Superabsorbent Polymer Composite (SAPC) Materials and their Industrial and High-Tech Applications

Von der Fakultät für Chemie und Physik

der Technischen Universität Bergakademie Freiberg

Genehmigte

DISSERTATION

zur Erlangung des akademischen Grades

doctor rerum naturalium

(Dr. rer. nat.)

vorgelegt

von   Deyu Gao

geboren am   27 Februar 1954   in Heilongjiang, V. R. China

Gutachter: Univ.- Prof. Dr. Habil. Berthold Thomas, Freiberg

Univ.- Prof. Dr. Habil. Robert B. Heimann, Freiberg

Univ.- Prof. Dr. -Ing   Peter Eyerer, Stuttgart, Pfinztal

Tag der Verleihung: 28. Februar 2003

Preface

The information contained in this thesis has been acquired over many years in several research organizations around the world. Essential parts were obtained during a research sojourn at Freiberg University of Mining and Technology, Freiberg, Germany between November 1997 and October 1999, sponsored by BMBF under auspice of the German-Chinese Bilateral Agreement on Cooperation in Science and Technology (WTZ). The results of this research are contained in section 3.2 (UV-irradiation polymerization), 3.3, 3.4(gas chromatography), 4.1(FTIR), 4.2(NMR), 4.3(XRD), 4.4(DSC), 5.1.2(mechanical properties), 5.2(thermal properties), and 6.8 (moisture sensor). Additional information was gather during a research assignment to the Department of Manufacturing Technology, Alberta Research Council (ARC), Edmonton, Alberta, Canada under the umbrella of a scientific exchange agreement between Heilongjiang Academy of Sciences and ARC. I worked there from October 1991 to June 1993 under the supervision of Professor Dr. Robert B, Heimann. The results of this research are described in section 3.1 (Electron beam polymerization), 5.1.1 (rheology), 5.3 (pH sensitivity), 5.4 (salt effect), 5.5 (electric properties), 6.2 (application in mining industry), 6.6 (dewatering of fuel) and 6.7 (strengthening of concrete).

The remaining work contained in this thesis was performed at the Technical Physics Institute (TPI) of Heilongjiang Academy of Sciences, Harbin, China in particular section 6.1 (application in oil industry), 6.4 (soil amelioration) and 6.5 (sealing of electric cable). Finally, research described in section 3.5 (pulse radiolysis, polymerization) was carried out during a research sojourn at Osaka University, Japan from October 1988 to April 1990.

In dealing with a material as multi-faced and versatile as superabsorbent polymer composite (SAPC) many preparatory and analytical methods have to be applied to fully comprehend this interesting and widely applicable class of materials. We are far from a complete understanding of its properties. Hence this thesis is only a small stepping stone towards a more comprehensive description of polymer-clay compounds. In particular, its technical application in industry, agriculture and cilviculture, medicine and general daily life has only began to be seriously considered.

Table of Content

0.0 EXECUTIVE SUMMARY

Expanding clay/polyacrylamide composites have the capacity to absorb large amounts of water while retaining good mechanical strength and high damping characteristics, and therefore represent a new and promising class of hydrogel materials. Bentonite (montmorillonite) has been used as expanding clay mineral and a superabsorbent poly(acrylamide)-bentonite composite (SAPC) material has been prepared using electron beam and UV light irradiation.

Characterization of SAPC using XRD, SEM, DSC, TGA, FTIR and NMR (^{27}Al, ^{29}Si and ^{12}C) showed that the structure of SAPC was that of acrylamide combined with montmorillonite in three different ways: a. AM intercalated in the lamina of montmorillonite in bimolecular layers bound by van der Waals force and hydrogen bonds; b. AM bonded to the montmorillonite surface by hydrogen bonds; c. AM in free state as a polymer string network.

Experimental results of rheological, mechanical, and thermal properties of SAPC showed a fully cross-linked structure and higher mechanical strength and thermal stability.

Application of SAPC in oilfields (enhanced oil recovery), for environmental protection (acid mine tailing abatement), agriculture (plantation, seedling), in electric industry (cable sealing), petrochemical industry (fuel dewatering), civil engineering (concrete additives) and sensor industry (sensor materials) showed a high potential of this class of materials for environmentally compatible and economically viable uses.

0.0 ZUSAMMENFASSUNG

Quellfähige Verbundwerkstoffe aus Ton und Polyakrylamid können grosse Quantitäten von Wasser absorbieren, behalten aber dabei eine hohe mechanische Festigkeit und gute Dämpfungseigenschaften und stellen daher eine neue Klasse von Hydrogelen dar mit potentiell interessanten technologischen Eigenschaften. Solche superabsorbierende Verbundwerkstoffe (SAPC) werden durch Polymerisation mit einem Elektronenstrahl oder Bestrahlung mit UV-Licht hergestellt.

Die Untersuchung der Eigenschaften von SAPC mit Hilfe von XRD, SEM, DSC, TGA, FTIR und NMR (^{27}Al, ^{29}Si und ^{12}C) zeigen, dass in der SAPC-Struktur das Akrylamid (AM) mit Montmorillonit in dreierlei unterschiedlichen Weisen verbunden ist: a. AM interkaliert in den Zwischenschichtraum von Montmorillonit in bimolekularen Schichten, die durch van-der-Waals-Kräfte und Wasserstoffbindungen verknüpft sind; b. AM gebunden an der Oberfläche von Montmorillonit durch Wasserstoffbindungen; c. AM als freies Polymernetzwerk.

Die Ergebnisse der rheologischen, mechanischen und thermischen Untersuchungen von SAPC zeigen eine völlig vernetzte Struktur mit vergleichsweise hoher mechanische Festigkeit und thermischer Stabilität.

Die Verwendung von SAPC bei der Ölgewinnung (Erhöhung der Ausbeute), im Umweltschutz (Reduzierung saurer Berge), der Agri- und Silvikultur (Pflanzen, Samenbau), der petrochemische Industrie (Entwässern), im Bauingenieurwesen (Zementbeimischung) und als Sensorsubstanz demonstriert, dass SAPC ein hohes Potential für umweltfreundliche und wirtschaftliche alternative Zwecke hat.

0.0 摘要

膨胀性黏土/聚丙烯酰胺复合材料可以吸收大量水并保持优异机械强度和流变特性，是新一代的凝胶材料。本文使用电子束和紫外线照射制备了聚丙烯酰胺/膨润土（蒙脱土）超级复合吸水材料（SAPC）。

使用X-射线衍射（XRD），扫描电镜（SEM），热分析（DSC，TGA），红外（FTIR）和核磁共振（NMR^{27}Al，^{29}Si ，^{13}C）等方法表征 SAPC 结构证明丙烯酰胺以三种不同的方式与蒙脱土结合：a. AM 通过 van der Waals 力和氢键以双分子层嵌入蒙脱土层间，b. AM 通过氢键与蒙脱土表面结合 c. AM 作为聚合物网络以自由状态存在。

流变学、力学、热性能等实验结果表明 SAPC 是完全交联结构并具有较高机械强度和热稳定性。

应用实验显示了 SAPC 在油田（二次采油）、环保（酸性尾矿处理）、农业（种植，育苗）、电力（电缆封水）、燃料工业（燃料脱水）、民用工程（混凝土添加剂）和传感器（敏感材料）等领域有广阔的应用前景。

0.0 概要

膨脹性黏土/ポリアクリルアミドの複合材料は大量の水を吸収すると同時によい機械性質と水分を保持する性質があるので，新しいハイドロゲールを代表している。ベントナイト（モントモリロナイト）は膨脹性黏土礦物として電子線と UV の照射によって， スーパー吸水性ポリアクリルアミド/ベントナイト複合材料をつくる。

XRD，SEM，DSC，TGA，FTIR と NMR（^{27}Al，^{29}Si and ^{13}C）を利用して SAPC の構造は解明されている。SAPC は アクリルアミド（AM）とモントモリロナイトと三つの結合方式により複合されている。a. AM は van der Waals force と水素結合によってモントモリロナイトの層間に二分子層 を形成し， b. AM は水素結合によって モントモリロナイト表面に接着し， c. AM は自由な状態でポリマーストリングの網状組織になる。

流動學と機械と熱の實驗結果により，SAPC は完全な架橋結構と高機械強度と熱の安定性があることはわかっている。

油田（enhanced oil recovery），環境保護（acid mine tailing abatement），農業（plantation, seedling），電氣工業（ケーブル シーリング），石油工業（燃料脱水），土木工事（コンクリート 添加物），センサー工業（センサー 素材）なとの應用結果により，SAPC は環境適應性と經濟性があり，ひろい應用前景があることが示されている。

1.0   INTRODUCTION

It is well known that there are many water absorbing materials such as pulp, paper, cotton etc which were conventionally used as sanitary towel and diaper. Those materials absorb water by its capillarity hence their water absorption capacity is usually less than 20 g water/g absorbent.   Another property of these materials is that the absorbed water can be squeezed out by an externally applied pressure. In the 1960's, researchers developed crosslinked polyacrylamide[1] which had the properties of absorbing up to 15-75 times of body exudate and retaining it under pressure of up to about 2.5 p.s.i..   At that time, the inventor of this material called it 'Hydrocoloidal Absorbent'. Comparing with traditional materials there was a big improvement, however, the absorption capacity was still low.   In the 1970's, at the Dept. of Agriculture of U.S. (Peoria, NRRL) a new material was developed which could absorb more than 1000 times of its weight of water and was called superabsorbent polymer (SAP)[2].   In 1974, disposable diapers were commercialized[3].   The world output of SAP increased from more than 100,000 tons in 1987 to 350,000[4] (400,000 ton[5]) in 1994. And in 1996, only one company (Hüls) produced 180,000 ton of SAP[6].   The production of SAP is increasing in two-digit speed at present time.

On the other hand, the application of clay-polymer composites attracted more and more attention in recent years[7].   Traditionally, clays are used as filling material for the purpose of improving material properties and reducing product cost. In 1985, an inorganic-organic composite (Superabsorbent Polymer Clay composite, SAPC) was prepared by intercalating acrylamide into an expandable smectitic clay, e.g. bentonite using γ-ray radiation-induced polymerization[8].   This preparation technique was improved and some of the properties of the composite material were studied[9].   The new material shows good absorption capacity to liquid water and water vapor. The absorption capacity can be as high as 2000 grams water/gram SAPC. Also, the material shows an interesting physico-chemical and electromechanical reaction to environmental changes such as temperature, moisture, electric fields, concentration changes of chemical species, and pH[10].   The product has been used in oil fields for enhanced oil recovery processes[11] and in other areas such as agriculture, forestry[12] etc.   In this thesis, the preparation of superabsorbent polymer composite (SAPC) using bentonite and organic monomer, its structural characterization and properties as well as its application in basic and commodity industries and high-technology fields are studied in detail.

2.0   BASIS PRINCIPLES OF SUPERABSORBENT POLYMERS

General properties of superabsorbent polymers

As mentioned above superabsorbent polymer can absorb water up to several thousand times of its own weight and keep this water under pressure. The absorbed water can be released slowly when the SAP is put in dry air to maintain the moisture of the environment. Most SAPs are in principle crosslinked hydrophilic polymers.

Because of these unique properties, SAPs have many novel potential applications in various areas. For example, they can be used in baby diapers, sanitary towels[13,14] athletic garment, as carrier of contamination prevention agent used as ship bottom painting to prevent the formation of microorganism[15], adhesives and food packing etc. In agriculture and horticulture[16], it is being used as plant growth medium to improve the water retaining property of sandy soil, in civil engineering as friction reducing material for placing pipe for sewage transport, in environmental protection, as sludge dehydrating treatment agent for solidifying waste and to absorb heavy metal ions such as Cr^{3+} and Co^{2+}. Using the same technology of SAP, Mijima prepared urea absorbing material which could be used to remove urea from urine in artificial kidneys[17], and Hirogawa prepared alcohol absorbing material[18] which can absorb about ten times of its weight of methanol.

There are many kind of methods to prepare SAP with various starting materials[19], such as copolymerizing hydrophilic monomer with a cross-linking agent, grafting monomer with starch[20], cellulose[21], synthetic fiber[22], and polysaccharide[23], cross-linking linear hydrophilic polymer with polyvalent metal ions[24] or organic multifunctional group materials etc. The product of SAP can be in the form of small particles, powder, fiber, membrane, microbeads and even liquid[25].

The SAPs can be classified with different methods. From a morphological point of view they can be divided into particle, powder, spherical, fiber, membrane and emulsion types etc. The morphology of SAP is designed to respond the different requirements of the applications. For example, the powder product can be put in the mutilayers sheet to form sanitary napkins and diapers, the particle and spherical product can be used as deodorant, fiber product can be used as antistatic electric fiber, membrane product can be used as antifost sheet and emulsion product can be used in soaking and painting.

From a material resources point of view, SAP can also be divided into natural macromolecules, semi-synthesized polymer, and synthesized polymers. From a preparation method point of view, it can be classified as graft polymerization, cross-linking polymerization, networks formation of water-soluble polymer and radiation cross-linking etc. There are many types of SAPs in the present market. Mostly, they are crosslinked copolymer of acrylates and acrylic acid, and grafted starch-acrylic acid polymer that are prepared by reverse suspension and emulsion polymerization, aqueous solution polymerization, and starch graft polymerization.

Water absorption capacity (WAC) is the most important characteristic of SAP. There are many ways to measure WAC, however, there is no standard yet. Usually, the WAC is measured using volumetric method, gravimetric method, spectroscopic method and microwave method. The volumetric method is to measure the volume changes of SAP (or the water) before and after the absorption, the gravimetric method is to measure the weight changes of SAP, the spectrometric method is to measure the changes the UV-spectrum of the SAP and the microwave method is to measure the microwave absorption by energy changes.

The water absorption capacity (WAC) of the SAPs depends upon its composition and structure generated from the preparation method, as well as the presence of electrolytes in the

water.   For example, the WAC of SAP can be thousand gram water/gram SAP when in contact with pure water, but when it is put into water containing urine, blood and metal ions, the WAC will be reduced to only one tenths of its maximum value.

Water absorbed in the SAP can exist in three states, 'bound' water, 'half-bound' water and 'free' water. 'Free' water shows a freezing point when the environment temperature is changed around 0°C, however, this freezing point cannot be seen with the 'bound' water. The 'half-bound' water shows property between them. The bounded water in SAP usually is 0.39-1.18 g/g[26].   Most water in the SAP is free water.   Tatsumi studied the effect of chemical structure on the amount of microwave absorption of water in various polymer films at 9.3 GHz. The microwave absorption was directly proportional to both the volume increase of the sample film and the amount of water in the polymer[27].

The principle of water absorption by polymer can be illustrated by the Flory theory[28] of an ionic network.

$$Q^{5/3} = \{(1/2 \times i/V_u \times 1/S^{1/2}) + (1/2 - X_1)/V_1\} \times V_0/\nu \qquad (1)$$

where Q: maximum swelling ratio of SAP, i: electronic charge on the polymer structure per polymer unit, V_u: polymer repeating unit volume, S: ionic strength of solution, X_1: interaction parameter of polymer with solvent, V_1: molar volume of solvent, in a real network, V_0: un-swollen polymer volume, ν: effective number of chains.   These parameters in the equation formed a balance of the swelling which can be further defined as follows: $1/2 \times i/V_u \times 1/S^{1/2}$: ionic strength on both polymer structure and in the solution, $(1/2 - X_1)/V_1$: the affinity of network with solvent, V_0/ν is cross-linking density.   The equation shows that the water absorption power mainly from the osmotic pressure, the affinity of water and polymer, and the cross-linking density of the network.

The swelling process of SAP can be explained as follow: the solvent tries to penetrate the polymer networks and produced the 3D-molecular network expanding, at the same time, the molecule chain between the crosslinked points thus decreasing the configuration enthalpy value. The molecule network has an elastic contractive force which tries to make the networks contract. When these opposed forces reach an equilibrium, the expansion and contraction reach a balance too.   In this process, the osmotic pressure is the driving force for the expansion of swelling, and the network elastic force is the driving force of the contraction of the gel.

At present, hydrophilic crosslinked superabsorbent polymers (SAP) such as modified acrylates and acrylamides are under scrutiny to develop a variety of products for industrial applications including chemomechanical ("intelligent") materials that convert chemical energy into mechanical motion[29,30]. The equilibrium swelling of such hydrogels is sensitive to environmental stimuli of either chemical or physical nature such as changes in pH[31,32], ionic strength of the surrounding solution[28], temperature[33], photo-irradiation[34] and electric field[35] that may influence the size, shape, solubility and degree of ionization of the gel.   By applying an electric field to a swollen gel in a solution, the gel can be made to contract and expand reversibly, thus simulating muscle action.   Also, research is ongoing worldwide to develop sensors and actuators based on those materials to monitor biochemical activity, pressure and strain rate.

One example of a hydrogel with an intelligent (smart) property responding to an environment stimulus is the pH-response polymer gel. Usually, the pH responsive gel is a molecular structure composed of a crosslinked network and ionizable groups in the network. These groups ionize in different pH and ionic solution. During the changing of the network structure and the ionic concentration with the environmental pH, effects arise such as the

generation of osmotic pressure, changes of the ionic groups and changes of the ionization degree. The hydrogen bond is changed, which in turn causes the gel to change in volume and mass. Besides the homogeneous polymer, the pH responsive gel can also be a block polymer (or interpenetrating polymer) composed of physically crosslinked non-polar rigid and soft structures such as block polymers containing polyurea (rigid) and polyethyleneoxide (soft).

Another example is a temperature-sensitive gel which can respond to a temperature stimulus to change its conformation. At low temperature the gels swell as the large molecule chains extend by hydration. When the temperature reaches to a certain value, rapid dehydration takes place. Because of attraction of hydrophobic groups, the molecule chain contracts. A typical hydrogel with temperature-responsive property is polyisopropylacrylamide. Polyacrylic acid and poly(N, N- methylene bisacrylamide) inter-penetrate polymer network gels also contract at low temperature due to hydrogen bond formation. At higher temperature, the hydrogen bonds weaken and the gel swells. Phase transition of the gel is a phenomenon of discontinuous change of the volume of the gel with the change of the environmental factors.

When a light-sensitive gel is being exposed to UV or visible light irradiation, isomerization or light decomposition takes place on the light-sensitive group. Due to the changes of conformation and dipole movement, the gel swells. For example, the derivative of triphenylmethane A changes to isolated triphenylmethane B. By heating or photochemical reaction it can return to the A state.

Most intelligent hydrogels are homogenous materials that contract or expand uniformly. If the material is built up with different original materials, it will bend to a special designed shape according to the original material to prepare an artificial hand for a robot. This is similar to a shape-memory alloy. These materials can be used in drug delivery system, artificial membranes for the eye, biosensors etc. Beside these rather high-tech applications, polymer/montmorillonite composites attracted attention in recent years[7] as new materials with improved properties and reduced product cost for applications such as a water-plugging agent in enhanced oil recovery operations and a soil amelioration material in agriculture[36].

Intercalation mechanism

SAP composite (SAPC) is prepared by intercalating a monomer into the interlayer space of sheet silicates. Typical silicates are montmorillonite, talc, Li-montmorillonite, zeolite, vermiculite etc. The most applicable silicate are three-layer (2:1) clay minerals. The basic structure unit is composed of an aluminum oxide (octahedral) layer between two silicon oxide (tetrahedral) layer such as montmorillonite. In the interlayer space, there are exchangeable cations such as Na^+, Ca^{2+}, Mg^{2+} etc, which can exchange with inorganic metal ions, organic cationic surfactant and cationic dyes.

Whether the intercalation and the associated planar expansion can proceed or not mainly depends upon the reaction free enthalpy (ΔG). If the $\Delta G < 0$, this process can go spontaneously. For an isothermal process, $\Delta G = \Delta H - T\Delta S$, $\Delta G < 0$, $\Delta H < T\Delta S$ is required. To meet the above condition, there are two processes in three ways

Exothermal process: $\Delta H < 0$, and $\Delta S > 0$,
$$\Delta H < T\Delta S < 0$$
Endothermal process: $0 < \Delta H < T\Delta S$.

The ΔH term is mainly composed of the strength of the interaction between the monomer or

polymer molecule and the clay, and the polymerization enthalpy of monomers in the interlayer of clay. The entropy change (ΔS) is related to the restricted state of solvent, monomer and polymer molecules, and the entropy of polymerization of the monomer in the layer.

According to the combination process, the intercalation can be divided into two types. 1. monomer intercalation and in-sit polymerization: disperse the monomer, intercalate it into the silicate interlayer space, and execute the polymerization; 2. polymer intercalation: mix the melted or dissolved polymer with the silicate by a mechano-chemical or thermo-dynamic chemical function to finish the intercalation process. As a practical method, this can be further divided into (i) solution method and (ii) melting method. Combining the above ways, four practical processes are generated: 1. melting intercalation of polymer, 2. solution intercalation of polymer, 3. melting intercalation and subsequent polymerization of the monomer and 4. solution intercalation and polymerization of the monomer. In this thesis, the 4th option, monomer solution intercalation was adopted and the details will be discussed.

3.0   PREPARATION OF SAP COMPOSITE

As indicated above that SAP is a kind of hydrophilic polymer with crosslinked structure generated in several ways such as copolymerizing monomers with cross-linking agents, cross-linking the linear polymer with multivalent metal ions or multifunctional organic chemicals, grafting monomers onto base materials, and hydrolysising the hydrophobic polymer etc.

Theoretically, there is a wide range of inorganic materials with expendable layers potentially available that conceivably can be utilized for the preparation of superabsorbent composites. Concerning the expendability, water affinity (hydrophilicity) and availability, bentonite[+] was chosen to prepare the composite.

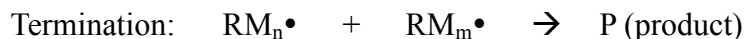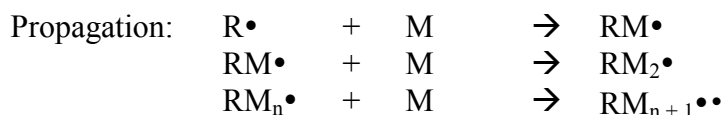### 3.1   Preparation of SAPCs by radiation polymerization with an electron beam

Ionizing radiation-induced polymerization has many advantages in terms of process controllability, products purity etc[37]. The radiation-induced polymerization is a chain reaction in which a large number of chemical changes may follow each single act of ionization or excitation. The polymerization of monomers involves at least three separate stages, i.e. chain initiation, chain propagation and chain termination, and these may be modified by further reactions such as chain transfer. Radiation intervenes primarily only in the initiation stage, acting as a means of starting the reaction which then continues independent of it. This is not longer true at very high radiation intensities where primary radicals produced can intervene directly in the termination mechanism. The number of growing chains which can react with each other also depends on the radiation intensity, which is therefore of considerable importance in polymerization.

The use of radiation polymerization has a number of distinct advantages when compared with the usual chemical techniques. The latter require catalysts which may be incorporated in the polymer and then remain as an impurity which may continue to react. With radiation, on the other hand, no impurities are introduced although trapped radicals may still be present in the solid polymer. The polymerization can occur under a variety of conditions; as a liquid, in the gas phase, as solid, in emulsions or dispersions. The temperature conditions needed for initiation by catalysts are not necessarily those most suitable for chain propagation, whereas with radiation the initiation step is almost temperature independent. Hence a reaction temperature may be chosen that is most suitable for the propagation step. Radicals can be produced uniformly throughout the system whatever it physical state is. In particularly polymerization in the solid state is possible. During chemical polymerization, its exothermal nature produces a rise in temperature which results in an increased rate of dissociation of the chemical catalyst. In radiation polymerization, this temperature rise has little effect on the initiation step, the number of primary radicals depending only on the instantaneous radiation intensity. Much closer control of the reaction is therefore possible[38].

The polymerization initiated by radiation can be illustrated as follows.

Initiation: M(monomer),   S(solvent) $\rightsquigarrow$ R•(radical)

[+] Bentonite is defined as a sedimentary rock consisting to a large proportion of expandable clay minerals with three-layer structure (smectites) such as montmorillonite, beidellite, nontronite etc. Additional minerals frequently found in bentonite are quartz, feldspars, zeolites etc.

Propagation: R•   +   M   →   RM•

RM•   +   M   → RM_2•

RM_n•   +   M   → RM_{n+1}••

Termination: RM_n•   + RM_m•   →   P (product)

In the preparation of SAP composite, monomers are acrylamide (AM) or other species containing the vinyl group, and the product itself is SAP. Some studies on AM/bentonite system have been done with gamma ray irradiation[39]. In this section, an alternative polymerization method using electron-beam irradiation will be mainly discussed, and in section 3.2 polymerization by UV radiation will be considered.

Materials

N,N-Methylene bisacrylamide (MBAM), acrylamide (AM, Electrophoresis Reagent, Isolab. Inc.), acrylic acid (AA, AR Aldrich), sodium hydroxide (NaOH), sodium carbonate (Na_2CO_3, AR, Mallinckrodt Canada Inc.), sodium bentonite (Avonlea, Saskatchewan), with chemical composition of SiO_2 58.66%, Al_2O_3 16.36%, Fe_2O_3 4.7%, CaO 2.0%, MgO 2.11%, Na_2O 1.96%, K_2O 0.1%, TiO_2 0.2% CEC 75-90 were used as received without further purification. The sodium bentonite contains 79% of Na-montmorillonite, 9.5% of Quartz, 3% of feldspar, 2% of gypsum and 1.5% of other minerals.   Its cation exchange capacity (CEC) is 820 meq/kg[40].

Equipment

Electron Accelerator AECL I-10/1 with an electron beam energy of 9 MeV.

Sample preparation method

The sample preparation procedure was as follows (unless specifically indicated). Sodium bentonite was suspended in distilled water in a concentration of 30 % by weight.   Then, the solution was mixed with AM aqueous solution (30 %) for 2 hours for intercalation.   After that, MBAM (2% aqueous solution) was added and the mixture was purged with nitrogen gas to replace the oxygen in the solution.   Finally, the solution was irradiated at preset temperature and dose rate with an electron beam from the Electron Accelerator AECL I-10/1 with electron beam energy of 9 MeV.   After irradiation, the solidified samples were cut into small pieces, dried and analyzed.

To get some insight into response of the water absorption capacity to various pertinent process parameters, a parameter sensitivity survey was performed.   The results are shown in sections 3.1.1 to 3.1.5 for AM/bentonite and in 3.1.6 for AA/bentonite.

3.1.1   Effect of additives

During the polymerization process, some chemical materials usually can change the polymerization rate[41,42], even the reaction mechanism and therefore the product property. Additives were used in this study to adjust the hydrophilicity and cross-linking density which affects the water absorption capacity (WAC) of SAP.   The Box-Behnken statistical design method[43] was used to study the effect of additives on the polymerization system. With this design, more information could be obtained with a minimum number of experiments. First, the basic conditions important in the radiation induced polymerization were determined, such as temperature, dose rate, and total dose. Then the concentrations of three of the most important additives (sodium hydroxide, sodium carbonate and N,N-methylene bisacrylamide), were used as independent factors. The results of this design are shown in Figure 1.
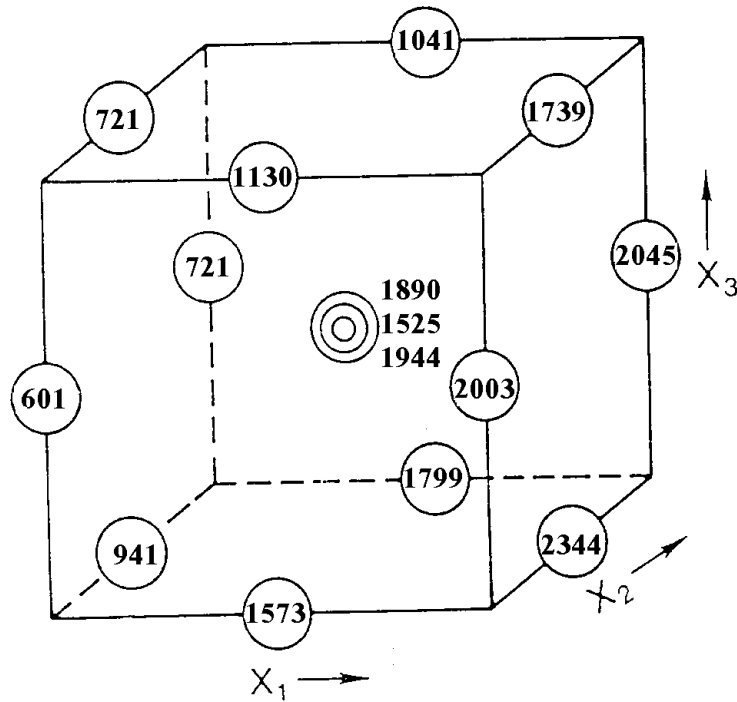
Figure 1. *Box-Behnken Design (additives effect).* x_1: *NaOH (0, 0.5, 5%);*
x_2: *Na$_2$CO$_3$ (0, 1.5, 3%);* x_3: *MBAM (0, 0.02, 0.04%), dose: 20 kGy, 20 ^{o}C.*
Data in the figure were the water absorption capacity (WAC) of the samples in
g water/g SAP.

At irradiation conditions of 20 kGy, 20 ^{o}C, increasing concentration of NaOH and Na$_2$CO$_3$ inhibit the polymerization and cross-linking reactions. Hence, the WAC of the product will be increased due to an increase in hydrophilicity and a decrease in cross-linking density. The MBAM benefited the cross-linkage greatly. However, threshold amounts of MBAM are needed in order to form a required cross-linkage between the linear molecules. The crosslinkage could take place even without addition of MBAM, if the irradiation dose is high enough. Although the MBAM had benefited the cross-linking reaction, and promoted the formation of a gel, it reduced the water absorption capacity in accordance with the Flory theory (see above section 2.0). The computation method to determine the coefficients of the polynomial of the Box-Behnken design is shown in Appendix 1.

Factor significance

To evaluate the effects of the factors, the minimum factor significance (F) was calculated according to the equation

$$F = t_{d.f}^{\nu} \bullet \sigma(s) \bullet (2/mk)^{1/2} \qquad (2)$$

where F: minimum significant factor effect, $t_{d.f}^{\nu}$: student "t" at confidence level ν for number of degree of freedom (d.f) in the estimate σ(or s), σ: standard deviation from triplicated center point, m: number of "+" in the column ($\equiv$ number of "+" signs in column). In this calculation, k: number of replicates = 1, d.f.: degree of freedom = (number of runs -1) = 14, ν = 0.95, $t_{14}^{0.95}$ = 2.14 (double-sided test), C: number of center points=3. The F values were

$F_M = 2.14 \times 228 \times (2/4)^{1/2} = 345$ for main effects
$F_I = 2.14 \times 228 \times (2/2)^{1/2} = 488$ for two-factor interactions
$F_Q = 2.14 \times 228 \times (1/mk + 1/C)^{1/2} = 330$ for quadratic effects

By evaluating Figure 1 it is obvious that the water absorption capacity Y is strongly dependent in a moderately sense on x_1; strongly dependent in a negative sense on x_3, and weakly dependent in a positive sense on the x_2.

Hence the concentration of NaOH (x_1) is the most important factor to maximize Y when the concentration of Na_2CO_3(x_2) and MBAM(x_3) are held at low levels. The interaction term(x_2x_3) shows that Na_2CO_3 and MBAM are weakly dependent on each other.

In the data analysis, it is supposed that the general polynomial for this model can be fitted by the method of least squares

$$Y = b_0 + \sum b_i x_i + \sum b_{ij} x_i x_j + \sum b_{jj} x_{jj}^2 \tag{3}$$

Putting (see Table A-1) of coefficients of this design into the equation, one obtains the full polynomial:

$$\hat{Y} \times 10^{-3} = 1.79 + 0.687x_1 + 0.037x_2 - 0.296x_3 - 0.241x_1^2 - 0.204x_2^2 - 0.197x_3^2 - 0.02x_1x_2 - 0.01x_1x_3 - 0.086x_2x_3 \tag{3a}$$

To simplify the polynomial, one omits the non-significant factors and obtains a reduced equation:

$$\hat{Y} \times 10^{-3} = 1.79 + 0.69x_1 - 0.30x_3 - 0.24x_1^2 - 0.20x_2^2 - 0.20x_3^2 \tag{3b}$$

The predicted values of $Y_{calc.}$ were calculated using the reduced polynomial and are shown in Table A-1 last column. Quality of the fit of the data to this polynomial can be estimated using a Fisher test:

$$F = \sigma_{LF}^2/\sigma_{error}^2 = 4374/51951 = 0.084 \leq 2.48 \; (F_{table}{}^{44})$$

From the latter calculation, it can be inferred that the polynomial model can provide a reasonable representation of the experimental results.

3.1.2 Concentration effect

Because the polymerization system was an aqueous solution, the AM and bentonite concentrations not only affected the reaction speed, but also affected greatly the post-treatment process of the product when solid product are desired. This is because in the post-treatment process the water has to be removed from the product so that a solid product could be obtained. The concentration had an obvious effect on the cross-linking process. Below a certain concentration, the system could not even be cross-linked to form a gel due to the longer distance between the molecules and weak strength of the chain. Figure 2 shows that the concentration has a great effect on the WAC because it affects the SAPC cross-linking density. With the decrease of concentration, the WAC increased linearly due to the less cross-linkage in the network of the composite. When the concentration dropped below a certain value, the linear PAM molecules cannot approach each other close enough to form cross-linkages, and thus the structure of the molecule cannot be changed from linear to a network. This resulted in dissolution and collapse of the samples when put into an aqueous solution for swelling. On the other hand, higher concentration systems benefit the cross-linking process, but decreased the WAC.
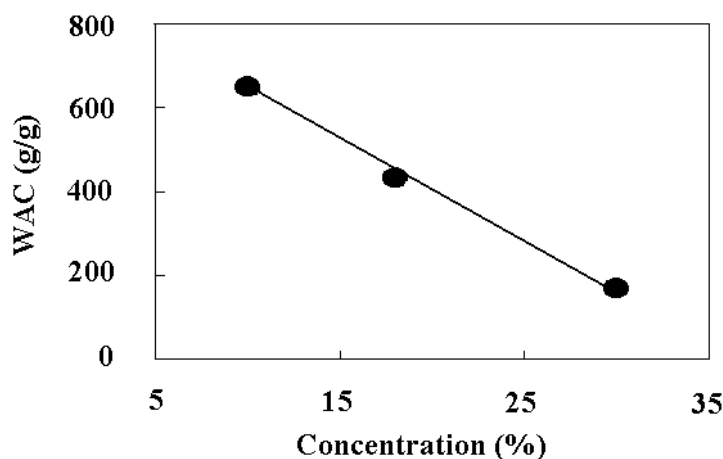
Figure 2. *Effect of concentration on the water absorption capacity, irradiation dose: 23 kGy.*

Moreover, because the AM can generate a great amount of heat during its polymerization (81.5 kJ/mol), too high a concentration of AM would make the system become too hot and also too viscous to be handled. In order to get higher WAC of SAP and more convenience of post-treatment, proper concentration of the system should be chosen, although higher concentrations could benefit the post-treatment process.
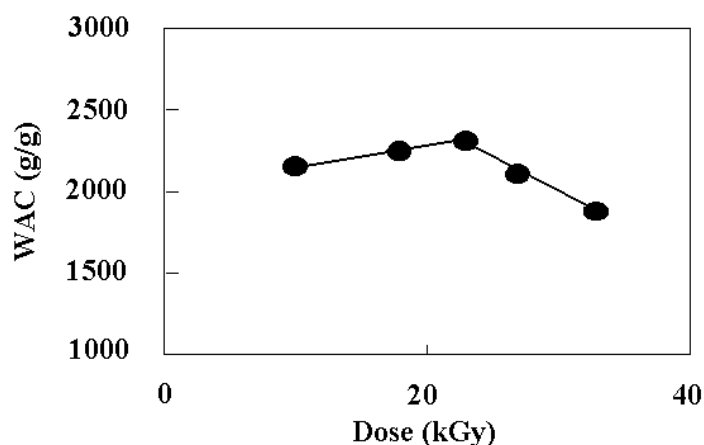
3.1.3 Effect of irradiation dose

Figure 3. *Effect of irradiation dose on water absorption capacity (c=28%)*

The solution used in the experiment contains 28% solid content (AM:bentonite=1:1) and 0.02% of MBAM, 3% of NaOH and 1.05% of Na_2CO_3. The results are shown in Figure 3. It can be seen that a lower irradiation dose cannot form enough cross-linked points in the SAPC which could efficiently hold the whole SAPC structure together, so gelation of the solution did not occur. Too high a dose irradiation produced too many cross-links which in turn decreases the WAC. Therefore a proper dose should be selected.
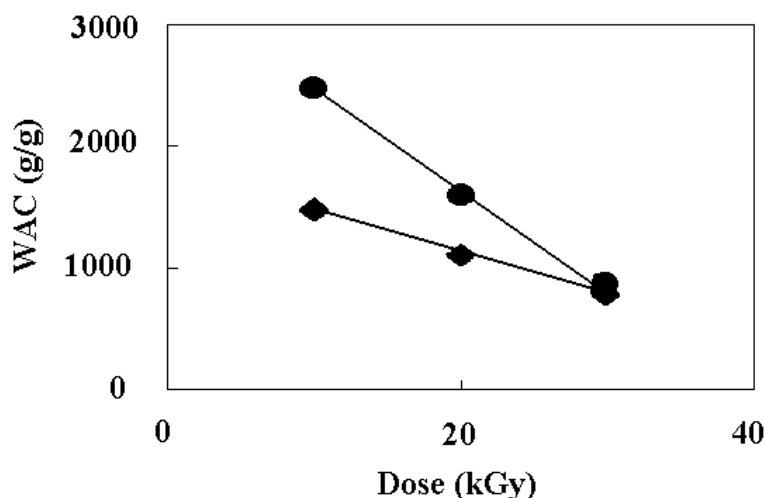
3.1.4   Effect of irradiation atmosphere

Figure 4. *Effect of irradiation atmosphere on the water absorption capacity.*
●*: In air;* ◆*: In N$_2$ atmosphere.*

The irradiation atmosphere could affect the polymerization rate since the oxygen in the solution inhibits the initiation process of polymerization by combination with radicals. The atmospheric effect was studied in a solution as in the previous experiment. Six samples were divided into two groups, three of them were polymerized in nitrogen gas atmosphere, and the others in air. After irradiation, the WAC was measured. The results obtained at different condition are shown in Figure 4. In the lower dose range, the difference of WAC between the sample purged with nitrogen gas and the one which was not purged is very large. But, when the dose goes higher, the difference becomes small. This is because in the electron-beam induced polymerization the reaction time is very short. The induction period could be not ignored although it was very short too. But with increasing reaction time, the induction period become relatively shorter. This is the reason why at high doses the difference becomes smaller and finally goes to zero.

3.1.5   Effect of acrylamide/bentonite ratio

The study of the effect of the AM/bentonite ratio was done at an irradiation dose of 10 kGy at a solid concentration of 28%. The results are shown in Figure 5.

From Figure 5 it can be seen that increasing AM/bentonite ratios increase the WAC of SAPC. Low ratios, i.e. small amounts of AM cannot form a crosslinked network structure so that the bentonite collapses during the WAC measurement.

3.1.6   Preparation of polyacrylic acid/bentonite composite

In the following section, the feasibility of the preparation of SAPC using acrylic acid (AA) and bentonite by irradiation with an electron beam will be discussed as well as the effect of important processing parameters on the water absorption capacity (WAC).

Effect of neutralization degree

It is well-known that in the polymerization process, the pH of the solution affects the polymerization rate. Higher neutralization degree (degree of the neutralization is a ratio of acrylic acid neutralized with NaOH) inhibited the monomer to be polymerized as in the polymerization of pure AM system. On the other hand, a lower neutralization degree accelerated the polymerization rate, increased the polymerization degree and the cross-linkage density, and
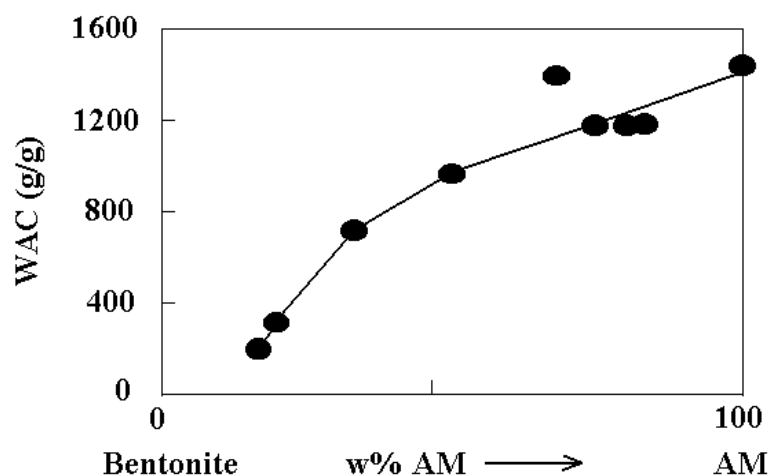
therefore, decreased the WAC as shown in Figure 6.

***Figure* 5.**   *Effect of the AM/Bentonite ratio on the water absorption capacity. Dose: 10 kGy.*
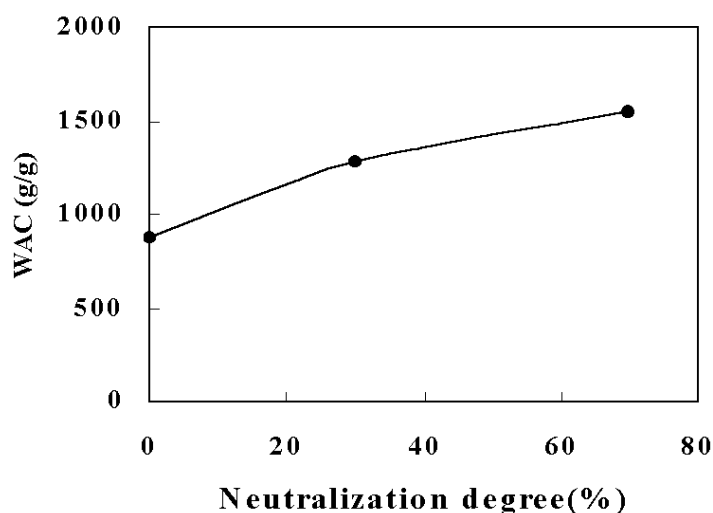

***Figure* 6.**   *Effect of neutralization degree of AA monomer on WAC. Dose:20 kGy; Nitrogen gas; AA/bentonite =1/1.*

Effect of irradiation dose

In Figure 7 it can be seen that to form a network structure, a certain irradiation dose is needed just as shown in AM polymerization.   At a lower irradiation dose, parts of the samples dissolved because not enough network structure was formed.   But after sufficient network structure had formed, a higher irradiation dose resulted in the decrease of WAC.   The higher the dose is, the lower the WAC becomes. Figure 7 shows that the AA/bentonite system has an optimum dose range of about 10 kGy to yield a maximum WAC of about 1500 g/g. Comparing to the polymerization of acrylamide/bentonite (see Figure 3), the optimum dose for AA is lower.   This may be due to the higher cross-linking reactivity of the AA.
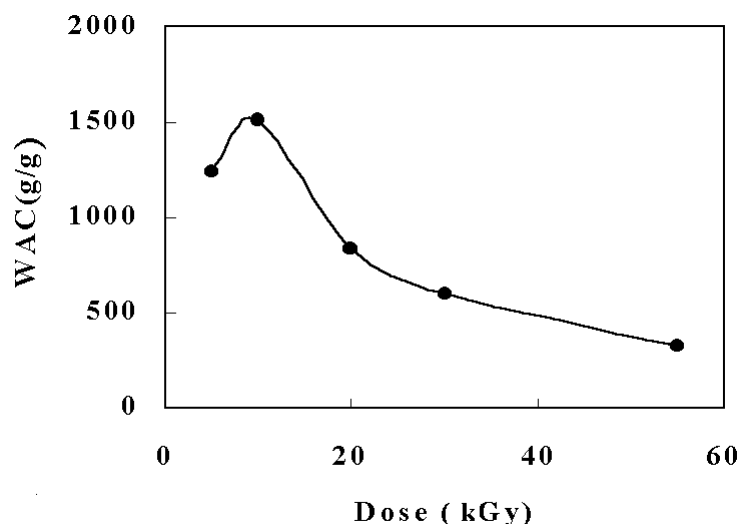
Figure 7. *Effect of irradiation dose on the WAC. Concentration 40 %, nitrogen atmosphere, AA/bentonite =1/1.*

Effect of cross-linking agent

As pointed out in the AM/bentonite system, the cross-linking agent of MBAM has a very large effect on both the network structure and the WAC of the Poly(AA)/bentonite composite. In order to form a network structure, some MBAM is needed. More MBAM will produce too many cross-linked points, which affects negatively the WAC of the samples. Figure 8 shows that the WAC decreased by the addition of MBAM.
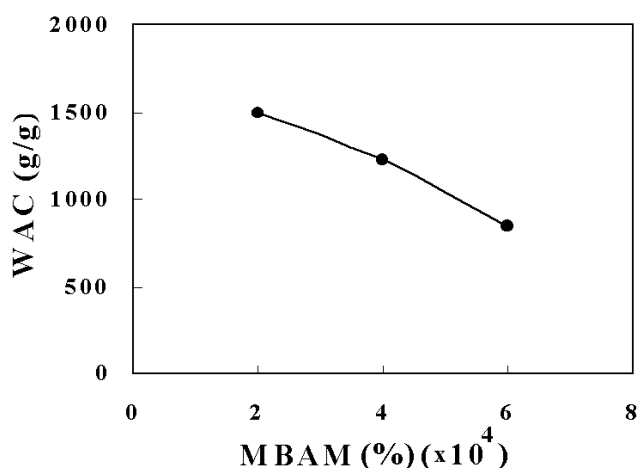
Figure 8. *Effect of MBAM on WAC. Dose:20 kGy, nitrogen gas, AA/bentonite=1/1.*

Effect of acrylic acid/bentonite ratio

The sodium bentonite influences the gel strength of the SAPC. Increasing the AA/bentonite ratio decreased the WAC of SAPC in a non-linear way (see Figure 9). This is possibly related to the increase of the polymerization rate and the changes of the crosslinked structure by an increase of the AA/bentonite ratio, i.e. the formation of cross-linked structure after the AA polymerized. However, too low AA/bentonite ratio can not form sufficient cross-linked points, so the sample structure would collapse in the solution.

Figure 9. *Effect of AA/bentonite ratio on WAC. Dose:20 kGy*
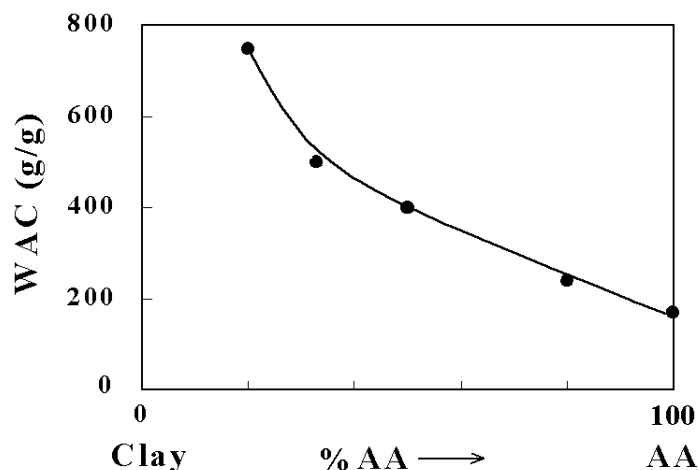
Effect of concentration

As in the AM/bentonite system (see Figure 2), higher concentration of AA decreased the WAC of SAPC as shown in Figure 10. High concentrations made the post-treatment process easy, but on the other hand, it generated too much polymerization heat that made the process difficult to control. By theoretical calculation, the highest concentration of AA in polymerization system initiated by an electron beam should not exceed 30%-w/w.
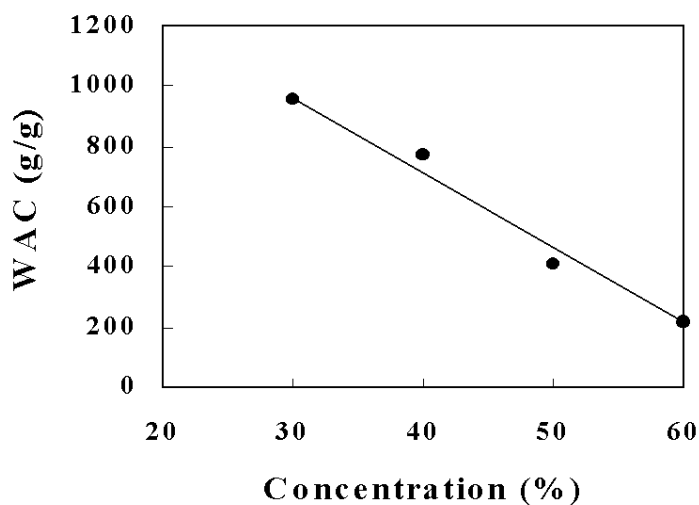
Figure 10. *Effect of AA concentration on WAC.*

3.2   Preparation of SAPCs by polymerization initiated by UV irradiation

Materials

Potassium persulfate and sodium hydroxide (AR, Merck KG, Germany), AM (GC, Fluka Chemie AG, Switzerland), AA (GC, Fluka Chemie AG, Switzerland), MBAM (Fluka Chemie AG, Switzerland), Eosin gelb, sodium vinylsulfonate (VSNa) (30% aqueous, Fluka Chemie) and sodium styrenesulfonate (SSNa) (Fluka Chemie) were used.

The bentonite (SÜD-CHEMIE AG) had the following chemical composition: water content of <14%, SiO_2 64.9%, Al_2O_3 19.4%, Fe_2O_3 3.3%, CaO 1.2%, MgO 2.3%, Na_2O 1.9%,

K_2O 0.4%, heating loss 5.3%[45]. By XRD analysis, the following mineralogical phase composition was found: Ca montmorillonite approx. 70-85%, quartz approx. 3-4%, feldspar approx. 7-8%, cristobalite approx. 4%[+]. The bentonite was dried at a temperature of 120 °C for 24 hours to remove the water content before being used as precursor materials for SAPC. Other chemicals were used as-received without any additional treatment.

Some basic conditions

The UV-induced polymerization experiments were carried out using an UV lamp (Solimed-Quartzlampen, TA150) with an output power of 140 W.

The amount of photons applied to the system is one of the most important factors during polymerization of acrylamide initiated by UV light. Due to the weak penetrating property of UV compared to an E-beam, silica glass vessels with better UV transparency than ordinary glasses were used.

The viscosity of the bentonite solutions were checked to determine the concentration ranges of the experimental system. The results are shown in Table 1. It is apparent that the dispersion speed of the bentonite was faster in the AANa solution than in the AM solution. The higher electrolyte concentration of the former caused a faster dispersion speed. Solutions with different concentrations of NaOH had different dispersion speeds. The viscosity of the solution showed the same trend. Solution of AM with 30 % concentration turned into a gel-like material after addition of bentonite. On the other hand, the AANa solution was not viscous at all.

Table 1.   Dispersion speed of bentonite in various solutions and their viscosities

	AANa (30%)	NaOH (4%)	NaOH (0.5%)	H_2O*	AM (30%)
Concentration of bentonite (%)	8	8	8	8	8
Relative dispersion speed of bentonite	very fast	fast	medium	slow	very slow
Viscosity of solution	non viscous	non viscous	viscous	very viscous	gel-like

*: *deionized water*

3.2.1   Polymerization initiated by UV irradiation

Acrylamide

Acrylamide is the most important material in the preparation of SAPC. To exclude the influence of bentonite on the UV-induced polymerization, preliminary studies on the polymerization of pure acrylamide using two kinds of photosensitizer, Eosin gelb and potassium persulfate[+], were carried out. Those two kinds of photosensitizer had different effects on the AM polymerization system. The results are shown in Table 2. The potassium

---

[+] The mineralogical composition of this bentonite deriates from the Saskatchewan bentonite used in previously (see section 3.1) in that it contains less quartz and more feldspar as the latter. However, since both minerals do not add to the swelling capacity of the clay this difference appears to be negligible. On contract with NaOH, the Ca-montmorillonite will transform to Na-montmorillonite through ion exchange.

[+] Sometimes this compound is called potassium peroxidisulfate, $K_2S_2O_8$.

persulfate had a more pronounced accelerating effect on the polymerization of acrylamide. Hence the polymerization was completed in about 10 min. But, at the experimental condition, the addition of Eosin gelb had no effect on the polymerization system of AM even if the system was irradiated for more than 30 min and higher concentration of Erosin gelb were used.

Table 2.   Effect of photosensitizers on the polymerization of AM*

Photosensitizers(%)		Remarks
$K_2S_2O_8$	Eosin	
-	-	not polymerized
0.32	-	polymerized
-	0.16	not polymerized

AM 30 g/100ml solution, room temperature, UV 13 min.

Sodium acrylate

The sodium acrylate was prepared by adding the theoretically required amount of sodium hydroxide solution to the aqueous acrylic solution cooled in a water bath under stirring to prevent polymerization induced by the heat generated during the neutralization reaction.   The pH of the solution was adjusted to about 7 with NaOH. The concentration of the solution was adjusted using a volumetric flask. The specific gravity of the AANa solution with a concentration of 30 % was about 1.15 g/ml. The polymerization of the sodium acrylate was carried out at the same condition as the acrylamide. The experimental results are shown in Table 3. It is obvious that the photosensitizers behave in the same way towards polymerization of the sodium acrylate as of the acrylamide.   The potassium persulfate had an accelerating effect on the polymerization of acrylate, while Eosin gelb showed a very weak effect. In fact, there was no gelation occurred in the solution even though the irradiation time was 3 times longer (30 min) than the initiation time using potassium persulfate. The solution become little viscous that means it partially polymerized.

From the experiments described above, it can be concluded that the potassium persulfate did indeed more effectively accelerate the UV-induced polymerization of AM and AANa, and hence it was used for this purpose in the further study.

Table 3.   Effects of photosensitizers on the polymerization of AANa*

Photosensitizers(%)		Remarks
$K_2S_2O_8$	Eosin	
-	-	not polymerized
0.32	-	polymerized
-	0.16	partly polymerized

AANa 30ml/100ml solution, room temperature, UV 11min.

Sodium styrenesulfonate and sodium vinylsulfonate

Because SSNa and VSNa are important co-monomers on the preparation process of the SAPC for its application in sensors, in the study, 20 g/100g aqueous solution of SSNa and 30 g/100g of VSNa were tested under the same polymerization condition as above. The experimental results showed that none of the two monomers could be polymerized by addition of potassium persulfate and Eosin gelb itself due to the poor polymerization activity. However, both of them could be co-polymerized together with the high activity monomer of acrylamide using potassium persulfate as photosensitizer.

3.2.2   Effects of $K_2S_2O_8$ concentration on gelation

After investigation on the feasibility of UV-assisted polymerization of pure AM and AANa solutions, the polymerization of the intercalation system of AM in bentonite was studied. In the experiments, the polymerization system consisted of a mixture of an aqueous solution containing 2% of NaOH, 0.08% of MBAM, 12% of AM, and 8% of bentonite. The bentonite powder was dispersed into the solution under stirring. The distance from the samples to the UV lamp was kept constant at 10 cm. The results of the experiment using different concentrations of potassium persulfate in the polymerization system are shown in Table 4. It can be concluded that $K_2S_2O_8$ had a good initiation effect of the polymerization in the concentration range of 0.02 - 0.08%.

Table 4.   Effect of $K_2S_2O_8$ concentration

$K_2S_2O_8$(%)	Remarks
0.02	gelled
0.04	gelled
0.06	gelled
0.08	gelled

UV 30 min

3.2.3   Effect of NaOH concentration

A set of experiment was designed to study the effect of the NaOH concentration on the polymerization system. The conditions for the experiments were identical to the experiments described above with the exception of the difference in the NaOH concentration. Figure 11 shows the water absorption behavior of SAPC samples. The water absorption capacity (WAC) increased with increasing concentration of NaOH. However, the hydrogels formed were found to become soft with an increase in NaOH concentration. It is suggested that this was due to incomplete polymerization caused by the slow polymerization rate which affected the cross-linking density of the gel and hence caused the gel to soften.
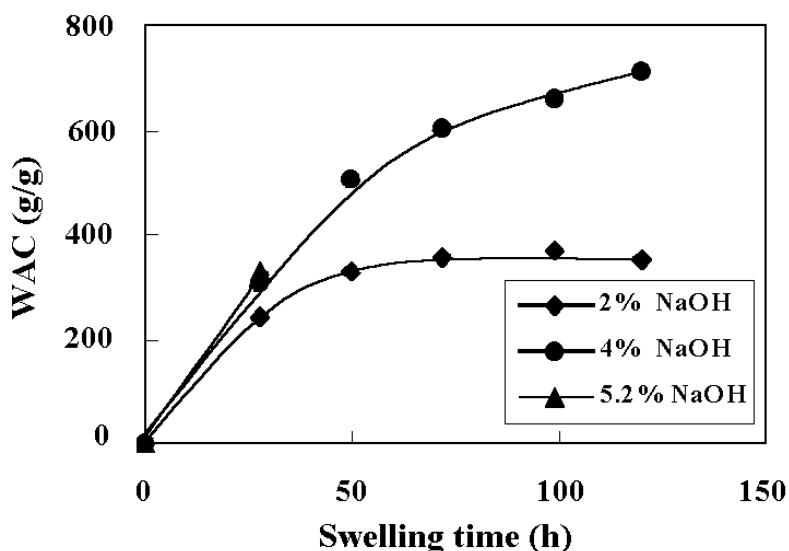
Figure 11. *Effect of NaOH and swelling time on WAC*
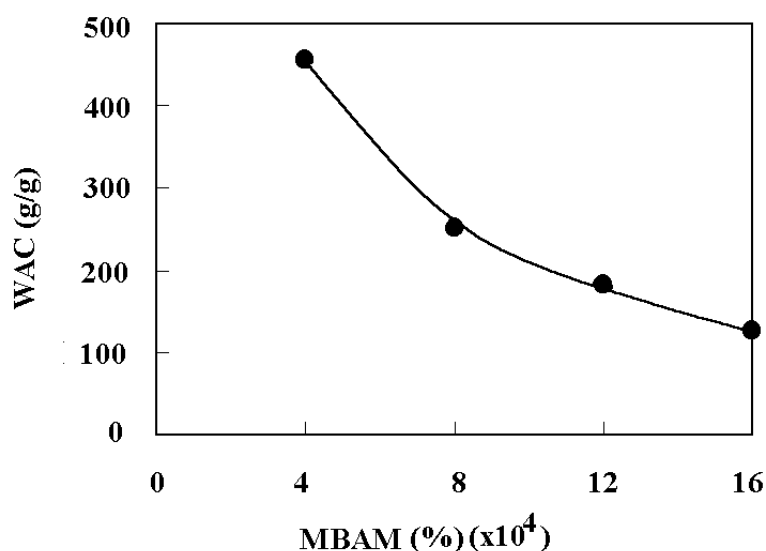
3.2.4 Effect of MBAM concentration

Figure 12. *Effect of methylene N, N-bisacrylamide (MBAM) concentration on WAC of SAPC*

A solution containing 8% of bentonite, 12% of acrylamide, 1.6% of sodium hydroxide and 0.08% of potassium persulfate was used in the polymerization. The results of the experiments evaluated in terms of the WAC are shown in Figure 12. The appearance of the hydrogels formed in the experiments showed that with increasing MBAM concentration the gels became hard and brittle. In contrast with the effect of NaOH, this was attributed to a high cross-linking density in the SAPC structure induced by the MBAM.

3.2.5 Box-Behnken design for the additive effect in the preparation of SAPC

Factors and levels

From the experiments described above, it can be concluded that the concentrations of sodium hydroxide, methylene N, N-bisacrylamide (MBAM), and potassium persulfate were

three important factors to be considered in the study. To evaluate the effects of additives on the UV induced polymerization system, a Box-Behnken design with three factors varied at three levels was used to optimize the properties of the resulting SAPC. The three factors and their three levels are shown in Table 5.

Table 5. Factors and levels for the Box-Behnken design

Parameter	Level 1 **(-)**	Level 2 **(0)**	Level 3 **(+)**
x_1, NaOH (%)	1	2	4
x_2, MBAM (%)	0.02	0.04	0.08
x_3, $K_2S_2O_8$ (%)	0.04	0.08	0.12

The schematic sketch of the Box-Behnken design space and the experimental results (water absorption capacity) are shown in Figure 13.
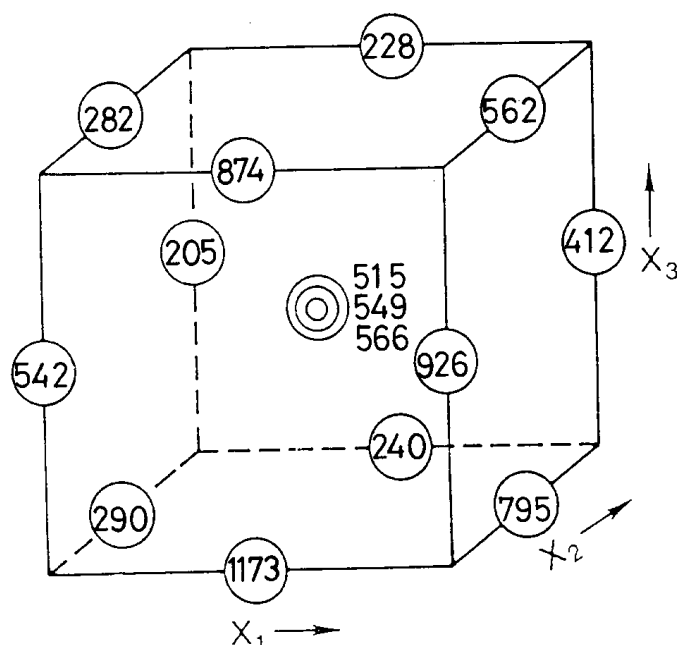

Figure 13. Schematic illustration of the Box-Behnken design space with experimental data points indicated. The numbers refer to the WAC of the resulting SAPC samples.

The experimental results were evaluated in terms of WAC. Appendix 2 shows the experiment results and the calculated values of the design.

Factor significance

The factor significance was calculated as in the previous section. Results were

$$F_M = 2.14 \times 26 \times (2/4)^{1/2} = 39$$
$$F_I = 2.14 \times 26 \times (2/2)^{1/2} = 56$$
$$F_Q = 2.14 \times 26 \times (1/mk + 1/C)^{1/2} = 38$$

If the effect of the factor is larger than F in absolute terms then it can be considered statistically significant. The coefficients b_1, b_2, and b_{11}, b_{22} are much larger than the

respective F values, and x_1, x_2, x_3 and x_1^2 and x_2^2 can therefore be considered the most significant factors.

Hence it can be concluded that the water absorption capacity (WAC) of the SAPC is strongly dependent, in a positive sense, on x_1, strongly dependent, in a negative sense, on x_2, and also weakly dependent, in a positive sense, on x_2x_3, x_2^2 and, in a negative sense, on x_3 and x_1^2. From the probability plot of the coefficients shown in Figure 14, a similar conclusion can be drawn, even though only the factor x_2 shows a significant distance from the straight line that indicates a Gaussian probability, i.e. normal distribution of the factor coefficients. On the other hand, the probability plot of the residuals indicates that the statistical model used, i.e. the fitted polynomial rather faithfully reflects the true shape of the response surface (Figure 15).
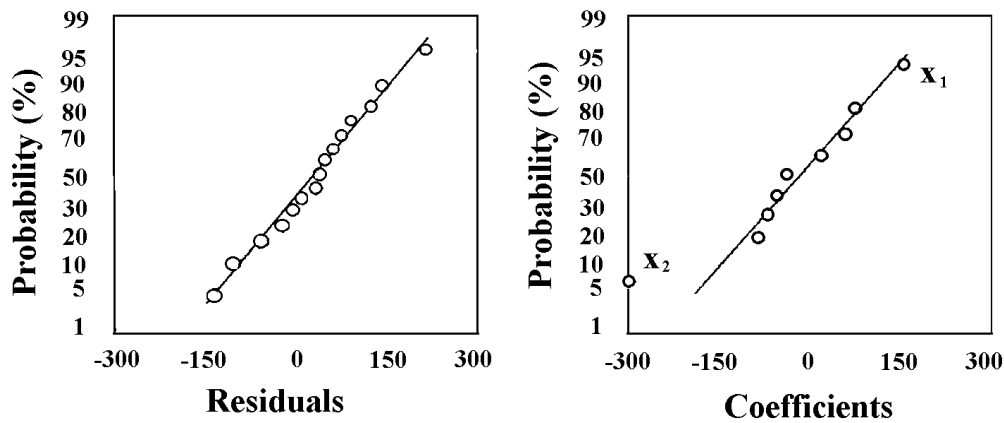

Figure 14. *Probability plots of the residuals and the factor coefficients*

The polynomial equation that would interpret the dependence of the water absorption capacity (WAC) of the SAPC on the selected parameters is

$$\hat{Y} \times 10^{-3} = 0.543 + 0.16x_1 - 0.304x_2 - 0.069x_3 - 0.044\ x_1x_2 - 0.056x_1x_3 +$$
$$0.072x_2x_3 - 0.086x_1^2 + 0.061x_2^2 + 0.022x_3^2 \tag{4a}$$

To simplify the polynomial, one omits the statistically non-significant factors and obtains the reduced polynomial:

$$\hat{Y} \times 10^{-3} = 0.54 + 0.16x_1 - 0.30x_2 - 0.07x_3 + 0.07x_2x_3 - 0.09x_1^2 + 0.06x_2^2 \tag{4b}$$

From above equation one can infer that the NaOH concentration x_1 has a strongly positive effect on the WAC, the MBAM concentration x_2 has a strongly negative effect on the WAC, and the $K_2S_2O_8$ concentration x_3 has a rather small negative effect on the WAC. There are also, to some extent, two-factor interaction effects of $K_2S_2O_8$ with NaOH, and $K_2S_2O_8$ with MBAM. The quadratic factors of the concentrations of NaOH and MBAM also have some weaker effects on the WAC as shown in the curvature of the response surface (Figure 15).

Hence the WAC of the SAPC can be controlled using the simplified equation in practical studies. The experimental results can also be predicted by this equation. Figure 15 shows the response surface of equation (4b) with x_3 fixed at a constant coded level of 0 (0.08% $K_2S_2O_8$).
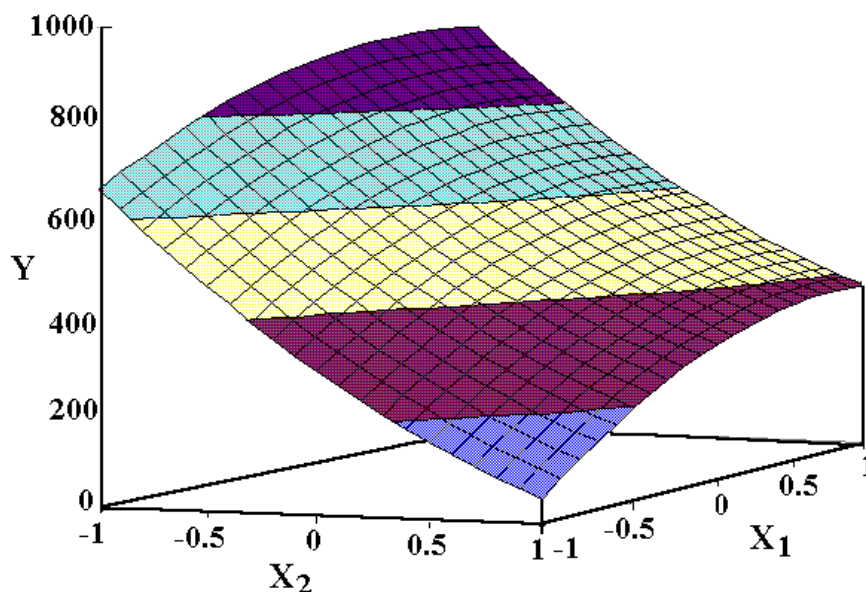
Figure 15. *Response surface of the water absorption capacity (WAC) of superabsorbent polymer composite (SAPC). X_3 was held constant at a coded level of 0 (=0.08% $K_2S_2O_8$)*

3.3 Improvement of the preparation technique (AM/AANa/bentonite system)

Some of the proposed application fields of SAPC require a pH-neutral product, in particular in the biomedical, pharmaceutical, cosmetics, and food industries. Previous SAPC preparation processes were carried out in an aqueous alkaline solution. To improve the preparation technique, it is desirable to prepare SAPC using an alternative co-monomer system with a neutral pH value in the solution.

The polymerization system of AM and AANa solutions have been studied, respectively. In the experiments described below, the polymerization system which intercalated the co-monomer of AM and AANa into bentonite was studied. In the polymerization experiment, fixed compositions with 0.04% of MBAM and 0.04% of potassium persulfate were used. The experiment was carried out at room temperature. Before irradiation, the solution was purged with nitrogen gas to remove the oxygen dissolved in the solution. Irradiation was carried out with an UV lamp at a distance of 10 cm.

First, the polymerization of co-monomers of AM and AANa without bentonite was studied using UV irradiation. The experimental results evaluated in terms of the gelation time (gel formation time) are shown in Figure 16. It is evident that the gelation time is related to the composition of the solution. With increasing AM/AANa ratio, the gelation time increases, reaching a maximum of 47 minutes at a composition ratio of 75%, then decreases again. The WAC of SAPC of the experiment shown in Figure 17 displays almost the same curve shape as the gelation time.
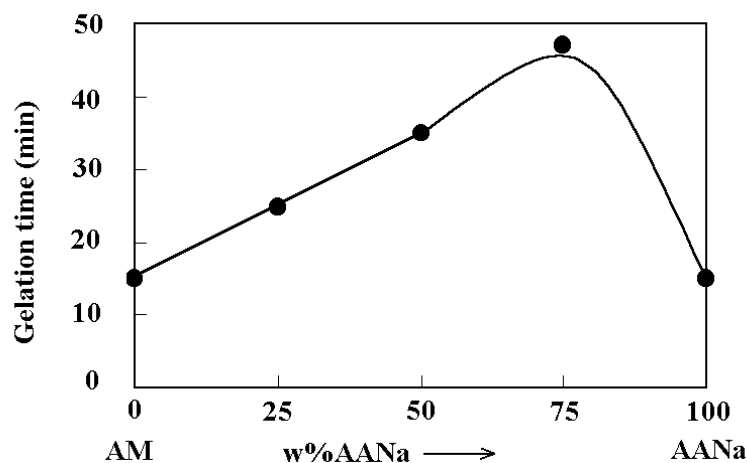
Figure 16. *Dependence of the gelation time on the AM/AANa ratio*

This suggests that a higher cross-linking density may be achieved during fast gelation that impeded the absorption of water.
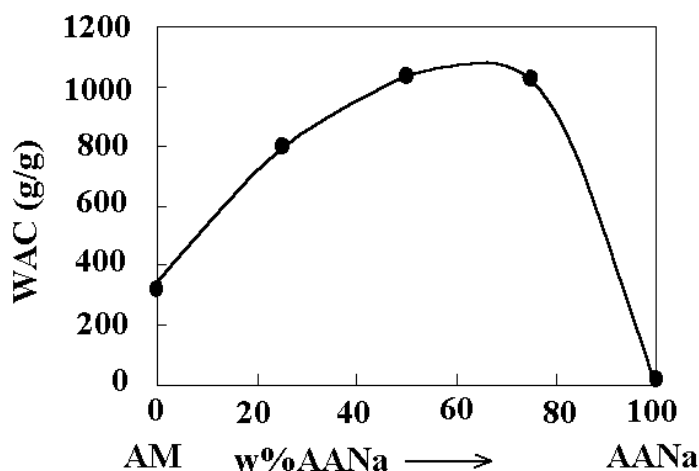

Figure 17. *Dependence of the water absorption capacity (WAC) on the AM/AANa ratio.*

Further studies were performed on the polymerization behavior of the AM/AANa/bentonite system. The concentrations of MBAM and potassium persulfate were fixed in this study at levels of 0.06% and 0.12%, respectively.

The stability of AM/AANa/bentonite solutions is shown qualitatively in Table 6. It was found that the bentonite separated from the AANa solution during the irradiation process. Though the mixture with a high AANa concentration was shaken several times to homogenize the solution during the polymerization it still separated. Moreover, the solution was very difficult to polymerize by UV irradiation.

This separation of bentonite from the AANa solution suggests that the intercalation of the AANa monomer into the bentonite layer space is inhibited due to the separation of the two components. In fact, although the water absorption capacity of the SAPC increased with increasing AM/AANa ratio (Figure 17), the highest ratio of AANa to AM in the co-monomers can not exceed 1:1 in the polymerization of AM/AANa/bentonite mixture solution.

Table 6. Stability of the AM/AANa/bentonite solutions

AM / AANa / Bentonite	Remarks
1 / 0 / 1	Homogenous
3 / 1 / 4	Homogenous
1 / 1 / 2	Slightly separated
1 / 3 / 4	Separated
0 / 1 / 1	Separated

Further experiments were carried out to clarify this point. The UV irradiation experiments were carried out after the samples were purged with nitrogen gas. The composition of the samples and the experimental results are shown in Table 7. The polymerization rates of the three samples investigated were different. Sample with high AM content polymerized first. There was a long induction period for the sample with low AM content. But, after the induction period, it polymerized very fast too. This showed that the polymerization of AANa was more difficult than that of AM.

Table 7. Preparation of AM/AANa /bentonite copolymer composite

AM/AANa/bentonite	MBAM (2%) ml	$K_2S_2O_8$ (4%) ml	Concentration (%)	Polymerization Speed
1 / 3 / 4	0.6	0.6	44	Slow
2 / 2 / 4	0.6	0.6	44	Medium
3 / 1 / 4	0.6	0.6	44	Fast

The water absorption capacity of the samples is shown in Figure 18. From Table 7 and Figure 18 it can be concluded that a high AM/AANa ratio produced samples has a fast polymerization rate but a low water absorption capacity (WAC). This is perhaps because all the polymerizations are carried out at a same condition. The addition of bentonite changed the polymerization reactivity. The system with high AM monomer content polymerized fast, after it polymerized, cross-linking occurred that reduced WAC of SAPC.
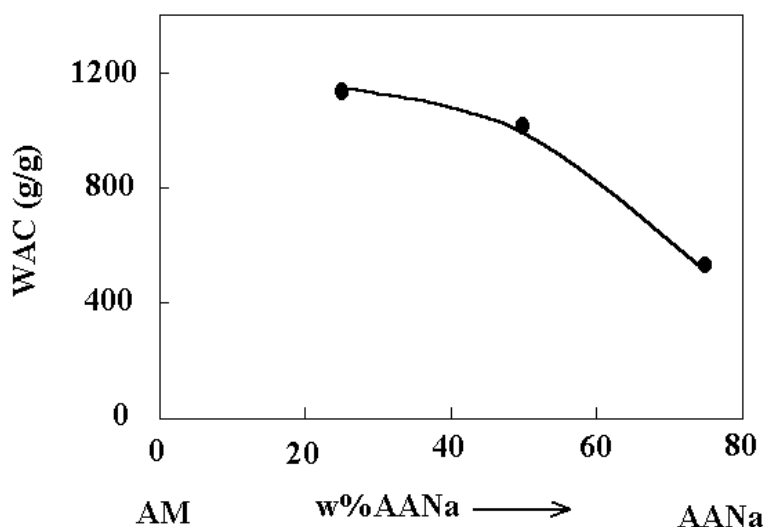
Figure 18. *Effect of the AM/AANa/bentonite ratio on the water absorption capacity (WAC) of SAPC*

Study of coating SAPC on the balance vessel

To measure the dynamic water absorption, SAPC was coated to the inner surface of a balance vessel to produce a thin membrane. The procedure was as follows.
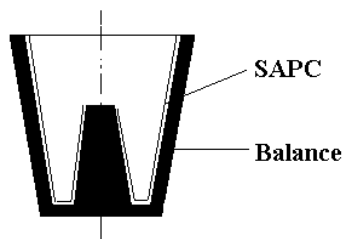

Figure 19. *Schematic illustration of the coating on the balance vessel*

Material with a composition of AM/AANa = 1:1, and MBAM and $K_2S_2O_8$ concentrations of 0.1% was used. Before coating the material onto the surface of the vessels, the solution was purged with nitrogen. Subsequently the solution was poured into the balance vessels, and poured out again to leave only a small amount of solution adhering to the surface. Then, the solution layer was polymerized with UV light to form a thin membrane. The thickness of the membranes was between 50 and 100 μm as calculated by taking the inner surface area of the balance vessel and the mass of SAPC used on the surface.

3.4   Measurement on the residual acrylamide in SAPC by GC

The residual AM in SAP products is an important factor that greatly limits its application. In this measurement, the unreacted AM was extracted from SAP by refluxing and filtration. The measurement was carried out in a 0.2% NaCl aqueous solution using a SP7100 Gas Chromatograph at the condition of thermal zone of injector of 220 °C, and detector of 280 °C. The carrier gas used was helium with a flow rate of 20 ml/min. Calibration of the measurement was carried out with a standard method.   The standard sample with 20 ppm acrylamide in 0.2% NaCl showed a small hump at the retention time for acrylamide. All samples showed no hump

or peaks in the gas chromatograph. This might indicate that the AM concentration in the samples was lower than the value of 20 ppm as shown in Table 8. The measurement showed that there was less than 4 mg/g of residual AM monomer in the SAPC. To make further measurements, the extract was concentrated by distillation for 8 and 28 times respectively. However, still no residual AM was detected. This means that the products can meet a wide range of requirement from the viewpoint of health in applications where the presence of monomer may cause a cytotoxic response.

Table 8 Analysis results of residual AM monomer in SAP

Sample	SAPC (g)	0.2% NaCl in water (g)	Reflux time (h)	Acrylamide in extract (ppm)	Acrylamide in gel (mg/g)
A	0.5004	101	3.5	<20	<4
A	0.4990	100	3.5	<20	<4
A	0.5021	100	3.5	<20	<4
B	0.4990	100	3.0	<20	<4
B	0.5000	100	3.0	<20	<4
B	0.5060	100	3.0	<20	<4
B*	0.5002	200	3.5	<20	<0.5
B**	0.5002	200	3.5	<20	<0.1

*Concentrated to 1/8, **concentrated to 1/28*

3.5 Radiation polymerization of vinyl monomers included in cyclodextrin

This section is to discuss the radiation induced polymerization process of p-styrenesulfonate in the presence of cyclodextrins using pulse radiolysis method since this might have a similar polymerization mechanism the results may shed some light on the polymerization of SAPC.
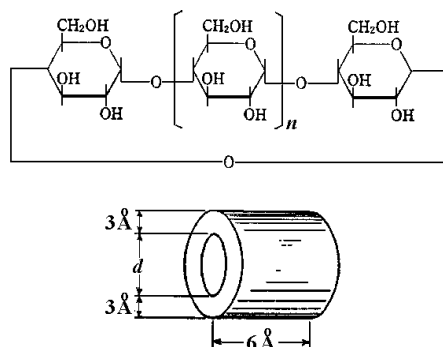
Figure 20. *Structure of cyclodextrins (from Takemoto, Inclusion Compound[46]). The diameter (d) of α, β, γ cyclodextrins is 4, 6 and 8Å, respectively.*

Unlike the sheet silicate montmorillonite, the cyclodextrins (CDs) are cylindrical compounds composed of glucose (Glc) units with hydrophobic cavities (see Figure 20) that form inclusion complexes with various organic molecules in aqueous solution[47,48]. The most common of them are α-, β- and γ-CDs consisting of six, seven and eight Glc units, respectively. The host-guest stoichiometry depends on the sizes of the CD cavities and that of the guest molecules. Inclusion complexes involving two guest molecules in a single cavity are well characterized for γ-CD, which has a large cavity compared with α- and β-CDs. The complexation of aromatic substrates by γ-CD promotes the formation of excimers[49,50,51,52,53]. It has also been reported that Diels-Alder reactions are accelerated by β-CD through hydrophobic binding of the reactants into the cavity, but not by α-CD, which has a smaller cavity[54,55]. In the experiment, the effect of the CD complexation of propagating radicals on the polymerization of sodium p-styrenesulfonate (SSNa) in aqueous solution was examined.

3.5.1 Experimental

The polymerization SSNa was initiated by γ-irradiation from a ^{60}Co source (dose rate, 500 Gy/h) without using conventional radical initiators in order to eliminate any additional effect due to the complexation of the initiators by CDs. The effects of α- and γ-CDs added to an aqueous solution of SSNa were examined under nitrogen at room temperature. Pulse radiolysis experiments were undertaken to investigate the effects of the CDs on the lifetime of the propagating radicals under the same conditions as the polymerization experiments. An L-band linear accelerator operating at 28 MeV and at a pulse width of 8 ns was used for the pulse radiolysis. Gel permeation chromatography of the polymers was performed on TSK-Gel 6000 PW$_{xL}$ and 3000 PW$_{xL}$ columns connected in series with a mixed water-acetonitrile solution (9:1 in volume) of 0.1 mol dm^{-3} NaNO$_3$ as an eluent at a flow rate of 1.0 cm^3/min. The molecular weights of the polymers were calculated by using a calibration curve based on sodium poly(p-styrenesulfonate) standards (Polymer Laboratories, Mn=5400-780 000). These experiments were carried out at the Institute of Scientific and Industrial Research, Osaka University, Japan.
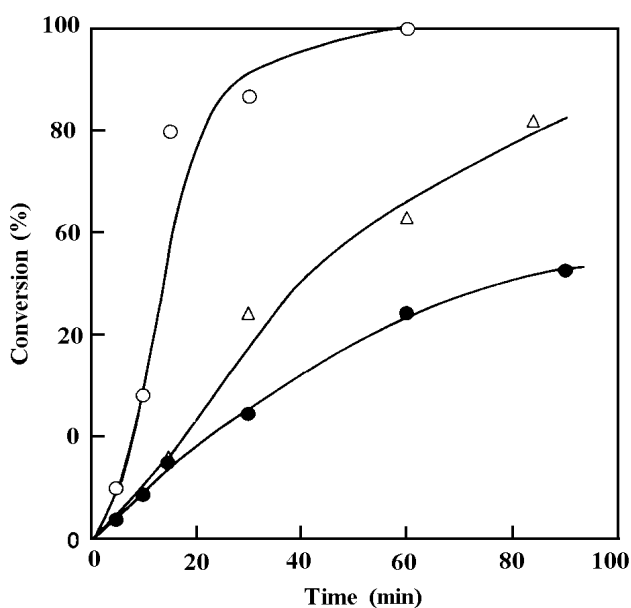
3.5.2 Results and discussions

Figure 21. *Time-conversion curves for the aqueous solutions of SSNa in the absence (Δ) and presence of α-CD (●) and γ-CD (O):[CD]/[SSNa], 1/2 (mol/mol).(Ref. 41)*

Figure 21 shows the time-conversion curves for the polymerization in the absence and presence of the CDs. The conversions were determined by measuring the 255 nm absorption related to the monomer. The decrease in this absorption, caused by the irradiation, was accompanied by an increase in the 225 nm absorption due to the polymer. The polymerization was accelerated by γ-CD and retarded by α-CD. The G values for monomer consumption at an irradiation time of 15 min were 2.4×10^2 and 1.2×10^5 for the CD-free and γ-CD-added solutions, respectively; the G value represents the number of the consumed monomer molecules per 100 eV energy absorbed by the medium. Figure 22 shows the dependence of the degree of conversion on the CD concentration. For the γ-CD system, appreciable acceleration is attained at [CD]/[SSNa] of 1/2 (mol/mol). This might be attributed to the contribution of a 1:2 γ-CD-SSNa complex.
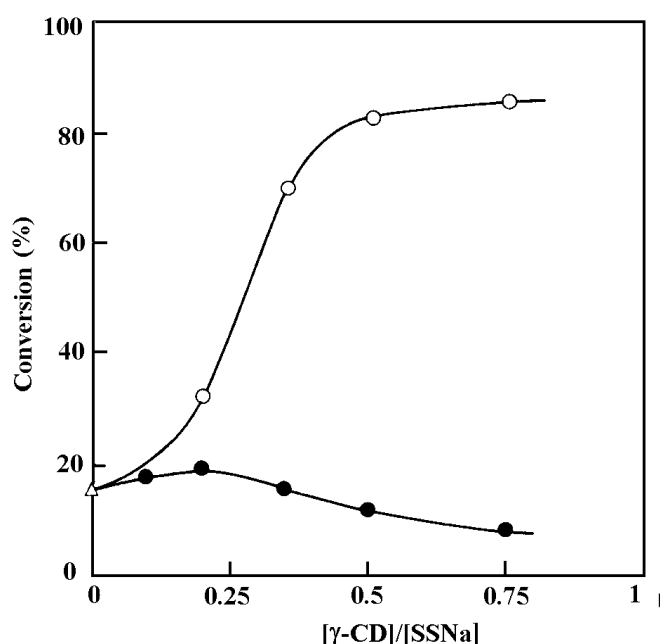

Figure 22. *Dependence of the conversion on the concentration of α-CD (●) and γ-CD (O) at an irradiation time of 15 min.(Ref. 41)*

It is known that the propagating radicals of styrene derivatives have an absorption band at around 320 nm[56]. Figure 23 shows the decay curves of the 320 nm absorption observed by pulse radiolysis of the CD-free and CD-added solutions. The decay of the propagating radicals become slow in the presence of the CDs. This indicates that the propagating chain ends are included in the CD cavities and hence are not accessible anymore. The retarding effect is more significant with γ-CD than with α-CD. The yield of the propagating radicals is slightly decreased by the addition of the CDs. The initiating species produced in the irradiated aqueous solutions are H atoms and OH radicals; G values are 0.6 and 2.95, respectively[57]. It is natural to consider that a fraction of the initiating species reacts with the CDs to give the less reactive CD radicals, α-hydroxyalkyl type radicals, through hydrogen abstraction. The binding of the hydrophobic vinyl groups of the monomer molecules is also considered to be responsible for the decrease of the yield of the propagating radicals.
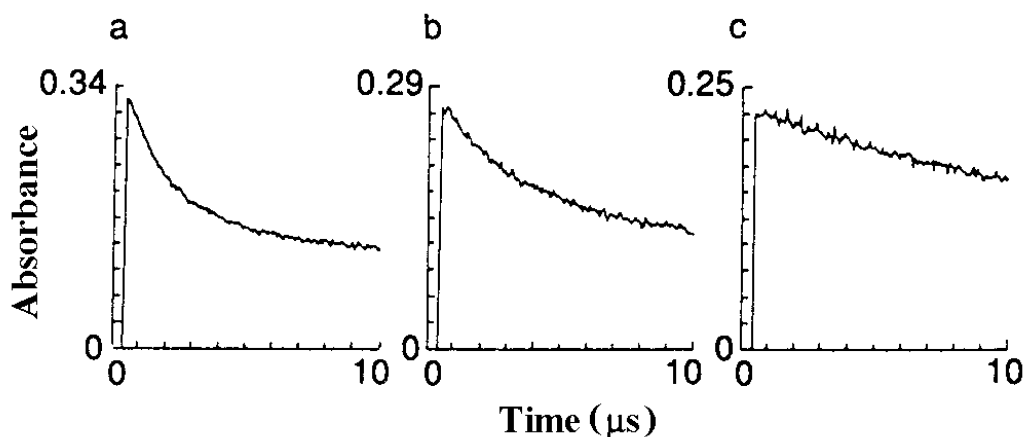
Figure 23. *Decay of the 320 nm absorption due to propagating radicals in the absence (a) and presence of α-CD (b) and γ-CD (c): [CD/[SSNa], 1/2 (mol/mol).(Ref.41)*

The results obtained in this study can be interpreted in terms of the binding of the propagating chain ends of the polymers within the CD cavities as follows. For the α-CD complex, the propagation reaction as well as the bimolecular termination reactions is inhibited because of the small size of the CD cavity. On the other hand, in the larger γ-CD cavity, the propagation reaction is not inhibited because of the binding of both the propagating chain end and the vinyl group of the monomer molecule. The hydrophobic effect accelerates the propagation reaction as reported for the Diels-Alder reactions. The bimolecular termination reaction is inhibited by the binding of the propagating chain ends in the CD cavities. The inhibition of the termination reaction enhances the polymerization in the γ-CD system as well as the hydrophobic effect.

The decay of the propagating radical was visibly more retarded by γ-CD than by α-CD (Figure 23). At a [CD]/[SSNa] ratio of 1/2, both complexed and dissociated radicals are formed and contribute to the recombination reaction in the α-CD system. However, if the formation of the 1:2 γ-CD-SSNa complex is favored, the termination reaction occurs between the complexed radicals in the γ-CD system. This might explain the difference between the α- and γ-CD systems.
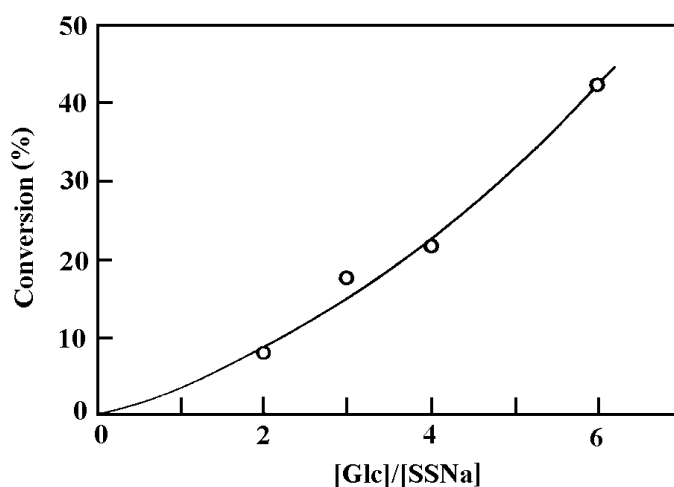

Figure 24. *Dependence of the polymer yield on Glc concentration at an irradiation time of 15 min at 0 ⁰C: [SSNa]=0.25 mol dm⁻³.(Ref. 42)*

The polymerization was also accelerated by Glc, but the effect was much smaller than that of γ-CD when compared at the same concentrations (Figure 24). In contrast with γ-CD, no saturation is observed in the concentration dependence up to a value of [Glc]/[*SSNa*]=6 examined. An aggregation of the hydrophobic styryl groups in the presence of Glc may be responsible for the acceleration of the polymerization.
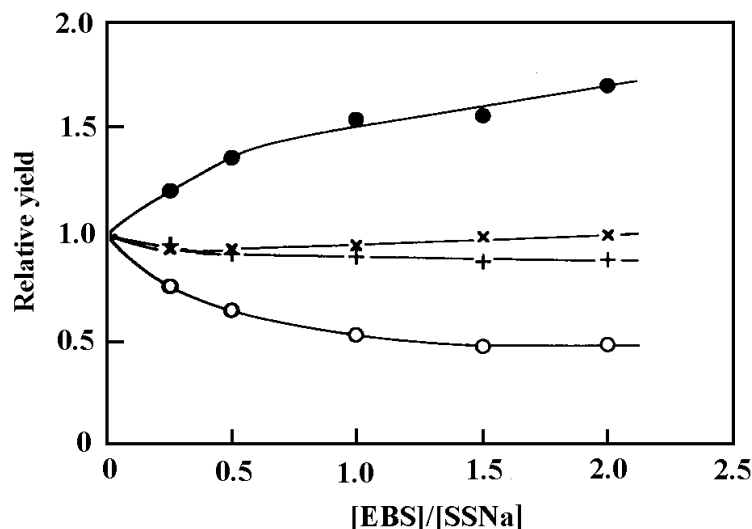

Figure 25. *Polymer yields relative to those in the absence of EBS plotted against [EBS]/[SSNa] for the SSNa (0.25 mol dm^{-3}) solutions at 0 ^{o}C. Additive and irradiation times:(o) γ-CD (0.125 mol dm^{-3}) 15 min; (●) α-CD (0.125 mol dm^{-3}) 15 min; (+) Glc (1.0 mol dm^{-3}) 30 min; (×) none. 60 min. (Ref. 42)*

Figure 25 shows the changes in polymer yield caused by the addition of sodium *p*-ethylbenzenesulfonate (EBS) to the solutions containing α- and γ-CDs, and Glc. The polymer yield in the presence of γ-CD is decreased by EBS. This can be attributed to the complexation of EBS competing with that of SSNa. On the other hand, the polymer yield in the presence of α-CD is increased by EBS, demonstrating that the inhibition of the polymerization by α-CD is also due to the CD complexation. As expected, the polymer yield for the solution containing Glc is hardly affected by EBS, and nor is that for the pure SSNa solution. Similar result were obtained with sodium benzenesulfonate in solutions containing γ-CD and Glc; for the solution containing α-CD the effect of benzenesulfonate could not be examined because of the deposition of the inclusion complex. For the solution containing γ-CD the relative polymer yields at [EBS]/[SSNa] above 1.5 are almost constant at about 0.5, although at an irradiation time of 15 min no polymer is obtained in the pure SSNa solution. This means that the acceleration of the polymerization in the presence of γ-CD is not only due to the 1:2 complexation but also due to some additional effect not disturbed by EBS. A hydrophobic aggregation similar to the case of Glc may be responsible for the accelerating effect of γ-CD. An aggregation of the 1:2 complexes is suggested by the molecular weight distributions of the polymers as described below.
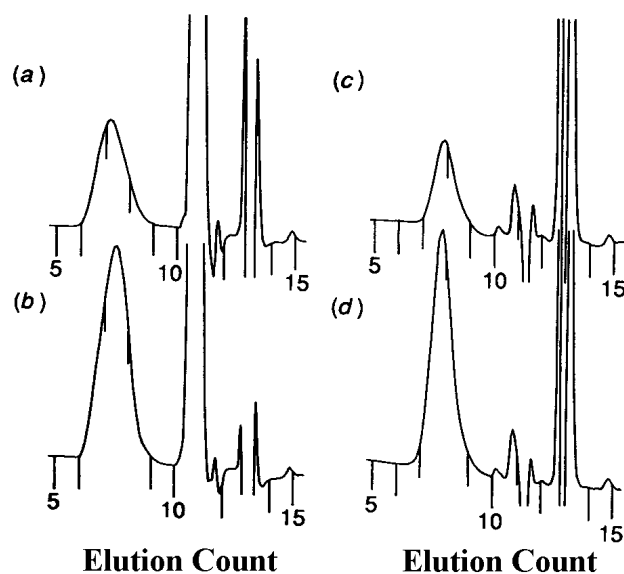
Figure 26.   *Gel permeation chromatograms for (a) the SSNa (0.25 mol dm⁻³)* *solution (0.25 mol dm⁻³ 6 min; (b)* **γ**-CD (0-.125 mol dm⁻³) 15 min; (c) none, 30* *min (d) none 60 min. (Ref. 42)*

Figure 26 shows the gel permeation chromatograms for the solutions irradiated in the absence and presence of γ-CD ([γ-CD]/[SSNa] =0.5); the solutions were submitted to chromatography after dilution with a ten-fold volume of the eluent solution.

Table 9.   Effects of CDs and Glc on the molecular weights of polymers obtained at 0 °C

Additive (mol/dm³)	Irradiation time/min	Conversion (%)	M_n	M_w/M_n
none	30	19	4.4×10^4	2.5
none	60	41	4.1×10^4	3.1
none	120	82	4.2×10^4	2.8
γ-CD(0.125)	6	31	1.3×10^5	4.0
γ-CD(0.125)	12	62	2.1×10^5	4.1
γ-CD(0.125)	30	87	5.3×10^4	3.8
α-CD(0.125)	60	28	2.6×10^4	2.6
α-CD(0.125)	120	49	2.4×10^4	2.4
Glc(1.0)	15	18	1.0×10^5	3.0
Glc(1.0)	30	45	1.1×10^5	2.9
Glc(1.0)	60	73	1.0×10^5	2.7

M_n= number-average molecular weight, M_w = weight-average molecular weight, M_w/M_n= polydispersity index.

The peaks at elution counts of 7-8 are assigned to the polymers and those at around 11

and 14, superposed with impurity peaks (ghost peaks), are assigned to γ-CD and the monomer, respectively. It can be seen that higher molecular weight polymers are produced in the presence of γ-CD. The values of M_n and M_w/M_n are listed in Table 9 together with those for the solutions containing α-CD and Glc. The M_n value of the polymer produced in the presence of γ-CD decrease with irradiation time, whereas those for the other systems are independent of irradiation time. The M_w/M_n ratios for the γ-CD system are also larger than those for the other systems. The M_n value increases in the presence of Glc, whereas it decreases in the presence of α-CD.
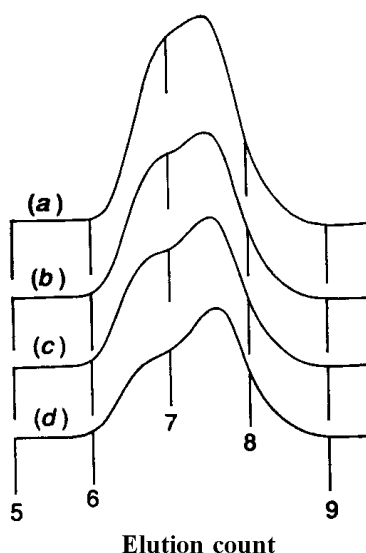

Figure 27. *Molecular weight distributions of the polymer produced in the SSNa (0.25 mol dm-3) solutions containing γ-CD at an irradiation time of 15 min at 0 °C: [γ-CD]/[SSNa]; (a) 0.30. (b) 0.25, (c) 0.20. (d) 0.15. (Ref.42)*

Figure 27 shows the molecular weight distribution curves of the polymers obtained at [γ-CD]/[SSNa] =0.15-0.30. They are clearly bimodal indicating a contribution of propagating species having different reactivities to the polymerization. The relative height of the higher molecular weight peak increases with increasing γ-CD concentration. Thus, the higher molecular weight peak is assigned to a product of the complexed propagating radicals, and the lower one to a product of the dissociated propagating radicals. The independent propagation of the complexed and dissociated radicals can be explained by assuming an aggregation of the 1:2 complexes of SSNa with γ-CD. This is to say, the 1:2 complexes and the dissociated SSNa polymerize separately through aggregation at these γ-CD concentrations.

The radiation chemical yields (G values) of the initiating species are 0.6 and 2.7 for H and OH, respectively[58]. The G values for polymers, G(polymer), were calculated from the G values for the monomer consumption and the Mn values. The G(polymer) values in the presence of γ-CD were in the range 24-33. The number of polymer molecules per initiating radical, G(polymer)/G(radical), is 7.3-10. This corresponds to the minimum yield since all of H and OH could not initiate the polymerization in the presence of γ-CD which reduces the yield of the propagating radicals as shown by the pulse radiolysis experiments. The large G(polymer)/G(radical) values suggest that a chain transfer to the monomer occurs, and that the molecular weights of the polymers depend mainly on the competition between the propagation and the chain transfer to the monomer, but are hardly affected by the termination. This means

that the formation of the higher molecular weight polymers is attributed to an acceleration of the propagation and/or a deceleration of the chain transfer to the monomer in the presence of γ-CD. The chain transfer to γ-CD may also occur but should not be important since the M_n value increases in the presence of γ-CD.

It is interesting that the propagating radical is included in the γ-CD cavity resulting in the change in reactivity. The propagation is the addition of the α-carbon of the propagating radical to the β-carbon of the monomer, whereas the chain transfer is the H-transfer from the β-carbon of the propagating radical to the β-carbon of the monomer. Therefore, higher molecular weight polymers are produced if the α-carbon of one of the monomers in the 1:2 complex is close to the β-carbon of another monomer and the β-carbons are separated from each other in the γ-CD cavity. Thus, a possible explanation of the formation of the higher molecular weight polymers is the configuration of the monomers in the γ-CD cavity of the 1:2 complex. The decrease in the M_n value with irradiation time, occurring only in the presence of γ-CD, may be due to the 1:1 complexation, which becomes important as the monomer concentration decreases during polymerization.

For the solution containing α-CD the G(polymer)/G(radical) value is about 3.1. In this case, the Mn value seems to depend on the competition between the propagation and the termination as well as on the competition between the propagation and the chain transfer. Thus, the suppression of the propagation by the complexation of the monomer with α-CD may result in the decrease in the Mn value. Similarly, in the presence of Glc, the (polymer)/(radical) value is less than 2.5, and the increase in the Mn value may be attributed to the promotion of the propagation by the hydrophobic aggregation.

3.5.3   Conclusions

The radiation-induced radical polymerization of SSNa is accelerated in the presence of γ-CD. The contribution of the inclusion complexes is demonstrated by the effect of EBS. The dependence of the polymer yield on γ-CD concentration suggests a 1:2 host-guest complexation. The aggregation of the 1:2 complexes is proposed to account for the independent propagations of the complexed and dissociated radicals resulting in the bimodal molecular weight distributions of the polymers obtained at [γ-CD]/[SSNa] = 0.15-0.30. The accelerating effect of Glc is also interpreted in terms of the hydrophobic aggregation. The formation of the higher molecular weight polymers in the presence of γ-CD may be attributed to the configuration of SSNa in the 1:2 complexes.

From the polymerization mechanism of CD/SSNa inclusion complex, it can be inferred that the polymerization of SAPC will first occur in monomers outside the interspace of montmorillonite because the high concentration of radicals generated in the water solution during the irradiation of electron beam.   However, in the interlayer of montmorillonite, there are still radicals generated by the high energy e-beam due to their high penetration capacity, that will induce the polymerization of AM inside the layers.   This is why high-energy irradiation is superior the chemical initiation method although it can be induced by heat and other techniques.

The process of ionizing-radiation induced polymerization in the preparation of SAPC using AM (AANa) and bentonite just as the polymerization of SSNa accelerated by the γ-CD and inhabited by the α-CD.   It has obvious advantage over the general chemical method. In the latter, to initiate the polymerization on AM intercalated in the montmorillonite, a problem is intercalating the initiator into the base material.   From a point of view of the initiation process the radiation method is obviously superior over the chemical one.

4.0   STRUCTURAL CHARACTERIZATION OF SAPCs

Equipment and methodology

(i) The FTIR spectra were acquired with a Nicolet 510 FTIR spectrometer.

(ii) A Bruker MSL 300 Nuclear Magnetic Resonance Spectrometer was used for ^{13}C, ^{27}Al and ^{29}Si NMR analyses.

(iii) X-ray diffraction (XRD) analyses were performed with a Rigaku Ru-200B automated powder diffractometer using a horizontal goniometer equipped with a graphite crystal monochromator and a rotating copper anode operated at 40kV, 80 mA and a scanning speed of 2 degrees/min. The samples were mounted on glass slides using an acetone suspension.

(iv) The scanning electron microscope (SEM) was a Hitachi X-650, equipped with both energy dispersive (EDS, 30 mm^3 Si(Li) detector; TN5402) and wavelength dispersive spectrometers (Western Research Centre, Canada Mineral and Energy Technology). The EDS on the Hitachi X-650 SEM has a thin window which allows for the detection of carbon and oxygen in the samples.   The Hitachi X-650 SEM was also equipped with a DN302 cold stage for the examination of fast frozen samples.   The fast freezing of bentonite-water samples maintains the morphology or the relationship between various components. By keeping the sample frozen on a cold stage in the electron microscope, it was possible to image the bentonite and also to get compositional information from the X-rays emitted as the electron beam strikes the sample. In order to better reveal the structure of the samples with various components, the temperature of the cold stage in the electron microscope was maintained at ca. 90 K by an Oxford ITC4 nitrogen heat exchanger and temperature-controller unit to dry the material by sublimation away the water.   The analysis process was that each sample was placed onto a Cu stub and immersed in nitrogen slush. While frozen, the sample was fractured under vacuum inside the Emscope SP2000 and subsequently transferred into the SEM chamber for observation. Secondary electron images of the samples were acquired at 25 kV and stored in the Tracer Northern TN8502 image analysis system. To investigate water-swollen samples, a JEOL JSM-5300 LV "environmental" microscope was used at 1 Torr water pressure made available by Souquelec Ltee, Montreal, Quebec, Canada.

(v) Differential scanning calorimetry data were obtained with a Perkin-Elmer DSC-4 with TADS controller at a heating rate of 10^oC/min to a maximum temperature of 400^oC, and thermogravimetric analyses were done using a TGA-951 with a Dupont 910 DSC Data Station 1090.

4.1   FTIR spectra analysis

Figure 28 shows spectra of sample A (a copolymer of AM and AANa without bentonite with a composition of AM:AANa = 1:1); sample B (a composite material prepared from AM and bentonite with a composition of 1:1); sample C (prepared using co-monomers of AM, AANa and bentonite with a weight ratio of AM/AANa/bentonite = 1:3:4); and sample D (a composite material prepared from co-monomers of AM, AANa and bentonite as in sample C but with different composition of AM/AANa/bentonite = 1:1:2).   Figure 29 shows the FTIR spectrum of the original Ca-montmorillonite.
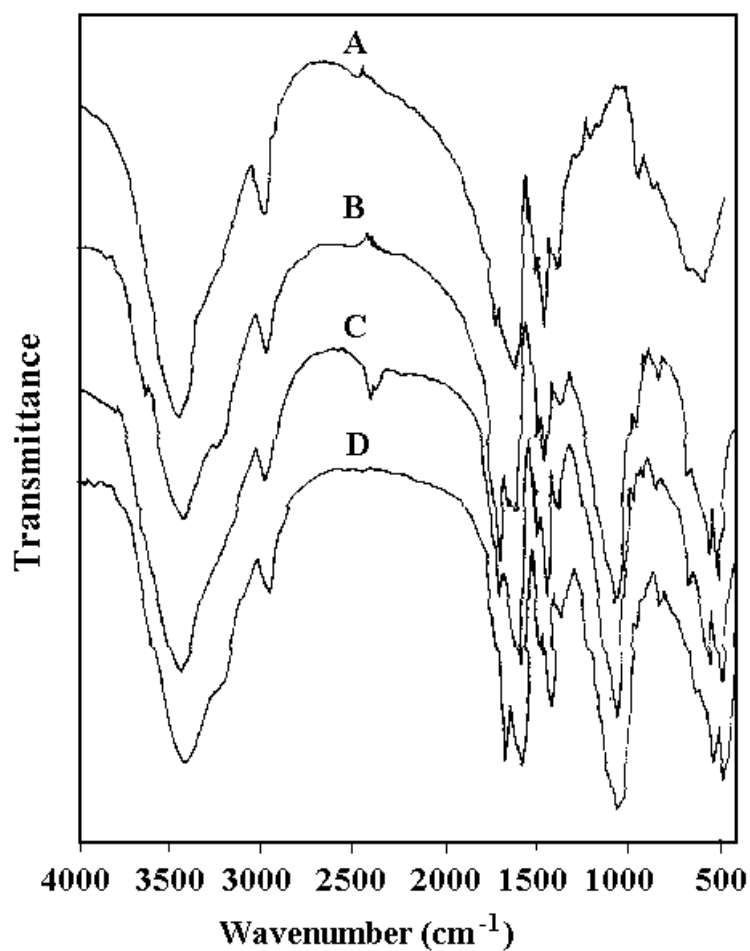
Figure 28. FTIR spectra of SAPC of A: AM/AANa (1:1) copolymer; B: AM/bentonite (1:1) composite; C: AM/AANa/bentonite (1:3:4) composite; D: AM/AANa/bentonite (1:1:2)
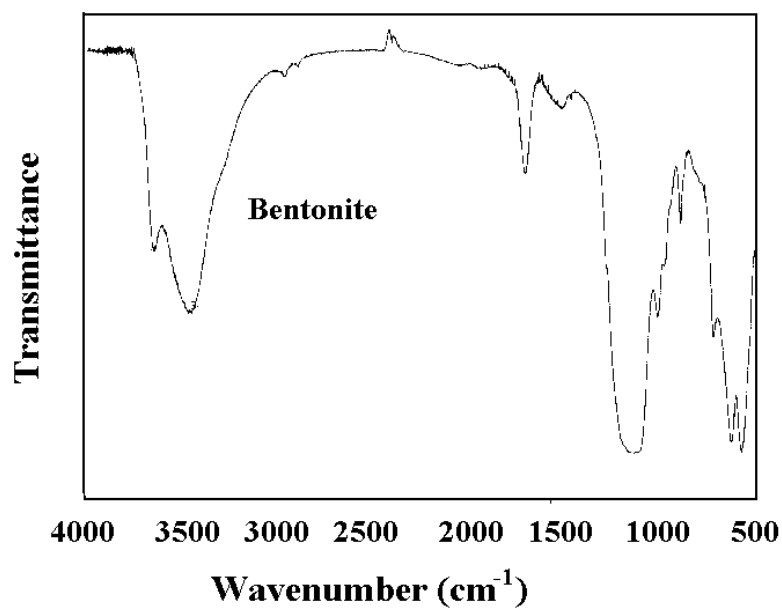

Figure 29. FTIR spectra of the original bentonite (Ca-montmorillonite).

The IR peaks in the spectra and their assignment for the composite materials, copolymer and bentonite are shown in Table 10. From the FTIR spectra in Figure 28 and 29, and Table 10 it can be concluded that the characteristic peaks of the composite were mainly a superposition of the peaks from both AM/AANa and bentonite materials. There were only small differences in the peaks positions caused by the intercalation of monomers into the bentonite.

Table 10. Assignment of FTIR bands of AM/bentonite, AM/AANa/bentonite composite, AM/AANa copolymer and pure bentonite.

AM/bentonite (cm^{-1})	AM/AANa/ bentonite(cm^{-1})	AM/AANa (cm^{-1})	Bentonite (cm^{-1})	Assignment
3632m	3605vw	3616vw	3637m	ν(OH)
3404vs	3420vs	3435vs	3451vs	ν(OH)
3192vw	3182vw			ν(NH)
2938s	2938s	2938s	2923w	ν(CH)
1667vs	1679vs	1674s	1622s	ν(C=O)
1571vs	1568vs	1565vs		ν(C=O)
1454m	1454m	1452m	1436m	δ(NH)
1408s	1408s	1404s		δ(NH)
1322s	1322s	1323s		δ(CH)
		1182w		δ(NH$_2$)
		1120w		δ(NH)
1047vs	1049vs	1047w	1049vs	(Si-O)
917m	919m		918m	(Al-OH)
845m	856w	856m		γ(CH)
799m	804m		799s	(Si-O-Al)
		788m		
625m	623w	624w	623m	(Si-O-Al)
523s	529s		535s	(Al-O-Si)
		519s		
467vs	473vs		473vs	(Si-O-Fe)

vs: very strong, s: strong, m: middle, w: weak, vw: very weak.

Figures 30 and 31 show FTIR spectra of dry SAPC and SAPC with 95% absorbed water (Figure 30) as well as dry SAP and SAP with 95% absorbed water (Figure 31). In both spectra, the peaks of the organic components become smaller with increasing water content, while the ratio of the peaks related to water and the peaks at 1675 cm^{-1} increases remarkably.

The FTIR peaks and their possible assignment show that with increasing water content, only the water peaks at positions of ca. 3400, 1600 and 1400 cm^{-1} remain.
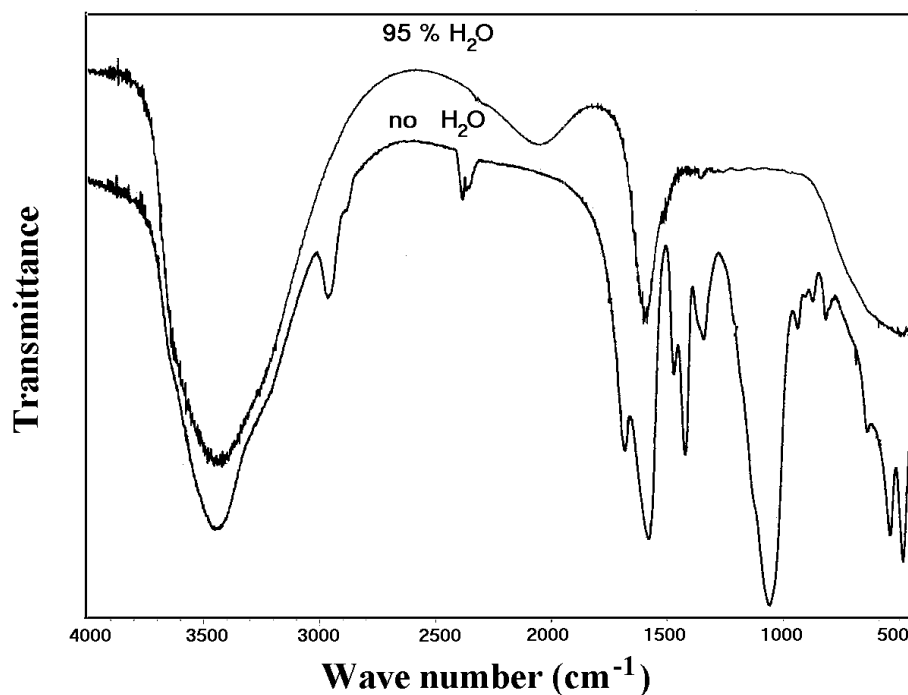
Figure 30. *FTIR spectra of SAPC (sample C) with different water contents*
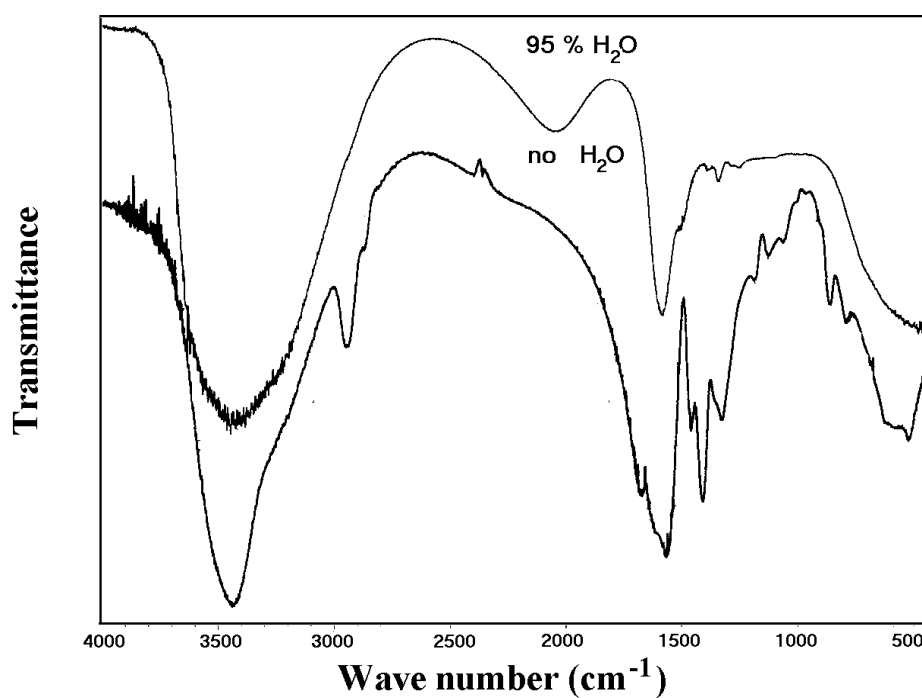
Figure 31*. FTIR spectra of SAP (sample A) without bentonite with different water contents*

4.2   NMR (^{13}C, ^{27}Al and ^{29}Si) analysis

NMR (^{13}C, ^{27}Al and ^{29}Si) analyses were carried out on the same set of samples.   A

commercial product (Cabloc CTF, Fa Stockhausen) was used for comparison. The ^{13}C NMR analyses results are shown in Table 11 and Figure 32.

Table 11. ^{13}C NMR analysis results

	A	B	C	D	Commercial product
AM/AANa	1/1	1/0	1/3	1/1	0/1
Polym./bentonite	1/0	1/1	1/1	1/1	1/0
CS_{Peak1} (ppm)	43.6	41.7	44.6	42.7	43.0
CS_{Peak2} (ppm)	184.7	180.8	184.7	182.7	185.1
H_1/H_2	1.99	1.79	1.45	1.6	1.89

CS: Chemical shift; H: peak height (the peak height of H2 contains the side bands around 190 ppm).

The ^{13}C NMR peak centered around 40 ppm is related to the carbon of the methylene (-CH_2-) and the methyne (-CH-) groups, and another large peak at about 180 ppm indicates the carboxyl groups (-COONa) and (-$CONH_2$). Two smaller peaks next to the second peak are spinning sidebands. The ^{13}C NMR spectra showed that the basic shape of the peaks of different samples were the same, but the positions and the widths of the peaks at 40 and 180 ppm varied from sample to sample that were prepared in slightly different ways. The spectrum of AM/bentonite had the lowest chemical shift of 41.7 and 180.8 ppm, whereas in spectrum with the addition of AANa, the peaks shifted to higher values. For AM/AANa=1:1, the value were 42.7 and 182.8 ppm, and with AM/AANa=1:3 were 44.6 and 184.7 ppm, respectively. The commercial product has a chemical shift of 43.0 and 185.1, and the sample with AM/AANa=1:3 but without bentonite has 43.6 and 184.7 ppm, both of them were higher than that of the AM/bentonite composite. This may be caused by any of the following: different degrees of crystallinity among polymers; different degrees of polymerization and cross-linking density; differences in the degree of association of the amide groups with surrounding cations, in particular the strength of the hydrogen bonded with the oxygen in the silicate sheet of the montmorillonite and; lastly, different amounts of carboxyl groups formed by the hydrolysis of amide groups and the original materials.

However, since these spectra do not include any information on the chemical changes of the carbon environment, it might be concluded that there was no chemical change (bonding) on C.
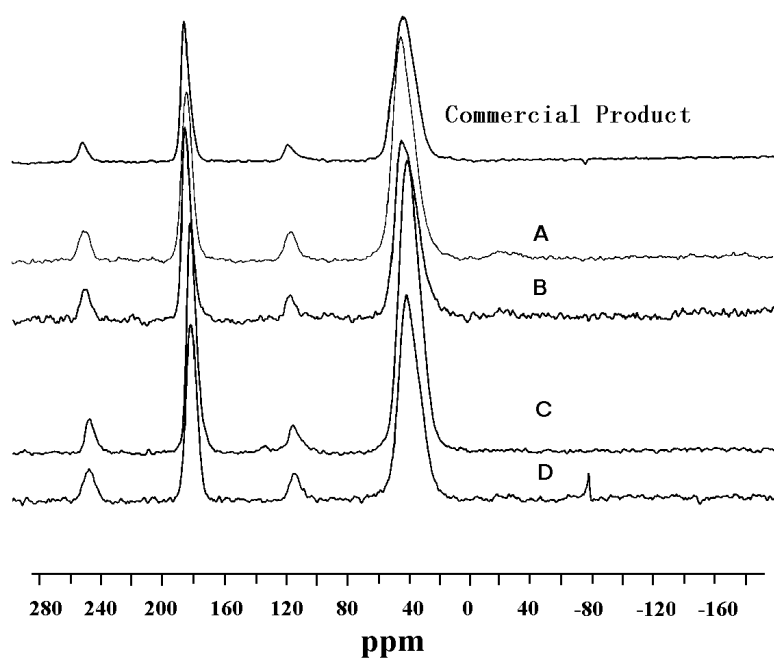
Figure 32. *75.47 MHz ^{13}C NMR spectra of A: AM/AANa (1:1) copolymer; B: AM/bentonite (1:1) composite; C: AM/AANa/bentonite (1:3:4) composite; D: AM/AANa/bentonite (1:1:2) and commercial product*

Figure 33 shows the ^{27}Al NMR spectra of SAPC samples measured at γ_{rot} = 15000 Hz (rotation frequency), $D\Phi$ = 0.5 s (time between scans), D5 = 5 ms (pulse length), BF1 = 78.205 MHz (basic frequency of transmitter) and NS = 5000 (number of scans).
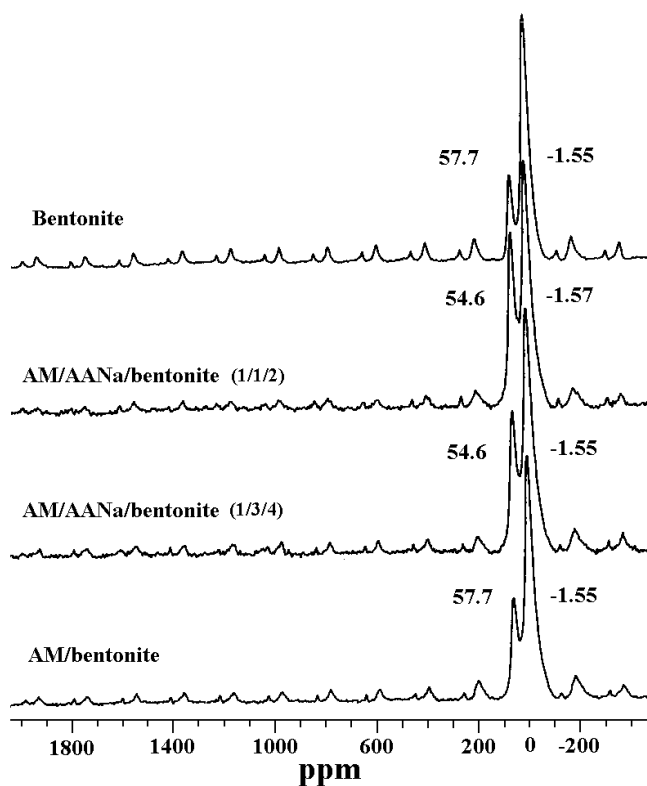
Figure 33. *^{27}Al NMR spectra of SAPC samples (γ_{rot} = 5000 Hz, BF1 = 59.6 MHz, $D\Phi$ = 2 s and NS = 1352). The chemical shifts were not corrected for second order quadrupol interaction.*

In the [27]Al spectra, the peaks at -1.55 and about 54.6 ppm were assigned to Al^{VI} (octahedral Al) and Al^{IV} (tetrahedral Al), respectively. The chemical shifts of peak 1 and peak 2 as well as their shapes in the spectra of the AM/bentonite and pure bentonite samples were identical. However, the peaks in the spectra of AM/AANa/bentonite were different. In the spectrum of AM/AANa/bentonite = 1:3:4, the peak 1 was the same as for pure bentonite, but peak 2 shifted from 57.7 to 54.6 ppm. In the AM/AANa/bentonite = 1:1:2, peak 1 and peak 2 both were shifted. Differences can also be seen in the peak heights. The relative height of peak 2 in the AM/AANa/bentonite spectrum is obviously greater than in the pure bentonite and AM/bentonite samples. This means that the relative proportion of Al^{VI} and Al^{IV} coordination had changed.   Generally, the radius (R) of Al in the structure of layered silicate is different, depending on the position it occupies.   Their values usually are $R_{Al(IV)}$=0.047 nm, $R_{Al(VI)}$ =0.061 nm, $R_{O(IV)}$=0.13nm and $R_{O(VI)}$ =0.132nm[59].   The radius ratio of aluminum and oxygen $R_{Al(IV)}/R_{O(IV)}$ is 0.047/0.13=0.361, which is in the range of the tetrahedral of 0.225-0.414, hence Al(IV) can occurs in tetrahedral coordination.   The radius ratio of $R_{Al(VI)}/R_{O(VI)}$ is 0.061/0.132=0.452, which is between the values of 0.414-0.7322, therefore it is suitable to occur in octahedral coordination. The different peak heights in these materials suggests the ratio of Al^{IV}/Al^{VI} being different and therefore a structural difference exists.
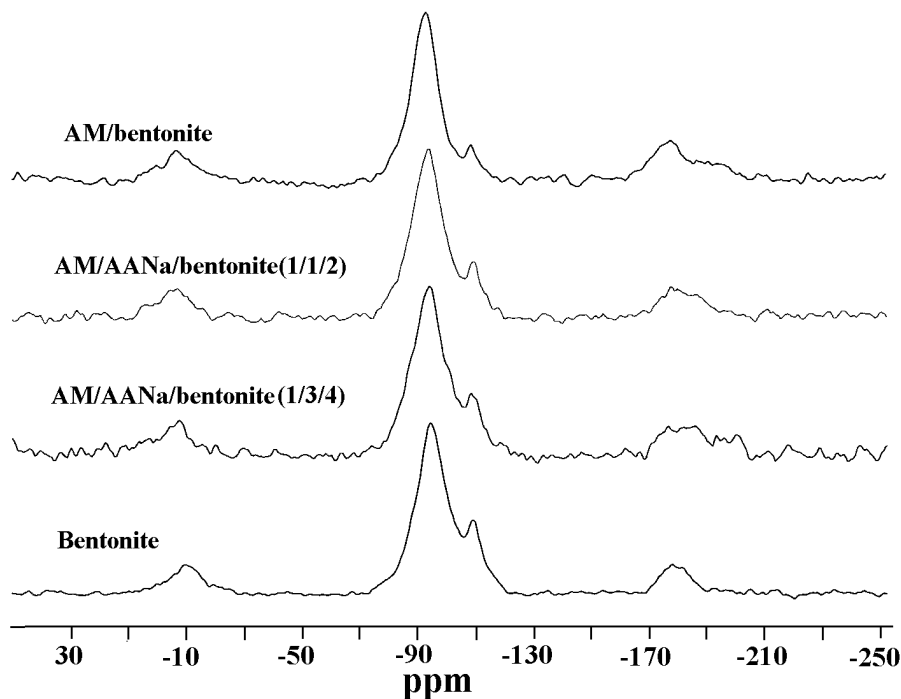
Figure 34.   *^{29}Si NMR spectra of SAPC (γ_{rot} = 5000 Hz, BF1 = 59.6 MHz, DΦ = 2 s and NS = 1352).*

Figure 34 shows the ^{29}Si NMR spectra of SAPC samples measured at γ_{rot} = 5000 Hz, BF1 = 59.6 MHz, DΦ = 2 s and NS = 1352.   In the figure, the peaks of [29]Si at about -110 ppm can be assigned to Q^4 (quaternary silicon oxygen bridges) groups, and those at about -94 ppm to Q^3 (tertiary silicon oxygen bridges) groups.   The peak positions of the different samples are the same and there is only a small difference between them.   The broadened peaks of the samples may be due to paramagnetic effects probably associated with Fe impurities in the samples**.**   However, it cannot be excluded that because of the Al(IV) content Q^3(1Al) group also occur.

These findings together with the result of the FTIR analyses mean that there is no major chemical change of the polymer chain associated with the intercalation. The interaction between bentonite and polymer was not related to bonding involving the carbon atoms. This is a further confirmation that van der Waals forces and hydrogen bonds are the cause of coordination complexes with interlayer cations and thus constitute the predominant means of attaching the poly(acrylamide) to the montmorillonite crystal lattice as outlined below (see p.52).

4.3   XRD Analysis

X-ray diffraction analyses were carried out according to the standard method (Cu-Kα). Results are shown in Figure 34.
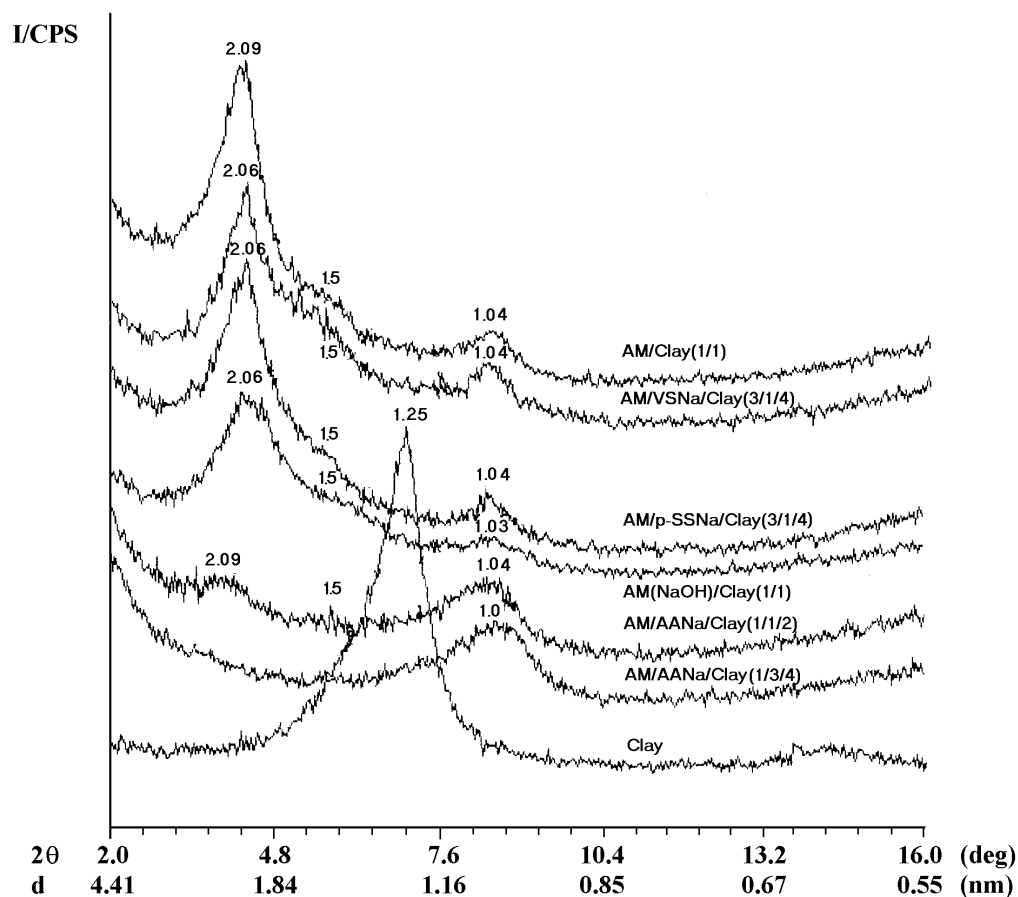
Figure 35.   *XRD pattern (CuKα) of bentonite (A) and SAPCs with different compositions*

In the XRD analyses, the same sample series as for the FTIR and NMR investigations were used. Comparing the XRD pattern of these samples (Figure 35), it can be concluded that the interplanar spacing (001) of SAPC products were changed by the intercalation.   Samples with different compositions showed different XRD pattern.   In the spectrum of the AM/bentonite composite, the largest interplanar spacing was 2.09 nm. This spacing enlargement was due to the intercalation of AM into the bentonite interlayer space in accordance with previous results[9,10] (see Gao, D.: Preparation and Property Improvement of a Superabsorbent Polymer Composite- A final report on the joint research activities at ARC, 1993; and Gao, D. and Heimann, R.B. in Polymer Gels and Networks 1993, 1, 225-246). At about 1.05 nm, there remained a peak tentatively assigned to the (002) spacing of bentonite.

Table 12. Summary of XRD peak positions

	Peaks position (nm)		
Bentonite(Ca-montmorillonite)	1.25	1.5	
AM/AANa/Bentonite=1/3/4	1.0		
AM/AANa/Bentonite=1/1/2	1.04		2.09
AM/Bentonite(NaOH)=1/1	1.03	1.5	2.06
AM/SSNa/bentonite=3/1/4	1.04	1.5	2.06
AM/VSNa/Bentonite=3/1/4	1.04	1.5	2.06
AM/Bentonite=1/1	1.04	1.5	2.09

Table 12 summarizes the XRD analysis results showing the changes in XRD peak positions. SAPC composed of sodium vinylsulfonate (VSNa) and sodium styrenesulfonate (SSNa) showed that the intercalation could also take place in the co-polymerization systems (AM/VSNa/bentonite, AM/SSNa/bentonite). The intercalation increased the basal spacing from 1.25 to 2.09 nm (Fig.35). But, the addition of sodium acrylate had a different effect on the XRD curves. The peak at 1.5 nm (Ca-montmorillonite) disappeared and with the addition of AANa over a ratio of AANa/AM = 3/1, the peak at 2.09 nm disappeared too. This was due to the replacement of Ca with Na, and the spacing, too large to be measured with the normal XRD equipment, might be caused by the collapse of the bentonite structure.

The value of the (001) interplanar spacing changed from 1.25 nm (hydrated complex with Na^+ as exchangeable interlayer cation) to 2.09 nm which indicates that the polymer was intercalated into the bentonite. The expansion of the interlayer region was thus about 0.84 nm. Ogawa et al[60] suggested that acrylamide is absorbed into the interlayer space in a bimolecular arrangement to form a 2.0 nm-compound. The intercalation mechanism is thus similar to the familiar swelling of smectites by polar polyalcohols such as diethylene glycol and glycerol. Those molecules produce two-layer complexes with basal spacings of 1.78 nm[61] that is the sum of the layer thickness of diethylene glycol, 0.76 nm and the desolvated Na-smectite, 1.02 nm.

4.4 SEM/EDX studies

The SAP composite investigated by energy-dispersive X-ray analysis (EDX) shows the typical X-ray pattern of sodium bentonite. At lower incident electron energy, the carbon peak from the polymer is clearly visible. This confirms the fact that AM was intercalated into the bentonite.
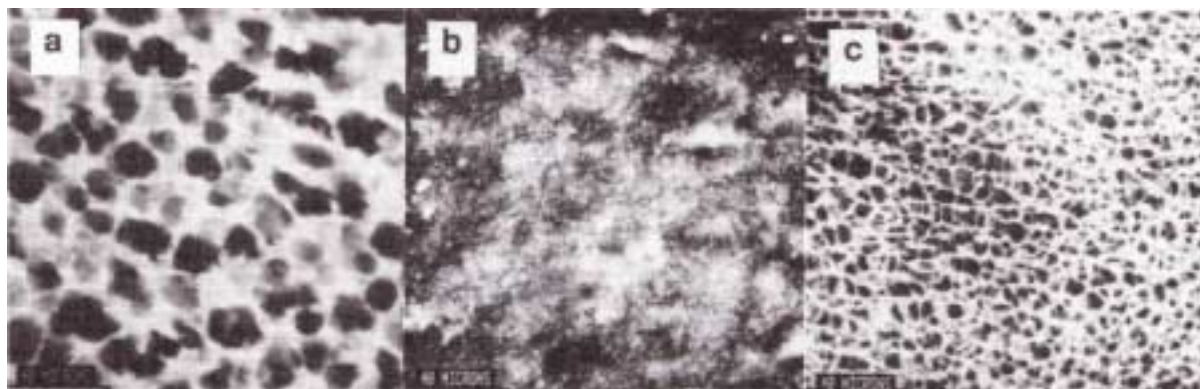
Figure 36 *SEM micrographs (Hitachi X-650) of freeze-dried samples of (a) bentonite (30% solid content); (b) SAPC (30% solid content); (c) SAPC (1.5% solid content). (Ref. 10)*

Figure 37. *Scanning electromicrographs (JEOL JSM-5300 LV "environmental" microscope) of poly(acrylamide)(a) and SAP (b, c) at 1 Torr water partial pressure.(Ref.10)*

In order to minimize interpretational problems, the morphology of similar samples prepared in exactly the same way were compared. The secondary electron images of bentonite and polymer/bentonite composite in the water-saturated state are compared in Figure 36. It is obvious that the pure bentonite structure (a) is much more porous and fragile than that of the composite with the same water content (b). The porosity of the pure bentonite sample with solid content of 30 % is even higher than that of the composite sample with a solid content of only 1.5 % (c). After further addition of water, the structure of the pure bentonite collapsed rapidly but the SAP composite kept its shape, supported by the intercalated polymer, to an even higher saturated state. This was confirmed by rheological measurements (see section 5.1.1). In addition, the uncoated swollen poly(acrylamide)/ bentonite composite samples were investigated at 1 Torr water vapor pressure with a JEOL JSM-5300 LV series microscope as shown in Figure 37. The PAM/bentonite ratio had a great effect on the microstructure of the SAP. The pure PAM (left) shows a tightly compressed structure while the sample with a PAM/bentonite ratio of 1/4 shows a structure with open pores (middle, right). This finding suggests that the structure of the SAP may consist of polymer chains as the skeletal backbone of the material in which the bentonites are intercalated and in turn are strung together by the polymer chains. Moreover, the bentonite enhances the stiffness of the polymer structure. Thus a schematic structural picture arises as illustrated in Figure 42.

4.5 Thermal Analysis

Four samples were investigated by differential scanning calorimetry (DSC) under identical conditions (sample weight: 9-12 mg, heating rate: 10 ^{o}C/min; maximum temperature: 400 ^{o}C, nitrogen atmosphere). Figure 38(a) shows the thermogram of pure Na-bentonite that

reveals only a small peak between 120 °C and 145 °C (maximum: 128 °C), presumably related to the release of water absorbed onto the external sites of the bentonite platelets.

Figure 38(b) shows the thermogram of pure poly(acrylamide) with two distinct endothermic peaks between 200 °C and 270 °C (maximum: 253 °C), and between 270 °C and 311 °C (maximum: 279 °C). Beyond 312 °C, the material shows a big jump in endothermic activity presumably associated with partial decomposition. Figure 38(c) shows the smooth thermal response curve of a starch-based superabsorbent polymer isolated from commercially available diapers ("Huggies"). This should be compared to the DSC curve of a PAM/bentonite composite shown in Figure 38(d). There is a broad endothermic peak between 230 °C and 350 °C that consists of at least three overlapping peaks. Gaussian-Lorentzian deconvolution of the composite peak resulted in peak maxima at 259 °C, 282 °C, 310 °C and 329 °C. The individual peaks may be associated with the three possible states of monomer bonding shown in Figure 43. Since it is reasonable to assume that water absorbed at the A, B and C-sites will have differing binding energies, the peak structure of the DSC curve reflects these differences. Theoretically, water associated with C-sites ('free' polymer) should have the lowest binding energy. Thus, the first (and second) peaks in Figure 38(d) at 259 °C and 282 °C may be related to water absorbed by the 'free' polymer by different binding modes, the third peak at 310 °C may be related to water absorbed by PAM situated at B-sites, and the fourth peak at approximately 329 °C may be related to water absorbed by polymer intercalated in the interlayer space of the bentonite (A-sites). The assignment of the first and second peaks are corroborated by the occurrence of the water release peaks at 253 °C and 279 °C in pure PAM (Figure 38 (b)).
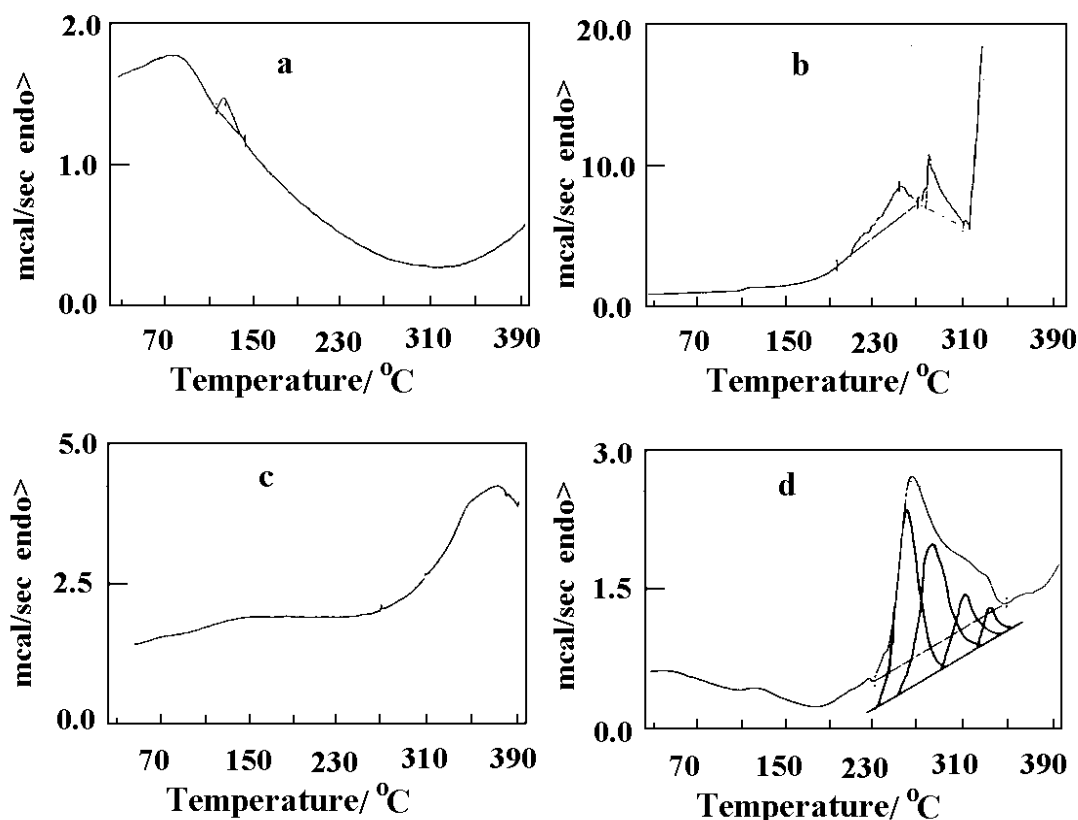
Figure 38. Differential Scanning Calorimetry (DSC) curves of bentonite (a), poly(acrylamide) (b), starch-based SAP from commercially available diapers (c), and poly(acrylamide)/bentonite SAP composite (d). (Ref.10)

Thermogravimetric analysis (TGA) was done using a TGA - 951 with Dupont 910 DSC Data Station 1090. Compared to the pure PAM, the SAPC had a smaller derivative (Figure 39). This reduction may be caused by the intercalation of the polymer into the bentonite.
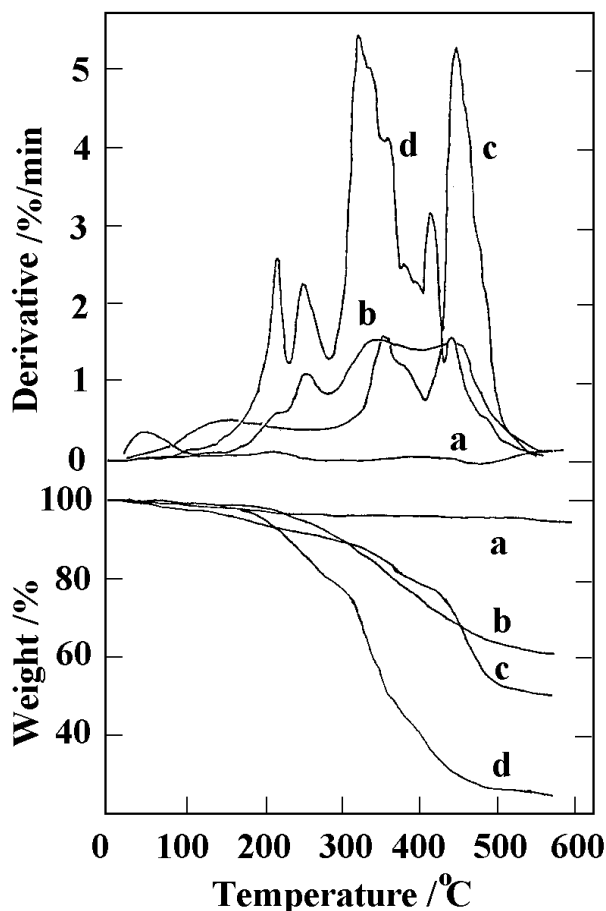
Figure 39. *Thermogravimetric (TG) curves of bentonite (a), poly(acrylamide)/ bentonite SAP composite (b), commercial starch-based SAP (c), and poly(acrylamide) (d). (Ref. 10)*

4.5.1 DSC analysis of SAPC

The measurements (Linseis DSC) were carried out in a nitrogen atmosphere with a flow rate of 2 ml/min. All samples were weighed before and after the DSC measurement, and second or third DSC scanning runs were made using the same temperature program. The curves of the second run were used as baseline in the resulting analysis process. The temperature rising programs selected were 1, 3, 5 K/sec according to the requirement of the measurement.

The SAPC gels for the DSC analysis contained 80 % of water. The amount of hydrogel sample used for each DSC measurement was about 25 mg. The calibration factor of the DSC equipment used in the measurement was as in Appendix 5 (Figure A-1,2), following the equation $K = 10.05 + 2.14 \times 10^{-2} T$ (mW/K).

Results of the DSC measurements of SAPC (gel, 80% of water)

Table 13. Position of DSC peaks of SAPCs and bentonite

|	Heating rate(K/min)	Mass (mg)						
A	5	26.06	Peak position (°C)	113.4	135.4	138.7	162.3	203.3
			(ΔT, mK)	6269	1194.5	1247	316.3	169.8
			(heat flow, mW)	78.22	15.47	16.23	4.28	2.45
	3	25.61	Peak position (°C)	103.8	128.3		168.3	203.0
			(ΔT, mK)	5626.7	700.0		152.1	169.8
			(heat flow, mW)	69.05	8.95		2.08	2.44
	1	13.14	Peak position (°C)	60.6	99.0			
			(ΔT, mK)	1099.4	140.3			
			(heat flow, mW)	12.47	1.70			
B	5	25.73	Peak position (°C)	114.6	133.7	160.3	255	
			(ΔT, mK)	6269	879	213.1	179.8	
			(heat flow, mW)	82.88	11.35	2.87	2.79	
	3	25.46	Peak position (°C)	97.8	120.5	165.4	227.1	246.1
			(ΔT, mK)	4829	630.3	181.8	196.5	212.5
			(heat flow, mW)	58.64	7.96	2.47	2.94	3.26
C	5	25.10	Peak position (°C)	114.7	133.1	158.5		
			(ΔT, mK)	6269	961.3	223.0		
			(heat flow, mW)	78.39	12.40	3.00		
	3	25.56	Peak position (°C)	102.6	123.3	165.8	210.7	
			(ΔT, mK)	4971.3	460	154.3	187.4	
			(heat flow, mW)	60.87	5.84	2.10	2.73	
D	5	25.44	Peak position (°C)	110.5		126.0		
			(ΔT, mK)	6269		1019.9		
			(heat flow, mW)	77.83		13.00		
	3	26.31	Peak position (°C)	102		120.5		
			(ΔT, mK)	5479.4		554.7		
			(heat flow, mW)	67.03		7.01		
E	5	25.33	Peak position (°C)	117.6		232.3		253.8
			(ΔT, mK)	5479.2		229.6		237.8
			(heat flow, mW)	68.85		3.45		3.68
	3	25.74	Peak position (°C)	102.1	119.1	226.3	244.6	
			(ΔT, mK)	3719.9	561.2	211.6	225.8	
			(heat flow, mW)	45.51	7.07	3.15	3.45	
F	5	25.76	Peak position (°C)	115.3		195.3		242.4
			(ΔT, mK)	6252		213.1		225.1
			(heat flow, mW)	78.26		3.03		3.43
	3	25.22	Peak position (°C)	102.8		144.8		228.5
			(ΔT, mK)	3717.8		175.3		224
			(heat flow, mW)	45.55		2.30		3.35
G	5	25.10	Peak position (°C)	111.5		133.5		161
			(ΔT, mK)	6269		667.7		168.6
			(heat flow, mW)	77.96		8.61		2.27
	3	25.73	Peak position (°C)	99.4		124.3		167.5
			(ΔT, mK)	5531.5		574.2		140.1
			(heat flow, mW)	17.36		7.29		1.91

G: bentonite
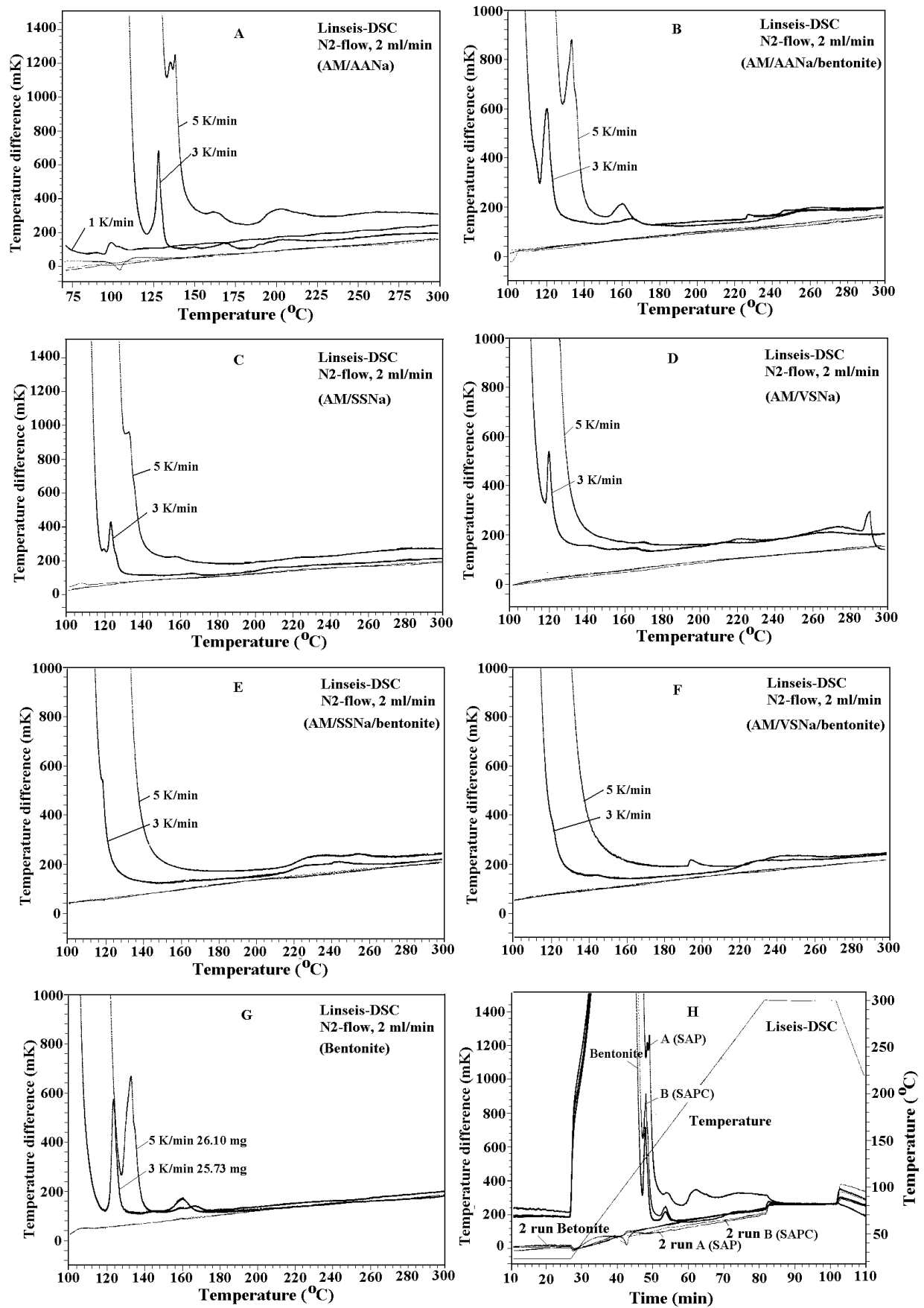
Figure 40.   *DSC curves of samples*

Sample A (Figure 40A) was a copolymer prepared by copolymerization of acrylamide (AM) and sodium acrylate (AANa) without bentonite. The ratio of AM to AANa was 3:1.

Comparison of the temperature program of 5 K/min, 3mK/min and 1 K/min showed that generally the fast temperature rising program generated large peaks and slower temperature rising speeds generated small peak with the peak positions shifted to the low temperature side. In the 3 K/min program, the second peak was obviously separated from the first one compared to that of 5 K/min and there were no big peak with that of 1 K/min. The height of the peak decreased and some peaks even disappeared. All peaks in the DSC measurement were endothermic peaks.

Sample B (Figure 40B) was a composite material prepared from acrylamide, acrylic acid and bentonite. Curves of almost the same shape were obtained from the sample A. There were four peaks in the 5 K/min temperature program and five peaks in the 3 K/min temperature program. After the measurement, the color of the sample was unchanged compared to the sample of sample A, which changed its color from white to dark brown. The shape of the samples was not changed while the sample A foamed in the process of heating at high temperature.

Sample C (Figure 40C) was a copolymer prepared by copolymerization of acrylamide and sodium styrenesulfonate. The measurement conditions were the same as before. The DSC curves were quite different compared to the former samples. There were two obvious peaks in the DSC curves and also some ambiguous peaks. The slower temperature increase generated sharp peaks at lower temperature position.

Sample D (Figure 40D) was prepared by polymerization of AM with sodium vinylsulfonate. Curves of sample D were similar to sample C. There were two peaks in both curves of 5 K/min and 3 K/min temperature programs. The second peaks in 5 K/min is at 126.0 ºC which is very small compared to the obvious peak at 120.5 ºC in 3 K/min.

Sample E (Figure 40 E) was prepared from acrylamide, sodium styrenesulfonate and bentonite. The test results of DSC were quite different from the sample C without bentonite. There are no obvious peaks on the DSC curves except the big peak of water desorption which started at 117.6 °C for the 5 K/min program and 102.1 ºC for the 3 K/min program. Perhaps, peaks at lower temperature were obscured by the large first peak that extended to almost 140 ºC for the 5 K/min program. On the other hand, at temperatures below 200 ºC, there was a broad and low endothermic peaks which maybe was due to the glass transition or curing of the network because the polymerization of this sample was not carried out as smoothly as for the other SAPCs. The appearance of sample E after the test was light brown.

Sample F (Figure 40F) was prepared from acrylamide, sodium vinylsulfonate and bentonite. It showed similar results as sample E.

The measurement conditions of raw bentonite (Figure 40G) without any treatment before the measurement were the same as for sample A and B. The peak shape, peak height, peak number and peak position were similar to the curves of sample B. Fast heating causes the peaks to be shifted to higher temperature. The appearances of the samples were not changed after the measurement.

Comparison of the DSC curves of sample A (SAP), B (SAPC) and bentonite are shown in Figure 40H, measured at a temperature program of 5 K/min. The three curves had their peaks at almost the same position except the sample A had an additional peak at 60 min (200 ºC). The sample B (SAPC) was in a position between the sample A (SAP) and the bentonite. All three curves showed a good accordance on their base line, especially at 300

°C.   Comparison with the 5 K/min program showed that the different DSC curves of three different materials had different peak position on their second peak in the measurement of the 3K/min temperature program.   However, all other features of those curves were similar to 5 K/min.
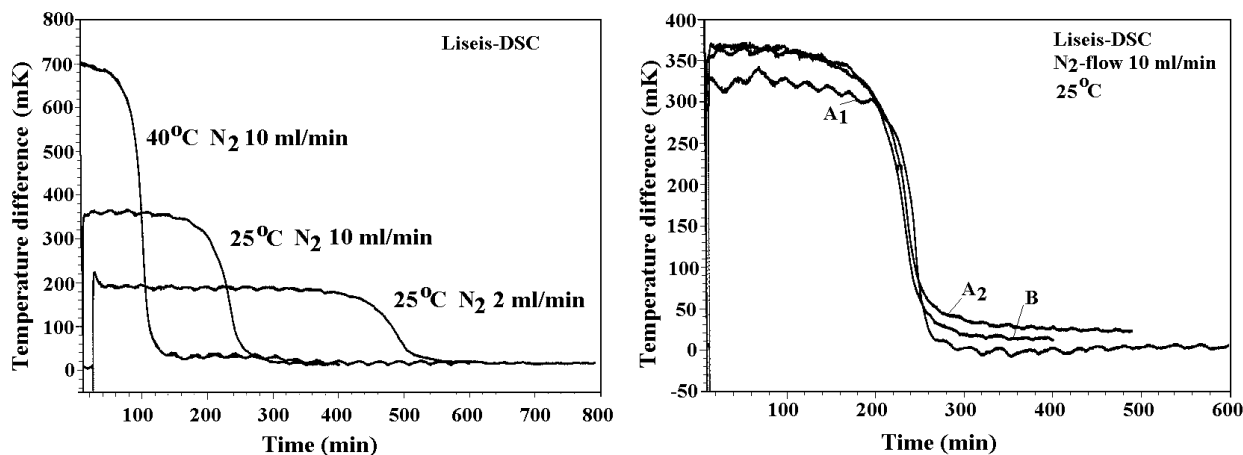

Figure 41. *DSC isothermal curves of SAPC B with different measuring condition (left), and the comparison of isothermal curves of SAPC B, SAP A (right).*

Isothermal measurements of some SAPC samples were carried out at various temperatures and nitrogen gas flow rates as shown in Figure 41(left) for sample B.   From Figure 41 it can be seen that the higher temperature (40 °C) caused rather fast water desorption. Within 130 min, the temperature difference reached an almost constant level. To reach this level of constancy at an isothermal temperature of 25 °C, 260 min were needed. Hence the water desorption at 40 °C was twice as fast as that at 25 °C when all the other conditions were fixed.   Moreover, on slowing down the nitrogen gas flow rate from 10 ml/min to 2 ml/min, the time needed for this desorption to reach the same level was almost 560 min, hence twice as long as the former one.   The temperature differences for the three measurements were 700 mK (7.63 mW), 370 mK (3.92 mW) and 195 mK (2.06 mW), respectively.

Comparison of isothermal measurement of sample A and sample B are shown in Figure 41(right).   These curves show almost the same isothermal water desorption properties.   Both samples desorbed most of the water in about 240 min at the same condition of a nitrogen gas flow rate of 10 ml/min with an isothermal temperature of 25 °C.

From the appearance of the heat-treated samples we can see that the thermal stability of sample B (SAPC) was higher than that of the sample A (SAP).   This means that intercalation of acrylamide and other chemicals into the interlayer of montmorillonite formed a stable structure. This may provide a wide usage of the composite materials in relatively high temperature application fields.

Intercalation mechanism of AM and bentonite

The intercalation mechanisms of bentonite with polymer such as poly(acrylamide), poly(vinyl alcohol), polyacrylate salts, and poly(ethylene glycol) were studied in the past[62-67]. Gu Qun studied the crystallization kinetics and morphology of poly(ether ester)/montmorillonite composite[68]. Wang Yizhong studied the copolymerization of styrene grafted on the montmorillonite[69] and polyethylene oxide/montmorillonite intercalation compound[70], and Chen Guohua studied to use the montmorillonite and polymer to prepare a polymer/montmorillonite nanocomposite[71]. Wu Qiuju studied the synthesis and characterization of polyaniline/bentonite hybrid with extended chain conformation of polyaniline[72]. Oya studied the bentonite mineral/polypropylene nano-composites[73]. However, poly(acrylamide) has received particular attention because of its superior water absorption capacity.

Acrylamide (AM) monomer polymerizes at $85^{\circ}C$. If intercalated into bentonite, however, higher polymerization temperatures are required because the restricted motion and intermolecular separation by the layered bentonite material impedes cooperative interaction of monomeric species. Thus, either higher temperatures are required or other techniques must be applied such as irradiation with γ-rays[8], electron beams[9] or UV radiation (this thesis). At temperatures exceeding $400^{\circ}C$ the polymer structure collapses owing to the degradation of the poly(acrylamide)[74,75].(see Figure 39 d)
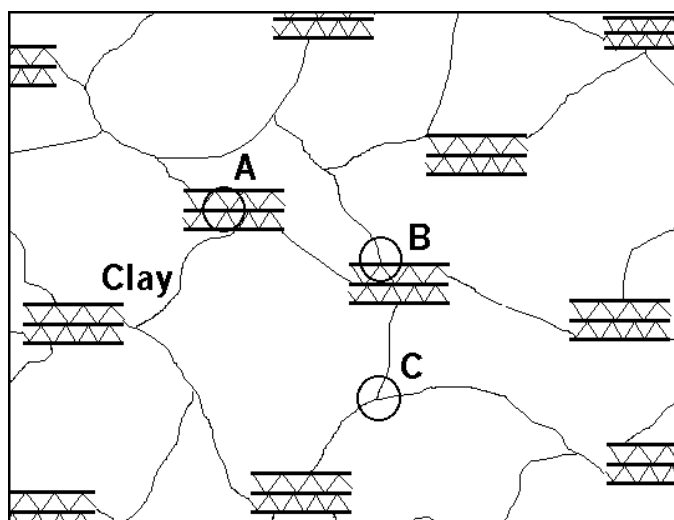
Figure 42. *Schematic structure of a poly(acrylamide)/bentonite composite SAP. A-site: Polymer intercalated into the lamina of bentonite, B-site: Polymer attached to the surface of bentonite particles, C-site: Free polymer network. (Ref.10)*

The kinetics and mechanisms of the intercalation and polymerization processes are complex and not known in much detail. Ogawa *et al*[60] assumed that during interaction of AM with montmorillonite a coordination complex might be formed by bonding to interlayer exchangeable cations and hydrogen bonding with surface oxygen atoms. In this thesis it is conjectured that there are three kinds of states in the composite structure as shown in Figure 42. First, AM intercalated into the interlayer space of bentonite is weakly bound by Van Der Waals forces and hydrogen bonds to the hydrated interlayer cation and the silicate layer, respectively (Figure 42, A-site). Secondly, AM is bound to the bentonite surface by hydrogen bonds with exchangeable surface cations in the structure of bentonite (Figure 42, B-site) according to

$-Na^{\delta+}-OH^{-}...H\ N^{+}-C-C-$ or $-Al^{\delta+}\begin{smallmatrix}O\\ \\O\end{smallmatrix}C-R-$
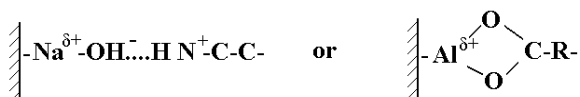
Finally, a `free' polymer network is formed between the bentonite particles (Figure 42, C-site) that links the bentonite platelets to each other via polymer strands. Because initially AM exists at all three bonding sites in the sample, on exposure to ionizing radiation simultaneous polymerization occurs. Therefore, the overall structure of the composite will be quite complex. It is our current understanding that it is this complex structure that imparts to the composite material better performance in terms of water absorption capability and thermal stability when compared to material that had only the intercalated polymer at A-sites[60].
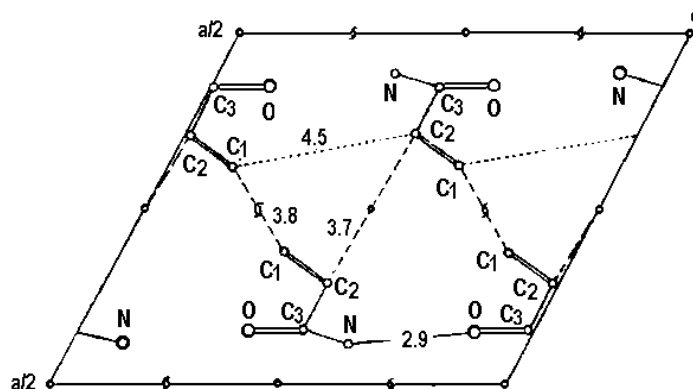

Figure 43.   *Crystal structure of acrylamide (010 plan), (Isakov[76], unit = Å.).*

The crystal structure of acrylamide has been investigated by Isakov (Figure 43). The unit cell contains four molecules that are arranged to conform to a monoclinic $P2_1/c$ lattice with $a_0 = 0.8408$ nm, $b_0 = 0.5792$ nm, $c_0 = 0.9777$ nm; $\beta = 118°34'$; N = 4. In the unit cell parallel to the (010) plane, the AM molecules are arranged in two layers with their carbonyl groups parallel to <100> and the C-C bond parallel to <001>.   The AM will interact with the montmorillonite structure as follows.   The two intercalated layers will expand the silicate sheets of the montmorillonite by a distance $c^* = c_0 \sin(180-\beta) = 0.859$ nm. This is in accord with Ogawa's suggestion that the oxygen of the carbonyl group forms a Van Der Waals-type bond with the exchangeable ion, and the NH_2 group forms hydrogen bonds with the oxygen of the silicate sheet[61]. Figure 44 shows a sketch of the possible molecular conformation of the poly(acrylamide)/montmorillonite intercalation complex.   The orientation relations are $(010)_{PAM} \parallel (010)_{montmorillonite}$ and $<c^*>_{PAM} \parallel <001>_{montmorillonite}$.   In the desolvated stage the intramolecular distance between equivalent $CH_2=$ groups (C_1) of neighboring molecules is 0.38 nm (dashed lines) (see Figure 43). The dotted lines between C_1 and C_2 groups of adjacent molecules indicate the formation of a polymer chain by 'head to tail' arrangement with a distance of 0.45 nm. Since this distance is longer than that between C_1 and C_1 ("head to head" polymerization), the latter mechanism has a higher probability. The positions of the Na atoms in the intercalated PAM mesh are tentative.   Hydrogen atoms are not shown.
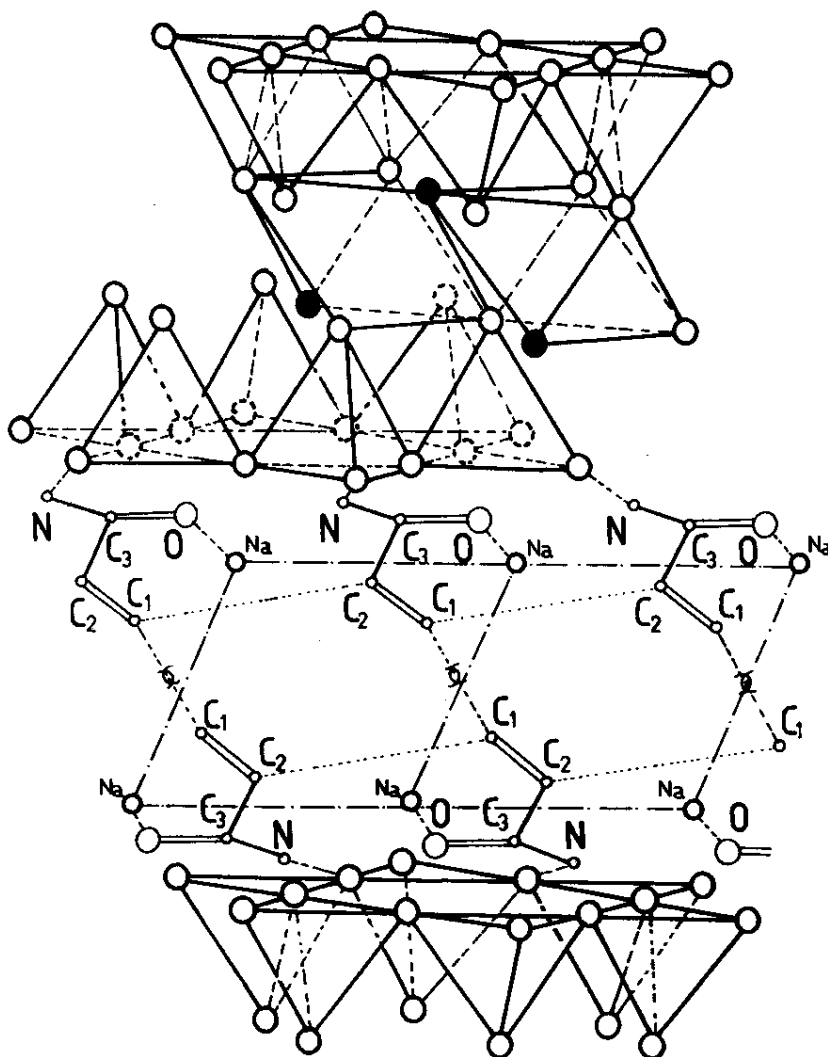
Figure 44. Schematic conformation of a bi-molecular layer of acrylamide intercalated into the interlamellar space of Na-montmorillonite parallel <001>. (Ref. 10)

5.0   PROPERTIES OF SAPCs

5.1   Rheological and mechanical properties

SAPC hydrogels show very interesting rheological and mechanical properties that suggest their use as mechanical energy-damping agents and moisture-driven actuator for a large variety of applications (see 6.10).   In particular as shown in the following section, SAPC hydrogel network structures are exceptionally resilient when exposed to shear strain with high perturbation frequencies.   Even with high water contents they retain rheological properties akin to true solids despite their viscoelastic nature.   This is augmented by the fact that SAPC hydrogels loaded with up to 95% of water still act like solids when pressure is exerted on them, i.e. the water cannot easily be squeezed out but is retained in the cellular network formed by the intercalation of polymer into the interlayer of expanding clay minerals (see Figure 37).

5.1.1   Rheological properties

The data reported in this section have been acquired during a study performed at Alberta Research Council in cooperation with the Department of Chemical and Materials Engineering, University of Alberta[77].

Strain and frequency sweeps were conducted on SAPC samples containing 95, 85 and 50% water.   Also, stress start-up and relaxation transients were determined.   Finally, the concentration dependence of the shear modulus $G'(c)$ was measured at low and high angular velocities, and the critical solids content determined below which a cube of SAPC would collapse under its own weight.

The experimental conditions used are shown in Appendix 3.

Strain sweeps

Measurement of G' at $\omega = 0.1$ rad/s for a range of γ^o covering almost four orders of magnitude are shown in Figure 45 for all three materials.   The curve for 50 % water appears superficially to achieve a linear limit (absolute flatness at low γ^o), but such is not the case, as is discussed below.   Although G'' are not displayed here, it is relevant to comment that $G'' << G'$. Since these properties are defined in the context of complex numbers, in terms of the complex modulus $G^* \equiv G' + i\,G''$, it is clear that the absolute value of G^* (determined by stress amplitude) is dominated by the storage modulus, $|G^*| \cong G'$.   This is one indicator of the solidlike nature of the hydrogel composites, since a more fluid-like material would be characterized by viscous behavior (energy loss by viscous dissipation) so G'' would be larger and contribute more substantially to $|G^*| = [(G')^2 + (G'')^2]^{1/2}$.
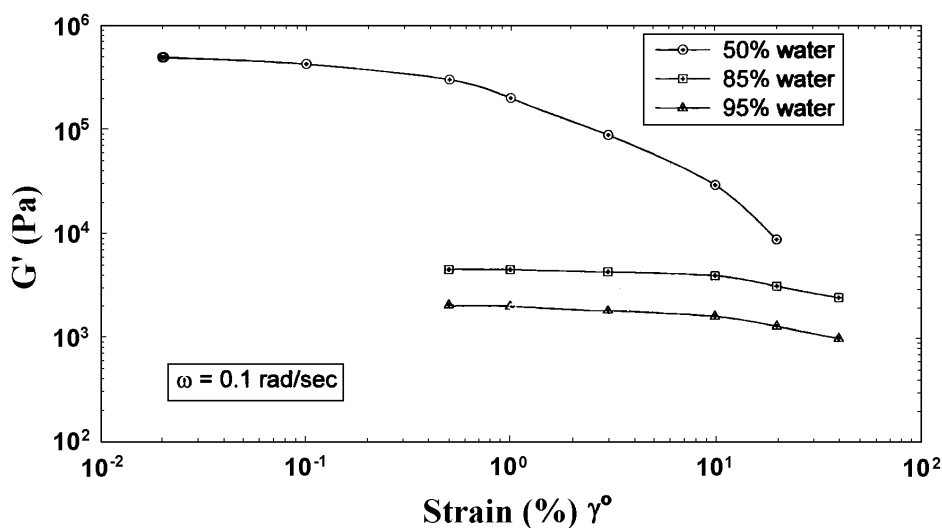
Figure 45*. Strain sweeps to determine onset of nonlinearities in dynamic testing, where strain is controlled as $\gamma = \gamma^o \sin\omega t$. Frequency was $\omega = 0.1$ rad/sec for all materials, which strain oscillation amplitude γ^o varied. Both platens of the parallel-plate shearing assembly were modified by a coating of "wet-and-dry" abrasive paper. (Ref. 77)*

An alternative interpretation[78], of stress data in dynamic testing is in terms of a pair of viscosity parameters, η'(ω) and η''(ω) that are related to the dynamic viscosity η^* by $\eta^* =$

η'-$i\eta''$. Basic definitions require that $\eta' = G''/\omega$, and $\eta'' = G'/\omega$, so that only one set of properties (e.g., G' and G'') needs to be reported for complete characterization of the linear viscoelastic behavior of a given material. These definitions also require that $|\eta^*| = |G^*|/\omega$. Given the dominance of G' over G'' for these materials, it is useful to note that $|\eta^*| \cong G'/\omega$ so that Figure 45 ($\omega = 0.1$ rad/s) results for G' can be used to give approximately $|\eta^*| \cong G'/\omega = 10\ G'$ and is rigorously converted to $\eta'' = 10\ G'$.

Frequency sweeps

The plots of $G'(\omega)$ and $G''(\omega)$ are given for polyacrylamide/bentonite hydrogels with various water contents in Figure 46. For 95% water (Figure 46a), results are displayed for two strain amplitudes, $\gamma^\circ = 5$ and 10%. These plots confirm that $G' >> G''$, as stated above, but show a slight difference between the two γ°. This demonstrates that the case $\gamma^\circ = 10\%$ was just barely within the nonlinear testing regime (see Figure 45) and that the $\gamma^\circ = 5\%$ data in Figure 46a, are more reliable for representing linear viscoelasticity.
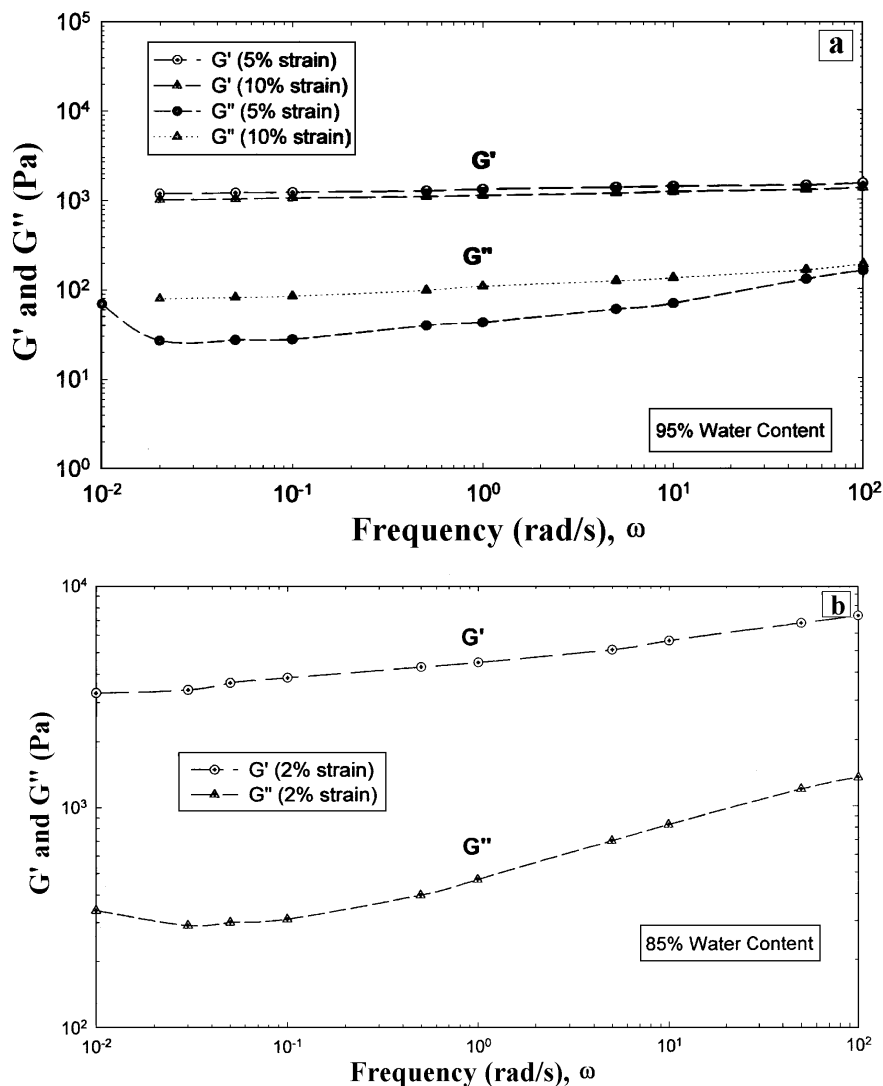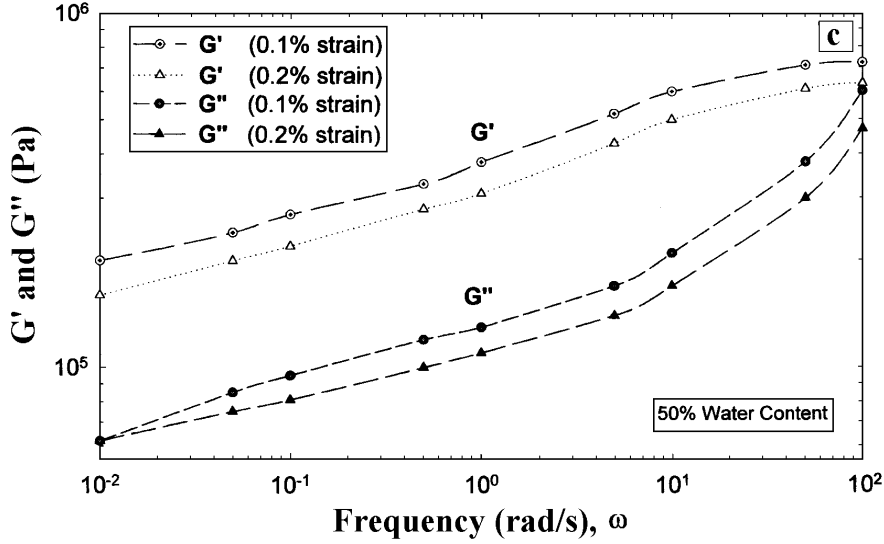
Figure 46 *Frequency sweeps (ω-dependence of G' and G") for all materials investigated. Several strain amplitudes γ'' were used to assess the possible influence of nonlinear effects, as shown on each figure. (a) 95% water, (b) 85% water and (c) 50% water. (Ref. 77)*

All testing for 85 % water samples (Figure 46b) was done at γ^o = 2%, so the possible influence of nonlinearities cannot be assessed, but from the results of Figures 45 and 46 it might be assumed to be small. However, for 50% water content (Figure 46c), the use of γ^o = 0.1 and 0.2% do not lead to exact superposition of results, which shows some nonlinearities still to be present, so that the γ^o = 0.1 % data should be regarded as more representative of linear behavior. Figure 45 agrees, for 50 % water samples, that γ^o=0.1% is almost down into the fully linear regime, but that γ^o= 0.2% is not.

The impressive strength (or "stiffness) of these materials is indicated by the magnitudes of $G'(\omega)$ in Figure 45, inasmuch as the value of G' for the majority component (water) is G'= 0. The fact that G'>>0 reflects a substantial presence of true solids (bentonite and rubber), and also the existence of a network structure, composed of the crosslinked polymer and the bentonite linkage sites.   The flatness of the three $G'(\omega)$ curves indicates that *these network structures are very stable when exposed to a wide range of perturbation frequencies*, even though the effective rate of shear (γ^o = $\omega\gamma^o$) also covers several orders of magnitude.   Clearly, the materials do not disassemble at any frequency (as long as the applied stress magnitude is low).   *Regardless of the high water content, the gels do not flow like fluids until a true rheological yielding occurs*, when the network is torn apart by higher applied stresses that exceed the yield stress.

Figures 46a, b and c collectively reveal unexpected behavior in the ratio G''/G' = tan δ, where δ is the phase difference between the oscillating γ(t) imposed and the responding material stress τ(t).   For 95 and 85% water case, tan δ ≅ 0.1, which could be interpreted as surprisingly high degree of 'relative fluidity' in view of the fact that these materials were phenomenologically solid-like bodies.   Dropping the water content to 50% led to an abrupt jump of tan δ to the range of 0.4-0.5.   This jump is better understood in terms of the solids concentrations (*c*) passing from the semidilute regime (c = 5% and 15%) to the concentrated solid regime (*c* = 50%); under these circumstances tan δ = 0.4 - 0.5 could still be considered surprisingly high 'fluidity'.

The ω-dependence of $G''(\omega)$ in Figure 45 is not close to flat, but it is not expected to be.

If we regard the hydrogel volumes as composed primarily of water (50-95%, here) energy dissipation (i.e., energy loss) effects might be thought to be controlled by the viscosity of water ($\eta_w = 10^{-3}$Pa.s).   Since $G'' = \eta'\omega$, the approximation $G'' \cong \eta'_w\omega$, (perhaps useful at extremely low solids content) shows that some ω-dependence in G'' is required.   The enhancement of G'' above the extremely low approximation for water ($G'' = 10^{-3}\ \omega$ Pa) implies that a major contribution is being made by the viscous component of the network (bentonite particle linkages, plus crosslinked polyacrylamide) at the prevailing solids concentration, $G'' \equiv \eta'(c)\omega$. The expected behavior of $\eta'(\omega,\ c)$ is to have a steep drop-off ('ω-thinning' as ω increases beyond negligible values.   This behavior results in the appearance of the shallow minimum in $G''(\omega) = \eta'(\omega) \times \omega$ observed in Figures 46a and b. Although Figure 46c exhibits no minimum, the $G''(\omega)$ curve display a concave-up shape arising from the same superposition of dual contribution to G'': [decreasing $\eta'(\omega)$] × [linearity increasing ω].

The fact that $G''(\omega)$ generally shows an increase (and not a ω-thinning) with ω increase over four orders of magnitude demonstrates that *the hydrogels retain excellent mechanical energy-damping ability over a wide frequency range.* Moreover, that ability is enhanced over that of the water component above by several orders of magnitude, despite the anticipated 'ω-thinning' of the solids component over the same frequency range.

Stress start-up/relaxation transients

The shear stress transient $\tau^+(t,\ \gamma)$ is used to define the transient modulus (relaxation modulus G_r) $G_r = G^+(t) = \tau^+/\gamma$, so to present $G_r = (t)$ also suffices to convey τ^+ when γ is given.

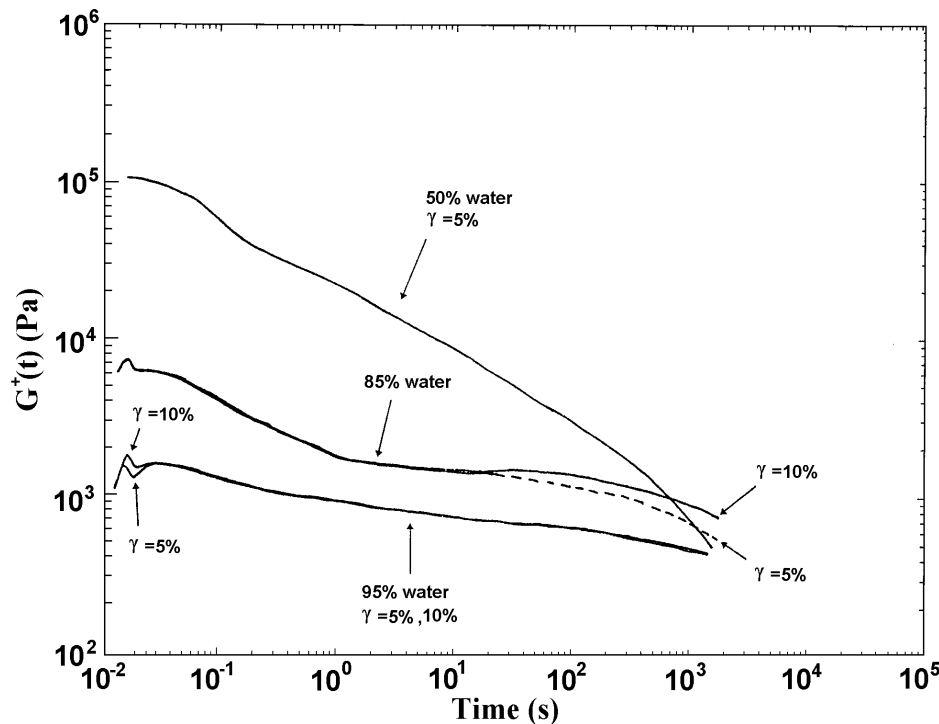***Figure 47.*** *Transient shear modulus $G^+ \equiv \tau^+/\gamma$ for the start-up shear stress τ^+ response of SAPC hydrogel with water contents between 95 and 50% (for detail see text). (Ref. 77)*

These moduli are displayed in Figure 47, for all three water-content cases. For 95% water content, the use of two strains (γ =5%, 10%) produced identical results for $t > 0.03$ s, with only a minor difference in the short-term oscillation in the first 0.02 s. There is somewhat greater nonlinearity displayed for samples with 85% water, as becomes apparent at long times, where the data for $\gamma = 5\%$ and 10% diverge slightly for $t > 20$ s. However, even at $t = 2000$ s the difference is only about 3% in $G^+ = G_r(t)$. Based on these results for water contents of 95 and 85%, the case for 50% water was tested only at $\gamma = 5\%$; no short-term oscillation at short times could be detected. For all three materials, the $\tau^+(t)$ transients peaked at about $t = 0.02$ s for all γ.

Ranges of kinematic variables

The linear viscoelastic properties have been measured over a wide range of time and rate variables, with t in $G^+(t)$ tests covering t from 10^{-2} to 2000 s (over 5 orders of magnitude) and ω in $G'(\omega)$ test ranging from 10^{-2} to 10^2 (4 orders of magnitude). The onset of nonlinearities was found at lower γ for the firmer materials (e.g., $\gamma^o = 0.2\%$ for G' in samples with 50% water, but $\gamma^o = 10\%$ for samples with 95% water, with similar results for γ in G^+ tests). These strain values are within normal ranges, but the reasons for the onset of those nonlinearities is not clear. At sufficiently large γ all materials must exhibit rheological nonlinearities, and with polymeric systems this can arise when the polymer coils are substantially distorted from their rest state of spherical symmetry, isotropy, and Gaussian mass distribution, to assume ellipsoidal symmetries and orientation. Additional factors arise in 'structured' system, when microscopic deformations can break down or otherwise alter the microstructure even when molecular-level nonlinearities are negligible. This is most likely the case for the hydrogel/bentonite composites.

Concentration dependence

A major objective of this study was to determine how the water content affected the various viscoelastic strength parameters. It is sometimes helpful to represent this dependence in terms of the materials solids content (c) which includes both bentonite and polyacrylamide in equal amounts. This is demonstrated by comparing the set of three curves for $G'(\gamma^o; c)$ in Figure 45 and for $G^+(t; c)$ in Figure 47. The anticipated increase of modulus with c is clearly shown there, over the whole range of γ and t. The same results emerges for $G'(\omega, c)$ over the whole range of ω as observed by inspection of Figures 46a, b, and c collectively. This c-dependence is made more explicit in Figure 48, where $G'(c)$ is displayed for both the low-ω regimes (10^{-2}s^{-1}) and the high-ω regime (10^2s^{-1}). In both regimes, the data plotted on semilog coordinates are essentially linear, signifying exponential dependence on c:

$$G'(\omega,c) = G'_0(\omega)e^{AC} \qquad (5)$$

where A(ω) determines the slopes in Figure 48 and G'_0 is the intercept at $c = 0$. Because the $c = 0$ limit corresponds mathematically to both no bentonite and no polymer, G'_0 must be carefully interpreted. The zero-polymer limit would normally give $G' = 0$ (no elasticity), but in fact we find that $G'_0 > 0$. We suspect this results is a consequence of sample preparation procedure, wherein acrylamide polymerization and cross-linking are completed before the post-treatment steps of adding water or removing water were performed. Thus, the extrapolated $c = 0$ limit (or, 100% water) does not have its usual significance, and the material performs viscoelastically in this limit. This also explain why G'_0 is weakly ω-dependent as well; the two lines in Figure 48 give $G'_0 = 8.5 \times 10^2$ and 7.5×10^2 Pa at $\omega = 10^2$s^{-1} and 10^{-2}s^{-1}, respectively. The closeness of these two values is consistent with the matrix behaving as a crosslinked rubbery network, which should exhibit a broad $G'(\omega)$ plateau in a certain middle range of ω so that only a minor sensitivity to ω should be expected to appear (increasing weakly with ω, as found here). The

exponential c-dependence of $G'(\omega,c)$ in Figure 48, and likewise the corresponding viscosity parameter $\eta''(\omega,c) = G'/\omega$, is probably a manifestation of bentonite component of the solids. Equation 5 resembles strongly the functional form for enhancement of concentrated suspension viscosity by rigid particulates of irregular shape[79]. To make the resemblance more complete, Equation 5 would have to be re-cast in terms of bentonite volume fraction (ϕ) and the maximum packing fraction (ϕ_{max}). This would make Equation 5 capable of extrapolation more reliable to the high-ϕ limit ($\phi \to \phi_{max}$), where its current form does not increase with c fast enough to represent the enormous G' values expected at higher c as $c \to c_{max}$.
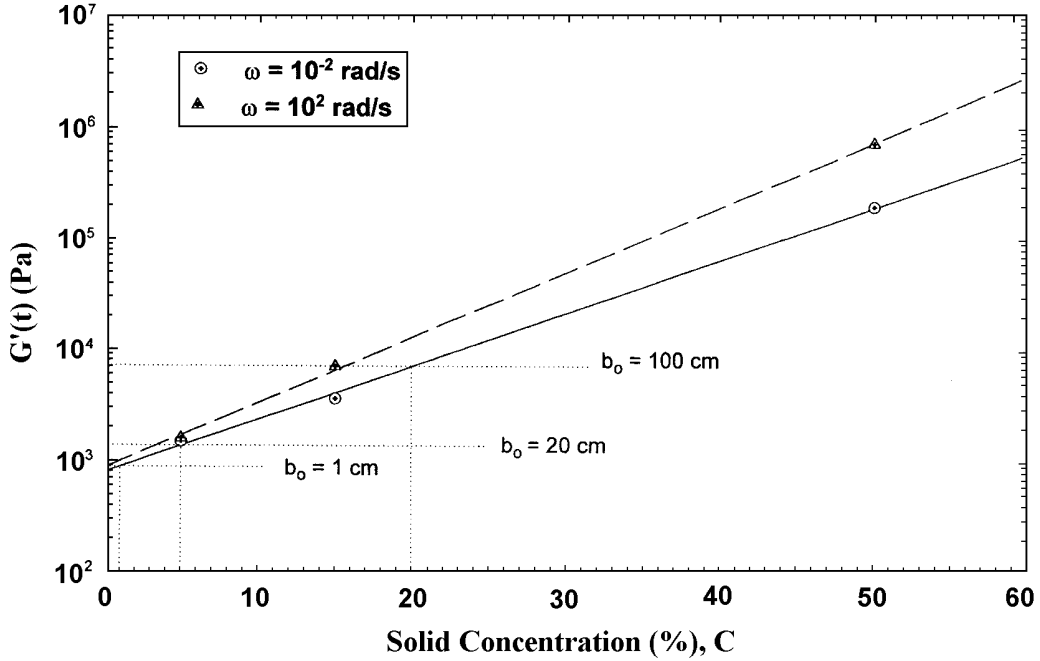
Figure 48 *Dependence of G' on solids concentration, c. The ω-sensitivity of this relationship is demonstrated by showing G'(c) for the lowest ω (10^{-2} rad/s) and highest ω (10^2 rad/s) employed in this study; for all other ω, results are intermediate. Values of b_0 correspond to the largest size of a material cube of a given solids concentration that is mechanically stable (see text). (Ref. 77)*

Critical solids content

Even though the samples tested here were clearly solid-like and did not flow spontaneously as fluids, this class of hydrogel composite could have an unacceptably low strength for various technical applications. In the absence of yield stress measurement, the data on $G'(c)$ could be used to evaluate the adequacy of the strength of a given materials or to estimate the solids concentration needed to fabricate a composite for a given service requirement.

It is first necessary to define the critical amount of deformation or strain that can be tolerated in service (γ_{crit}) and then determine whether the stress (τ) encountered in service can cause $\gamma > \gamma_{crit}$. This leads to the concept of the critical modulus that permits the critical strain $G_{crit} = \tau / \gamma_{crit}$. By identifying the low-ω storage modulus in Figure 48 and Equation (5) with G, one thus can obtain G'_{crit} and the corresponding required solids contents c_{crit}.

This general technique will now be used to demonstrate in practical terms the 'solidity'

of these hydrogels.   Considering a cube of dimension b_0 and accepting its strength to be barely sufficient if the force of gravity causes it to collapse only to a height b_1, the resulting body will have an unchanged volume $V = b_0^3$ but expanded lateral dimensions.   The critical strain in compression is thus $\gamma_{crit} = \Delta b / b_0 = (b_0 - b_1) / b_0$.   This condition is defined as a collapse to half the original height, $b_1 = b_0 / 2$ so $\gamma_{crit} = 1/2$.   Gravitational force on the original cube is $F = mg = \rho b_0^3 g$ (ρ = sample density), causing an initial compressive stress $\tau_0 = F / A_0 = F / b_0^2 = \rho b_0 g$ so that the critical compression modulus is $E_{crit} = \tau_0 / \gamma_{crit} = 2\rho g b_0$.   For incompressible materials, the unidirectional modulus (E) in compression or tension is related to the shear modulus (G) by $E = 3G$.   One can also identify the static shear elastic modulus G with the dynamic elastic storage shear modulus $G'(\omega)$ at low ω, from which one obtains $G_{crit} = G'_{crit} = 2\rho b_0 g / 3$.   Next, the $G'(c)$ relationship must be inserted. From Figure 48 and Equation 5, $G'_{crit} = G'(\omega)\exp(A c_{crit}) = 2\rho b_0^3 g/3$, from which $c_{crit} = (2.303 / A) \log (2\rho b_0 g/3 G_0)$.

This result, using the density of water, is superimposed on Figure 48.   For a 1-cm cube, unacceptable solidity ($\gamma_{crit} = 1/2$) corresponds to solids content below $c \cong 1\%$.   The highest-water-content samples ($c = 5\%$) was sufficiently 'solid' to confirm to this criterion, as no slumping was observed with wither the test specimens ($b_0 = h = 0.2$ cm) or the larger bulk materials ($b_0 > 5$ cm).   At $c = 5\%$, G' is found to be about 1300 Pa (see Figure 48) and this equals G_{crit} when $b_0 = 3G' /2\rho g = 20$ cm.   Considering a much larger object, using the same γ_{crit} criterion, for $b_0 = 1$ m such a cube would be stable ($\gamma < 1/2$) for $c \geq 20\%$, predicting that a hydrogel composite of this composition could securely retain an enormous volume of water. The general observation of the $c = 15\%$ samples tested here (which should be slightly weaker than the $c = 20\%$ examples cited above) certainly confirm the 'solidity' of that material when handled as specimen disks of diameter 5 cm and thickness 0.2 cm, with the additional impression that a body of dimension 1 m made of the same material would not have been stable (in agreement with these calculations).   Similarly, handling the $c = 50 \%$ material confirms impressively that it would easily have been stable if 1 m in size.

Time and rate effects in viscoelasticity

Linear viscoelastic properties are expected to depend on t and $1/\omega$ in equivalent ways-i.e., $G'(\omega)$ should have the same value as $G_r(t)$ when $t = 1/\omega$.   This principle can be tested by using Figures 46 and 47 together.   One selects arbitrarily $t = 10^2$ s in Figure 47, corresponding to $\omega = 10^{-2}$ rad/s in Figure 46.

The comparison of $G'(10^{-2})$ with $G_r(10^2)$ shows good agreement for 95% water samples ($G' = G_r = 1200$ Pa) and for 85% water samples ($G' = G_r = 3700$ Pa) but not for 50% water samples.   For the latter, $G'(\omega = 10^{-2}s^{-1}) = 2 \times 10^5$ Pa, while G_r ($t = 10^2$ s) = 4500 Pa.   This discrepancy is likely due to artifacts introduced by anyone or all of the following: loading trauma, slip of the samples during measurements and presence of a yield stress.   For further detail see Gao et al[77].

Conclusions

The bentonite/polyacrylamide composites have the capacity to absorb large amounts of water while retaining good mechanical strength and high damping characteristics, and therefore represent a new and promising class of hydrogel materials.

Rheological results showed a fully cross-linked structure resembling a visco-elastic rubber-like material.   Dynamic and stress relaxation tests showed that the water-swollen poly(acrylamide)/bentonite composite hydrogel behaved rheologically as a viscoelastic crosslinked structure in the range of 50 - 95 % water content.   Frequency sweep and step strain measurements indicated that with increased water content the material responded more quickly

to mechanical deformation.

The strengthening effect of the bentonite concentration was found to be exponential, G' = $G'_0\exp(Ac)$, over a wide range of frequencies of sinusoidal dynamic testing, with a weak ω-dependence appearing as $G'_0(\omega)$ and $A(\omega)$. Further work is needed to explore the factors determining A.

Internal consistency checks of data on $G^+(t)$ and $G'(\omega)$ at various strain levels were shown to be capable of establishing approximate values of τ_y or bounds on τ_y.

The rheological behavior of SAPC hydrogel networks is hence exceptionally resilient when exposed to shear strain with high perturbation frequencies. Even with high water content up to 95% they retain properties resembling those of true solids. In particular, a SAPC block of 1 m side lengths containing 80% of water would be dimensionally stable at a dynamic elastic storage modulus G' of 10 kPa, i.e. it would not slump under its own weight. This opens up very interesting applications in fields where vibration damping is required.

5.1.2 Mechanical properties

Experiments were carried out to evaluate SAPC for applications as actuators responding to the presence of water, for example as safety shut-off valves.

The measurement of the swelling power of SAPC was carried out using equipment shown in Figure 49. The principle is that after water is introduced into the cylinder, the SAPC will swell, and its expansion force will press a given mass upward. In the experiment, the work and power generated by swelling of an SAPC hydrogel was measured.
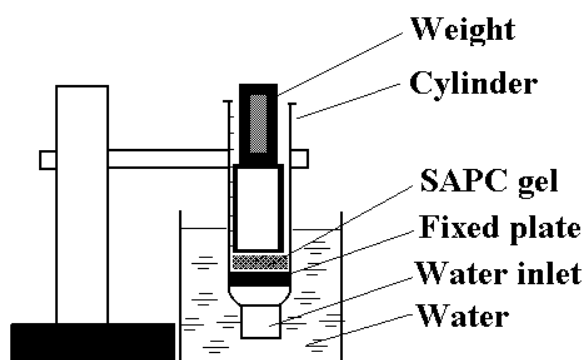
Figure 49. *Schematic setup of the mechanical property measurement of SAPC (power generated by swelling of SAPC)*

The experimental conditions were as follows: weight on the top of the gel disk was 51g; WAC of the gel was 320 g/g (24 h); and the scale on the cylinder was calibrated using standard meter. Samples A to C were SAPC hydrogel blocks (A, B) and membrane (C), respectively containing 70% water. Samples designated by M (Table 15) were dry samples. The results are shown in Tables 14 and 15.

Table 14. Results of mechanical property test

	Work ($J \times 10^4$)	Thickness of SAPC (mm)	Mass of Weight (g)	Swelling time (h)
A	34	2.85	51	23
B	72	2.05	51	70
C	78	0.44	142	23

From above experiments it is obvious that the efficiency of the device depended on the shape and the mass of the gel disks. The swelling speed is yet too slow to build a functional actuator, and needs to be improved by appropriate engineering of the process of SAPC preparation.

A set of membrane samples was prepared with different compositions and cut to disks 1 cm in diameter.   The experimental results are shown in Table 15 which display the work and power generated by swelling of SAPC in standard units.

Table 15.   Expansion work and power of SAPC

No	Work ($J \times 10^4$)	Specific work * ($J \times 10^4$/g)	Power (W)	Specific power * (W/g)	Thickness of SAPC (μm)	Swelling time
A(gel)	34	539	4.1×10^{-8}	6.5×10^{-7}	2900	23 h
B(gel)	72	1546	2.8×10^{-8}	6.1×10^{-7}	2000	70 h
C(gel)	78	7813	9.4×10^{-8}	9.4×10^{-6}	442	23 h
M1001	2	359	1.1×10^{-6}	2.0×10^{-4}	59	4 min
M1018	56	360	2.4×10^{-6}	1.6×10^{-4}	20	4 min
M1020	11	465	4.7×10^{-6}	2.0×10^{-4}	31	4 min
M1014	14	1257	5.9×10^{-6}	5.2×10^{-4}	14	4 min
M1015	17	1206	7.1×10^{-6}	5.0×10^{-4}	15	4 min

Data were calculated by a relation of 1 g.cm/s = 9.80665 $\times 10^{-5}$ W (1 W = 1 J/s).
* Data normalized to 1 g SAPC;   M: dry membrane samples.

From the experimental data above, we can infer that the power generated by an expanding SAPC gel under the set conditions is 6×10^{-7} - 9×10^{-6} W per gram SAPC in bulk and membrane hydrogel state with 70% water, and 1.6 - 5×10^{-4} W per gram of SAPC in dry membrane form.

Big bulky SAPC blocks and longer swelling times can produce higher work. However,

the power (the capacity to do work in unit time) is smaller. The thinner the SAPC material is, the faster it swells and the more power it generates per unit mass.

The relationship of work and power with time are shown in Figures 50 and 51.
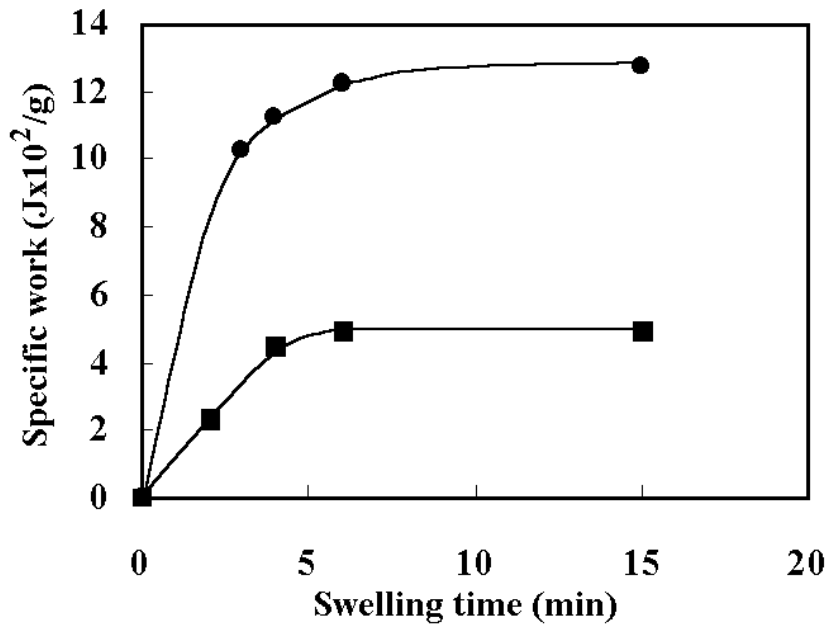

Figure 50. *Specific works generated by the swelling of SAPC. Thickness:* ● 14 μm, ■ 31 μm.
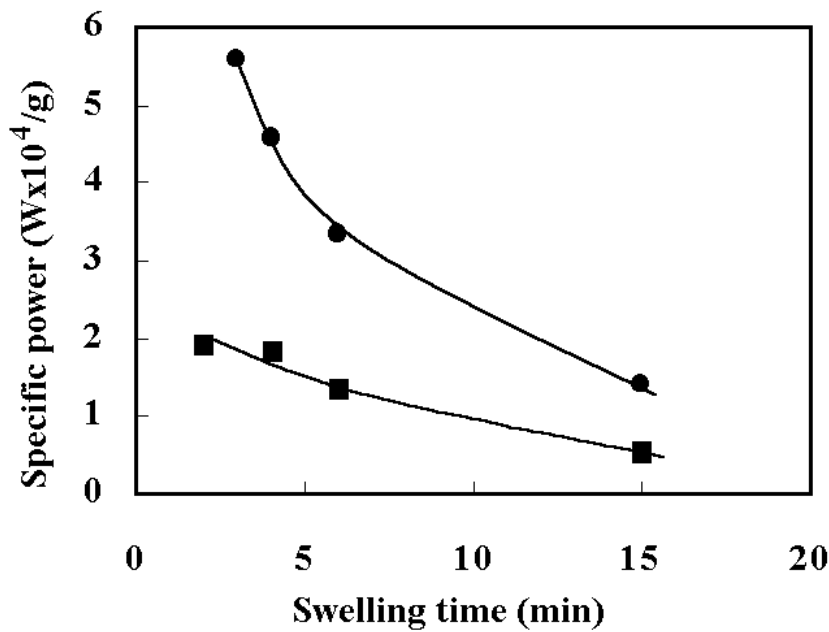

Figure 51. *Specific powers generated by the SAPC. Thickness:* ● *14 μm,* ■ *31 μm.*

The specific work generated by the swelling of SAPC increases with time to a constant value after about 4 to 6 minutes swelling time, but the specific power decreases accordingly.

5.2 Some thermal properties of SAPC

5.2.1 Heat storage capacity of SAPC

This experiment was designed to estimate the heat storage ability of SAPC. The aim of this experiment is to measure the thermal property of SAPC to develop its application in the field of health care, for example to develop efficient heating pads for patients suffering from rheumatism and other ailments for application of constant moderate heat is beneficial.

The experiment conditions were as follow. In a glass vessel preheated to a temperature of 54 °C and equipped with a thermometer, one gram of SAPC and 200 ml of water with the same temperature of 54 °C were added separately. The vessel was then positioned on a thermal insulation plate. The temperature of the water was recorded in a preset time schedule. The temperature of air surrounding the vessel was 20°C. For the purpose of comparison, a blank test was carried out under exactly the same condition but without addition of SAPC. The schematic experimental setup is shown in Figure 52.

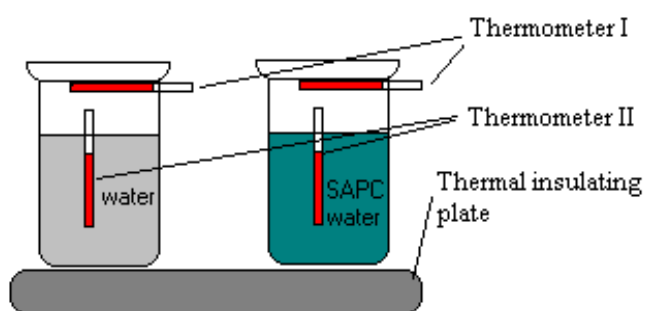***Figure 52***. *Experimental setup to measure the heat storage capacity of SAPC*
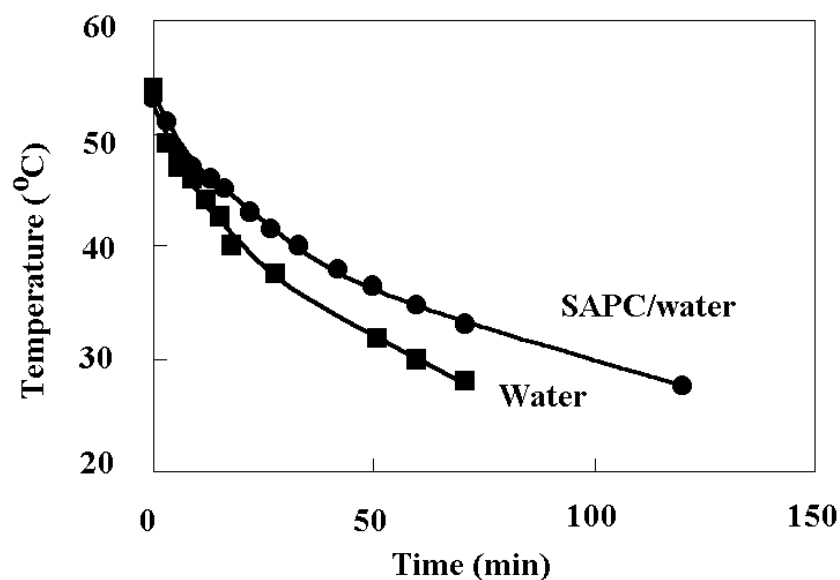

Figure 53. *Temperature retaining properties of SAPC. (environmental temperature: 20 °C)*

The data shown in Figure 53 was measured with the thermometer II (see Figure 52). As shown in Figure 53, the addition of SAPC decreased the heat loss and slowed the temperature drop by a factor of 1.5 - 2.0 times compared to pure hot water.

To compare the heat loss of the two different systems, the temperature above the water level was recorded with thermometer I. Figure 54 shows the temperature difference recorded by thermometer I.
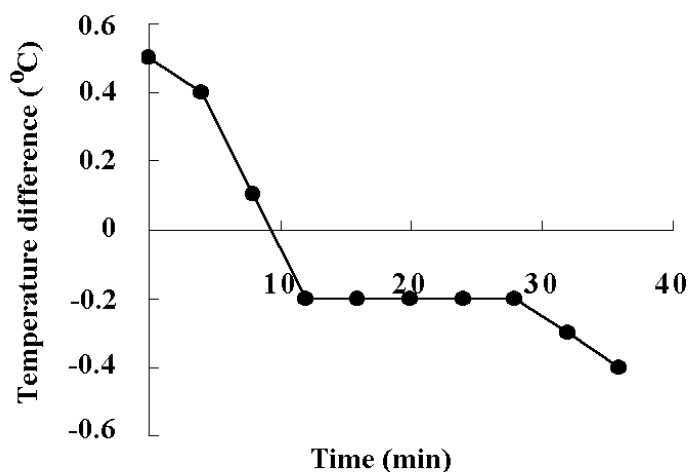

Figure 54. *Temperature difference above the water level of pure water and SAPC-water mixture systems (T$_{water}$ - T$_{SAPC/water}$)*

From Figure 54 it is obvious that at the beginning of the experiment, the temperature above the pure water was higher than the temperature above the SAPC/water mixture system, but, after about 10 minutes, the temperature was lower than that of the SAPC/water mixture system. The reason is probably that at the beginning of the test, although the temperature of the two systems was the same, the temperature above the pure water was higher than that of the SAPC/water system because the pure water system releases heat faster than the SAPC/water system. But, since the temperature drop of the pure water system is faster than that of the SAPC/water system, after a while, temperature in the pure water system dropped which was lower than that of the SAPC-water system, and so did the temperature above the water level.

This suggests that the reason for the SAPC/water system to keep its temperature longer than the pure water system was that the water molecules were blocked in the network of the SAPC and hence their movement was restricted. This prevented heat loss and kept the higher temperature for a longer time. This suggestion is supported by the observation that the temperature in the water system was almost the same from center to surface (homogenous), but in the SAP/water system, the temperature in the center of the glass vessel was much higher than that at the surface of the system. An approximate temperature gradient of 2~3 ^{o}C was observed.

5.2.2. Thermostability of SAPC

The purpose of this test was to estimate the thermal stability of the SAPC. In the experiment, the SAPC samples were treated in an oven with pre-set temperature. After treatment, the WAC of the samples were measured using distilled water to see the effect of heat treatment. After the heat treatment, the appearances of some samples were changed. The results are shown in Table 16.

Table 16. Compositions and the appearances of the SAPCs after the heat treatment

	Composition (%)			120 ^{o}C	170 ^{o}C	200 ^{o}C
	AM	Bentonite	AANa			
a	60	40	-	NC	B	B
b	50	50	-	NC	NC	SB
c	25	-	75	NC	NC	NC
d	75	-	25	NC	B	B

NC: no change; B: bloated; SB: slightly bloated.

Heat treatment changed the appearance of some SAPC. Samples with higher sodium acrylate content showed a higher thermostability.

Table 17. Thermostability of SAPC with different AM/AANa composition

	AM/AANa/Bentonite	170 ^{o}C	200 ^{o}C
e	1 / 4 / 5	NC	NC
f	1 / 1 / 2	NC	NC
g	4 / 1 / 5	NC	B

Table 17 shows the relationship between thermostability and composition of SAPC clearly, i.e. the sodium acrylate component increased the thermostability.

The effects of heat treatment on the water absorption capacities of SAPC are shown in Figure 55.
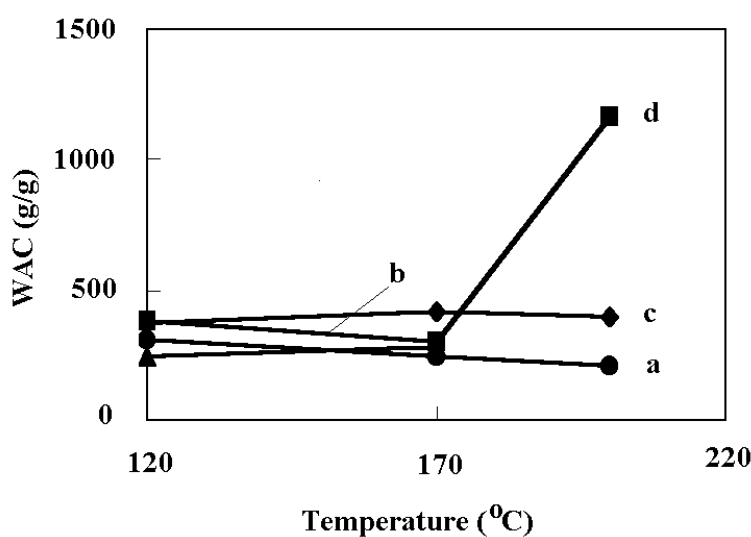
Figure 55. Effect of heat treatment on the WAC of SAPC

From Figure 55 it can be concluded that below 170°C there was no effect of the heat treatment on the WAC of SAPC samples. After the temperature has risen to 200°C, the

WAC of sample d (AM-AANa) rose greatly. This might be caused by the destruction of some of the bonds in the structure during the heat treatment, which decreased the cross-linking density. However, the 200°C temperature treatment had no effect on the other samples. This means that the SAPC in general has a rather good thermostability.

5.3   pH sensitivity of SAPC hydrogels

Because SAPC can be considered a polyelectrolyte, it is sensitive to the ionic strength of the surrounding solution as well as its pH. Investigations of the effect the pH variation has on the swelling capacity of the SAPC were performed using a set of SAPC gels that were contacted at 23 °C with electrolyte solutions having different pH values. After that the water swelling ratios were measured. The pH values of the solutions were adjusted with hydrochloric acid (for pH less than 7) and sodium hydroxide (for pH higher than 7), and monitored with a Metrohm 654 pH-meter. It is well known that the swelling equilibria are determined basically by three different factors: (i) the free mixing enthalpy of the polymer network chains with the solvent, (ii) the osmotic pressure resulting from the mobile counterions surrounding the fixed charged groups within the network, and (iii) the swelling pressure of the polymer network ,i.e. the elastic retractile response of the network.
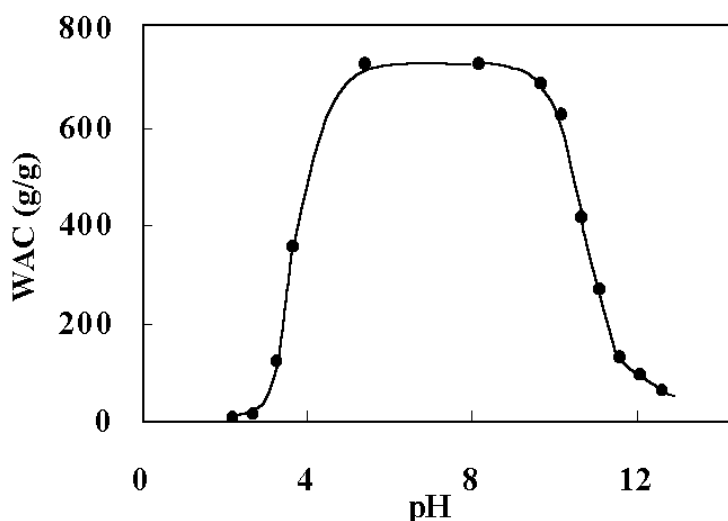
Figure 56 *Dependency of the swelling ratio (grams of water/gram of SAPC) on the pH of the surrounding solution. (Ref. 10)*

It was found that the pH of the solution had a pronounced effect on the swelling equilibrium. Figure 56 shows that the swelling ratio of SAPC was strongly affected by the pH of the solution in contact with the SAPC. The solutions at lower pH had a somewhat stronger effect on the swelling ratio than those at a higher pH. In the pH range between 5-10, the water absorption capacity (WAC) reached a maximum while below a pH of 5, the capacity began to decrease and stabilized at a very low level pH = 2.   This was presumably due to the fact that on the pH decreases, the sodium carboxylate group on the polymer network was protonated. This in turn decreased the degree of ionization and the charge on the network hence decreasing the swelling ratio. The behavior of the absorption capacity in the alkaline region was symmetrical to that in the acidic region. At pH=14, the swelling capacity decreased to nearly zero. Here, the pH increase led only to an increase in the charge density of the surrounding solution that increased the degree of ionization of the network. As a result, the swelling ratio did not decrease as dramatically as in the lower pH region.
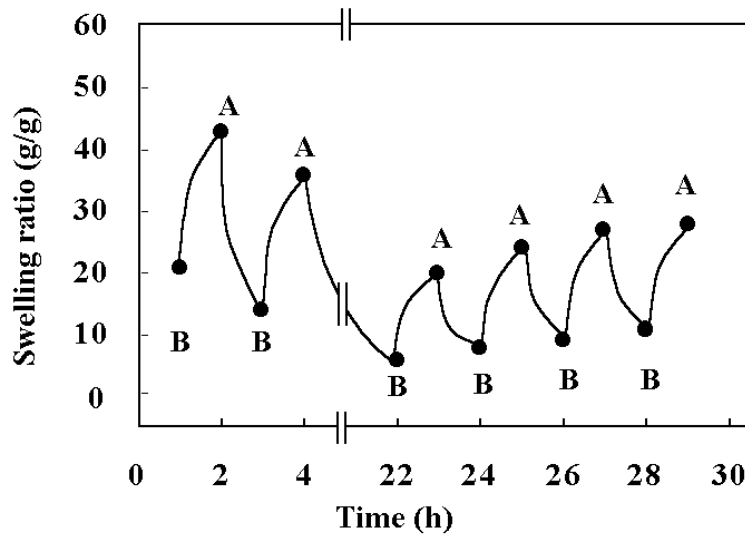
Figure 57 *Dependency of the swelling ratio (grams of water/gram of SAPC) on the time in pH cycling tests (A: pH = 3.6; B: pH = 2.5). (Ref. 10)*

In order to study the response of the system to cycling of the pH of the solution, pH-values of 2.5 and 3.6 were selected as alternative test points. The experimental procedure was to put a piece of SAPC hydrogel into the solution of pH 2.5 for one hour, weigh it and, after washing it with distilled water, put it into a solution of pH 3.6 for another hour. Figure 57 shows the effect of pH cycling on the swelling ratio. Note that the swelling ratio is lower than that shown in Figure 56, because the gel was contacted with solution for only one hour and is thus not saturated. It can be seen that this treatment had an obvious effect on the swelling behavior of the SAPC gel. By controlling the pH of the solution it is possible to control swelling (expanding) and shrinking (contracting) of the gel. This property of the SAPC could be used, for example, in applications such as the design of physiologically sensitive controlled drug delivery device, and could also be used as a chemomechanical material to convert chemical energy changes into mechanical movement for sensor or actuator applications simulating muscle activity and acting as chemical valves or oscillating switches[29]. However, at this point in time the rate with which a saturation equilibrium is being reached is still too low to seriously consider applications in which this property can be meaningful exploited.

5.4 Salt Effect

Because the SAPC is a kind of polyelectrolyte, it is very sensitive to the electrolyte concentration of the solution. Based on the simplified Flory swelling equation (cp eq. (1))

$$Q_m^{5/3} \cong A/S + B \qquad (6)$$

where $A = (i/2Vu)^2/(v/V_0)$, and $B = (1/2 - X_1)/V_1]/(v/V_0)$.

the swelling ratio Q is proportional to the 3/5 power of the reciprocal ionic strength, S i.e. it obeys approximately a relationship of $Q \propto \sqrt[5]{1/S}$. From this equation, we infer that Q will sharply drop at the very beginning when putting a small amount of salt into solution although in practical terms, Q is not correctly proportional to the reciprocal ionic strength in 3/5 power due to a slight change of parameter x_1 which is caused by the change of concentration. Usually, when a SAPC sample with a WAC of more than 1000 g/g in pure water is put into a saline solution, the WAC will drop to several tens g/g. This phenomenon, is usually called the 'salt effect'.

The salt effect has been studied by changing the type of ionic charge (positive or negative such as sulfonate or alkyl groups containing monomers)[80] and ionic strength etc. From a different point of view, here two different methods to study the salt effect were used: one was using a dry SAPC sample; and the other was using swollen ones.   Table 18 and Table 19 show that the salt concentration has a great effect on the WAC of SAPC in either case.   In the first case (Table 18), the SAPC was gradually swelling up to a balanced value of WAC and then stopped; while in the later case (Table 19), though the samples were saturated with distilled water and absorbed a great amount of water before being put into the saline solution, it would release the water that it absorbed and thus decrease the WAC value down to the same value as in the first case. This means that the WAC of a sample is only a function of the salt concentration and other inherent properties.   It will not be affected by the swelling route.

Table 18. Effect of the salt concentration on the WAC of dry SAPC

	Salt concentration (%)				
	0	0.1	0.9	2.9	10.0
W(g/g)	1251	219	86	60	47

Table 19. Effect of the salt concentration on the WAC of the swollen SAPC

	Salt concentration (%)		
	0	1	3
W1	1251	83	58
W2	852	72	53
W3	383	54	41

5.5   Electric properties of SAPC hydrogel

Some hydrogels show sensitivity to electric field changes[29] that influence swelling and shrinking properties of the gel by altering the content of absorbed water, thus changing the physical sample dimensions. Different rates of movement of ions in the outer and inner parts of the material, affected by the electric field, generate a stress field that gives rise to molecular rearrangement by expansion or contraction.   This can in principle be used to create hydrogels simulating the action of muscles or tendons.

To study the behavior of the material in an electric field, a D.C. electric supply with a pair of electrodes was utilized whose electric potential could be varied between 1 and 15 volts and its current between 0-1 amperes. The direction of the current could be changed as well.

Solutions with concentrations of 0.1 mol/L of different cations and anions were used. In the cationic groups, Na^+, K^+, Ca^{++}, Mg^{++} and Fe^{+++} were used with only Cl^- as counterion in solution. In the anionic group, Cl^-, Br^- and NO_3^- were used with Na^+ as counterion in solution. The results of the tests are shown in Table 20. The one-valent cations showed a larger effect than

the two-valents and three-valents cations. This resulted from the lower absorption capacity of the gels for the high valent cations which could induce physical cross-linkage of the function groups on the surface of the gel. It is obvious that under the conditions selected in multi-valents cation solution, the gel shrank only weakly if at all.

Table 20. Relative mass change (%) of a SAPC strip immersed in 0.1 mol/L solutions of various cations (counterion: Cl^-) and anions (counterion: Na^+).

Charge	K^+	Na^+	Ca^{++}	Mg^{++}	Fe^{+++}	Cl^-	Br^-	NO_3^-
Relative mass change (%)	7.2	5.6	0.9	0.9	0	5.6	0.9	4.4

Electric potential of 12.5 V for 2 min.

Before applying an electric field, the SAPC hydrogel was cut into bar shape and was saturated with a solution that would be used in the electric field experiment later. The gels showed a large variety of electric field responses depending on the nature of the surrounding solution. In NaCl solution at a constant electric field, the SAPC gel swelled adjacent to the negative pole, but shrank adjacent to the positive pole. The magnitude of these changes depended upon the value of the electric potential, the current strength and the charging time.
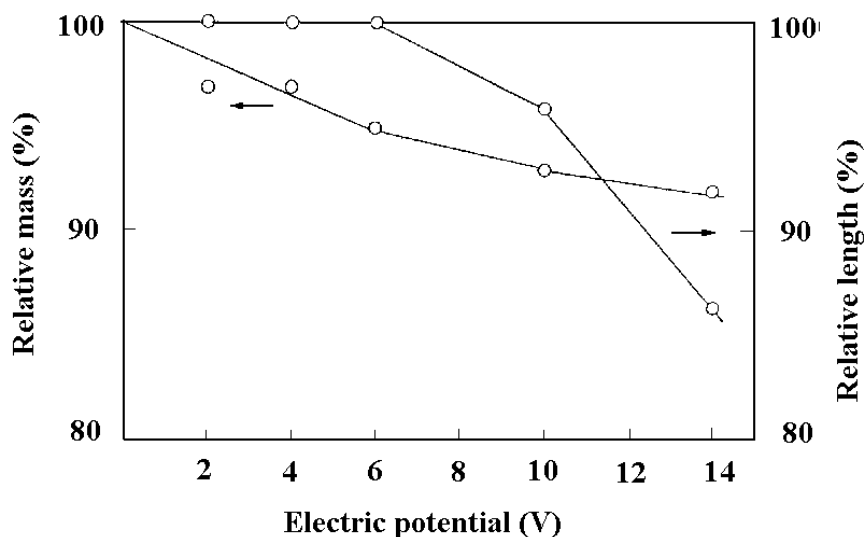
Figure 58. *Changes in mass and length of a SAPC strip as a function of the electric potential (t=2min). (Ref. 10)*
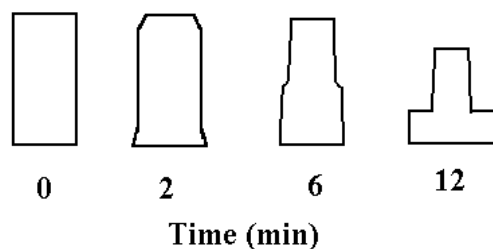
Figure 59. *Schematic illustration of the electric field effect on a strip of SAPC.*

In gel collapse experiments in distilled water, the samples were cut to a prismatic shape with dimensions of 20 x 8 x 8 mm. The two ends of the gel bars were compressed to fit onto a pair of electrodes made from graphite with the size of 50 x 30 mm. Figure 58 shows the change in mass and length of a SAPC hydrogel sample as a function of the electric potential. The

collapse of the gel was accelerated by the voltage increase of the electric field beyond 6 volts. A different trend was observed in the experiments using the charging time as a variable. Figure 60 shows a linear relationship between the change in weight and length, and time. The shape and the geometrical dimensions of the originally prismatic SAPC gel sample changed over time as shown schematically in Figure 59. These changes are dependent on the conductivity of the solution. They were observed in saline solutions regardless whether the electrodes touched the gel samples or not. In distilled water, however, contact between the electrodes and the sample was required to affect the collapse of the gel. In addition it was observed that the ionic strength of the surrounding solution strongly affected the rate of gel collapse, being accelerated in solutions with high ionic strength.

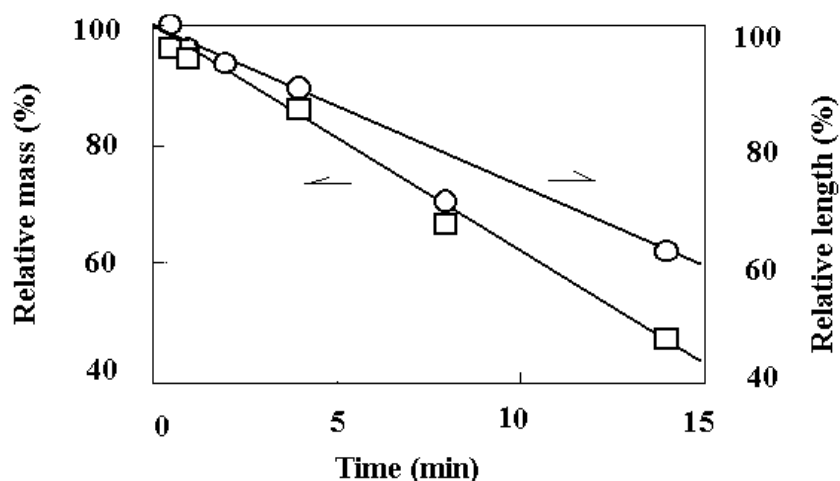***Figure 60*** *Changes in mass and length of a SAP strip as a function of time (V=14V). (Ref. 10)*

To test the chemomechanical properties of the material in a second set of experiments, flat gel samples were cut with a 820 Rotary Microtome (Scientific Instruments). To detect the expected effect, the gel was held between two electrodes in a D.C. field whose polarity could be reversed. The mechanism of the chemomechanical properties of the SAP hydrogels is presumably related to the movement of ions in the outer and inner regions of the gel. In equilibrium with water or an electrolyte solution, the absorption capacity of a gel is related to the ionic strength of the solution and the structure of the gel by the Flory equation. The equation can be reduced to

$$Q^{5/3} = A\mathbf{i}^2/\mathbf{S} + B, \tag{7}$$

where $A = (1/2V_u)^2/(v/V_o)$, $B = (1/2 - X_1)V_1/(v/V_0)$.

The driving force for the SAPC gel to move under a chemomechanically induced stress is related to differential expansion (swelling) and contraction. The swelling equilibrium is then determined by the osmotic pressure and the elasticity. When a gel in solution is subjected to an electric field, the anions and cations in both the solution and the polymer network are being attracted to the corresponding electrodes. Hence the initial swelling equilibrium will be broken, and to establish a new equilibrium the gel is forced to expand or contract. Three classes of surfactants were studied: anionic (sodium lauryl sulphate, sodium octanesulfonate), neutral (Triton X100), and cationic (dodecyl-ethyldimethylammonium bromide, tetrapropylammonium bromide). In neutral and cationic surfactants, the cations tend to go to the negative electrode and the anions to the positive electrode as well in solution as in the SAPC gel. Since the concentration of cations in the SAPC gel at the negative pole is

much higher than at the positive pole due to the electric field attraction, the gel will expand in order to react to the charge density difference established between outer and inner parts of the gel. On the other hand, the gel will contract at the positive pole. As a net result, the gel strip will bend towards the positively charged side. Figure 61 shows a photograph of an actual experiment showing the bending of a SAPC strip in an electric field at a potential of 14 volts applied for 30 seconds in an anionic surfactant (sodium laurylsulphate, 0.02mol/L). The central picture refers to uncharged situation. In the left picture, the positive pole is on the right side, in the right picture, the positive pole is on the left side. The SAPC gel strip shows bending away from the positive pole towards the negatively charged side.   This unexpected behavior requires additional investigations.
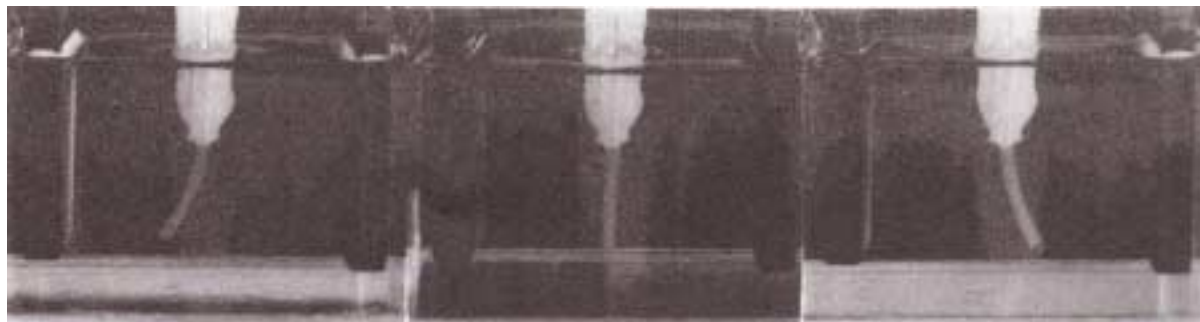

Figure 61. *Bending of a strip of SAPC in an anionic surfactant in an electric field (U = 14 V, 0.5 min). (Ref. 10)*

6.0   APPLICATIONS OF SAPCs

6.1   Application in enhanced oil recovery (EOR)

The oilfield experiments using SAPC as plugging agent were carried out in Jilin[81], Daqing[82], Panjin[83] oil fields to meet the need of enhanced oil recovery (EOR)[84].   After long year operation of water flooding, the water content in crude oil increased which actually decreased the oil output. The higher water content in the crude oil may cause many problems such as increased corrosion, sand production, emulsion formation and disposal, etc.   It is an urgent need to reduce the water content in the crude oil.   One of the methods to reduce the water content is to adjust the oil pay in the oil-producing well.   Requirement for the SAPC used for the deep cross-section adjustment of the underground in the water injection well must have several characteristics such as control of the product particle size, water swelling capacity, initial swelling speed, temperature resistant property, salt resistant property, degradability etc. The experiment on the well-core showed that the weak cross-section adjustment agent gel having a property of larger touch-deformation was good for the enlargement of the distance and dimension.

SAPC used in the experiment has the following technological requirements e.g. controllable particle size, proper WAC, and swelling speed.   Furthermore, during the whole process of injection (20-180 min) the swelling rate must be controllable.   The product's salt resistance should be less affected by the mineral content of the water, and hence the SAPC should be suitable for plugging and cross-sectional adjustment of the oil production well in high-salt oilfields.

The experiments on migration performance of SAPC hydrogel particles in porous media for plugging application was carried out using well core. After driving the oil in the forward direction, the plugging agent was injected reversibly. The result showed that in the

well core with lower permeating rate, the outflow decreased with increasing injection time.

The fluidity of hydrogel particles was monitored by the changes of the pressure during different injection periods. In the pre-water driving, pressure was kept on a constant value.   However, in the particle injection, the general trend was an increase in pressure but with large excursions. There were oscillations caused by the movement of particles in the pore space or pore throats. The pressure decreased with the outflow of the particles from the well core.   It shows that the particles have an effect on plugging and migration movement.

The effect of hydrogel particle on the recovery ratio tested using replicated sand-filled pipes showed that the particles could preferably improve the flow direction of liquid and increase the crude oil recovery ratio. Using these sand filled pipes, oil driving property of hydrogel particles was measured.   Results showed that the hydrogel particles had a preferable oil-driving effect on oil recovery ratio and could decrease the residual oil in the driving water.

Influence of the injection speed on the injection pressure showed that at low injection rate the change of injection pressure was small and reached gradually an equilibrium.   When the injection rate was high, the injection pressure went up quickly, the pressure fluctuated and showed an upward trend.   Therefore, to maintain a large amount of injected particles, low flow rate injection should be used.

Effect of the particle concentration on the injection quantity showed that different particle concentrations had different effects on the water injection pressure and the plugging effect.   The higher the injection concentration is, the faster the pressure goes up due to the particles resorted on the entrance.   The pressure after the injection in the case of high concentration injection decreased quickly and went down to the level of low concentration injection.   Hence the plugging effect of high concentration was almost the same as that of low concentration injection.   This means that the high concentration is not favorable to the injection and that to achieve large amount of particle injection, it is necessary to use a low concentration injection method.

The oilfield experiment in Jilin oilfield (ninety three wells were treated using SAPC to adjust the water absorbing formation of the water well) had an effective ratio of the treatment of 100%. Without taking other major steps, the oil output in all oil wells around the water wells has obviously improved. The average increment of oil output was 220%.   This technology also was used in other oilfield such as Panjin Oilfield and Daqing Oilfield etc. The SAPC showed a high application potential in the EOR.

6.2   Mine waste treatment

Acidic drainage resulting from the oxidation of sulfide minerals is the single largest environmental problem facing the world mining industry today. Sulfide oxidation, which generally occurs at shallow depths above the water table, can result in the production of highly acidic pore water containing elevated levels of many heavy metals and other deleterious constituents. It is generally agreed that the production of acid is controlled by the availability of the oxygen at the sulfide surface. In tailings the primary mode of oxygen transport is diffusion through porous spaces. The recognition of this process has led to the suggestion of a multi-layered barrier which can minimize the amount of air infiltration[85,86]. Experimental studies based on this concept are being conducted at Noranda Technology

Center[87-89].   In this concept, a layer of fine silt or clay material is underlain by a layer of coarse sand. The layers would be placed in such a way as to enhance drainage of the coarse layer, thereby lowering the effective hydraulic conductivity to near zero as it approaches residual saturation. At this state (residual saturation), the coarse layer can not transmit moisture downward from the upper layer. The upper fine layer therefore can maintain full saturation over a prolonged period of time.

There is a large amount of mine waste in Canada which generates a big problem of acid drainage. The treatment of mine waste is of great importance in the view of environmental protection. Attempts have been made to attack the problem by covering the mine waste with SAPC.   Within the MEND (national Mine Environment Neutral Drainage) New Ideas initiatives, SAPC is used for the abatement of acid mine drainage.   When the SAPC fully hydrated, it can adsorb large amount of water and increases its volume significantly during the process. This very property of SAPC could be very useful in the area of acid tailing abatement. First, if a layer of SAPC-bearing composite material is placed on top of the acid tailings, the composite layer may constitute an impermeable barrier. This is because the high water-absorption capacity, strong moisture retention capability and large swelling pressure of SAPC will virtually "seal off" the tailings. Secondly, if a layer of SAPC-bearing composite material is placed at the bottom of a tailing pond as a liner, the composite material may prevent the seepage of the acid leachate into groundwater. The potentials of both options are evaluated.

The purpose of Phase I of the "impermeable Modified Clay Barrier" project is to demonstrate the effect of SAPC on the hydraulic conductivity and moisture retention characteristics of the cover material. In this chapter, the following aspects will be discussed: 1) methods and results of hydraulic conductivity and moisture retention tests, 2) the implication of the experimental results, and 3) a preliminary economic analysis of the SAPC application.

As the WAC of a pure bentonite is only about 10 g water/g. The WAC of the SAPC is about two orders of magnitude greater than bentonite. However, the salt effect can reduce the WAC of SAPC to one tenth if the water contains salts such as NaCl and $CaCl_2$ etc. From the results of pH effect on SAPC (see Figure 56), it is obvious that the hydration of SAPC is affected by both acidic and alkaline solutions and this detrimental effect is somewhat more pronounced in the acidic range than in the alkaline range. However, to keep things in perspective, it should be noted that in acidic solution with pH of 3.5, the WAC is still greater than 100 which is much greater than that of bentonite. The acidic solution is equally detrimental to the hydration of clay minerals.

To appreciate the effect of hydration of the SAPC on the hydraulic conductivity of a cover material, an artificial case should be considered. 1000 cm^3 of a porous medium (sand) with 40% of porosity and particle density of 2.60 g/cm^3 has a pore volume of 400 ml and total weight of the solids of 600 cm^3 x 2.6 g/cm^3 = 1 560 g. If one twentieth weight percent (0.05 wt%) of the solid is SAPC, the SAPC will weigh 1560 g x 0.05% = 0.78 g. upon hydration in fresh water. The SAPC will adsorb 0.78 g x 680 g/g = 530 g of water and the volume of the gel will be about 530 ml. Therefore the SAPC gel will be more than enough to fill out all the pore space in the porous medium. In reality, the WAC of the SAPC will be much less depending on the ionic strength of the solution. Nevertheless, this calculation does illustrate the high potential for SAPC to reduce the hydraulic conductivity of a porous medium. Based on this analysis, 1 wt% of SAPC was added to the sand and tailings in the experiments.

6.2.1   Experimental Methods

Materials

The materials used in this study include silica sand, bentonite clay, the SAPC, and acid tailings. The silica sand is commercial grade of 30-60 mesh (0.27-0.6 mm)size and was purchased from Sil Silica Inc. of Edmonton. The sand was used as received. The bentonite was purchased from Ward's. The X-ray diffraction analysis indicates that the sample contains a significant amount of quartz but no effort was made to purify the sample. The bentonite was used as received. The granular SAPC particles were ground to pass 325 mesh size sieve. The tailings are from Waite Amulet mine and were supplied by Noranda Technology Center. For moisture retention and hydraulic conductivity measurements, the tailings as received were oven-dried at 103°C overnight and aggregates larger than 1 mm were removed. The grain (particle) density of the tailings was measured using the standard "Density Bottle Method"[90] and found to be 3.09 g/ cm^3. The particle size distribution was determined by conventional sieving (for greater than 20 µm particles) and gravitational sedimentation (for less than 20 µm particles) methods. The tailings are composed of mainly silt and fine sand fraction as shown in Figure 62.
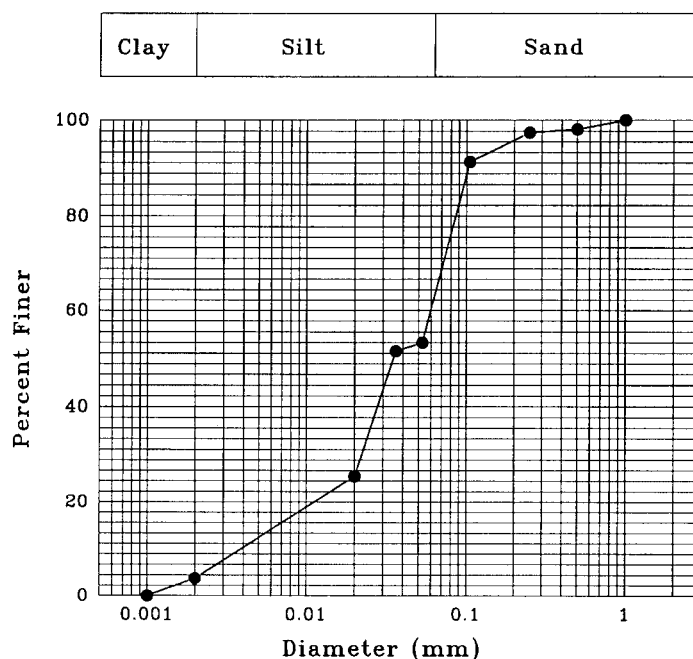
Figure 62. *Particle size distribution of the tailings.*

Seven samples were used for hydraulic conductivity measurements and six samples were used for moisture retention. These samples are: A) Silica sand (35-60 mesh); B) 99 wt% silica sand plus 1 wt% SAPC; C) 90 wt% sand plus 10 wt% Wyoming bentonite; D) Oven-dried acid tailings; E) 99 wt% tailings plus 1 wt% SAPC; F) 90 wt% tailings plus 10 wt% Wyoming bentonite; and G) 89 wt% tailings plus 10 wt% silt fraction and 1 wt% SAPC.

One weight percent SAPC was chosen for the reason stated in the previous section. Ten percent of bentonite were used because a composite mixture containing 8% bentonite is being investigated by Noranda Technology Center.   The bentonite sample used in this study contains some quartz. The bentonite concentration in the samples is thus comparable to that used by Noranda Technology Center.

6.2.2 Hydraulic conductivity measurement

The apparatus used to determine the hydraulic conductivity consists of a tube containing the porous medium, a fluid delivery and collection system, and pressure monitoring devices to determine the head loss during flow (Figure 63). The porous medium was contained in a stainless steel tube 305 mm long by 22.1 mm I.D.. The tube had sintered stainless steel frits with a nominal 10 micron pore size to contain the particulates at both ends. Near each end of the tube, there is a set of pressure taps at the side of the tube, connected to two differential pressure (DP) transmitters which measure head loss during flow. The pressure taps were spaced 195 mm apart. The two sets of DP cells have working ranges of 20 kPa and 200 kPa, respectively. The head loss was used to calculate the permeability of the pack. Pressure transducers at the inlet and outlet end of the tube also measured the flow pressure up to 5 MPa. A bypass line with an isolation valve connected the inlet and outlet ends of the flow tube. This line was used only during the saturation stage of the experiments.
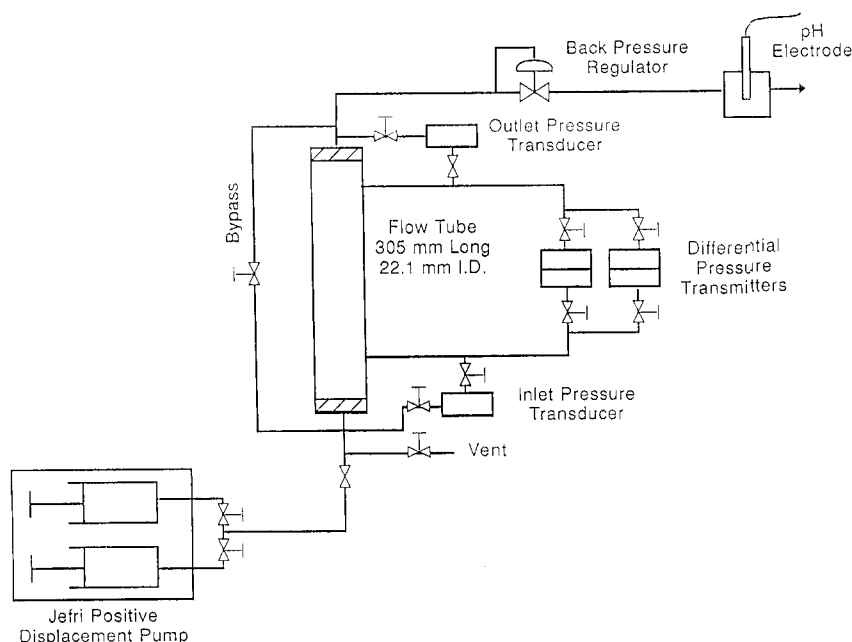
Figure 63. *Experimental apparatus for hydraulic conductivity measurements.*

A back-pressure regulator at the outlet end of the tube maintained the static fluid pressure at approximately 1 MPa. A syringe pump was used to inject de-ionized water into the porous medium at a constant rate over the course of the experiment. In a stable thermal environment (constant temperature), the pump was capable of fluid delivery as low as 0.1 cm^3/h at elevated pressures.

During packing, the flow tube was held in a vertical position in a vise and grounded to earth. Otherwise, a static charge will build up as a result of pouring the loose material into the tube. By grounding the tube, the static is discharged and this allows for a repeatable pack consistency.

The porous medium was slowly poured into the tube through a funnel while tapping on the vise with a mallet. After the tube was filled to the top, tapping was continued and more material added until there was no further change in the level of material in the tube. The weight of the porous medium was determined by difference between the weights of the empty and filled tube. Porosity of the pack was determined from the weight and grain density of material

in the tube and the volume of the tube.

After a sample was packed, the tube was mounted in the flow system. Air was displaced from the pack by flowing carbon dioxide through the tube. The tube was then evacuated to remove the carbon dioxide. In this way residual carbon dioxide that was not evacuated dissolved easily into the water as the core was saturated and was readily displaced as water flowed through the tube. The de-ionized water was then injected into both ends of the tube at a low rate to minimize the possibility of fines transport through the pack. The higher permeability sand and tailings packs saturated very quickly. For the samples containing bentonite and the SAPC, the saturation of the pack took several hours or more. After saturation, the flow rate was fixed. The flow pressure fluctuated at the beginning and then stabilized. The flow rate and differential pressure data were used to calculate the hydraulic conductivity of the sample with Darcy's law. The procedures were repeated several times by changing the flow rate to ensure that the hydraulic conductivity calculated was independent of flow rate.

Moisture retention curves

Moisture retention measurements were performed on six samples (A to F see p.86) using a standard "Pressure-Plate Extraction" method[91] . In this method, a sample is placed in a rubber ring which sits on a porous ceramic plate. The sample and the porous plate are then saturated from below. The plate is covered using a plastic sheet to prevent evaporation. After 24-hours or longer saturation, the plate is placed into a pressure pot. The pressure pot is sealed off and a gas pressure is applied to drive water out. When outflow has ceased, the sample is transferred to a tarred drying can and weighed. Then the sample is oven-dried at $105^{\circ}C$ and reweighed. The moisture retention is expressed as the equilibrium water content at a given pressure:

$$\text{Moisture retention} = [(\text{Weight}_{wet} - \text{Weight}_{dry})/\text{Weight}_{dry}] \times 100\% \qquad (8)$$

Each sample was run in duplicates and at five different equilibrium pressures (0.10, 0.33, 1.00, 5.00, and 15.00 bars).   In total, 30 tests were conducted in duplicates.

6.2.3   Experimental Results

Hydraulic conductivity

The results of the hydraulic conductivity tests are shown in Table 21. Samples A, B, and C are sand-based and the pure sand sample (A) provides a baseline for this group of samples. When packed, the medium size sand had a porosity of 36.5%. The saturation of this sample was very fast (in minutes). At a fixed flow rate, the differential pressure was fairly stable. Small variations in permeability may be due to temperature fluctuation or other instrumental deviations (Figure 64).

The permeability is calculated using Darcy's law:

$$\kappa = (Q/A)(\Delta l /\Delta p)\eta \qquad (9)$$

where κ is the permeability, Q the flow rate, A the cross-section area of the tube, Δl the distance between the pressure transducers, Δp the differential pressure, and η the viscosity. The hydraulic conductivity (K) is related to permeability by:

$$K = (\rho g/\eta) \kappa \qquad (10)$$

where ρ is the density of the fluid, g the gravitational constant. For water at room temperature, $\rho g/\eta$ is 10^5 s/cm. Therefore, if K is in cm/s and κ is in darcy (1 darcy (d) = 9.87×10^{-9} cm^2), K(cm/s) = $10^{-3} \kappa$ (d) or $10^{-6} \kappa$ (md).
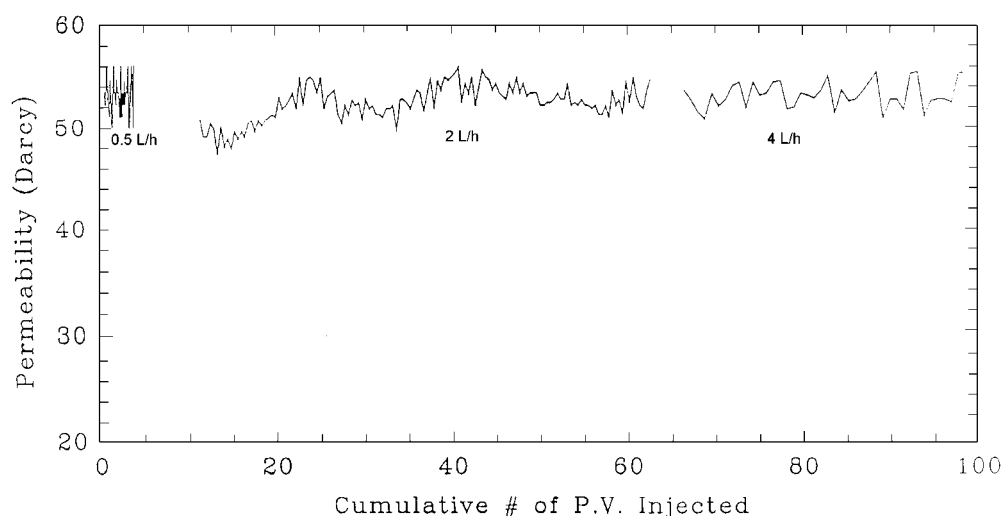
Figure 64. *Permeability of sample A (sand) to DIW at room temperature.*

When the flow rate changed from 0.5 l/h to 2.0 l/h and then to 4.0 l/h, the permeability stayed at 53 Darcy (or hydraulic conductivity at 5.3×10^{-2} cm/s) which is reasonable for this material. When 1 wt% of SAPC is mixed with the sand and packed (sample B), the porosity changed very little but establishment of saturation took much longer (a few hours). The permeability after the saturation was about 3 md (or hydraulic conductivity of 3×10^{-6} cm/s) but it slowly decreased to 1.9 md (or 1.9×10^{-6} cm/s) in 72 hours. This may indicate that the bulk of the SAPC was hydrated in a few hours but a small fraction of the SAPC was still hydrating and expanding in days. The hydraulic conductivity dropped four orders of magnitude from the pure sand. When the sample was removed from the tube after the hydraulic conductivity test, it showed some physical cohesiveness. When air-dried, the sample slowly became semi-consolidated. For sample C, the addition of 10 wt% of bentonite decreased the porosity to 33.1% but its hydraulic conductivity of was still twice as much as that of sample B. The effect of SAPC on hydraulic conductivity of the quartz sand is therefore at least 10 times greater than bentonite.

When packed, the tailings-based samples (D, E, and F) had larger porosity values than the sand- based samples. This is consistent with the fact that the particle size of the tailings is smaller than that of the sand used in this study. The pure tailing sample (D) had a porosity of 40.0%. The tailings must contain a significant amount of soluble material because the effluent was brownish in color and carried some fine particles. As a result, the permeability slowly increased over the course of the test. After 42.4 hours and 56.8 pore volume (pv) throughput, the test was terminated and the permeability at that point was 130 md (or hydraulic conductivity of 1.3×10^{-4} cm/s).

Table 21.   Porosity and hydraulic conductivity of test samples

Sample	Composition (wt%)					Porosity %	Throughput pv	Permeability md	Hydraulic conductivity cm/s
	Sand	Tailing	Clay	SAPC	Silt				
A	100	-	-	-	-	36.5	92.3	53000	5.3×10^{-2}
B	99	-	-	1	-	36.3	4.4	1.9	1.9×10^{-6}
C	90	-	10	-	-	33.1	17.7	3.9	3.9×10^{-6}
D	-	100	-	-	-	44.0	56.8	130	1.3×10^{-4}
E	-	99	-	1	-	43.9	63.2	180	1.8×10^{-4}
F	-	90	10	-	-	44.8	21.0	28	2.8×10^{-5}
G	89	-	-	1	10	30.1	2.4	<0.1	$<1.0 \times 10^{-7}$

When 1 wt% of SAPC was mixed with the tailings, the porosity was virtually unchanged. The effluent was still brownish and the hydraulic conductivity also increased with time. After 69.42 h and 63.2 pore volume, the test was terminated and the permeability at this point was 180 md (or hydraulic conductivity of 1.8×10^{-4} cm/s). This hydraulic conductivity value was even larger than that of the pure tailings but this increase was likely due to a greater amount of dissolution of the tailings during the much longer testing period and the larger throughput of fluids. In any case, it is fair to conclude that the effect of the SAPC is very limited when mixed with acid mine tailings. In contrast, when 10 wt% Wyoming bentonite was mixed into the tailings (sample F), the hydraulic conductivity decreased about one order of magnitude. Nevertheless, this decrease is still small compared to that of the sand-based system where a four orders of magnitude decrease was achieved.

The last permeability test (sample G) was performed to demonstrate that the performance of the SAPC might be improved if a sand sample contains some silts. The sand used in samples A, B, and C have a narrow size distribution (35 - 60 mesh).   Natural sand have a wider size distribution. Thus, when adding 10 wt% coarse silts (270 mesh) into sample G, the amount of SAPC was still 1 wt%. When packed, this sample had a quite low porosity at 30.1%. The saturation of this sample was very slow and the permeability was very low. At the very small flow rate (0.6 ml/hr), the accuracy of the syringe pump depends on a stable temperature over the course of the test. Because the temperature could not be controlled accurately during the test, only an upper limit of the permeability could be estimated at extremely low flow rates. Conservatively speaking, the hydraulic conductivity of this sample is less than 1×10^{-7} cm/s.

Moisture retention

The moisture retention results are shown in Table 22 and Figure 65. For pure sand (sample A), its moisture retention capability is very small even at very low pressure (1.2% at 0.1 bar). When 1 wt% SAPC was added (sample B), the moisture retention can be improved significantly. At each of five equilibrium pressures, the water contents of sample B (sand plus SAPC) are 20 times greater than sample A (sand only). Sample B and sample C (sand plus

bentonite) are comparable, indicating that the moisture retention capability of 1% SAPC is equivalent of 10% Wyoming bentonite. It should be noted that the equilibrium pressures used here are high. At lower equilibrium pressures, the moisture retention of the SAPC could be even better because the water adsorption capacity of the SAPC at zero pressure is very large. On the other hand, no significant improvement is shown when the SAPC is used with acid mine tailings. The moisture retention capability of sample E (tailings plus SAPC) is similar to that of sample D (tailings only), and both of which are a few percent less than sample F (tailings plus bentonite).

Table 22.   Moisture retention

Sample	Composition wt%					Equilibrium Pressure (Bars)				
	Sand	Tailing	Clay	SAPC	Silt	0.1	0.33	1.0	5.0	1 5
A	100	-	-	-	-	1.2	1.1	0.6	0.5	0.5
B	99	-	-	1	-	30.7	26.8	25.0	10.6	9.2
C	90	-	10	-	-	32.8	27.7	25.3	18.9	12.7
D	-	100	-	-	-	32.5	25.0	19.5	9.7	6.1
E	-	99	-	1	-	34.7	32.1	17.5	9.0	6.2
F	-	90	10	-	-	38.4	31.9	23.4	13.0	8.9

The moisture retention of sample G was not measured but it would have the best moisture retention among all the samples tested here.

A comment should be made here about the moisture retention results for the tailings-based samples. Because the tailings contain a significant amount of soluble materials, and some of these soluble materials are hydrated minerals (e.g. gypsum), during oven-drying these minerals will dehydrate. The weight loss from the mineral dehydration is included in the term (Weight$_{wet}$- Weight$_{dry}$) of equation (8). For instance, gypsum ($CaSO_42H_2O$) will dehydrate to anhydride ($CaSO_4$) at 60-70°C and this is accompanied by a 20% weight loss. The chemically bonded water lost during oven-drying would be recorded as physically adsorbed water in this conventional method for moisture retention measurement. Because of this, the reported moisture retention of the tailings-based samples could be significantly higher than actual values.
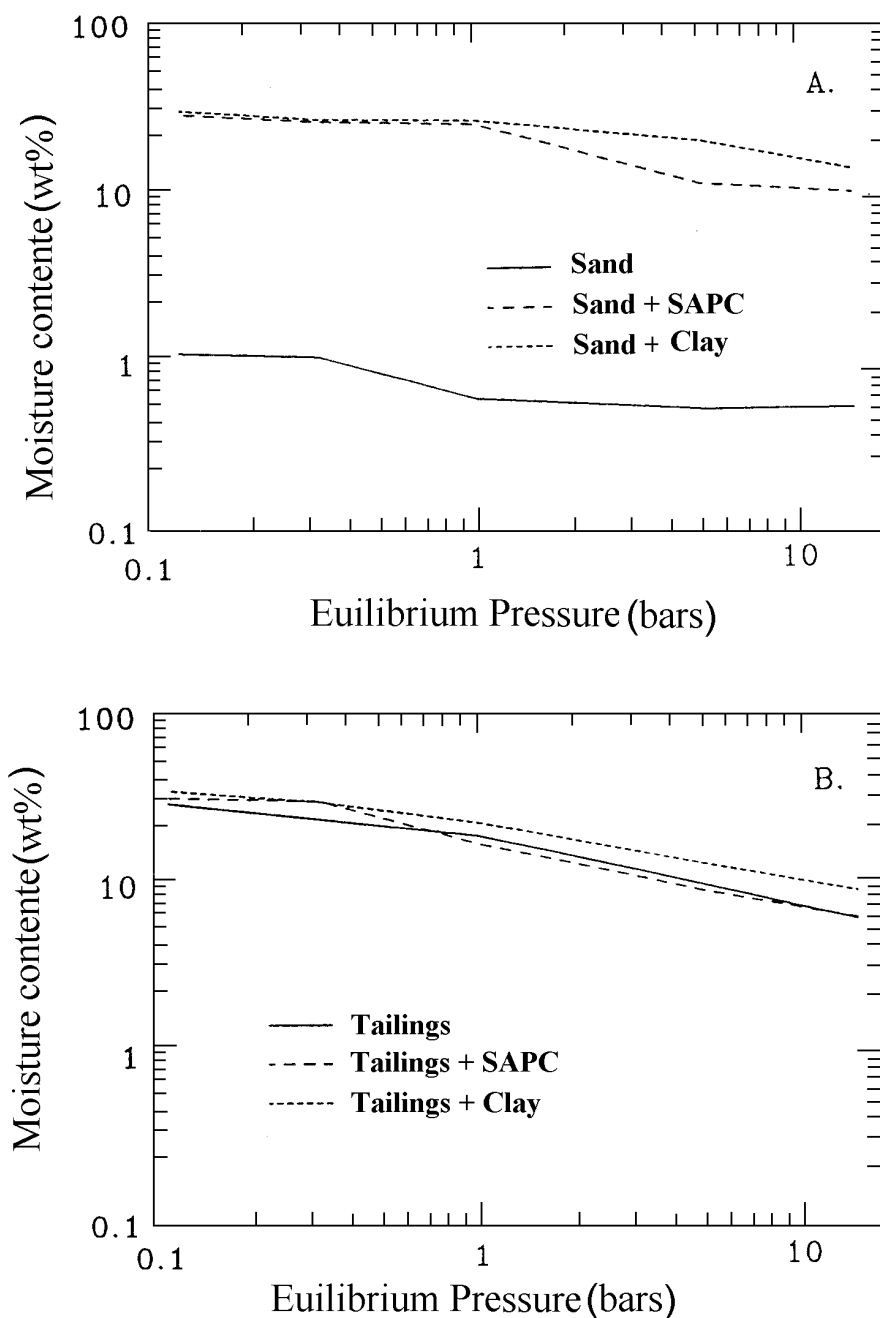
Figure 65. *Moisture retention curves. A) Sand-based samples: B) Tailings-based samples.*

6.2.4 Discussion and conclusions

SAPC performance in the sand samples

Both moisture retention and hydraulic conductivity data indicate that SAPC would be a very effective hydraulic barrier when used with sand. The good performance in the sand is due to the full hydration/swelling of the SAPC in the system. If the ionic strength of the solution is low, full SAPC hydration/swelling can be realized. Based on the WAC - salt concentration relationship, we infer that SAPC hydration/swelling would remain large even in moderate NaCl solution (< 0.1 M or 5800 mg/1). Moderate NaCl concentrations can also alleviate the poisoning effect of Ca^{2+} ions.

With the exception of sample G, the sand used in the test is fairly uniform and of medium size. The addition of 10 wt% silt fraction into the sand reduced the hydraulic conductivity of the SAPC/sand mixture. When SAPC is used with natural sand, its performance may be improved and the minimum concentration may be even lowered because natural sand always contain a variable amount of fine particles such as silt or clay.

SAPC performance in the tailings

The performance of the SAPC is poor when used with acid mine tailings. This is most likely due to the poisoning of SAPC by divalent cations leached out from the tailings (see section 5.4). Divalent cations can cross link the polymer branches and make the polymer network more "tight", therefore reducing the hydration of the polymer. In the oxidized tailings such as those used in this study, there is a large amount of gypsum (St-Arnaud, personal communication). Gypsum dissolves very fast in aqueous solution and will supply 15 mM Ca^{2+} (600 mg/l) to the solution at saturation. At this concentration, the hydration and the swelling of SAPC will be greatly suppressed.

Even if the SAPC is used with fresh mining tailings, its performance may be affected significantly. This is because pore water of the fresh tailings would be alkaline (pH 10) and would contain high calcium concentrations. However, if the calcium concentration can be reduced, the performance of SAPC in tailings can be improved. High pH is less detrimental than low pH.

Covers vs. liners

As mentioned before the SAPC can be applied either as a cover or as a liner for acid mining tailings. The experimental results indicate that SAPC is more suitable for the use in a cover. When a small amount of SAPC (1 wt% or less) is mixed with fine sand, the material will be an effective hydraulic barrier. Its moisture retention capability will increase dramatically. The SAPC and sand mixtures are physically cohesive, indicating that the SAPC has some "cementation" capability.

Because of the strong poisoning effect of divalent cations on SAPC, a question may arise as how to prevent divalent cations from entering the cover. This will be especially relevant when the cover is underlain by a layer of oxidized tailings. In reality, this may not be a serious problem. First, in the event of precipitation, the flow will be downward and the only way the divalent cations can get into the cover is through diffusion. Cation diffusion in the porous media requires a continuous aqueous phase in tailings which is rarely present. Second, after the SAPC is hydrated, divalent cations have to work their way through the gel. This process would be much slower. Finally, if a multi-layer concept is used, the impermeable SAPC-bearing layer would be underlain by a layer of coarse sand. The latter is at residual saturation which will eliminate the possibility of cation diffusion through it.

In summary, if a natural sand, silt, or till contains low to moderate amounts dissolved components, the use of a small amount of SAPC would make the natural material an effective hydraulic barrier. The performance of the SAPC-bearing material would be improved if a layer of coarse sand is placed underneath.

When used in a bottom liner, the SAPC will not function well because solution percolating through the acid mine tailings will poison the SAPC performance. Without the swelling of the SAPC, the liner would not be an effective hydraulic barrier.

Economics of SAPC application

The economics of SAPC application in acid mine abatement can not be fully evaluated until an optimum concentration is determined for a candidate cover material. It is certain however that only a small amount of SAPC (one weight percent or less) is needed in the cover. The cost for the SAPC production in any case would be much higher than Wyoming bentonite on a unit weight basis. However, for equal performance in moisture retention and as hydraulic barrier, the amount of SAPC required in the cover is only one tenth of bentonite or even less. Savings on transportation can be substantial. In addition, mixing SAPC with sand or silt will be very easy. Packing requirements may be not as strict since volume expansion of the SAPC is so large that it will fill all the pore space. *All these savings may outweigh the high material cost as the SAPC can be directly mixed with a natural geological material.* The amount of SAPC required could be even much less (as low as 0.2 wt%) when used with materials with low hydraulic conductivity such as certain fills or varved clays.

The real benefit of using SAPC is that it may provide technical advantages over other natural materials. For example, if no natural material can achieve the required technical specifications, or if more than one type of natural material (e.g. sand plus clay) has to be mixed in order to achieve these technical specifications, the application of SAPC may become an important alternative.

Conclusions

Preliminary tests with SAPC/sand mixtures show a significant potential for SAPC application in acid mine tailing abatement. The use of SAPC in the bottom liner of a tailing pond is not a viable option because of the poisoning effect by multi-valent cations on the SAPC. However, a SAPC- bearing cover should be an effective hydraulic barrier. Essentially, the cover would be an impermeable barrier and would retain its water saturation. The cost for this material may be offset by the savings on the transportation of the barrier material and construction of the cover.

6.3   Sludge dehydration

Research has been carried out to seek new application of SAPC using its water-absorption and retention properties. Unlike the water absorption and retention property used in the general situation, in sludge dehydration the water absorption property is used to absorb water from solid materials containing a high water content. Masuda studied dewatering of coal, activated sludge and metal plating sludge[92]. In comparison, the water content in some materials was lower by SAPC dewatering than that achieved by centrifugal dewatering, In the study, the residual water content of coal obtained by SAPC dewatering was much lower than that achieved by centrifugal treatment. The water content of the activated sludge and metal plating sludge was reduced to 80% by mechanical method compared with 72 and 60%, respectively by SAPC dewatering. This shows that sludge dewatering technology using SAPC could be applied to solidify city sludge to protect the environment.

6.4   Soil amelioration

The SAPC can be used as soil moisture retention agent or component of plant growth media for the improvement of soil quality as well as seed coatings. The function of SAPC in the soil is to absorb water from rainfall or irrigation, and releasing it slowly to meet the need of plants to grow. There are many ways to use SAPC in agriculture, such as to mix the SAPC with soil or to mix SAPC with the seeds, fertilizers and agricultural chemicals used in planting. Usually, only small amounts (0.05-0.1%) of the SAPC can greatly improve the property of the soil. In forestry, SAPC is used in tree transplanting and seedling. SAPC is spread over the

surface of the tree roots to prevent them from drying out in the transportation process.   Asano studied the water retention using 0.1-0.3% of SAPC and sea sand and used 0.1% SAPC in sandy soil.   As a result the yield of tomato was increased[93].   Since 1988, Japan has been carrying out a five years soil improvement project in Egypt[94].

In the draught area of northeast China, the SAPC has been used for the planting of sugar beet, soybean, rice etc.   The results of field experimental showed that the SAPC had a good effect on beet, soybean and rice production[12].

Table 23.   Effect of SAPC on sugar beet growth

SAPC (g/pot)	Average plant height (cm)	Average number of green leafs	Average Number of dead leafs	Largest leaf (cm)		Beet			Leaf weight (kg)	Sugar content (%)
				Length	Width	Length (cm)	Diameter (cm)	Weight (kg)		
10	72	32.5	15	40	34	21	11.5	1	2.75	6.0
7	69	20.0	17	37	23	22	9	0.8	1.6	5.5
0	57	21.0	15	30	22	16	9	0.78	1.9	5.5

Data in the table are averaged from three 20 m² areas.

Table 24.   Effect of SAPC on soybean growth

SAPC (g/pot)	Average plant height (cm)	Average number of main branches	Average pod number	Average output (kg/Mu*)	Increase of yield (%)
10	114	5	39	176.3	122.4
0	96	3	35	144.4	100

*1 Mu = 666.7 m². Data in the table are averaged from three 20 m² areas.

Table 25.   Effect of SAPC on rice seedling

| SAPC* (g/1.5kg soil)	Average leaf number	Average plant height (cm)	Average stock diameter(cm)	Average root number	Average branch ratio (%)	Average plant weight (g)
0	4.3	17.3	0.30	16.9	37	4.10
2	4.3	16.3	0.32	18.4	39	4.21
4	4.3	16.5	0.35	17.5	42	4.33
6	4.3	16.1	0.34	17.4	48	4.25

* The seedling experiments were done in Jiamusi, Ningan, Mishan, Wuchang, Yanshou, Tailai, and Huachuan cities and counties etc. Data were averaged from young plants of three 20 m² seedling beds.

The results showed that using SAPC in the production of soybeans and beats had an obvious draught-resistant effect and therefore increased the production output and the sugar content in beet.   It has also an obvious effect on rice seedling as simplifying the seedbed management, increasing the survival rate of the seedling, shortening the seedling stage and

increasing the production output. According to the assessment of Jiamusi (Heilongjiang) General Section, with the addition of SAPC, the seedling survival ratio increased from 80% to 95% and the morbidity by Liku (witherling) disease decreased from 19% to 2%[95].

6.5 Sealing material in electric industry

Using the water absorption and swelling properties, SAPC can be used as water leakage preventing material in the electric industry. In the battery industry, the traditional sealing materials are a mixture of bitumen, white wax and resin etc. The leakage is a problem of the battery in its usage. The SAPC was used as a sealing material to prevent the leakage of the fluid in the battery. There are three ways for the application of SAPC in the battery. First, the SAPC is used as leakage-proof material to prevent the leaking out of water generated by the chemical reaction in the battery. The second is the use of SAPC as septum material in the battery which will improve the structure of the battery and prolong its life time. The third is the use as electrolyte fluid carrier in the battery to improve the electrical property of the battery. The use of SAPC not only solved the problem of leakage but also prolonged the shelf life of the battery[96]. SAPC also can be used for electric cable production to stop water from entering the cable in case of damage of the cover wall of the cable. It can also prevent the water percolating into the cable from the junction. The principle of the usage of SAPC is as shown as follow
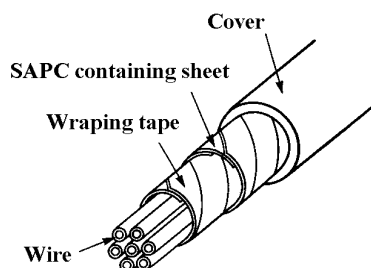
The application of SAPC in the cable production has been done in Jiamusi City, Heilongjiang, China and good results were obtained.

6.6 Dewatering of adulterated fuel[97]

In the gasoline and diesel oil processing industry, dewatering treatment is usually necessary because the water (free water and dissolved water) can often decrease the activity of catalysts and therefore decrease the reaction ratio of the reagent, corrode the transportation pipeline and jam the pipeline in form of frozen water. Distillation and absorption are the most commonly used method for removing water[98,99]. However, to further dry out the humidity in the fuel, these two methods are not suitable from the view of economics. To reduce the dewatering cost, SAPC was used to absorb moisture in the fuel.

Materials

Gasoline (Canadian Petroleum Exchange M-600, $\rho=0.684 g/cm^3$), diesel fuel (Canadian Petroleum Exchange D-28), deionized water and T_{20} (tritiated water, 1 mCi/g) were used in the experiment.

Super-dry gasoline was prepared at 23 ^{o}C using 10% (w/w) of molecule sieve 3A (activated in a vacuum oven at 325 ^{o}C for 24 hours) in nitrogen gas atmosphere for 24 hours.

To prepare radioisotope-traced gasoline 0.0226ml of T_{20} were put into a vessel containing 300 ml dried gasoline and mixed thoroughly. The water content is equivalent to the theoretical value of the moisture in the gasoline at this temperature. The scintillation solution was measured with scintillator.

Measurement of dewatering action of SAPC

A mixture of 0.2 ml traced gasoline and 3 ml of scintillation solution was prepared in a proportion of 1:30 (v/v) and injected into the measurement cell of the scintillator meter at 23°C.   The measurement was repeated twice and the average value of the two measurements was taken as a baseline.   Then, 0.53 g of SAPC particles (particle size 0.25-0.45 mm, dried at 100 °C for 100 h) were put into the traced gasoline. The water content was measured at sampling time intervals of 5, 10, 30, 60, 120 and 240 min respectively, by taking out 0.2 ml of gasoline and mixing them with 3 ml scintillation solution.

To see the influence of oil on the water absorption behavior of SAPC, comparison measurements were done.   Usually, when putting the SAPC into the gasoline/diesel fuel because the surface of the SAPC particles was covered by the fuel, an oil membrane was formed.   This SAPC was then taken out of the fuel and put into distilled water. The water absorption rate was measured.   As a comparison, a fresh SAPC sample was directly put in the water to see the influence of the oil membrane on the SAPC.   Results are shown in Figure 66.
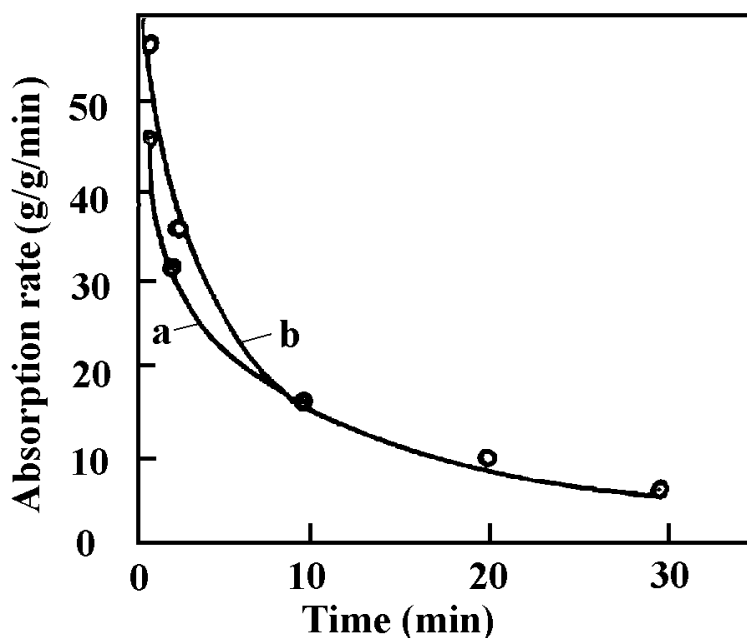

Figure 66. *Normalized absorption rate of water by SAPC (a) with and (b) without an oil membrane. (Ref. 97)*

The absorption rate of SAPC in the presence of an oil membrane slowed down during the first 10 minutes due to the delay for water to penetrate the oil membrane to reach the SAPC.   However, after then, the absorption rate is identical to the condition in the absence of an oil film. This result is in accordance with that of Basmadjian[100].

Absorption of free water in the fuel

Table 26. Absorption of free water in the fuel

	Fuel (ml)	Water (ml)	SAPC (g)	Water residual (ppm)*
Gasoline	25	1	0.5	111
Diesel	25	1	0.5	125

At 25°C, the dissolved water in gasoline/diesel is 125 ppm.

Table 26 shows that the SAPC can absorb all free water in the gasoline/diesel fuel. After the treatment, the residual water was close to the saturation concentration of dissolved water. The dewatering experiment also showed that the water absorption rate of SAPC in oil was close to that in the pure water in this experimental condition. This perhaps is because when the SAPC is put in the fuel it contacts with water in a dispersive phase and absorbs the free water before the surface of SAPC has been covered by oil membrane. And at this time, the environment of SAPC was the same as in the pure water so that the water absorption rate was not obviously influenced by the presence of oil.

Absorption of dissolved water

The water content in the gasoline was measured by a radio-tracer method[101]. The results are shown in Figure 67.
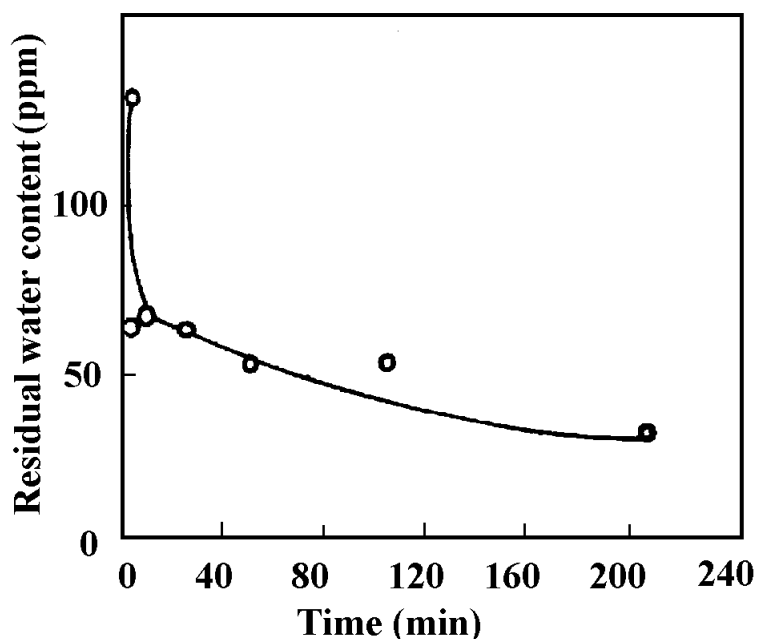

Figure 67.   Residual water content of gasoline treated with SAPC. (Ref. 97)

During the first 30 minutes, the amount of residual water decreased sharply, and then it slowed down. It is suggested that with the decrease of residual water, the probability of the SAPC surface to interact with the dissolved water molecule decreased.

Experiments showed that the SAPC could be used for absorbing water in the gasoline/diesel fuel. It can also be used to dewater other non-polar solvents. This property showed a high application potential. Because of the economical characters, SAPC can be used as a filling material for the gasoline/diesel dewatering.

6.7   Strengthening of concrete

Since the 1970's, cement matrix composites have been developed for applications, ranging from factory-fabricated units to field use[102].   Among the major advances achieved[103-106] are the formation of densified or warm-pressed cement pastes with properties approximating those of fired ceramics, the modification of the chemical composition of the cement, and the formation of macrodefect-free (MDF) cement prepared by special processing, for example employing water-soluble polymers such as poly(vinyl acetate) or hydroxypropylmethylcellulose followed by intense shear-mixing[107-109].   The strength of aluminous cements has been improved by using specific types of water-soluble polymers acting as a rheological aid during dough formation, and leading to a reduction in porosity and strengthening of the cement by increased polymer/cement interaction. SAPC has a potential application as an additive to improve concrete performance by acting as a water-reducing agent[110] to eliminate the negative effect of water on the hardening of cement. It can also act as an air-entraining agent[111] by virtue of the polar nature of the carboxyl group of polyacrylamide which may reduce surface tension and hence stabilize the fine foam of bubbles originating from the mixing process. This chapter deals with the application of SAPC in concrete preparation to obtain an aluminate concrete with improved compressive strength, tensile strength and modulus.

6.7.1   Samples preparation

The cement used in the experiment was an aluminate cement manufactured by Canada Cement Lafarge Ltd. To prepare the cement/SAPC paste, a statistical method[112] was employed to minimize the number of samples investigated without sacrificing the information content, and to obtain an estimate of the synergistic interaction of the factors chosen. Three factors at three levels each were selected according to a Box-Behnken orthogonal design. The variables investigated were the amount of SAPC added (X_1), the SAPC particle size expressed as a mesh number (X_2) and the cement/water ratio (X_3). These factors and their levels are shown in Table 27.

Table 27.   Factors and their levels used in the Box-Behnken statistical experimental design

Factor	Level		
	(-)	0	(+)
X_1. amount of SAPC (%)	0.2	0.35	0.5
X_2. grain size of SAPC (mesh)	20-40	40-60	>60
X_3. cement/water ratio (%)	32	36	40

To prepare the concrete samples, a procedure conforming to an ASTM standard (ASTM C 192-90a) was employed. A fixed cement:sand:gravel ratio of 1:1.18:1.86 by mass was used in the preparation of all concrete samples. The sand was screened with a sieve shaker (Fisher-Wheeler Model-5) equipped with a set of sieves with screen openings of 4 (4.75 mm), 8 (2.36mm), 16 (1.18 mm), 30 (0.6mm), 50 (0.3 mm) and 100 (0.15 mm) mesh.   Each portion of sand was prepared according to the ASTM C 33-90 standard, blended with a rotating mixer, and finally homogenized with a sample splitter (Gilson Screen Corporation Model SP-I). The particle size distribution of the sand, determined according to ASTM C 136-84a, was 25% (-2.36 + 1.18) mm, 25% (-1.18 + 0.6) mm, 30% (-0.6 +0.3) mm, 18% (-0.3 +0.15) mm and 2% < 0.15 mm. The gravel used was sieved to a size between 8 and 12.7 mm (ASTM C 33-90). The total moisture content of the aggregate was determined according to the ASTM C 566-89

procedure, and was found to be 0.14% for sand and 0.83% for gravel. The preparation procedure of the concrete was as prescribed by ASTM C 192-90a. After mixing, the pastes were poured into moulds made from PTFE and PVC pipe with a diameter of 5.08 cm (2") and a length of 10.16 cm (4"). One end of the pipes was closed by a PMMA plate and sealed with silicone grease. Air bubbles were removed by vibration using a rod-type vibrator. The samples were cured in saturated limewater at a temperature of $23^{o}C$ for 28 days. Each parameter combination was replicated five times. Three of the replicates were used for compressive strength testing and the two others were used for split tensile strength testing. The samples were tested immediately after being removed from the curing solution according to the relevant ASTM procedures on the 28th day.

6.7.2   Results and discussions

Aluminate cement paste

Adding SAPC to aluminate cement paste prepared with a cement/water ratio of 40% increased the average compressive strength $Y_{f,c}$ from 36.1 MPa (0% SAPC) to 40.5 MPa (0.2% SAPC) to 44.4 MPa (0.6% SAPC), the average modulus of elasticity Y_E from 7.8 GPa (0% SAPC) to 10.1 GPa (0.2% SAPC) to 11.1 GPa (0.6% SAPC), and the average split tensile strength $Y_{f.t}$ from 3.3MPa (0% SAPC) to 5.8MPa (0.2% SAPC) to 7.0 MPa (0.6% SAPC).

A Box-Behnken statistical design in the parameters X_1 (SAPC/cement ratio: 0.2, 0.35 and 0.5%), X_2 (SAPC particle size: 20-40, 40-60 and > 60 mesh) and X_3 (cement/water ratio: 27, 31 and 35%) showed that the compressive strength of aluminate cement paste increases parabolically with increasing water content and linearly with SAPC particle size but parabolically with a decreasing amount of SAPC. The modulus of elasticity shows the same trend. The split tensile strength increases linearly with increasing water content and parabolically with the amount of SAPC added.

Aluminates concrete

The effect of SAPC on aluminate concrete was evaluated by measuring the compressive strength ($Y_{f,c}$), the modulus of elasticity (Y_E) and the split tensile strength ($Y_{f,t}$). In general, the compressive strength, modulus of elasticity and split tensile strength increased on addition of SAPC. This is taken as an indication that the strength increase may be related to a delay in the hydration of the cement by keeping water away from the unhydrated cement mineral grains[113]. The addition of SAPC did not cause a noticeable difference in the macroscopic appearance of the aluminate cement. The experimental conditions and the statistical calculations are shown in Appendix 4 (Table A-3, A-5).

The average strengths of blank samples, prepared with a cement/water ratio of 36% without addition of SAPC, were $Y_{f,c}$ = 65 MPa, Y_E = 18.8 GPa and $Y_{f,t}$ = 5.26 MPa. Inserting the coefficients obtained from the Box-Behnken designs selected into the general polynomial equation and omitting the statistically non-significant factors, one obtains the reduced response polynomial

$$Y_{f.c} = 59.2 - 5.45x_2 - 6.25x_3 + 5.65x_{12} + 7.1X_1{}^2 + 6.37x_3{}^2 \qquad (10)$$

$$Y_E \times 10^{-3} = 18.1 - 1.960x_2 - 2.000x_3 + 1.675x_{12} + 2.065x_1{}^2 + 1.565x_3{}^2 \qquad (11)$$

$$Y_{f.t} = 5.78 + 0.133x_1{}^2 - 0.365x_2{}^2 + 0.255x_3{}^2 \qquad (12)$$

As shown in equations 10 to 12, the compressive strength of concrete, $Y_{f.c}$ increases linearly with decreasing mesh number of SAPC, that is, increasing particle size and cement/water ratio but parabolically with increasing amount of SAPC and cement/water ratio.

The modulus of elasticity, Y_E, shows the same trend. The split tensile strength, $Y_{f.t}$, increases parabolically with decreasing mesh number of SAPC, increasing amount of SAPC and increasing cement/water content.

From the reduced response equations (equations (10)-(12)) the predicted values $\hat{Y}$ and the residuals $(Y - \hat{Y})$ were calculated (Appendix 4, Table A-4). Probability plots of the empirical cumulative distribution[114] of the coefficients (left) and the residuals (right) are shown in Figure 68. The plots of the residuals indicate a reasonably good fit to a normal distribution, which confirms that the reduced response polynomials fit the experimental data at the selected level of confidence (v= 0.95 to 0.99, see Table A-5).
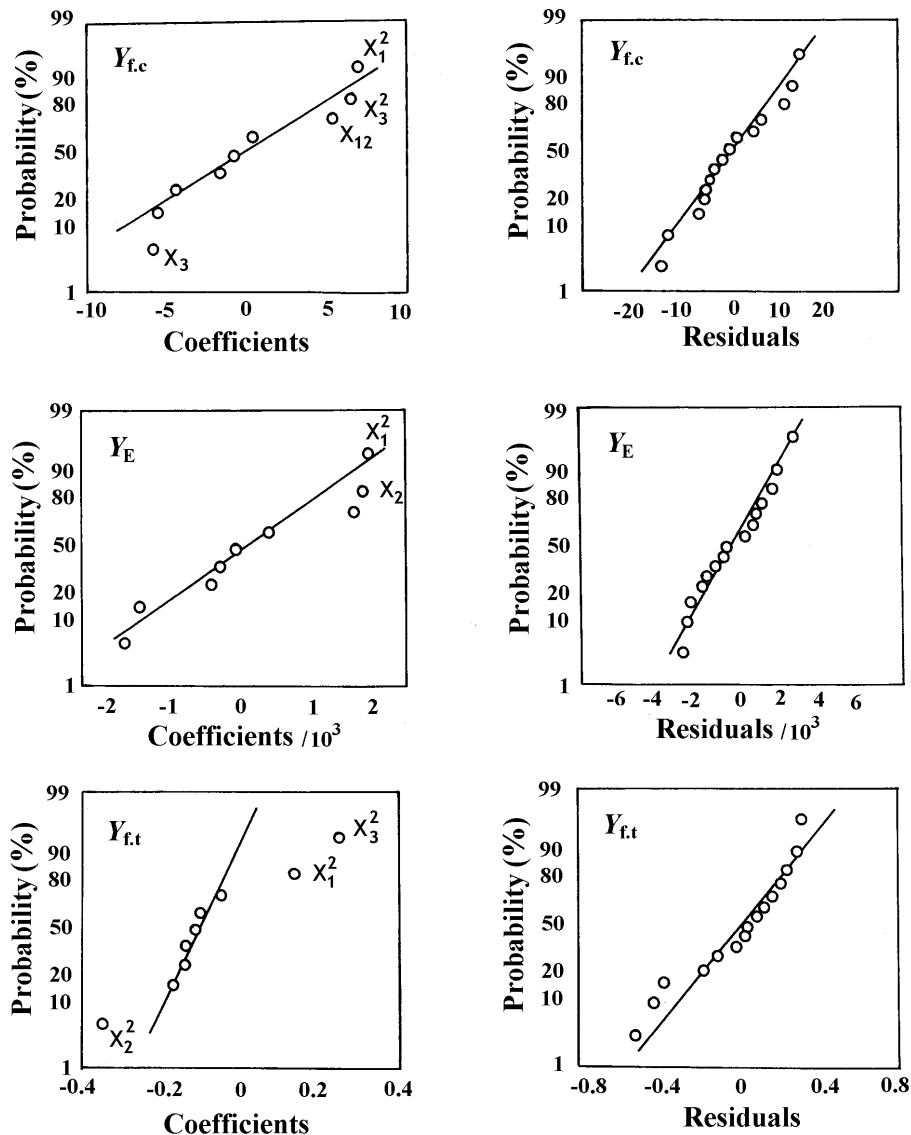

Figure 68 Empirical cumulative distribution of coefficients (left) and residuals (right) calculated from the reduced polynomials. (Ref. D. Gao, R.B. Heimann and S.D.B. Alexander, Advances in Cements Research, 9(35) (1997) 93-97)

To get a feeling for the precision of the fitted response surfaces, the average variances of the fitted values $\hat{Y}$, $V(\hat{Y}) = 1/n\sum V(\hat{Y}_i) = (p\sigma^2 (S))/n$ (with p the number of parameters fitted. $\sigma(S)$ the standard deviation calculated from the center points of the design and n the number of samples (= 15)), were calculated for the compressive strength, the modulus of elasticity

and the split tensile strength. These values were compared to the range of the fitted Ŷ values (Table A-4). For the compressive strength and the modulus no substantial lack of fit could be shown since the predicted changes of Ŷ are, respectively, 7 and 17 times the average standard error of Ŷ. On the other hand for the split tensile strength the predicted change of Ŷ is only 1.4 times the average standard error, thus indicating a rather imprecise fit as also indicated by the probability plot of the residuals (Figure 68).

Conclusions

From the analyses performed it can be concluded that the addition of SAPC as a superplasticizer/ additive to an aluminate cement had a positive effect on the mechanical properties of concrete made from this cement. The compressive strength and the stiffness, expressed by the modulus of elasticity, increased in a statistically significant way with increasing amounts of SAPC.

6.8   Application as chemical and moisture sensors

Principle of sensors for moisture, pH and ionic concentration changes

The functional principle is based on the sensitivities of a polyelectrolyte SAPC hydrogel to water vapor in air and to the ionic strength and pH values of a solution. As described in previous chapters (5.3-5.4) the volumetric change of the gel is a function of pH, ionic concentration and ionic charge of the surrounding solution. In principle, a moisture sensor could be built with SAPC hydrogel shaped to suit a silicon wafer-based integrated circuit. The basic structure of such a moisture sensor is that between the two electrodes a polymer material is placed to prevent a short circuit. As a sensing material, the polymer changes in response to environmental change and so does the electric signal. The key points of the functional properties are the sensor's sensitivity and response time[115-117]. To improve the latter property, usually a thin film is desired. Principally, polymer-based moisture sensors can be divided into four types:

a.   Resistance changes by ionization of polyelectrolyte membranes

By absorbing water (or water vapor), molecules at the surface of the polymer will be ionized, thus decreasing the resistance.

$$R - H + \ H_2O \ \Leftrightarrow \ R^- \ + \ H_3O^+$$
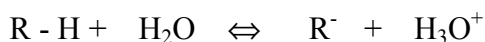
(R: all the other components except H)

b.   Resistance changes resulting from the polymer expansion

In a polymer membrane, electrically conductive materials, e.g. graphite, metals etc. are added. After absorbing moisture, the polymer expands, the distance between the conductive particles increases, and hence the resistance of the circuit becomes larger. In this structure, the particles will become separated, i.e. electrically isolated by the osmotic swelling of polymer resulting in a higher resistance.
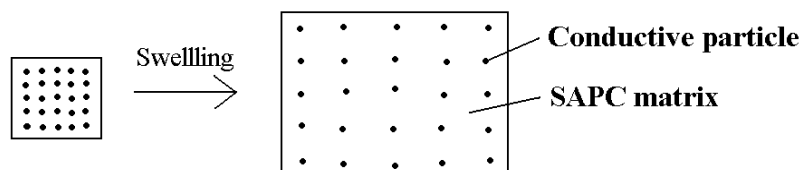

Figure 69. Schematic sketch of the resistance changes

c.   Capacity changes of the polymer membrane

With absorption of moisture by the SAPC, the apparent dielectric constant of polymer materials will change.

d.   Mass changes of the polymer membrane

The resonance frequency of a microbalance coated with a moisture-absorbing polymer will change in response to the absorption of moisture by the polymer.   This frequency change can be measured with a frequency counter and calculated principally by the equation

$$\Delta f / f = \Delta m / M \qquad (13)$$

where Δf: frequency change, Δm mass change of the polymer, M: mass of the electric element.   The equation shows that the change of the frequency is directly proportional to the change of mass.

One feasible practical measurement method could be based-on the differential frequency measurement shown in Figure 70.
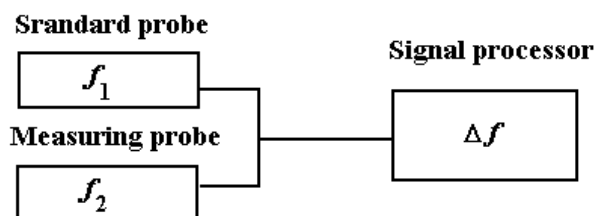

Figure 70.   *Principle of the measurement of the frequency*

The relationship between the resonant frequency f, and the mass change Δm (g) is given by the Sauerbrey equation[115]

$$\Delta f = -2.3 \times 10^6 f^2 \Delta m / A \qquad (14)$$

where the A is sensing area.

A chemical sensor with the ability to detect or measure toxic species for environmental monitoring can be prepared using the above principles. One of the concepts is to use the SAPC materials as a chemically sensitive material by measuring the changes of the electric resistance or the capacity of the material with a proper method thus constructing a chemical sensor. Another concept is to insert conductive particles into an insulating polymer matrix (SAPC). As the degree of swelling and hence the resistance measured is a function of the chemical nature of a vapor, chemical solvents of environmental significance can be detected and selectively measured.

6.8.1   Absorption of moisture in air by SAPC

Comparison of the water moisture absorption of SAPC with other absorbents

Absorption of moisture in air was done using SAPC and other absorbents. By comparison of water absorption curves of SAPC with molecule sieve 3A, and activated alumina and silica gels, it was found that in the range of relative humidity (RH) 11.31-100%, the SAPC has higher absorption ratio to the water vapor. Above RH 30%, the water absorption capacity of SAPC was far higher than that of the molecular sieve. Only for RH < 30%, the absorption capacity of SAPC is lower than that of molecular sieve. This is because

the difference in the form of water combination. SAPC is an intercalated composite of polyacrylamide-bentonite, under lower water vapor pressure the water absorption ability is close to that of the silica gel and activated alumina. However, after absorption of some water, the relative surface area of the latter decreased rapidly[118], and so did the water vapor absorption capacity. Therefore, SAPC showed higher absorption ability at both high and low vapor pressures. The reason that the molecular sieve had a higher absorption at low vapor pressure is due to its strong Coulombian force and the polarity thereof.
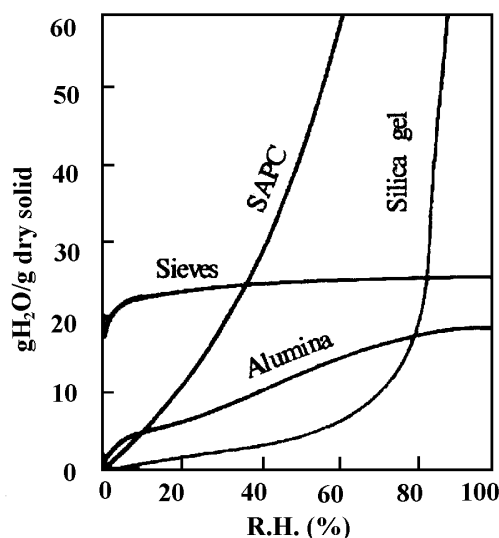

Figure 71. Comparison of SAPC with other absorbents (Ref. 97)

Measurement on the enthalpy of water absorption

To confirm the feasibility of using a thermal method to monitor the absorption process, an experiment was performed to determine the heat generated by the interaction of liquid water with SAPC using a standard reaction calorimeter (LKB 8700, LKB, Sweden). SAPC samples were sealed in a glass ampoule and installed in a thermally insulated reaction cell placed in a constant temperature bath as shown in Figure 72. Calibration and enthalpy determinations were performed using standard procedures[119,120]. To start the measurement, the ampoule was broken by the stirrer to allow the SAPC to make contact with water[121].
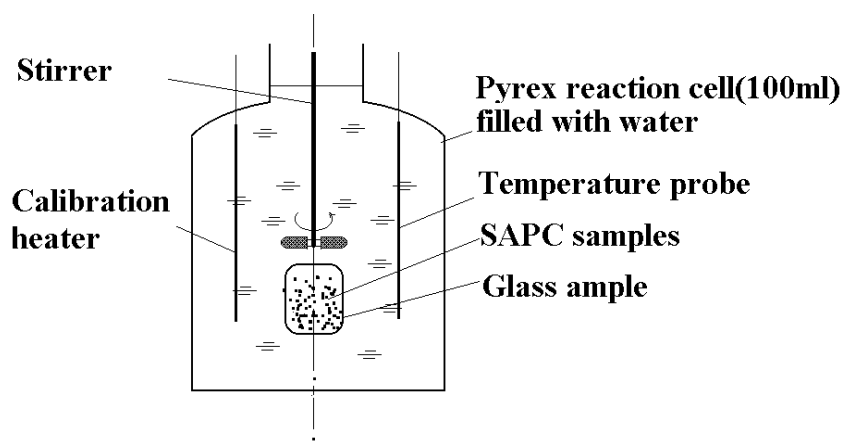

Figure 72. Scheme of the calorimetric cell. (Ref. 121)

The interaction enthalpies of SAPC with water were measured during an interaction time of 5 minutes. Table 28 shows that the interaction enthalpies were between 118.6 and 124.9 J/g. These values are smaller than 43.5 J/mol given in the literature[122] since the interaction time in the experiment was not sufficient for the reaction to reach completion. There are differences between the ΔH values of samples with various masses.   The higher the mass of the SAPC, the higher ΔH.   This is presumably caused by the heat loss of the measurement device.

Table 28.   Specific interaction enthalpies of SAPC on contact with water

Sample	Mass of SAPC (mg)	Mass of H_2O (g)	q (J)	ΔH (J/g)
SAPC 1	32.20	85.200	3.82	118.6
SAPC 4	33.55	85.200	4.19	124.9
SAPC 5	32.63	85.467	3.87	118.6

q: *measured heat exchanged, ΔH: Specific enthalpy per gram sample.*

A typical result of the measurement is shown in Figure 73.   It is obvious that there are two distinct processes, the wetting and diffusion/swelling process. The specific enthalpy of the wetting process, estimated from the calorimetric measurements for a water interaction time of 5 minutes, is exothermic near $\Delta H= -(120.7\pm3.6)$ J/g as following from the results in Table 28. Due to the complexity of the second process, its enthalpy could not be determined unambiguously. The duration of this process is so long that an estimation of an enthalpy value from the further slope of the calorimetric curve seems problematic. Bakass *et al*[123] used a similar calorimetric method to measure water absorption enthalpies, but the meaning of the values obtained is subject to many questions.
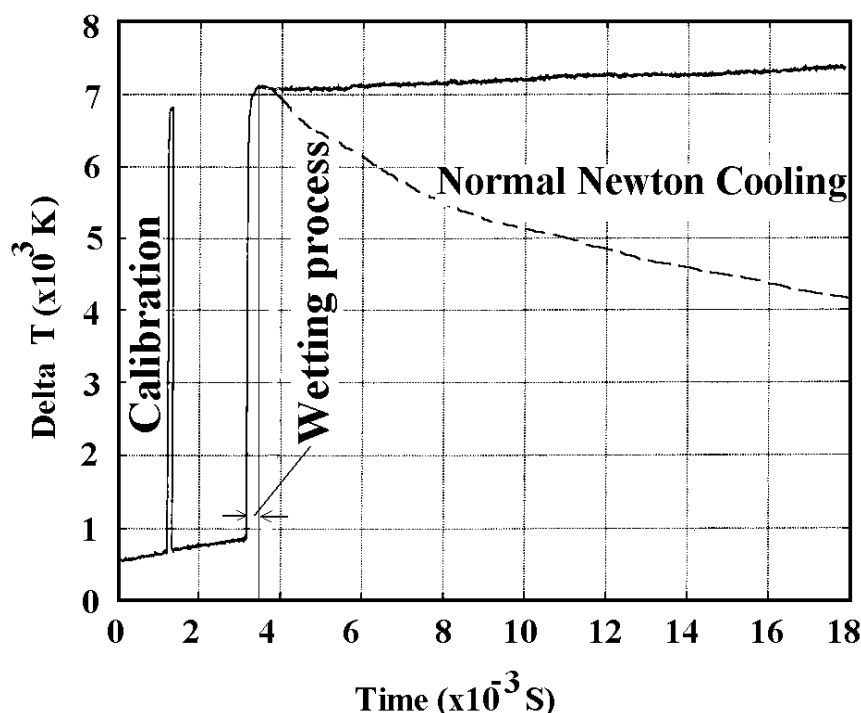
Figure 73. *Typical curve of the calorimetric measurements. (Ref. 121)*

Thermodynamic measurement of water moisture absorption

To measure the thermodynamic absorption behavior, a thermogravimetric analyzer was used (Q-Derivatograph; MOM Budapest, Hungary) and operated at isothermal mode at room temperature. A stream of argon gas containing different moisture levels was led over the sample. The moisture content was controlled with saturated salt solutions (LiCl, KCl, $Mg(NO_3)_2$ and H_2O), and expressed by their relative humidity value (RH). The mass of the samples used in this experiment was about 100 mg. The results are shown in Figure 74.

From Figure 74 it can be concluded that the moisture absorption of the SAPC was linear proportional to the relative humidity of the atmosphere. Further experiments were carried out using different experimental parameters such as the type of ionic species in the SAPC, the geometrical shapes and the mass of the samples. In these experiments, samples A, B, E and F were copolymers of AM with AANa, samples C and D were composites of AM/AANa and bentonite. samples A, B, C and D were constituted of fine particles with a diameter less than 0.125 mm, samples E and F were membranes. The masses of the samples A, B, C, D, E, and F were respectively, 106.7 mg, 95.9 mg, 105.7 mg, 102.3 mg, 23 mg and 16 mg. Figure 75 shows the dynamics of moisture absorption of SAP and SAPC samples with different compositions and geometries at 100% relative humidity.
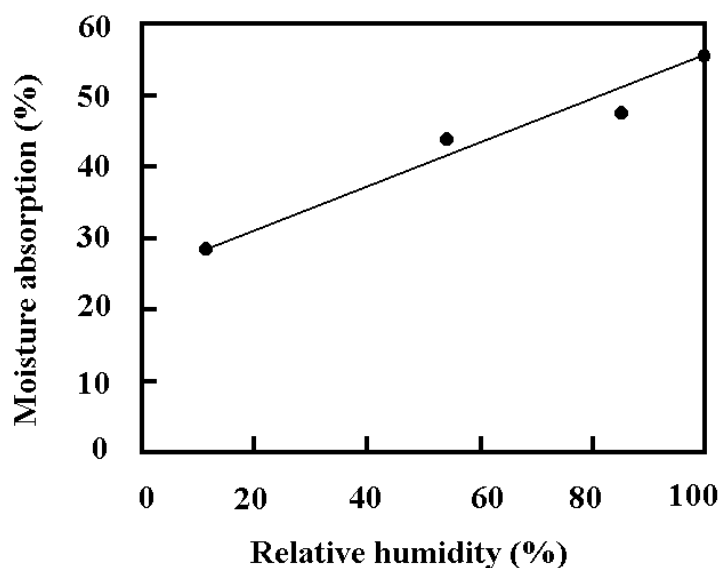
Figure 74. *Water moisture absorption of SAPC versus relative humidity (absorption time: 3000 min). (Ref. 121)*

To see the influence of SAPC mass on the water vapor absorption, data in Figure 75 were normalized to one gram. The addition of bentonite in the composite samples (C, D) strongly reduces the water absorption capacity in comparison to the pure SAP materials. The membrane samples (E, F) absorbed moisture much faster than the powder samples (A-D). At the beginning, the absorption rate was relatively fast because it occurred at the surface of the material. Later this process slowed down because of the saturation of the surface with water. However, since saturation takes place only at the surface of the material, the exterior water tends to diffuse into the interior, controlling the absorption rate by inward diffusion of water. This process is much slower than the former one, hence samples with a larger mass showed slow absorption rates. Since the powdered samples have large specific surface areas, they should absorb water vapor quickly. The reason that these samples absorbed water vapor slower than expected is due to the fact that the powdered samples are highly compacted. In addition, after absorption of some critical amount of water vapor the pore system will be plugged by the swollen hydrogel. This suggests that the moisture absorption rate of SAPC is predominantly controlled by the diffusion rate of water within the SAPC network. Because of the relatively short diffusion paths in the thin membrane samples, the absorption equilibrium can be reached more quickly. From this analysis, it is obvious that thinner membranes are needed to accelerate the absorption process in order to meet the requirements for sensor application.
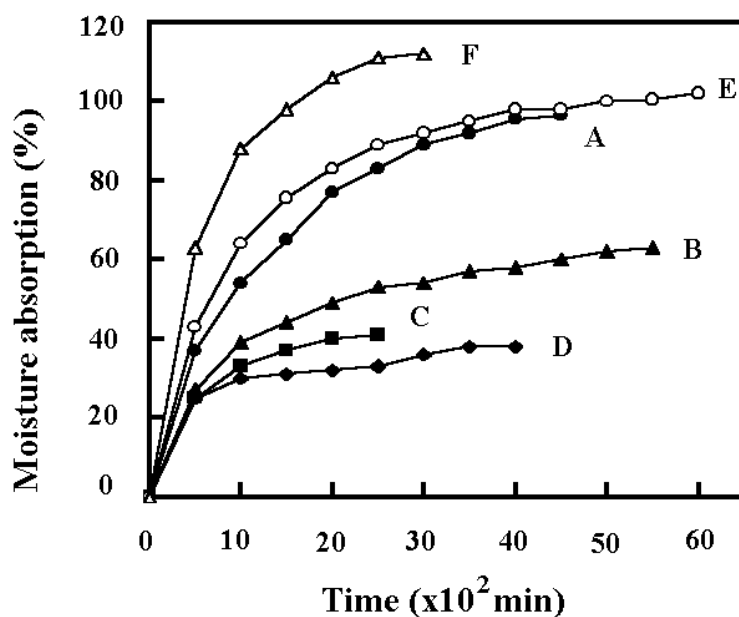
Figure 75. *Time dependence of the absorption by different SAP (A, B, E, F: copolymers of AM and AANa) and SAPC (C, D: composites of AM/AANa with bentonite) at 100% relative humidity (for detail see text). (Ref. 121)*

Layout of water moisture sensor

Based on the experimental results described above and from the point of practical application, membrane-type SAPCs were selected for further experiment. The schematic sketch of the experimental device of a prototype moisture/chemical sensor and the schematic diagram of the layout of the silicon transducer chip which was used for the measurement are shown in Figure 76.
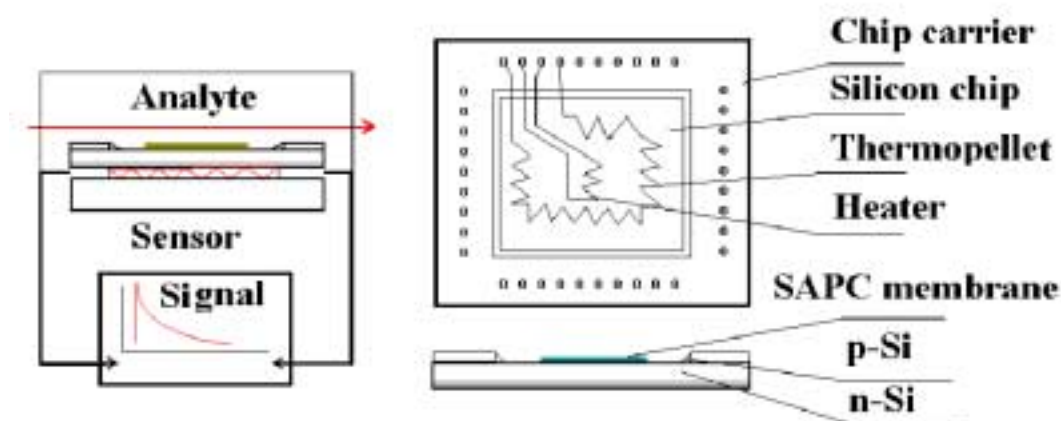

Figure 76. *Schematic sketch of prototype moisture and chemical sensor (left) and diagram of the layout of a silicon transducer chip (right). (Ref. 121)*
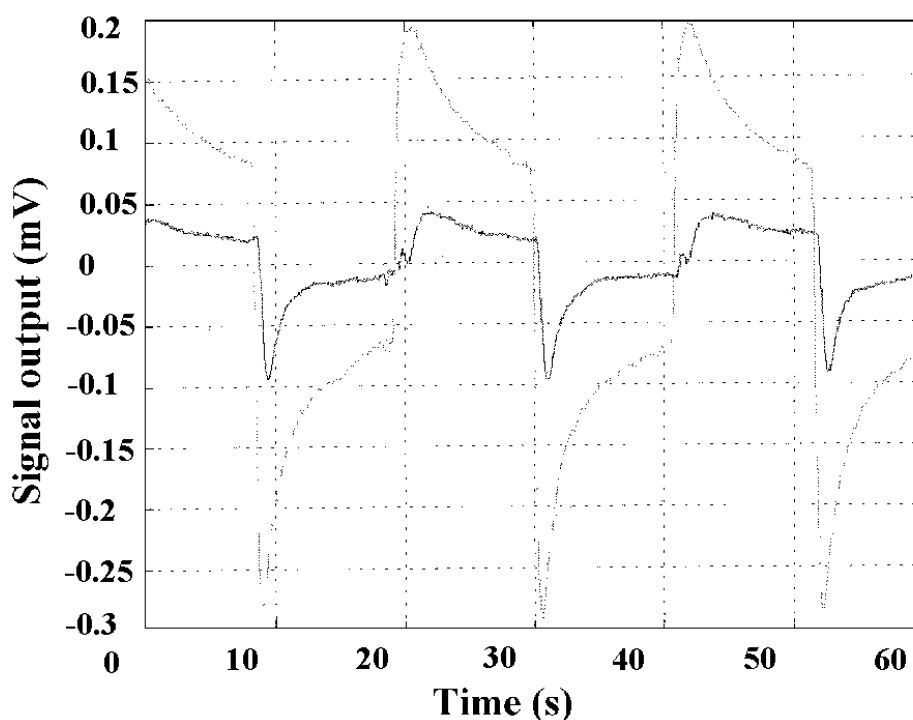
Figure 77.   *Voltage output of the moisture sensor produced from SAPC*

Figure 77 shows the voltage signal of the transducer in response to moist air (thin lines). The voltage changes from +0.2 mV to -0.3 mV during contact with moist air with a water content of 0.2%. Then dry air is led over the membrane to remove the moisture. This process takes about 12 seconds. The cycle is repeated. The heavy line shows the calibration curve obtained from air with zero percent of moisture. These results show that it is feasible to construct a moisture sensor based on SAPC.

To improve the response sensitivity of the materials to moisture and some organic vapors, SAPC with a new composition was studied. Sodium vinylsulfonate and sodium styrenesulfonate were used in the copolymerization of SAPC to improve the dynamic moisture absorption properties.

6.8.2   Water moisture absorption of various SAPCs

In the study, samples with different compositions were used to compare the water absorption ability. Results of the moisture absorption experiments are shown in Figure 78.

From Figure 78 it is obvious that all samples investigated were sensitive to water moisture to a different degree. Sample AM/AANa had the highest water absorption capacity but the time required to reach saturation was longer than for the others. Sample with composition of AM/VSNa/bentonite reached thermodynamic equilibrium first.   The response time of SAPC was improved compared to the previous experiments.
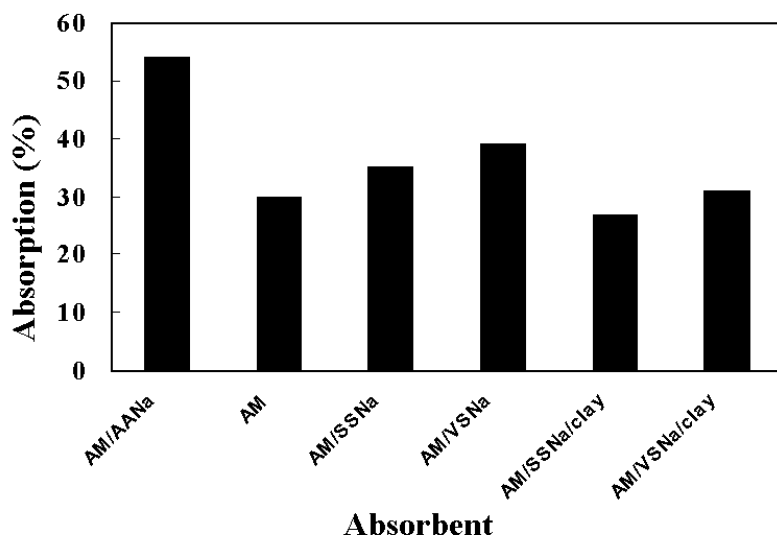
Figure 78. *Water moisture absorption of absorbents with different composition. Relative humidity of the atmosphere was 100%, absorption time 1000min. The masses of samples were about 100mg. Compositions were AM/AANa=7/3, pure AM, AM/SSNa=10/3, AM/VSNa=7/3, AM/SSNa/bentonite = 10/3/6, AM/VSNa/bentonite =7/3/4.*

6.8.3   Feasibility studies on chemical sensors

Materials used for chemical and biochemical sensors according to literature data

There are many kind of materials, that could be used in application as sensors. These materials combined with various transducers form a broad range of sensors for measurement in different fields of application.   Table 29 gives some examples.

Table 29.   Materials and measurement methods used for the sensor applications

	Matrix	Sensing Material	Target compound	Reference
1.	polymer	Cyclodextrin	Chlorobenzene	124
2.	PAM gel	ferrocene, enzyme	DADH	125
3.	PAM		Humidity	126
4.	ethylcellulose	Porphyrine	HCl	127
5.	gold electrode		ethanethiol, sulfide	128
6.	Ppy	TiO_2	O_2	129
7.	cellular	adsorbed fluorophore	NO_x	130
8.	polyimide film		Humidity	131
9.	gelatin film	fluorescent dye	Humidity	132
10.	poly(propagylalcohol)-sulfuric acid		Humidity	133
11.	polyelectrolyte		Humidity	134
12.	PVA	Poly(o-phenylenediamine)	Humidity	135

13. polymer		organic gas	136
14. polymer		n-octane, tetrachloroethane	137
15. ethylcellulose	t-phenylporphine	HCl gas	138
16. PPy/PE/Nylon	polyaniline	DMMP, NH$_3$, NO$_2$	139
17. Ppy	enzyme	Glucose	140
18. poly(3-hexylthiophene		hydrazine vapor	141
19. protein	Fluorescent dye	Glucose	142
20. gold nafion electrode		Humidity	143
21. alkanethiols	[HS(CH$_2$)(6)X]	acetic acid, alcohol	144
22. PVC (9.6%)	2-nitrophenyl octyl ether (87%), t-butylamonium, hexafluorophosphate	NO$_2$	145
23. PVA	TA, nafion	Humidity	146
24. poly[butyl methacrylate]		chloroform, (di)-chlorobenzene	147
25. PST and derivates		fluorinated compound	148
26. poly(thionaphtheneindole		Humidity	149
27. PPy/PVA		Methanol	150
28. Ppy	urease	NH$_3$	151
29. polyaniline		polar organic vapor	152
30. BMBT, PEI		CO$_2$, humidity	153
31. poly2,5-thienylene Vinylene		organic vapor	154
32. polymer		gas, odor, aroma	155
33. siloxane polymer		non-polar organic vapor	156
34. N-isopropylacrylamide		metal ions, glucose	157
35. polymer/macrocyclic calixarenes		organic pollutants	158
36. PPy/poly-3-methylthiophene		NH$_3$, H$_2$, CO	159

Scouting experiment on organic vapor absorption

To see whether it is possible to use SAPC as chemically sensitive material in a chemical sensor, an experiment was carried out to measure the absorption of organic vapors by SAPC.
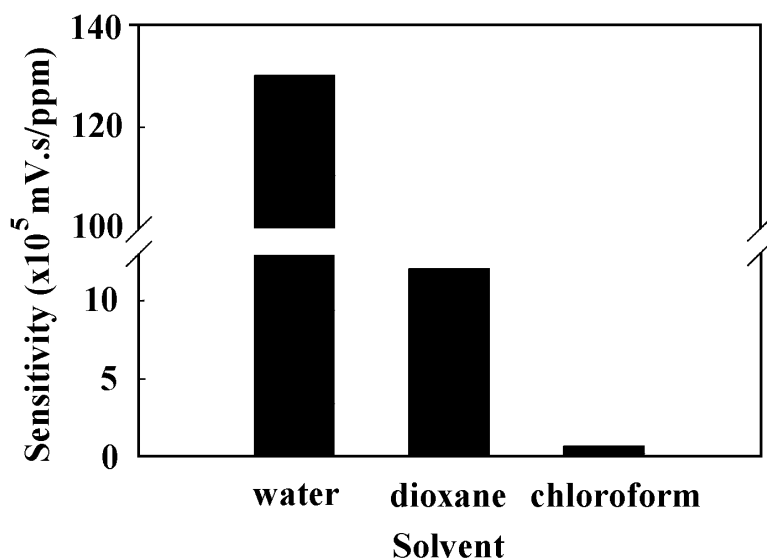
Figure 79.   *Comparison of signal sensitivities of different absorbates bound to SAPC. (Ref. 120)*

Figure 79 shows that the signal output sensitivities of the absorption of some organic solvent e.g. dioxane and chloroform to SAPC were 1.14×10^{-4} mVs/ppm and 6.23×10^{-6} mVs/ppm, respectively, one to two orders of magnitude lower than that of water (1.13×10^{-3}mVs/ppm).

6.8.4   Preparation of SAPC membranes

A thermally sensitive transducer was used to build a prototype sensor. In this experiment, the requirements for the sensor material were that it must adhere tightly to the surface of the silicon transducer and that it should have a good moisture sensitivity. From the experiments described above, a membrane-type SAPC was selected. As mentioned before, for a suitable material the sensitivity must be high and the thickness of the membrane must be thin and controllable. To obtain good control over the required properties of SAPC membrane, experiments on glass slides were carried out first. Because the available transducer required that only a square-shaped area with a side length of 4 mm should be covered by the SAPC membrane and that the membrane should be very thin to obtain the high sensitivity desired, the experimental conditions for the polymerization of SAPC material were quite demanding. The mass of the sample was only in the milligram range.   Glass slides with a dimension of 76 x 26 mm were used. Before the experiment, the glass slides were subsequently washed with detergent, and distilled water.

Particle size distribution of bentonite

One of the most difficult tasks was to adjust the large size of the commercial bentonite particles to the preparation of the thin membrane. The problem was solved by using a mill with agate vessel and balls to pulverize the bentonite to fine powders.   The diameters of the bentonite particles were measured with an optical microscope. The diameters of the milled particles were about 0.17 - 0.57 μm which is 50 times smaller than the original grain size (10 – 28 μm).

Preparation of membranes

The thickness of membranes prepared by UV-induced polymerization (see section 3.2) was controlled by controlling the volume and concentration of the monomer solution. To

achieve this purpose, concentrations of polymerization systems were strictly controlled with the method of dilution.
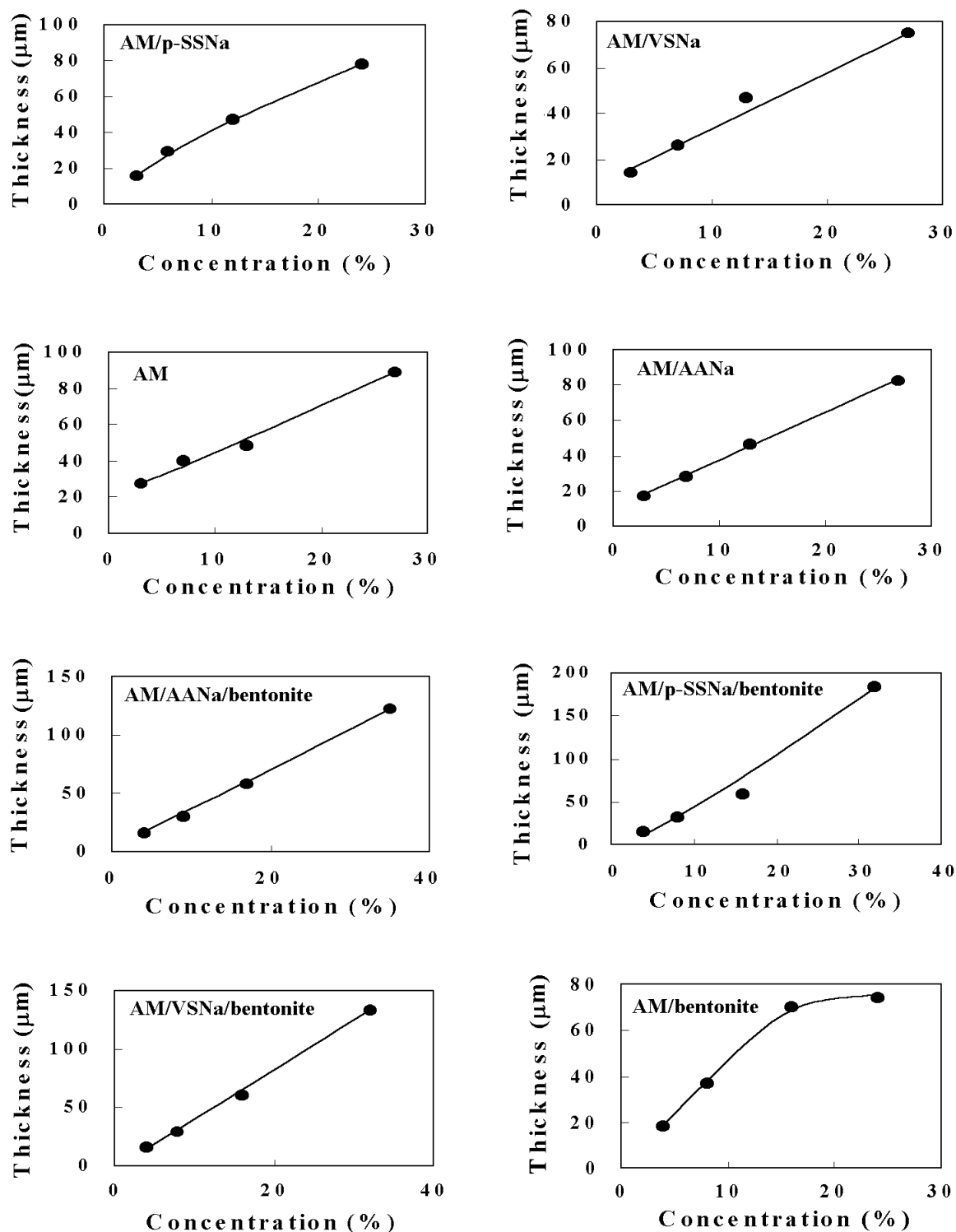

Figure 80. *Relationship between solution concentration and the thickness of a membrane; data were averaged from 4 different batches of experiments.*

In the experiments, membranes with various compositions (AM/SSNa, AM/VSNa, AM/AANa, AM, AM/SSNa/bentonite, AM/VSNa/bentonite, AM/AANa/bentonite and AM/bentonite) were prepared. The compositions of the stock solution in the experiments

are shown in Table 30.   The UV-irradiation was carried out at a distance of 10 cm for 10 minutes.

Table 30.   Compositions of the stock solutions

	AM (%)	AANa (%)	SSNa (%)	VSNa (%)	Bentonite (%)
A	17.5	-	6	-	-
B	17.5	-	-	9	-
C	26.5	-	-	-	-
D	17.5	9	-	-	-
E	17.5	9	-	-	12
F	17.5	-	6	-	12
G	17.5	-	9	-	12
H	26.5	-	-	-	12

The thickness of the membranes as a function of solution concentration are shown in Figure 80.   There is an approximate linear relationship between membrane thickness and solution concentration.

Preparation of thinner membranes

AM/AANa membrane

To prepare thinner coating membranes, a polymerization system with further diluted concentration was used in the experiment. A stock solution containing 17.5% AM, 9% AANa, 0.1% MBAM and 0.1% $K_2S_2O_8$ was prepared.   This solution was further diluted with distilled water for the use of polymerization. To decrease the surface tension of the solution, 10% ethanol was added. UV irradiation was carried out at a distance of 10 cm for 10 minutes (Figure 81).
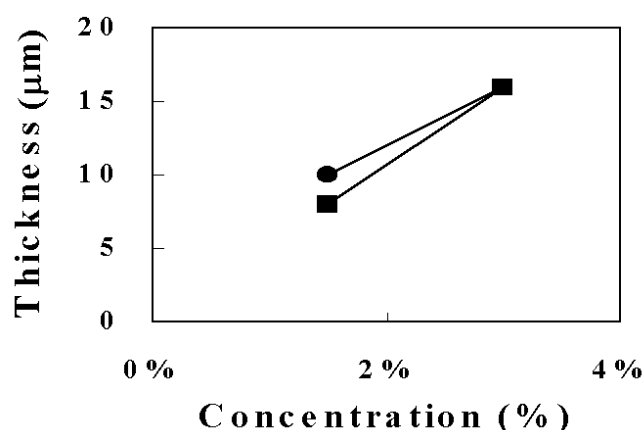

***Figure 81**.   Relationship between solution concentration and the thickness of a membrane; data were averaged from 4 different batch experiments.   ■ AM/AANa solution without other additives and ● same solution with addition of ethanol (10%).*

AM/SSNa membrane

In the experiment, a stock solution containing 17.5% AM, 6% SSNa, 0.1% MBAM and 0.1 $K_2S_2O_8$ was used.   UV irradiation was carried out at a distance of 10 cm for 10
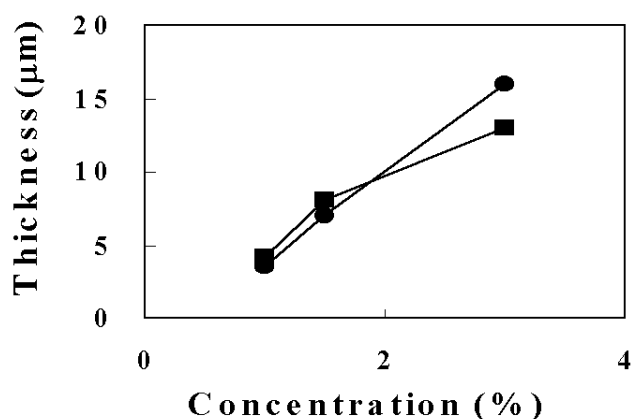
minutes for 10 min (Figure 82).

Figure 82.   *Relationship between solution concentration and the thickness of a membrane; data were averaged from 4 different batch experiments. .* ■ *AM/AANa solution without other additives and* ● *same solution with addition of ethanol (10%).*

AM/SSNa/TiO$_2$ membrane

To further improve the absorption properties and the selectivity to other chemicals of the SAPC materials, titanium dioxide of particle size 0.16 – 0.32 μm was used in the experiment.

Referring to the experiments with other materials, the preparation of membranes of AM/SSNa and TiO$_2$ was tried.   The preparation process was as follow.   First, a stock solution containing 15.4% AM, 7.7% SSNa, 0.1% MBAM and 0.1% K$_2$S$_2$O$_8$ was prepared (concentration = 23 %).   Then, TiO$_2$ was added to make its concentration of 11.5%.   The solution was further diluted with distilled water to a concentration of 4.4%.   UV irradiation was carried out at a distance of 10 cm for 10 minutes. The results showed that the thickness of the membrane was around 15 μm.

6.8.5   Dynamic measurement of the absorption of vapors

In the dynamic measurements, a thermochemical sensor with a silicon chip with integrated thermopiles was used as described on p116. The membranes were coated onto the surface of the silicon chips using method as described in the membrane preparation. Five kinds of samples, AM/VSNa, AM/VSNa/bentonite, AM/SSNa, AM/SSNa/bentonite and AM/SSNa/TiO$_2$, were utilized.

The preparation process of the membranes on the silicon chip was more difficult than on the glass slide because of the surface tensions of the solution as well as the difference of the wettability of the solution with the surface of the glass slide and silicon chips. To compare the reproducibility of the experiment, two parallel membrane samples were prepared under the same conditions using two silicon chips (chip *a* and chip *b*).   There was still a difference between the two silicon chips though much effort were put in the preparation process.   The maximum difference of the thickness of the membranes on chip *a* and chip *b* was less than 10%.

1. Absorption by AM/VSNa membrane

This membrane had a composition of AM: VSNa = 2:1. A set of measurements using different solvent vapors (water, dioxane and chloroform) was carried out with the same membrane. Data in Figures 83 to 100 were averaged from 10 cycles of the experiments. After the absorption, the appearance of the membrane changed from transparent to white. As observed in the thermodynamic experiments, the signal of the absorption of the organic solvent vapors is smaller than that of the water moisture (when normalizing to standard absorption). The reason for this will be discussed later.
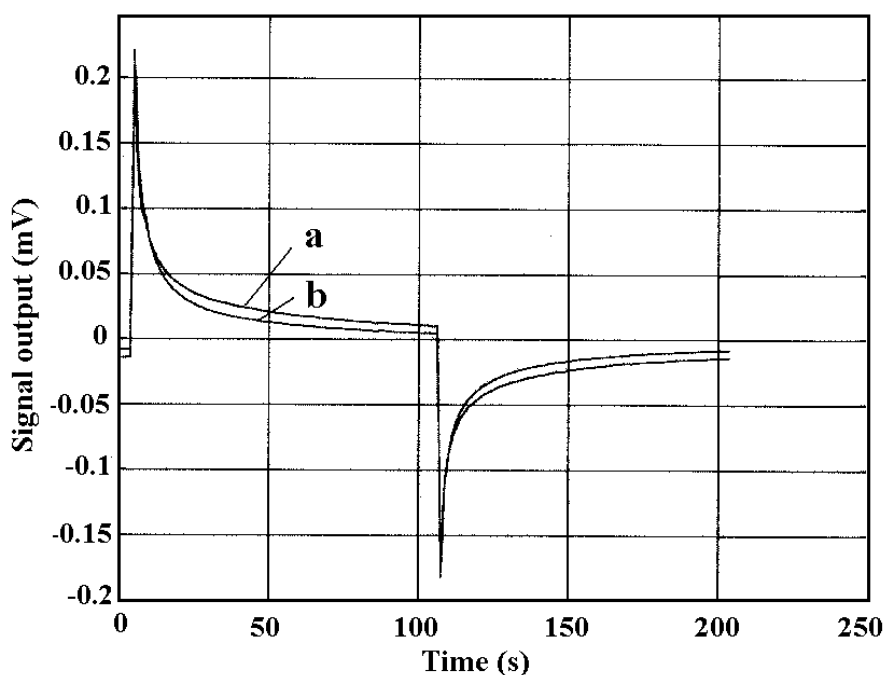
Water vapor

Figure 83.   *Mean value (10 cycles) of the water vapor (3456 ppm) absorption by an AM/VSNa (2/1) membrane on chip a and chip b.*
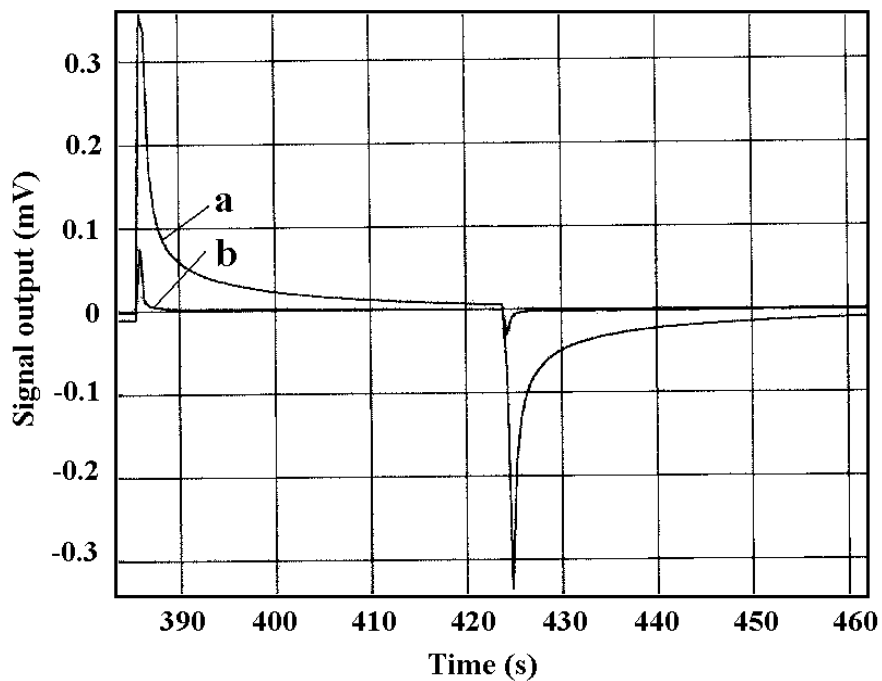
Dioxane

Figure 84. *Average dioxane vapor (34592 ppm) absorption by an AM/VSNa (2/1) membrane on chip a and chip b.*

Chloroform

Figure 85. *Average chloroform vapor (186300 ppm) absorption by an AM/VSNa (2/1) membrane on chip a and chip b.*

2. Absorption by AM/VSNa/bentonite SAPC membrane

Water vapor

Figure 86. *Average water vapor (3456 ppm) absorption by an AM/VSNa/bentonite (4/2/3) membrane on chip a and chip b.*

Dioxane vapor

Figure 87. *Average dioxane vapor (34592 ppm) absorption by an AM/VSNa/bentonite (4/2/3) membrane on chip a and chip b.*

Chloroform vapor

Figure 88. *Average chloroform vapor (186300 ppm) absorption by an AM/VSNa/bentonite (4/2/3) membrane on chip a and chip b.*

The absorption curves were obvious abnormal especially the curves measured with chip *b*.

Second run on the absorption of chloroform vapor by an AM/VSNa/bentonite SAPC membrane
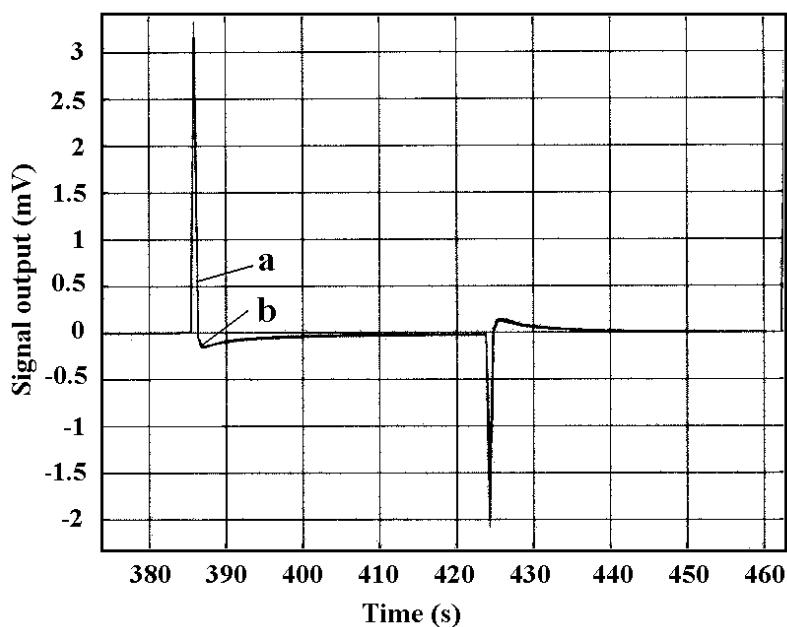
Figure 89. *Average chloroform vapor (186300 ppm) absorption by an AM/VSNa/bentonite membrane on chip a and chip b.*

3. Absorption by AM/SSNa membrane

Water vapor
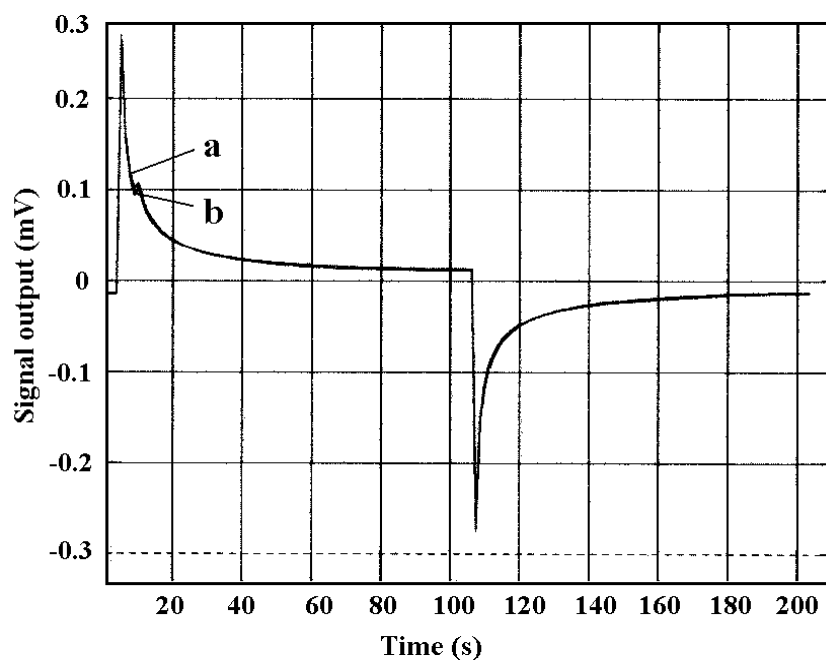
Figure 90. *Average water vapor (3456 ppm) absorption by an AM/SSNa (2/1) membrane on chip a and chip b.*
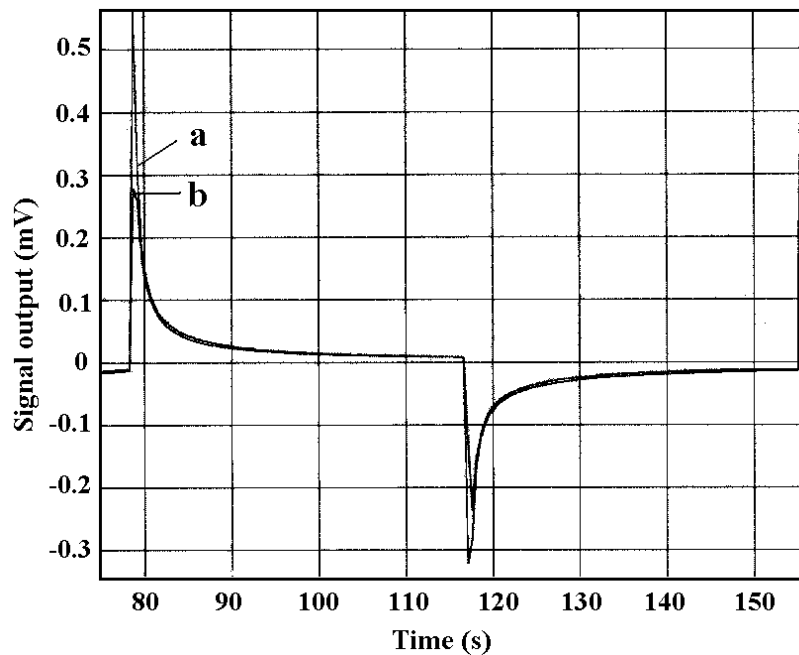
Dioxane vapor

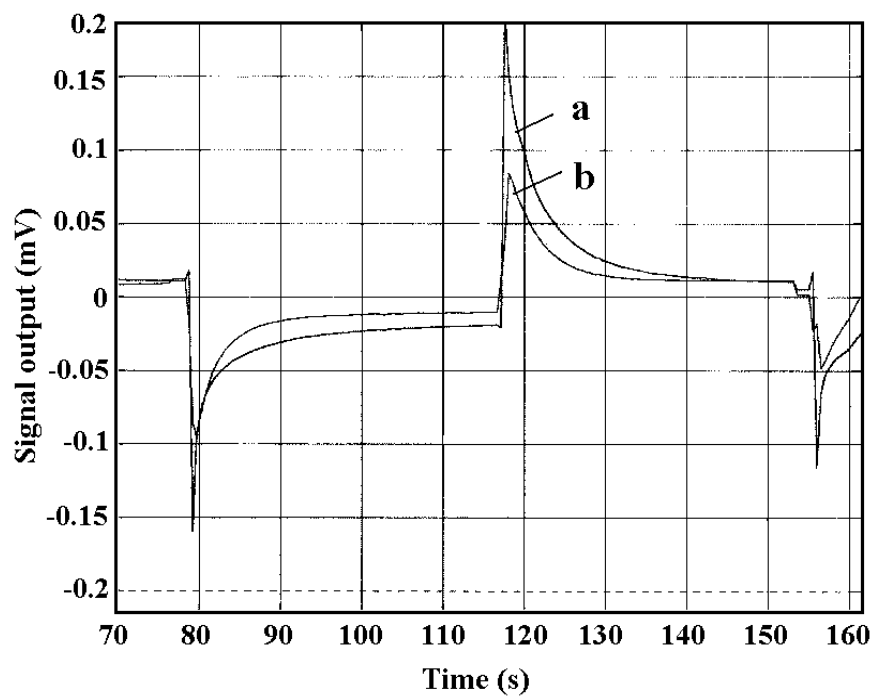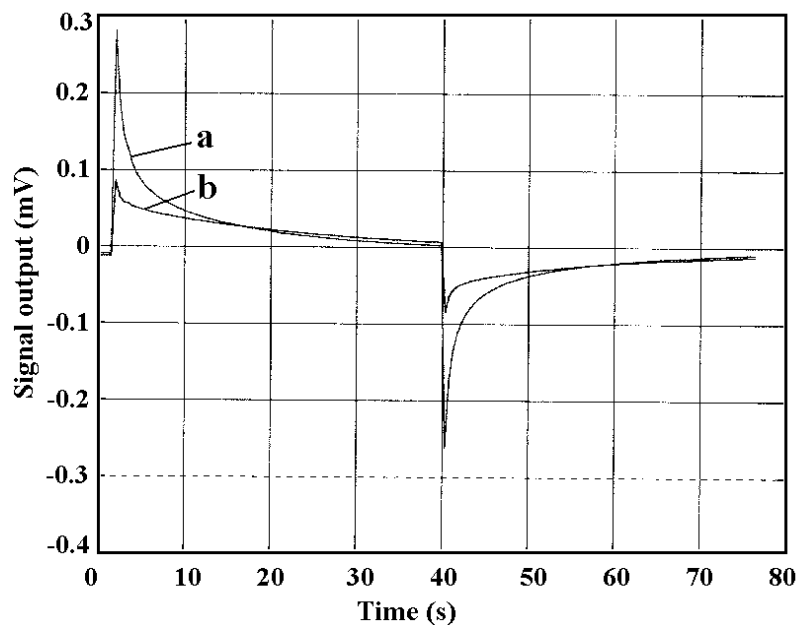**Figure 91.** *Average dioxane vapor (34592 ppm) absorption by an AM/SSNa (2/1) membrane on chip a and chip b.*
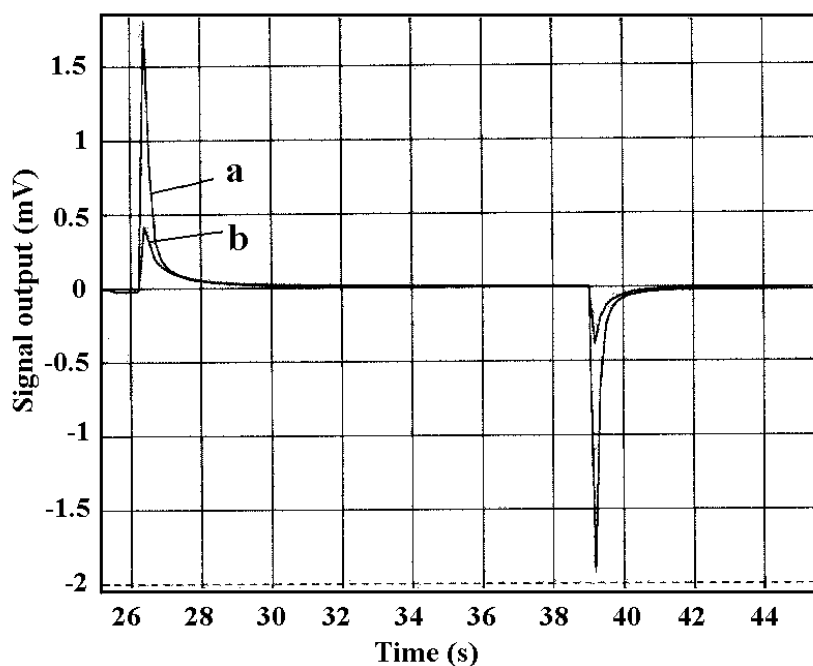
Chloroform vapor

Figure 92. Average chloroform vapor (186300 ppm) absorption by an AM/SSNa (2/1) membrane on chip a and chip b.

4. Absorption by AM/SSNa/bentonite SAPC membrane
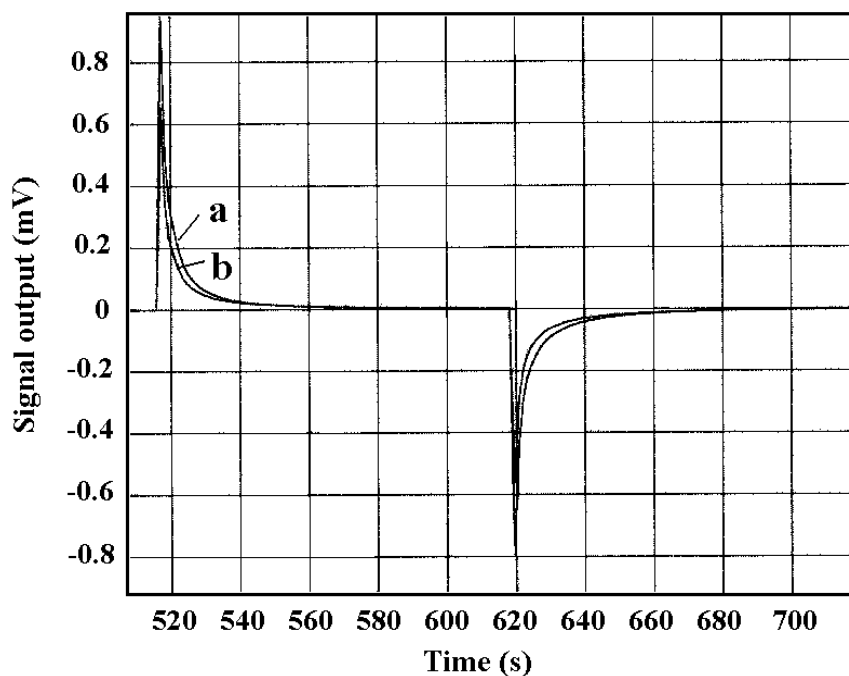
Water vapor

Figure 93. Average water vapor (3456 ppm) absorption by an AM/SSNa/bentonite (4/2/3) membrane on chip a and chip b.
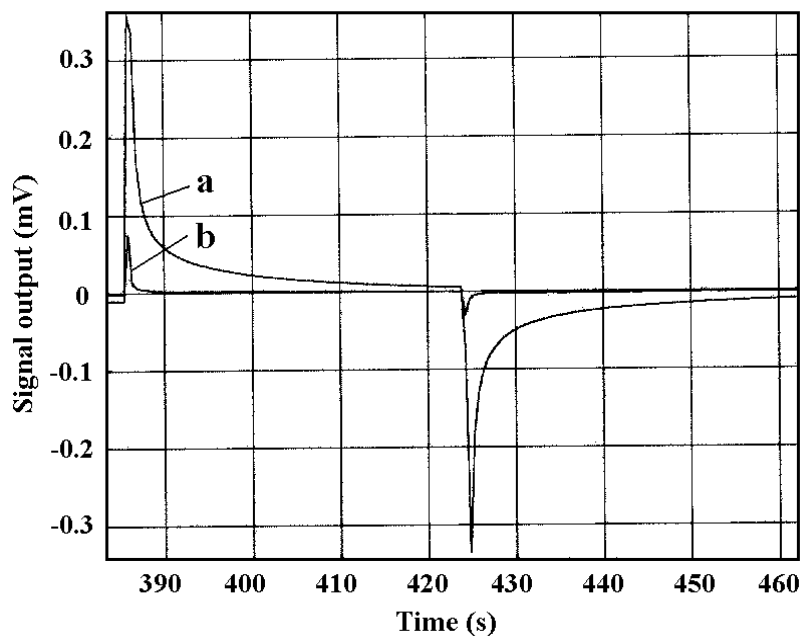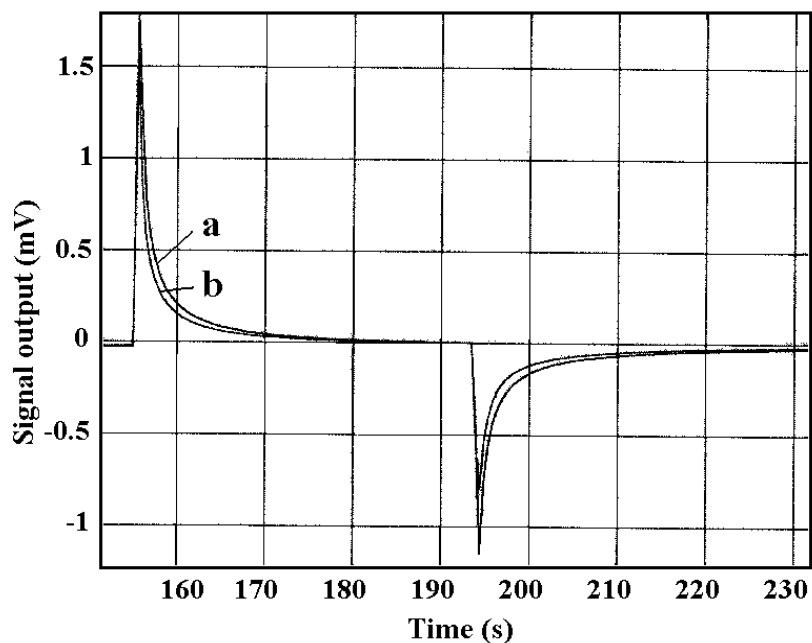
Dioxane vapor

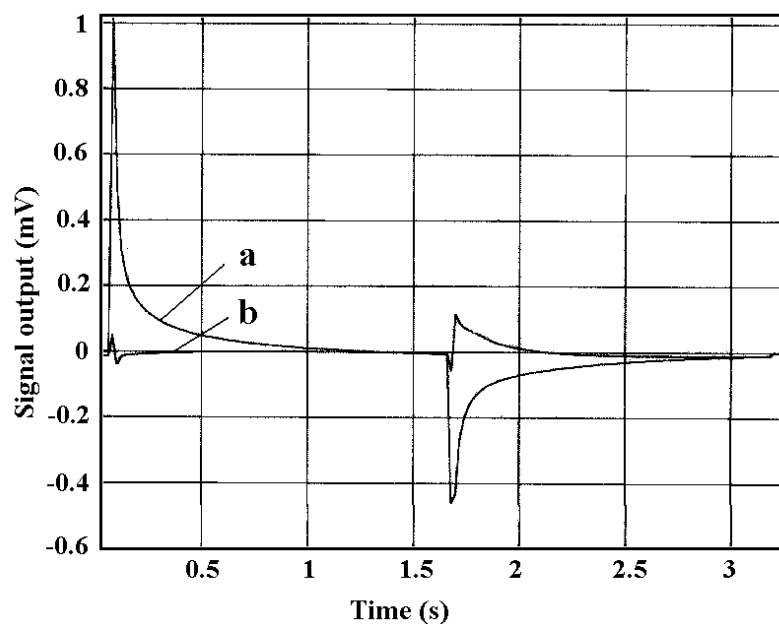*Figure 94.   Average dioxane vapor (34592 ppm) absorption by an AM/SSNa/bentonite (4/2/3) SAPC membrane on chip a and chip b.*

The absorption curves of chloroform was abnormal and showed the same phenomena as in other systems.

5. Absorption by AM/SSNa/TiO$_2$ membrane

Water vapor
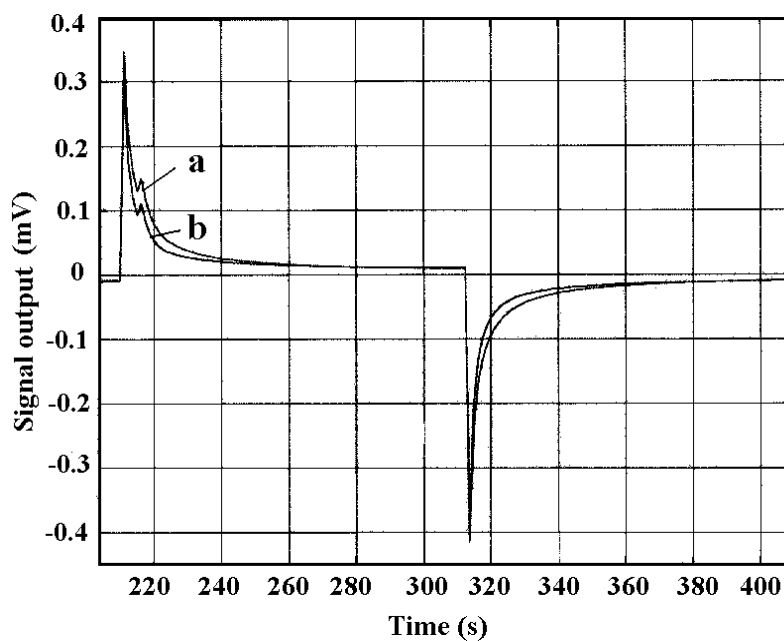
Figure 95.   Average water vapor (3456 ppm) absorption by an AM/SSNa/TiO$_2$ (4/2/3) SAPC membrane on chip a and chip b.
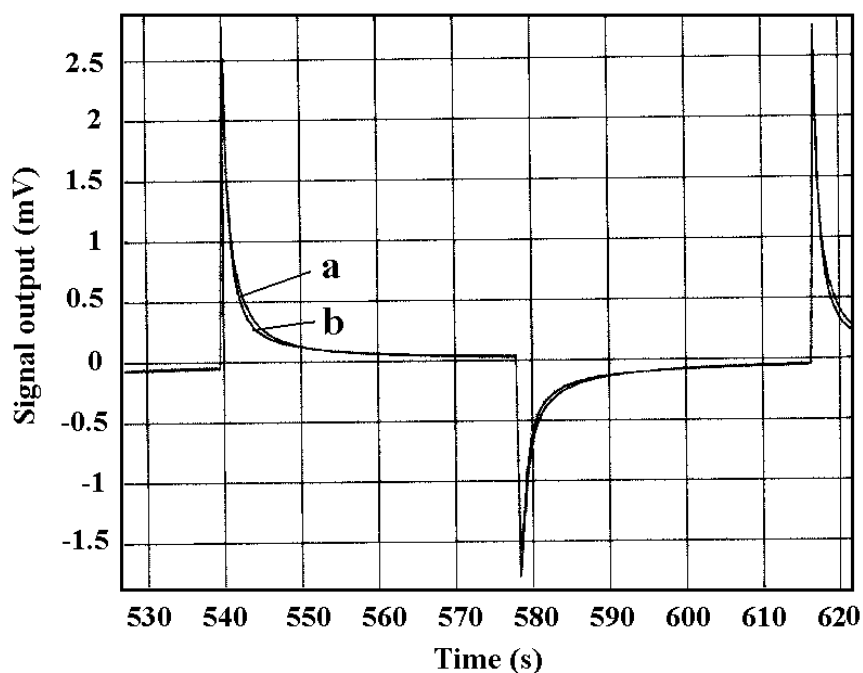
Dioxane vapor

Figure 96. *Average dioxane vapor (34592 ppm) absorption by an AM/SSNa/TiO$_2$ (4/2/3) SAPC membrane on chip a and chip b.*

6. Comparison on the absorption by various membranes

Absorption of water vapor
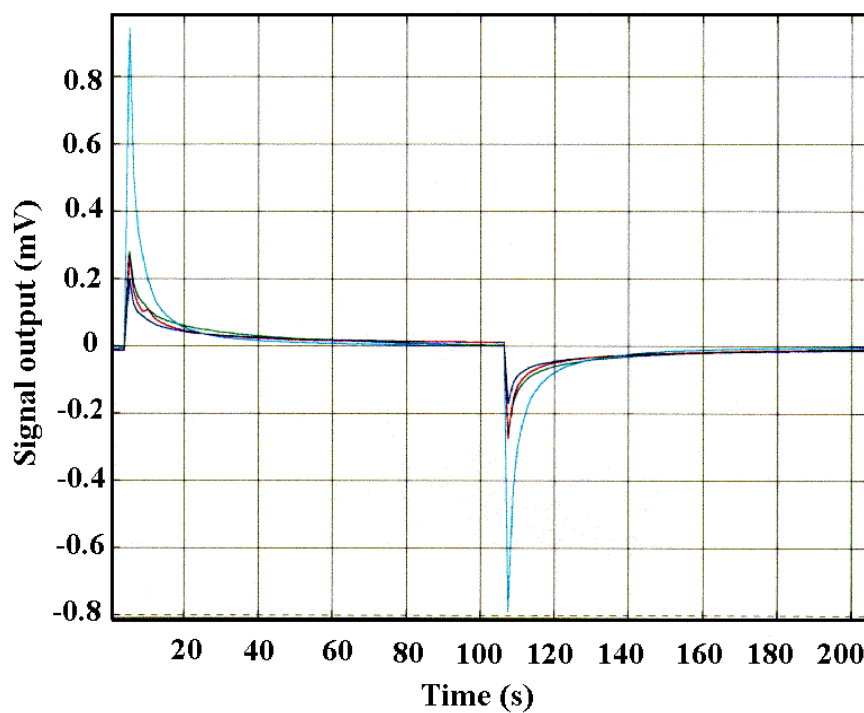
Figure 97. *Average water vapor (3456 ppm) absorption by SAP and SAPC membranes (on chip a) of AM/VSNa (blue), AM/VSNa/bentonite (green), AM/SSNa (red) and AM/SSNa/bentonite (light blue).*
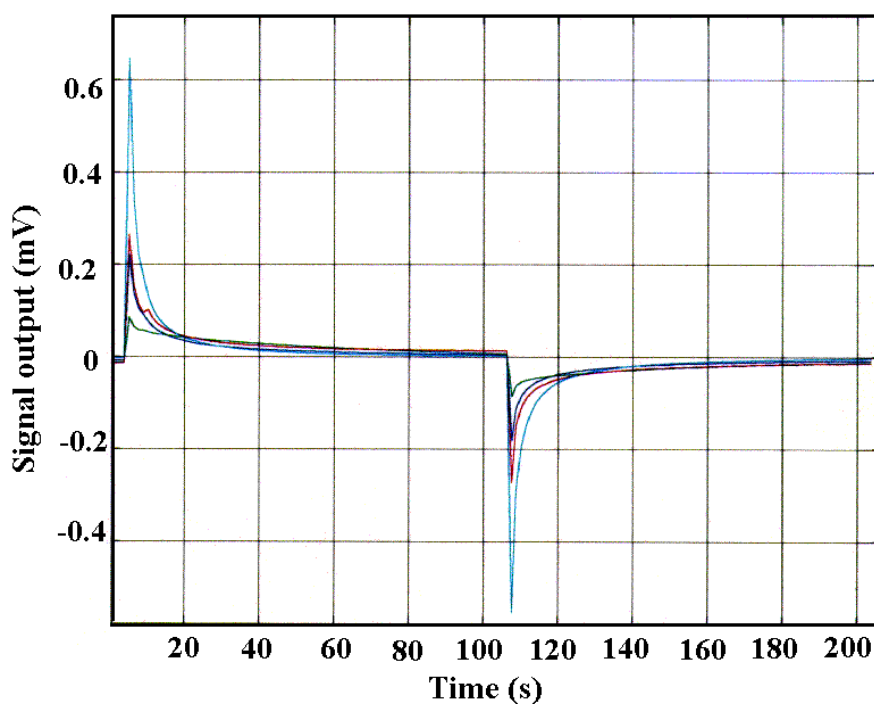
Figure 98. Average water vapor (3456 ppm) absorption by SAP and SAPC membranes (on chip b) of AM/VSNa (blue), AM/VSNa/bentonite (green), AM/SSNa (red) and AM/SSNa/bentonite (light blue)

Absorption of dioxane vapor
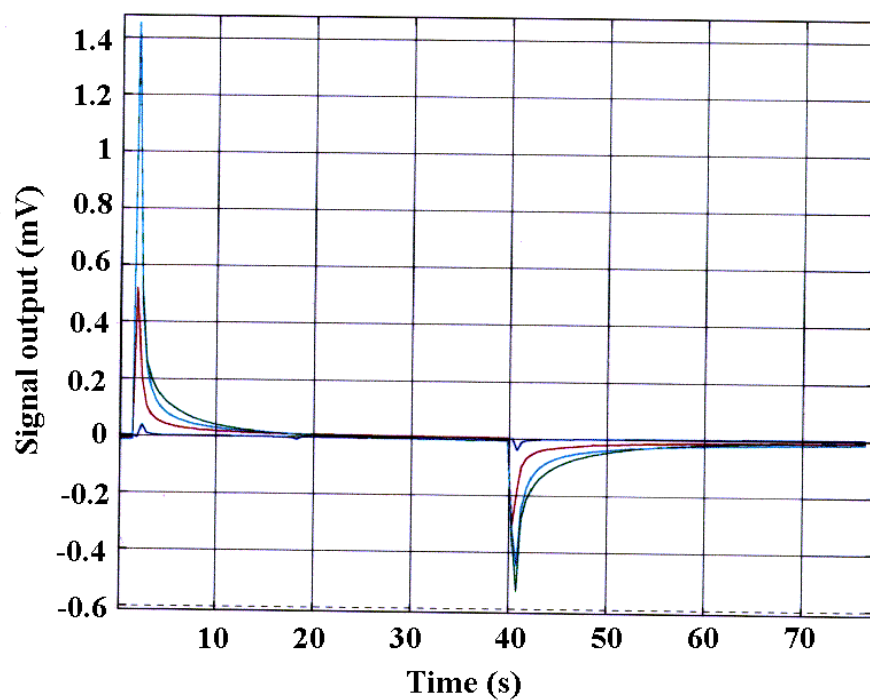
Figure 99. Average dioxane vapor (34592 ppm) absorption by SAP and SAPC membranes (on chip a) of AM/VSNa (blue), AM/VSNa/bentonite (green), AM/SSNa (red) and AM/SSNa/bentonite (light blue)
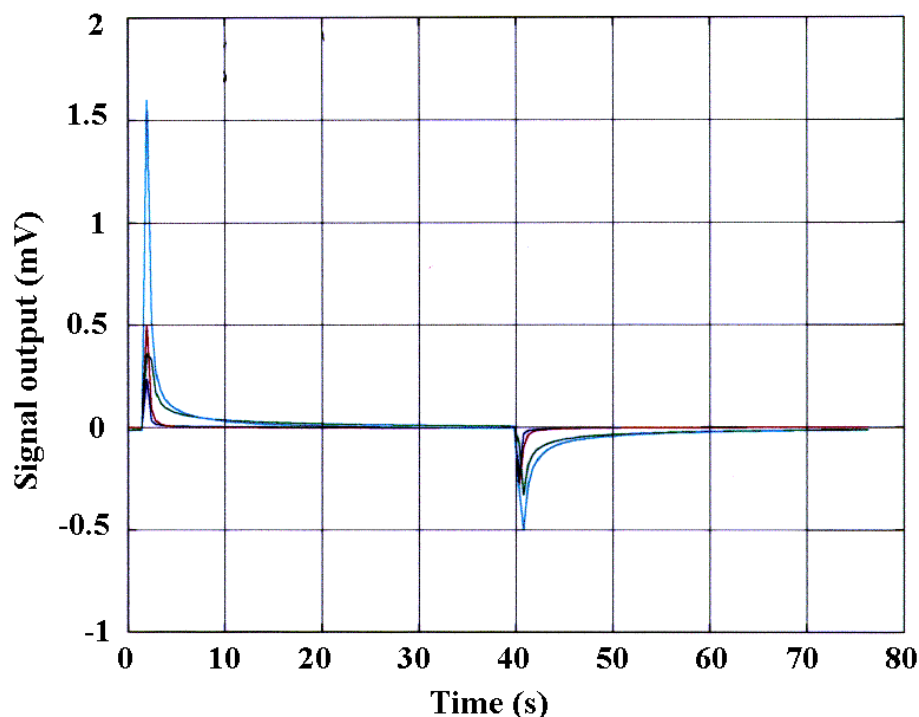
Figure 100. *Average dioxane vapor (34592 ppm) absorption by SAP and SAPC membranes (on chip b) of AM/VSNa (blue), AM/VSNa/bentonite (green), AM/SSNa (red) and AM/SSNa/bentonite (light blue)*

6.8.6   Summary of the dynamic absorption experiments

Looking at the absorption curves, it is evident that the SAPC membranes have a good water moisture sensitivity as well as a water desorption ability.   The sensitivity to dioxane is much less than that to water.   To the sensitivity to chloroform is still lower.   Moreover the absorption curves are not reproducible.   This is difficult to explain and thus needs further studies.   The curve (water and dioxane) shows that at the beginning, the SAPC has a high absorption rate that subsequently decreases.   The decrease of the water moisture absorption rate fitted with a computer shows a second order exponential decay of

$$R_{ab.Water} = 1.13\, e^{-t/1.74} + 0.2911\, e^{-t/8.80},$$

where the t is the absorption time.   The water moisture desorption process showed the same curve shape as that of the absorption. The desorption rate increased very quickly during the first several seconds, then it decreased   according to a similar second order exponential decay model expressed by the equation

$$R_{de.water} = -3.36\, e^{-t/0.92} - 0.38\, e^{-t/8.65}.$$

It is remarkable that the essential time constants agree rather well for both processes. However, in the case of dioxane vapor, the absorption and desorption curves of SAPC were obviously unsymmetrical (see Figure 84, 87, 91, 94, 96). The absorption shows a high and rather sharp peak but the desorption process has a low and broad peak.   The fitted absorption equation

$$R_{ab.dioxane} = 0.0039 + 41.91\, e^{-t/0.22} + 0.1774\, e^{-t/3.85}$$

showed decay of the absorption rate by a second order law.   The desorption equation was

$$R_{de.dioxane} = 0.0051 - 0.39\, e^{-t/0.91} - 0.057\, e^{-t/0.85}.$$

The exponents and the preexponential terms of the two dioxane absorption and desorption equations are so different from each other (also different from the water moisture absorption) that they suggest different mechanisms for absorption and desorption.

From the comparison above, one can conclude that the AM/SSNa/bentonite SAPC has the highest absorption to water moisture and the AM/SSNa/TiO$_2$ has the highest absorption to dioxane vapor. But, the absorption peak of organic vapor was obviously weaker than that of the water moisture. The reason for this is presumably related to differences in the absorption mechanism. The SAPC material had a stronger absorption peak of water moisture because the process was chemisorption and the organic vapor absorption was presumably governed by physisorption. Normally, chemisorption has activation energy levels of 60 - 400 kJ and physisorption only about 8-40 kJ[120]. The composite of AM/SSNa/TiO$_2$ had a lower sensitivity to water moisture absorption compared to AM/SSNa/bentonite, but it had the highest sensitivity for absorption of dioxane vapor. These results indicate that there is good potential for applications of SAPC as material to monitor water moisture and some solvent vapor for use in environmental sensors.

To check the reproducibility of the process, the absorption and desorption cycles were repeated more than a 100 times (Figure101) without noticeable decay of the maximum (about +1 mV) or minimum (about -0.8 mV) output voltages thus confirming the feasibility to utilize SAPC membrane to construct a functional moisture sensor.
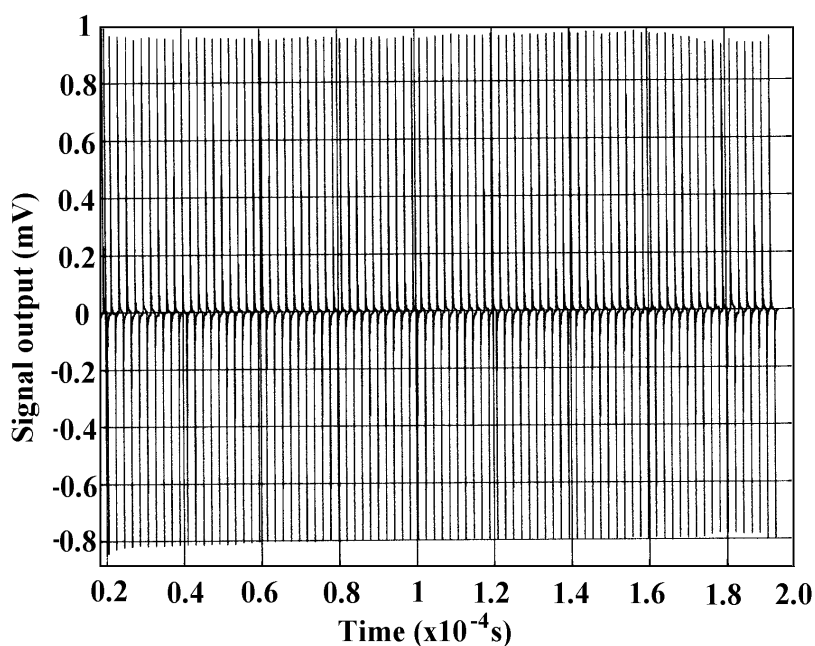
Figure 101. *Reproducibility of the output voltage signal of a moisture sensor coated with a 18 μm thick membrane of SAPC (AM/SSNa/bentonite). (Ref. 120)*

6.9   Other potential applications

Because of the smart (intelligent) properties of SAPC, it has a higher potential for high-tech application. In response to the environmental stimulus, the SAPC hydrogel can be used as artificial muscle, actuator and for drug delivery system (DDS). Brock, using a

similar hydrogel studied the basic principle of intelligent hydrogel as an artificial muscle[160]. In the study, he designed a device with two antagonist artificial muscles to control a single link thus to simulate the movement of the muscles. Also, he designed a linear actuator based on the PAN hydrogel fibers using an integral fluid irrigation system[161]. Kaetsu studied the DDS using hydrogel as an intelligent valve for controlled release of drugs[162]. The systems have a sensor-actuator gate consisting of polyelectrolyte hydrogel layer with immobilized enzymes inside fine holes of polyethylene terephthalate (PET) film and silicon wafer as base materials. Excimer-laser or ion-beam irradiation was used for the etching of holes in PET film and photo-lithography was used for the etching of silicon wafer. U.V. And gamma-ray irradiations were used for the polymerization and immobilization of electrolyte layers in the holes. Various kinds of signal responsive release systems such as pH responsive, substrate responsive, Ca^{2+} responsive, photo-responsive and electric field responsive systems have been developed using those techniques. This DDS technology can also be used in other fileds such as for the delivery of pesticide, plant-growth regulator and fertilizer in agriculture, fishery drug and hormone in aquaculture industry, fragrant of clothing and catalyst for chemical reaction etc[163].

Nüesch studied the bentonite/HDPE foil[164] as a flexible insulating and auto-sealing materials for the use in underground construction to prevent the leaking of ground water by auto-close the rips and holes of up to 3cm diameter through expansion of the Smectites. The bentonite foil is a thin (< 1mm), flexible, water-impervious HDPE-foil with an about 3mm pasted Na-Bentonite sheet which is superior to the conventional passive systems. The utilization of this sealing material is therefore of great meaning. The Na-bentonite e.g. Wyoming (USA) shows an up to 9-times volume-increase by expansion. This expansion in the Nano-area represents the actual self-healing potential which has neither freeze-thaw cycle nor cement-water disadvantageous influences. Calcium chloride solution in a concentration of 10g/l does not affect the expansion. So, it has not endangered the stability of bentonite due to the contact with cement-water.

Similar technology has been studied in Alberta Research Council, Canada by Zhou who used the clay/polymer composite as protective lining for landfills, construction waterproofing and other civil engineering applications[165]. All the above applications show higher application potential of SAPC in both industrial and high-technology fields.

7.   SUMMARY

1.   Expanding clay/polyacrylamide composites have the capacity to absorb large amounts of water while retaining good mechanical strength and high damping characteristics, and therefore represent a new and promising class of hydrogel materials. In this study, bentonite (montmorillonite) has been used as expanding clay mineral.

2.   It is feasible to use electron-beam irradiation to prepare superabsorbent polymer/clay composites (SAPC). The irradiation atmosphere affects the polymerization, the crosslinking process. There is a threshold ratio of the organic monomer in the SAPC. Below this threshold ratio, the polymer chains can not string the bentonite particles together to form a cross-linked network. High concentration of monomer benefited the polymerization, as well as the post-treatment process, but decreased the water absorption capacity of SAPC because of the higher cross-linking density. Furthermore, too high a concentration may cause the polymerization system to be too viscous to be handled. The polymerization heat limited the concentration of acrylamide in the polymerization system to below 30%. By properly controlling parameters such as irradiation dose, dose rate, atmosphere, the ratio of organic monomer to bentonite and the concentration of the system, SAPC with required quality and design properties could be obtained.

Acrylic acid or sodium acrylate can be used for preparation of SAPC by an electron-beam induced polymerization method. The neutralization degree of acrylic acid in form of pH value affected the polymerization process. In the process of AA/bentonite polymerization, an optimum irradiation dose was found where the highest water absorption capacity (WAC) of SAPC could be obtained. Increasing concentration of AA benefits the post-treatment process but decreased the WAC of SAPC. The highest concentration of AA in a solution can not be over 30%-w/w for getting a good polymerization.

3.   A novel route towards a superabsorbent poly(acrylamide)-bentonite composite (SAPC) material, utilizing UV radiation as a polymerization agent, was successfully developed. It was found that potassium persulfate has a sufficiently large accelerating effect on the radiation-induced polymerization of acrylamide monomer as well as sodium acrylate in the interlayer space of montmorillonite.

4.   Studies of the WAC in grams water absorbed per gram of SAPC, using a statistical experimental design of Box-Behnken type, showed that the most important factors influencing the WAC were the NaOH concentration (positive effect), the N, N-methylene bisacrylamide concentration (negative effect), and the potassium persulfate concentration (weakly negative effect).

5.   The maximum WAC obtained experimentally was 2344 g/g (electron beam) and 1175 g/g (UV), respectively but larger values are expected by further process optimization, for example by an increase of the radiation fluence of the UV source as well as variation of the polymerization temperature.

6.   Characterization of the SAPC by ^{27}Al NMR spectroscopy showed that intercalation of acrylamide into the interlayer space of montmorillonite caused a change in the relative proportions of Al^{VI} and Al^{IV} coordination. This could also be confirmed by XRD data that showed an increase of the interplanar spacing of (001) of montmorillonite from 1.25 nm to 2.09 nm consistent with the intercalation of two molecular layers of acrylamide.

XRD analysis of SAPC containing sodium vinylsulfonate and sodium styrenesulfonate showed that intercalation could also take place in the copolymerization system (acrylamide with sodium vinylsulfonate, sodium p-styrenesulfonate) which increased

the basal spacing from 1.25 to 2.04 nm. However, the addition of sodium acrylate had a different effect on the XRD curves. The peak at 1.5 nm (Ca-montmorillonite) disappeared when AANa was added in amounts exceeding an AANa/AM ratio of 3, and the peak of basal spacing could not be identified anymore. This was due presumably to the replacement of Ca by Na, and the newly formed spacings were too large to be measured with normal XRD equipment. Characterizations of SAPC using XRD, SEM, DSC, TGA, FTIR and NMR showed that the structure of SAPC was that the acrylamide combined with montmorillonite in three different ways: a. AM intercalated in the lamina of montmorillonite in bimolecular layers and bound by van der Waals force and hydrogen bonds; b. AM bonded to the montmorillonite surface by hydrogen bonds; c. AM in free state as a polymer string network.

7. Rheological results showed a fully cross-linked structure resembling a visco-elastic rubber-like material. Dynamic and stress relaxation tests showed that the water-swollen poly(acrylamide)/bentonite composite hydrogel behaved rheologically as a viscoelastic crosslinked structure in the range of 50 - 95 % water content. Frequency sweep and step strain measurements indicated that with increased water content the material responded more quickly to mechanical deformation. The strengthening effect of the bentonite concentration was found to be exponential, $G' = G'_0\exp(Ac)$, over a wide range of frequencies of sinusoidal dynamic testing, with a weak ω-dependence appearing as $G'_0(\omega)$ and $A(\omega)$. The rheological behavior of SAPC hydrogel networks is hence exceptionally resilient when exposed to shear strain with high perturbation frequencies. Even with high water content up to 95% they retain properties resembling those of true solids. In particular, a SAPC block of 1 m side lengths containing 80% of water would be dimensionally stable at a dynamic elastic storage modulus G' of 10 kPa, i.e. it would not slump under its own weight. This opens up very interesting applications in fields where vibration damping is required.

8. From the swelling behavior of SAPC, it can be inferred that the expansion power generated by an SAPC gel under the experimental conditions selected is 6×10^{-7} - 9×10^{-6} W per gram SAPC in monolithic gel form, and 1.6 - 5×10^{-4} W per gram of SAPC in membrane form. Big bulky SAPC blocks and longer swelling times can produce higher work. However, the power (the capacity to do work in unit time) is smaller. The thinner the SAPC material is, the faster it swells and the more power it generates.

9. Temperature retaining (heat storage) property tests proved that the SAPC could prevent heat loss in the aqueous solution and keep the temperature for longer periods.   This suggests a potential for application in the medical field, e.g. in heating pads.

Thermal stability experiments below 200 °C showed that within the experimental range, the SAPC had a higher thermal stability than the pure polymer system. This important finding suggests a wide application range for the SAPCs at elevated temperature.

10. SAPC is sensitive to the pH of the surrounding solution as well as to electric fields. These properties could be used to convert chemical energy into mechanical motion to simulate muscle action in robotics or as a means for controlled drug delivery systems etc.

11. The water absorption capacity (WAC) of SAPC is a strong function of the salt concentration; and follows the well-known Flory equation, $Q_m^{5/3} \cong A/S + B$, where $A = (i/2Vu)^2/(v/V_0)$, and $B = (1/2 - X_1)/V_1]/(v/V_0)$. Q is the swelling ratio, S is the reciprocal ionic strength of the solution.

12. The oilfield experiment in the Jilin Oilfield, China showed that during treatment of water wells with SAPC, the average increase of oil output was 220%. Hence, the SAPC showed a high application potential in EOR (enhanced oil recovery).

13. Preliminary tests with SAPC/sand mixture showed a significant potential for SAPC application in acid mine tailing abatement. The use of SAPC in bottom liners of a tailing pond is not a viable option because of the poisoning effect of multi-valent cations on the SAPC. However, a SAPC-bearing cover should be an effective hydraulic barrier. Essentially, the cover would be an impermeable barrier and would retain its water saturation.

14. Using SAPC in the production of soybeans and beets had an obvious draught-resistant effect and therefore increased the production output and the sugar content in beet. The SAPC has an obvious effect on the rice seedling in simplifying the seedbed management, increasing the survival rate of the young plants, shortening the seedling time, and increasing the production output.

15. Comparing to other absorbents such as molecular sieves, activated alumina and silica gels, in a range of relative humidity (R.H.) 11.3-100%, the SAPC has a higher absorption ratio to water vapor. Experiments showed that SAPC could be used for absorbing water in gasoline/diesel fuel. It can also be used for dewatering of other non-polar solvents.

16. The addition of small amounts (0.5%) of SAPC as a superplasticizer/ additive to an aluminate cement had a positive effect on the mechanical properties of concrete made from this cement. The compressive strength and the stiffness, expressed by the modulus of elasticity, increased in a statistically significant way with increasing amounts of SAPC.

17. Studies of the dynamic water vapor absorption behavior revealed that the absorption rate was initially very fast but later decreased with time. This suggests that the water vapor absorption rate of SAPC is controlled predominantly by the diffusion rate of water molecules in the SAPC network.

Thin films were produced for utilization in a moisture sensor. The thickness of the films could be controlled within the range of 4 to 400 μm. A working prototype moisture sensor was constructed using an SAPC membrane integrated with a silicon chip transducer. From this a reproducible voltage signal was obtained in response to the changing amount of water vapor in air.

Optimization of the membrane preparation techniques on the silicon chips proved the feasibility to tailor the membrane of moisture/chemical sensor that can be controlled in size, shape, and thickness.

18. Evaluation of dynamic absorption of various organic solvent vapors on SAPC was carried out using a thermochemical sensor. A composite of acrylamide/sodium p-styrenesulfonate/bentonite had the highest water moisture absorption sensitivity (275 nV/ppm). Composites of acrylamide/sodium p-styrenesulfonate/titanium dioxide had the best absorption to organic vapor (dioxane, 81 nV/ppm). These compositions have a high potential for application in moisture and chemical sensors, respectively.

8.   REFERENCES

1.   Harmon, S. Plains, US Patent 3 670 731 (1972).

2.   G.F. Fanta, RC. Burr, C. R. Russell, and C.E. Rist, J. Macrom. Sci. -Chem., A-**4**, (1970) 331; G.F. Fanta, RC. Burr, W.M. Doane, C. R. Russell, J. of Appl. Polym. Sci., **15** (1971) 2651-2660.

3.   Chemical Week, 21 (July 7, 1974).

4.   F. L. Buchholz, Trends Polym. Sci., **2**(8) (1994) 277-281.

5.   C. Hu, Technology and Market of Water-soluble polymers and Superabsorbent Polymers, Information Center of Chemical Industry of China (1995).

6.   Annual report 1996 of Hüls, Hüls Aktiengesellschaft, Marl Konzern-und Marktkommunikation (1997).

7.   B. K. G. Theng, Formation and Properties of clay-Polymer Complexes, Elsevier, Amsterdam (1974).

8.   Y. Rong, Y. Jiang, R. Li, L. Shen, Chinese Patent 85102156(1985).

9.   D. Gao, Preparation and Property improvement of Superabsorbent Polymer Composite, A Final Report on the Joint Research Activities at ARC, Edmonton, Canada (1993).

10. D. Gao, and R.B Heimann, Polymer Gels and Networks **1**, (1993) 225-246.

11. Experiment on the application of SAPC in water injection well for the adjustment of oil production cross-section, Department of Oil Well Operation of Jilin Oilfield, (1985).

12. Experiment on the SAPC as water retention agent, Beat Administration section, Zhaodong, Heilongjiang, China (1985).

13. Oya and Y. Kurokawa, J. of Mat. Sci., **19**(35) (2000) 1045-1050.

14. K. Saotome, JP Kokai Tokkyu Koho 98713(1986).

15. N. Hiroda, JP Kokai Tokkyu Koho 183762(1983), K. Saotome, JP Kokai Tokkyu Koho 203084 (1989).

16. M. Toyama, Chemistry **45**(2) (1990)108-110 (Japanese).

17. Y. Mijima, JP Kokai Tokkyo Koho 59353 (1988).

18. N. Hirogawa, S. Fijida, T. Masamizu, JP Kokai Tokkyo Koho 75016 (1988).

19. S.N. Bhattacharyya and D. Maldas, J. of Polym. Sci., Polym. Chem. Edition, **21** (1983) 3281-3290; P. K. Sahoo, H. S. Samantary and R.K. Sama, J of Appl. Polym Sci. **32** (1986) 5693-5703.

20. G. F. Fanta, E. I. Stout, W. M. Doane, US Patent 4 134 863 (1979).

21. S. Yang, Z. Zhang, Chemical World, **5** (1990) 213-215; J. Xiong, X. Li, Chemical World, **1** (1990) 18-21.

22. K. Saotome, Kobunshi Kako **8**(39) (1990) 403-406 (Japanese).

23. E. G. Muller, US Patent 4 333 461 (1982).

24. H. Tsubakimoto, T. Shidamura, H. Kobayashi, K. Okamura, JP Kokai Tokkyu Koho 144748(1987); JP Kokai Tokkyu Koho 14312 (1989); H. Tsubakimoto, T. Shidamura, H. Kobayashi, JP Kokai Tokkyu Koho 36309 (1986); H. Mitaku, Y. Hasuna, H. Kobayashi, T. Shidamura, JP Kokai Tokkyu Koho 249808 (1989); H. Kobayashi, H. Mitaku, T. Shidamura, T. Hoda, JP Kokai Tokkyu Koho 167306(1989).

25. H. Tashiro, JP Kokai Tokkyu Koho 284507 (1989) .

26. F. Masuda, Kokyusuiseiporima, Tomotachi Press, Tokyo (1988) (Japanese).

27. M. Tatsumi, S. Sonoda, Y. Kojima, T. Mitsuo and S. Yamamoto, Kobunshi Ronbunshu, **45**(2) (1988) 169-175.

28. P. J. Flory, Principle of Polymer Chemistry, Cornell University Press, New York (1953).

29. Y. Osada, R. Kishi and M. Hasebe, J. of Polym. Sci. Part C, **19** (1981) 303-308.

30. M. Suzuki, Int. J. Japan Soc. Prec. Eng., **25**(3) (1991) 169-174.

31. R. A. Siegel and B. A. Firestone, Macromolecules, **21**, (1988) 3254-3259.

32. L. B. Peppas and N. A. Peppas, Chem. Eng. Sci., **46**(3) (1991) 715-722.

33. T. G. Park and A. S. Hoffman, J. Appl. Polym. Sci., **46** (1992) 659-671.

34. Suzuki & T. Tanaka, Nature, **346** (1990) 345-347.

35. T. Tanaka, Science, **218** (1982) 467-469.

36. Y. Rong, Y. Jiang, L. Shen, G. Sun, D. Gao, P. Sun, Y. Liu, J. Hou, Selected Theses of Heilongjiang Acad. of Sci., (1988) 48.

37. A.J. Swallow, Radiation Chemistry. An Introduction, Longman Group Ltd. (1973).

38. Charlesby, Atomic Radiation and Polymers, Oxford, Pergamon press, (1960) 368.

39. Y. Rong, Y. Jiang, G. Sun, D. Gao, Proceedings. of 3rd China Radiat. Proces. Symp. (1990) 6.

40. R.M. Quigley, Atomic Energy of Canada Ltd. Report, AECL-7827, (1984).

41. D. Gao, Y. Yamamoto, K. Hayashi, J. Chem. Soc. Chem. Commun., (1990) 910.

42. Y. Yamamoto, S. Shiraki, D. Gao, Hydrophobic Acceleration of p-Styrenesulfonate Polymerization by r-Cyclodextrin, J. Chem. Soc. Perkin Trans. **2** (1993)1119-1122

43. G.E.P.Box and D.W. Behnken, Technometrics **2**(4) (1960) 455-475.

44. Statistics for Zhengjiao shejifa

45. Clays data (Süd-Chemie AG) (1997)

46. Y. Takemto, K. Miyada, K. Kimura, Inclusion Compound, Tokyo Kagakutomohito, Tokyo (1989).

47. M. L. Bender and M. Komiyama, Cyclodextrin Chemistry, Springer-Verlag, Berlin (1978).

48. J. Szejtli, Cyclodextrins and Their Inclusion Complexes, Akademiai Kiado, Budapest (1982).

49. Ueno, K. Takahashi, and T. Osa, J. Chem. Soc., Chem. Commun. (1980) 921.

50. D. F. Eaton, Tetrahedron, **43** (1987) 1551.

51. Ueno, I. Suzuki, and T. Osa, J. Chem. Soc., Chem. Commun. (1988) 1373.

52. Harada and S. Nozakura, Polym. Bull., **8** (1982) 141.

53. S. Hamai, J. Phys. Chem., **93**, (1989) 6527.

54. N. K. Sangwan and H.-J. Schneider, J. Chem. Soc., Perkin Tram. **2** (1989)1223 and references cited therein.

55. D. C. Rideout and R. Breslow, J. ,Am. Chem. Soc., **102** (1980) 7817.

56. Schneider and A. J. Swallow, Makromol. Chem., **114** (1968)155.

57. M. Anbar, Fundamental Processes in Radiation Chemistry, ed. P. Ausloos, Interscience, New York, (1968) 651.

58. G. V. Buxton, in The Study of Fast Processes and Transient Species by Electron Pulse RadioIysis, eds. J. H. Baxendale and F. Busi, D. Reidel. Dordrecht. (1982) 241.

59. Y. He, G. Gao, S. Shou, K. Jia, Mineralogy, Changchun Geology University Press., Changchun (1981).

60. M. Ogawa, K. Kuroda and C. Kato, Clay Science, **7** (1989) 253-251.

61. M. C. MacEwan, Trans. Faraday Soc. **44** (1948) 349-367.

62. S. Burchill, P. L. Hall, R. Harrison, .H. B. Hayes, J. I. Langford, W. R. Livinston, R. J. Smedley, D. K. Ross and J. J. Tuck, Clay Minerals **18** (1983) 373-397

63. TH. Stutzman, B. Siffert, Clays and Clay Minerals **25** (1977) 392-406

64. P. Espinasse and B. Siffert, Clays and Clay Minerals 27 (1979) 279-284

65. B. Siffert, P. Espinasse, Clays and Clay Minerals **28**(5) (1980) 381- 387

66. B. Siffert and Y. Bocquent, Colloids and Surfaces, **11** (1984) 137-143

67. K. Tanihara and M. Nakarawa, Nippon Kagaku Kaishi, **5** (1975) 782-789.

68. Q. Gu, D. Wu, G. Yi, G. zhang, Y. Yang, L. Wu, Chemical Journal of Chinese, **2**(20) (1999) 324-326.

69. Y. Wang, B. Wu and D. Yu, Chem. J. of Chinese Univ., **4**(26) (1999) 94-96.

70. Y. Wang, B. Wu and D. Yu, Chem. J. of Chinese Univ., **7** (20) (1999) 1143-1148.

71. G. Chen, M. Li and K. Yao, Polymer Mat. Sci. & Eng., **3**(15) (1999) 9-14.

72. Q. Wu, Z. Xue, Z Qi and F. Wang, Acta Polymerica Sinica, **5** (1999) 551-556.

73. Oya and Y. Kurokawa, J. of Mat. Sci., **35** (2000) 1045-1050.

74. Y. Sugahara, K. Kuroda and C. Kato, J. Materials Sci. **23** (1988) 3572-3577,.

75. Y. Sugahara, S. Satogawa, K. Kuroda and C. Kato, Clays and Clay Minerals, **38**(2) (1990) 137-143.

76. V. Izakov, Zh. Strukt. Khimii, **7**(6)   (1966) 898-900.

77. D. Gao, R.B. Heimann, M. Williams, J. Materials Sci. **34**   (1999) 1543-1552

78. J.D. Ferry, Viscoelastic Properties of Polymers, 2nd ed.(John Willy and Sons, Toronto,1970)

79. C.R. Wildemuth and M.C. Williams, Rheologica Acta **24**(1985) 75.

80. T. Shiga, Y. Hirose, A. Okada, T. Kurauchi, J. Appl. Polym. Sci. **47** (1993) 113-119.

81. Report on Adjustment of Water-Absorbing Formation in Water-Injection Well using SAPC, Downhole Operation Section, Jilin Oilfield (1989).

82. Application of SAPC in oilfield, Report of New Technology Application Station, Shuguang Oil Recovery Factory (1990).

83. Report on the Application of SAPC in Oilfield, Institute of Oil Recovery Technology of Daqing Oilfield (1989).

84. Y. Zhang, Report on the Application of SAPC in Oilfield, Technical Physics Institute of Heilongjiang Academy of Sciences (1986).

85. R.V. Nicholson, R.W. Gillham, J.A. Cherry, E.J. Reardon, Canadian Geotechnical Journal, **26** (1989) 1-8.

86. R.V. Nicholson, F.F. Akindunn, R.C. Sydor and R.W. Gillham, Proceedings of the Second international Conference on the Abatement of Acid Drainage, September 16-18, 1991 Montreal, Quebec (1991) 443-460.

87. E.K. Yanful, Proceedings of the Second international Conference on the Abatement of Acid Drainage, September 16-18, 1991, Montreal, Quebec (1991) 461 -485.

88. E.K. Yanful, and L.C. St-Arnaud, Proceedings of the Second international Conference on the Abatement of Acid Drainage, September l6-l8, l99l, Montreal, Quebec (1991) 487-504.

89. E.K. Yanful, Oxygen Diffusion through Soil Covers on Sulfide Mine Tailings, the ASCE Journal of Geotechnical Engineering **119** (1993) 1207-1228.

90. H.H. Head, Soil Technician's Handbook, Pentech Press, London (1989) 157.

91. B.H. Sheldrick, Analytical Methods Manual, Land Resource Research Institute, Ottawa, Ontario (1984).

92. K. Masuda and H. Iwata, Powder Technology, **63**(1990) 113-119.

93. J. Asano, M. Matsumoto, Nippon Sakkyu Kenkyukai Hapyokai, 1983, 8 :

94. M. Tooyama, Kagaku (Chemistry), **45** (2) (1990) 108-110 (Japanese).

95. Recommended Agriculture Technology, Agriculture Technology Generalizing Section of Heilongjiang (1998) 207.

96. Report on the application of SAPC in Harbin Battery Factory, Research Institute of Harbin Battery Factory (1985).

97. Y. Liu, D. Gao, J. Hou, RB. Heimann, H. Zheng, Y. Yang, Chemical Engineer, **3** (1996) 7-9

98. B.T. Brown, Chem. Eng. Prog., **8**(66) (1970) 54-60.

99. M. H. Moseman. CEP, February (1982) 78-83.

100. D. Basmadjian, The Adsorption Drying of gases and liquids, (1984).

101. D. R. Burfield. Ana. Chem.; 14(48) (1976) 2285-2287.

102. Frohnsdorff. and J. Skalny, Cement in the 1990s: challenges and opportunities. Philos. Trans. R. Soc. London. Ser. A, **310** (1983) 17-30.

103. D. M. Rov, Science, **255** (1987) 651-658.

104. J. F. Young, Mater. Res. Soc. Symp. Proc., **179** (1991) 101-122.

105. K. P. Groskurth, Mater. Res. Soc. Symp. Proc., **179** (1991) 273-282.

106. M. R. Silsbee, D. M. Rov and J. H. Adair, Mater. Res. Soc. Symp. Proc., **179** (1991) 129-144.

107. J. D. Birchall, A. J. Howard. and L.K. Kendall, European patent 0021682 (priority date 26 June 1979).

108. J. D. Birchall, Phil. Trans. R. Soc. London. Ser. A, **310** (1983) 31-42.

109. C. S. Poon, L. E. Wassell and G. W. Groves, Br Ceram. Trans. J, **86** (1987) 58-62.

110. L. Czarnecki and E. Osiecka, Bull. Liaison Lab. Ponts. Chaussees, **108** (1980) 29-36.

111. R C. Hewlett and J. F. Young, J. Mater. Educ., **9**, No. 4, (1987) 389-435.

112. S. Dowdy and S. Wearden, Statistics for research, Wiley, New York (1983).

113. D. D. Double, Phil. Trans. R. Soc. London. Ser. A, **310** (1983) 53-66.

114. G.E.R. Box, W.G. Hunter and J.S. Hunter, Statistics for experimenters. Wiley, New York, 1978.

115. B. R. Eggins, Biosensors: an Introduction, Wiley and Teubner (1996).

116. K. R. Rogers, Biosensor and Chemical Sensor Technology, ACS Washington (1995).

117. Costa and S. Miertus, Trends in Electrochemical Biosensors, London (1992).

118. Z. Shen, G. Wang, *Colloid and Surface Chemistry*, Chemical Industry Press. 1991.

119. W. Hemminger, G. Höhne, Calorimetry: fundamentals and practice, Verlag Chemie, Weinheim (1984).

120. C. Günther, R. Pfestorf, M. Rother, J. Seidel, R. Zimmermann, G. Wolf and V. Schröder, J. Thermal Anal., **33** (1988) 359

121. D. Gao, R.B. Heimann, J. Lerchner, J. Seidel and G. Wolf, J. of Mat. Sci. **36**(18) (2001) 4567-4571.

122. R.I. Masel, Principles of Adsorption and Reaction on Solid Surface. John Wiley & Sons Inc. New York (1996) 111.

123. M. Bakass, A. Mohnklisse, M. Ben Chanaa, M. Lallemant, Thermochimica Acta **206** (1) (1992) 309.

124. FL. Dickert, M. Tortschanoff, K. Weber, M. Zenkel, Fresenius, J. of Ana. Chem., **362** (1) (1998) 21-24.

125. HZ. Bu, SR. Mikkelsen, Ana. Chem., **78**(20) (1998) 4320-4325.

126. GQ. Wang, WS. Shen, GD. Zhang, GS. Zhang, J. of Nature Science of Heilongjiang University, (1996) 62-64.

127. K. Nakagawa, Sensors and Actuators B- Chemical, **52**(1-2) (1998) 10-14.

128. TAP. Rocha, MTSR. Gomes, AC. Duarte, JABP Oliverira, Ana. Communications, **35**(12) (1998) 415-416.

129. MI. Baraton, Nanotechnology, , **9**(4) (1998) 356-359.

130. SLR. Barker, R. Kopelman, Ana. Chem., **70**(23) (1998) 4902-4906.

131. M. Matsuguch, T. Kuroiwa, T. Miyagishi, S. Suzuki, T. Ogura, Y Sakai, Sensors and Actuators, **52**(1-2) (1998) 53-57.

132. MMF. Choi, OL. Tse, Ana. Chem. Acta, **378**(1-3) (1999) 127-134.

133. MJ. Yang, Synthetic Metals, **81**(1) (1996) 65-69.

134. SX. Pang, H. Grassl, H. Jager, J. of Atmospheric and Oceanic Tech., **13**(5) (1996) 1110-1115

135. K. Ogura, H. Shiigi, M. Nakayama, J. of Electrochemical Society, **143**(9) (1996) 2925-2930.

136. ET. Zellers, M.W. Han, Anal. Chem., **68**(14) (1996) 2409-2418.

137. K. Bodenhofer, A. Hierlemann, G. Noetzel, U. Weimar, W. Gopel, Ana. Chem. **68**(13) (1996) 2210-2218.

138. K. Tanaka, C. Igarashi, P. Tagliatesta, T. Boschi, Y. Sadaoka, J. of Materials Chem., **6**(6) (1996) 953-956.

139. GE. Collins LJ. Buckley, Synthetic Materials, **78**(2) (1996) 93-101.

140. M. Trojanowicz, ML. Hichmann, Electroanalysis, **8**(3) (1996) 263-266.

141. D. L. Ellis, MR. Zakin, LS. Bernstein, MF. Ruber, Ana. Chem., **68**(5) (1996) 817-822.

142. JS. Marvin, HW. Hellinga, J. of American Chem. Soc., **120**(1) (1980) 7-11.

143. LR. Jordan, PC. Hauser, GA. Dawson, Electroanalysis, **9**(15) (1997) 1159-1162.

144. XC. Zhou, L. Zhong, SFY. Li, SC. Ng, HSO. Chan, Sensors and Actuators B-Chemical, **42**(1) (1997) 59-65.

145. J. Langmaier, F. Opekar, Z. Samec, Sensors and Actuators B- Chemical, **41**(1-3) (1997) 1-6.

146. Wang, CD. Feng, SL. Sun, CU. Segre, JR. Setter, Sensors and Actuators B- Chemical, **40**(2-3) (1997) 211-216.

147. Z. Liron, K. Kaushansky, G. Frishman, D. Kaplan, J. Greenblatt, Ana. Chem., **69**(14) (1997) 2848-2854.

148. DB. Radloff, S. Kurosawa, K Hirayama, T Arimuram K. Otake, A. Sekiya, N. Minorura, M. Rapp, HJ. Ache, Mol. Cryst. and Liq. Cryst. Sci. and Tech. Section A - Mol. Cryst. and Liq. Cryst., **294** (1997) 439-442

149. G. Casaldboremeceli, N. Camaioni, G. Beggiato, M. Campos, CM. Mari, J of Appli. Electrochem., **27**(4) (1997) 441-447.

150. CW. Lin, BJ. Hwang, CR. Lee, Materials Chem. and Phy., **55**(2) (1998) 139-144.

151. S. Komaba, M. Seyama, K. Tanabe, T. Osaka, Electrochemica Acta, **42** (3) (1997) 383-388

152. V, Svetlicic, AJ. Schmidt, LL. Miller, Chem. of Materials, **10**(11) (1998) 3305.

153. K Korsah, CL. Ma, B. Dress, Sensors and Actuators, B. Chem., **50**(2) (1998) 110-116.

154. N. Dewit, E. Vanneste, HJ. Geise, LJ. Nagels, Sensors and Actuators, B. Chem., **50**(2) (1998) 164-172.

155. MEH. Amrani, RM. Bowdeswell, PA. Payne, KC. Persaud, Sensors and Actuators B-Chemical, **44** (1-3) (1997) 512-516

156. B. Zimmermann, J. Burck, HJ. Ache, Sensors and Actuators, B. Chem., **411**(1-3) (1997) 45-54.

157. J.H. Holtz, S.A. Asher, Nature, **389** (6653) (1997) 829-832

158. S. Rosler R. Lucklum, R. Borngraber, J. Hartmann, P. Hauptmann, Sensors and Actuators B- Chemical, **48**(1-3) (1998) 415-424.

159. L. Torsi, M. Pezzuto, P. Siciliano, R. Rella, L. Sabbatini, L. Valli, PG. Zmbonin, Sensors and Actuators B- Chemical, **48**(1-3) (1998) 362-367.

160. D. L. Brock, Dynamic model and control of an artificial muscle based on contractile polymers. MIT. A.I. Memo 1331 (1991).

161. D. L. Brock, W. Lee, D. Segalman, W. Witkowski, A Dynamic model of linear Actuator based on polymer hydrogel, MIT. A.I. Memo icim 944 (1991).

162. I. Kaetsu, K. Uchida, H. Shindo, S. Gomi, K. Sutani, Radiat. Phy. and Chem., **55**(2) (1999) 193-201.

163. I. Kaetsu, Kobunshi Mochiita Deribarishisutemu, (Delivery System with Polymer), Kobunshi Kako **37**(5) (1988) 243-248

164. R. Nüesch, Amart Bentonit-HDPE-Folien als active grandwassererabdichung in Tiefbau,

165. Accelerating Innovation -2001 Annual Report, Edmonton, Canada (2001) 22

Acknowledgments

Abbreviations:

AA	Acrylic acid
AANa	Sodium acrylate
AM	Acrylamide
aq.	Aqueous
d.f.	Degree of freedom
DSC	Differential Scanning Calorimetry
f	Frequency
FTIR	Fourier Transform Infrared spectroscopy
g.cm	Gram.centimeter
G^*	Modulus
G^+	Shear modulus
G	Storage modulus
H	Enthalpy
ΔH	Specific enthalpy per gram sample
i	Electronic charge on the polymer structure per polymer unit
K	Kelvin
mA	Milliampere
MBAM	Methylene N, N'- bisacrylamide
md	Millidarcy
meq	Milligramequivalent
min	Minute
mK	Millikelvin
MeV	Megaelectron-volt
mV	Millivolt
mW	Milliwatt
nm	Nanometer
NMR	Nuclear Magnetic Resonance
nV	Nanovolt
ppm	Parts per million
p.s.i.	Pound per square inch
Q	Swelling ratio
q	measured heat exchanged
Q_{ad}	Absorption heat
Q_r	Reaction heat
R	Radius
s	Second
S	Ionic strength of solution
SAP	Superabsorbent Polymer and/or co-polymer
SAPC	Superabsorbent polymer clay composite
SSNa	Sodium styrenesulfonate
TG	Thermal Gravimetric analysis
VSNa	Sodium vinylsulfonate
V	Volt
V_0	Un-swollen polymer volume.
V_1	Molar volume of solvent
Vu	Polymer repeating unit volume
W	Watt
WAC	Water absorption capacity

X_1	Interaction parameter of polymer with solvent
XRD	X-ray Diffraction
γ^o	Shear strain
ϕ	Fraction
η	Viscosity
ν	Effective number of chains in a real network
θ	Angular
σ	Standard deviation
τ	Sheer stress
ρ	Density
ω	Angular velocity

Appendix 1

Table A- 1. Computing of Box-Behnken design

No	$Y(x_0)$	x_1	x_2	x_3	x_1^2	x_2^2	x_3^2	x_1x_2	x_1x_3	x_2x_3	$\hat{Y}_{calc}$
1	2045	+	+	0	+	+	0	+	0	0	2080
2	2003	+	-	0	+	+	0	-	0	0	2000
3	721	-	+	0	+	+	0	-	0	0	700
4	601	-	-	0	+	+	0	+	0	0	620
5	1739	+	0	+	+	0	+	0	+	0	1740
6	2344	+	0	-	+	0	+	0	-	0	2340
7	378	-	0	+	+	0	+	0	-	0	360
8	941	-	0	-	+	0	+	0	+	0	960
9	1041	0	+	+	0	+	+	0	0	+	1030
10	1799	0	+	-	0	+	+	0	0	-	1830
11	1130	0	-	+	0	+	+	0	0	-	1150
12	1573	0	-	-	0	+	+	0	0	+	1550
13	1890	0	0	0	0	0	0	0	0	0	
14	1525	0	0	0	0	0	0	0	0	0	
15	1944	0	0	0	0	0	0	0	0	0	
Σ^+	21684	8131	5606	4288	10772	10921	10947	2646	2680	2614	16360
Σ^-			2641	5315	6657				2724	2722	2929	
$\Sigma^+-\Sigma^-$			5490	291	-2369	10772	10921	10947	-78	-42	-315	
$x_{0,i,ii,ij}$			1373	73	-592	1347	1365	1368	-39	-21	-158	
$b_{0,i,ii,ij}$	1786	687	37	-296	-241	-204	-197	-20	-10	-86	
σ^2	51951										4374
$V(b_{0,i,ii,ij})$	17317		6494		17317			12988			
S.E.$(b_{0,I,ii,ij})$	132		81		132			114			
Cov(b_0b_{ii})			-4329								
Cov(b_0b_{ij})			1082								

$Y(x_0)$: experiment results; $\hat{Y}_{calc.}$: calculated values

$\Sigma^+ = \Sigma x_i\, y_i\ (x = +)$;

$\Sigma^- = \Sigma x_i\, y_i\ (x = -)$;

$x_{0,i,ii,ij} = F_{0,i,ii,ij} = (\Sigma^+ - \Sigma^-)/x_i^+$ (factor effect)

$b_0\ = \ddot{y}_0,\quad \ddot{y} = \Sigma y_i\, /i$ (average value);

$b_i\ = A\{iy\},\ \{iy\} = \Sigma x_{in}\, y_n$;

$b_{ii}\ = B\{iiy\} + C_1\ \Sigma\{jjy\} + C_2 \Sigma\{lly\} - (\ddot{y}_0 /S)$;

$b_{ij} = D_1\, \{ijy\}$, i,j, first associates;
$b_{ij} = D_2\, \{ijy\}$ i,j second associates;

$\sigma = [(y_i - \ddot{y})^2/(n - 1)]^{1/2}$ (standard deviation)

$V(b_0) = \sigma^2/n_0$ (variance of b_0)

$V(b_i) = A\sigma^2$ (Variance of linear coefficients)

$V(b_{ii}) = [B + 1/S^2 n_0] \sigma^2$ (variance of parabolic coefficients)

$V(b_{ij}) = D_1 \sigma^2$ i,j first associates   (Variance of coefficients of 2-factor interaction)

$V(b_{ij}) = D_2 \sigma^2$ i,j second associates (Variance of coefficients of 2-factor interaction)

$Cov(b_0 b_{ii}) = -\sigma^2/S^2 n_0$;

$Cov(b_{ii}bjj) = [C_1 + 1/S^2 n_0]\sigma^2$ i,j first associates;

$Cov(b_{ii}bjj) = [C_1 + 1/S^2 n_0]\sigma^2$ i,j second associates.

Here, $A = 1/8$; $B = 1/4$; $C_1 = -1/16$; $C_2 = 0$; $D_1 = 1/4$; $D_2 = 0$; $S = 2$; $n_0 = 3$.

Appendix 2

Table A- 2. Master table for statistical calculations

No	$Y(x_0)$	x_1	x_2	x_3	x_1x_2	x_1x_3	x_2x_3	x_1^2	x_2^2	x_3^2	$\hat{Y}_{calc.}$	$\hat{Y}_{calc}-Y^*$
1	412	+	+	0	+	0	0	+	+	0	460	48
2	926	+	-	0	-	0	0	+	+	0	1068	142
3	205	-	+	0	-	0	0	+	+	0	140	-65
4	542	-	-	0	+	0	0	+	+	0	748	206
5	562	+	0	+	0	+	0	+	0	+	578	16
6	795	+	0	-	0	-	0	+	0	+	828	33
7	282	-	0	+	0	-	0	+	0	+	370	88
8	290	-	0	-	0	+	0	+	0	+	396	106
9	228	0	+	+	0	0	+	0	+	+	303	75
10	240	0	+	-	0	0	-	0	+	+	297	57
11	874	0	-	+	0	0	-	0	+	+	767	-107
12	1173	0	-	-	0	0	+	0	+	+	1049	-134
13	515	0	0	0	0	0	0	0	0	0	543	28
14	549	0	0	0	0	0	0	0	0	0	543	-6
15	566	0	0	0	0	0	0	0	0	0	543	-23
Σ^+	8159	2695	1085	1946	954	852	1401	4014	4600	4444		
Σ^-		1319	3515	2498	1131	1077	1114					
$\Sigma^+ - \Sigma^-$		1376	-2430	-552	-177	-225	287	4014	4600	4444		
$X_{0,i,ii,ij}$		319	-608	-138	-88	-113	144	502	575	556		
$B_{0,i,ii,ij}$	543	160	-304	-69	-44	-56	72	-86	61	22		
σ^2		675										
$V(b_{0,i,ii,ij})$	225	84			169			225				
$SE(b_{0,i,ii,ij})$												
$Cov(b_0b_{ii})$					-56							
$Cov(b_0b_{ij})$					14							

*Y: average $Y(x_0)$.   (Interpretations of the calculation see Table A-1)

Appendix 3

Experiments on the measurement of rheological property

Samples containing water contents of 95, 85 and 50% were all prepared by post-treatment of a base hydrogel containing approximately 70% water. The samples were first saturated with distilled water to some degrees and then were cut by hand to a disc shape of 2 mm in thickness and 50 mm in diameters and kept in air-tight plastic bags to prevent the evaporation of moisture.

Rheological (dynamic and step strain) measurements were carried out with a Rheometric Mechanical Spectrometer, model 800 (RMS800) fitted with a 2-2000 g Force Rebalance Transducer (FRT) to sense the material torque response under strain. Samples were contained between two horizontal parallel stainless steel platens of 50 mm diameter. In the RMS 800, the lower platen is driven to achieve the desired strain program $\gamma(t)$ in the sample. The upper platen in such testing remains stationary, transmitting torque from the sample to the FRT. Data are converted to the relevant material properties by computer software integral to the testing system. Material strain is reported as $\gamma = \theta R/h$, where the θ is the programmed angular displacement of the lower platen, R is platen radius, and h is the controlled separation of the platens (here, h $\cong$ 2 mm). While the γ - measure is actually the strain at the outer rim (γ_R), and γ is not uniform in the sample (varying with radial position, from 0 at the center to the maximum γ_R), the measured torque is completely dominated by conditions at the greatest radial position so that $\gamma \cong \gamma_R$ is a good rheological parameter to associate with shear stress and resulting torque measurements, and generally is used when reporting results from such testing.

Because the hydrogel composites were wet to the touch, despite their solid-like behavior, it was determined to avoid or minimize the possibility of sample slippage on the steel platens. A layer of abrasive paper was therefore glued to both platens prior to loading each sample. The modified surfaces, with the water-proof "wet-and-dry" abrasive paper (United Abrasives Inc., Willimmantic, CT, USA, grade 400A, particle size 21-24 μm) were found in preliminary tests to be superior to use of unaltered steel surfaces alone.

Samples were removed gently from their airtight bags and laid onto the lower platen in a concentric position, after which the upper platen was lowered until contact was made at approximately h = 2 mm. The uneven thickness of hand-cut samples led to uneven contact with platen surfaces, suggesting that more uniform surface contact might result by moving the upper platen further downward, exerting a small compression that would deform the uneven regions laterally. This was indeed possible for the samples of 95 and 85% water content, for which material was squeezed outward beyond the platens by 3-5 mm and then trimmed off. The samples with only 50% water were too stiff to be compressed enough to achieve this outflow, but were also trimmed to align with the platen rim.

In this sample configuration, the only mechanism for moisture loss during testing is evaporation from the sample/air surface at the platen rim. Such moisture loss would

cause increasing local solids concentration, and because of its location at r = R, a disproportionately high reading of torque. This potential problem was overcome by two precautions: (a) coating the free surface with a thin layer of silicone oil (moisture barrier) of viscosity sufficiently low to have no effect on torque measurements, and (b) closing an oven attachment around the platens and placing water-soaked tissues within it, thus saturating the atmosphere around the samples and eliminating humidity gradients that might drive the evaporation.

Linear viscoelastic properties are defined to characterize material sensitivity to time and rate variables i.e., $G'(\omega)$ and $G^+(t)$ and thus must be independent of nonlinearities in the form of residual dependency on testing parameters such as γ and γ^o. It was therefore necessary to determine what range of γ^o or γ would be sufficiently small so that nonlinearities would not appear, while using strain amplitudes as large as possible so that stress response of the samples would also be large and could be measured easily and accurately. These compromises are often found in the strain range of 1-10%, but must be found empirically for each material. In the present testing, G' was first measured at fixed ω (0.1 rad/s) for a wide range of γ^o (to be show below), from which it was found that G' was γ^o - independent for samples with 95% water if $\gamma^o \leq 10\%$, and for samples with 85% water if $\gamma^o \leq 5\%$. For samples with 50% water, it was difficult to find a γ^o sufficiently small to give a truly linear response (as will be demonstrated below), so that $\gamma^o = 0.1\%$ and 0.2% were chosen arbitrarily for further ω-testing; use of smaller γ^o did not produce material stresses large enough to measure. A similar investigation for $G^+(t)$ found most results to be independent of γ after the initial rapid stress build-up, so that in the stress relaxation regime ($t \geq 0.03$ sec) $G_r(t)$ showed little γ-dependency.

Appendix 4

Calculations for concrete experiments

Table A- 3. Coding of factor levels and experimental response*

No	x_1	x_2	x_3	x_1x_2	x_1x_3	x_2x_3	x_1^2	x_2^2	x_3^2	$Y_{f.c}$	$Y_E(10^3)$	$Y_{f.t}$†
1	+	+	0	+	0	0	+	+	0	64.5	18.1	5.76
2	+	-	0	-	0	0	+	+	0	72.1	22.3	5.01
3	-	+	0	-	0	0	+	+	0	46.0	13.9	5.86
4	-	-	0	+	0	0	+	+	0	76.2	24.8	5.54
5	+	0	+	0	+	0	+	0	+	62.0	19.6	5.80
6	+	0	-	0	-	0	+	0	+	78.6	22.9	6.20
7	-	0	+	0	-	0	+	0	+	68.7	20.3	6.21
8	-	0	-	0	+	0	+	0	+	81.2	25.2	6.43
9	0	+	+	0	0	+	0	+	+	62.7	17.9	5.78
10	0	+	-	0	0	-	0	+	+	56.8	17.5	5.50
11	0	-	+	0	0	-	0	+	+	62.5	20.8	5.56
12	0	-	-	0	0	+	0	+	+	73.9	22. I	5.82
13	0	0	0	0	0	0	0	0	0	55.5	17.5	5.91
14	0	0	0	0	0	0	0	0	0	65.9	20.8	6.06
15	0	0	0	0	0	0	0	0	0	56.0	15.9	5.36
Σ										982.9	299.6	86.79
Y_{ave}										65.5	20.0	5.79
$\sigma(S)$										5.8	2.5	0.37

The unit of Y is megapascals. The values σ (S) were obtained from the center points (runs 13-15).   † The $Y_{f.c}$ and Y_E values are the averages of three replicates; the $Y_{f.t}$ values are the averages of two replicates.

Table A- 4. Measured Y and predicted ($\hat{Y}$) values, and the residuals (Y- $\hat{Y}$) calculated from the reduced polynomials (Equations (10) – (12))

$Y_{f.c}$	$\hat{Y}_{f.c}$	(Y- $\hat{Y}$)	Y_E	$\hat{Y}_E$	(Y- $\hat{Y}$) ($\times 10^3$)	$Y_{f.t}$	$\hat{Y}_{f.t}$	(Y- $\hat{Y}$)
64.5	66,5	-2.0	18.1	19.9	1.8	5.76	5.55	0.21
72.1	66.5	5.6	22.3	20.5	1.8	5.01	5.55	-0.54
46.0	55.2	-9.2	13.9	16.5	-2.6	5.86	5.55	0.3l
76.2	77.5	-1.3	24.8	23.8	1.0	5.54	5.55	-0.01
62.0	66.4	-4.4	19.6	23.0	-3.4	5.80	6.17	-0.37
78.6	78.9	-0.3	22.9	24.0	-1.1	6.20	6.17	0.03
68.7	66.4	2.3	20.3	20.0	0.3	6.21	6.17	0.04
51.2	67.8	13.4	25.2	24.0	1.2	6.43	6.17	0.26
62.7	53.8	8.9	17.9	16.0	1.9	5.78	5.67	0.11
56.8	66.3	-9.5	17.5	20.0	-2.5	5.50	5.67	-0.17
62.5	64.8	-2.3	20.8	19.9	0.9	5.56	5.67	-0.1l
73.9	77.3	-3.4	22.1	23.9	-1.8	5.82	5.67	0.15
55.8	59.2	-3.4	17.5	18.1	-0.6	5.91	5.78	0.13
65.9	59.2	6.7	20.8	18.1	2.7	6.06	5.78	0.28
56.0	59.2	-3.2	15.9	18.1	-2.2	5.36	5.78	-0.42

Table A- 5. Calculation of the factor effects. Coefficients of the polynomial, and factor significance.

	$Y_{f.c}$	Y_E	$Y_{f.t}$
Effects of factors			
x_1	1.3	-325	-0.32
x_2	-10.9	-3920	-0.18
x_3	-12.5	-4000	0.27
$x_1 x_2$	11.3	3350	0.22
$x_1 x_3$	-2.1	800	-0.09
$x_2 x_3$	8.7	650	0.27
x_1^2,	14.2	4130	0.27
x_2^2	-3.1	-720	-0.73
x_3^2	12.74	3730	0.51
Coefficients for polynomials			
b_0	59.20	18100	5.78
b_1	0.65	-162	-0.159
b_2	-5.45	-1960	-0.09
b_3	-6.25	-2000	0.136
b_{12}	5.65	1675	0.11
b_{13}	-1.00	400	-0.045
b_{23}	4.40	425	0.14
b_1^2	7.10	2065	0.133
b_2^2	-1.56	-360	-0.365
b_3^2	6.37	1565	0.255
Factor significance*			
	$t_{0.99}$	$t_{0.95}$	$t_{0.95}$
F_M	6.94	2172	0.323
F_I	9.82	3073	0.457
F_Q	4.91	1536	0.228

Calculations see Table A-1. Here, F_M is the minimum factor effect for linear parameters; F_I is the minimum factor effect for two-factor interactions; F_Q is the minimum factor effect for quadratic parameters.

Appendix 5

Calibration factors for DSC analysis

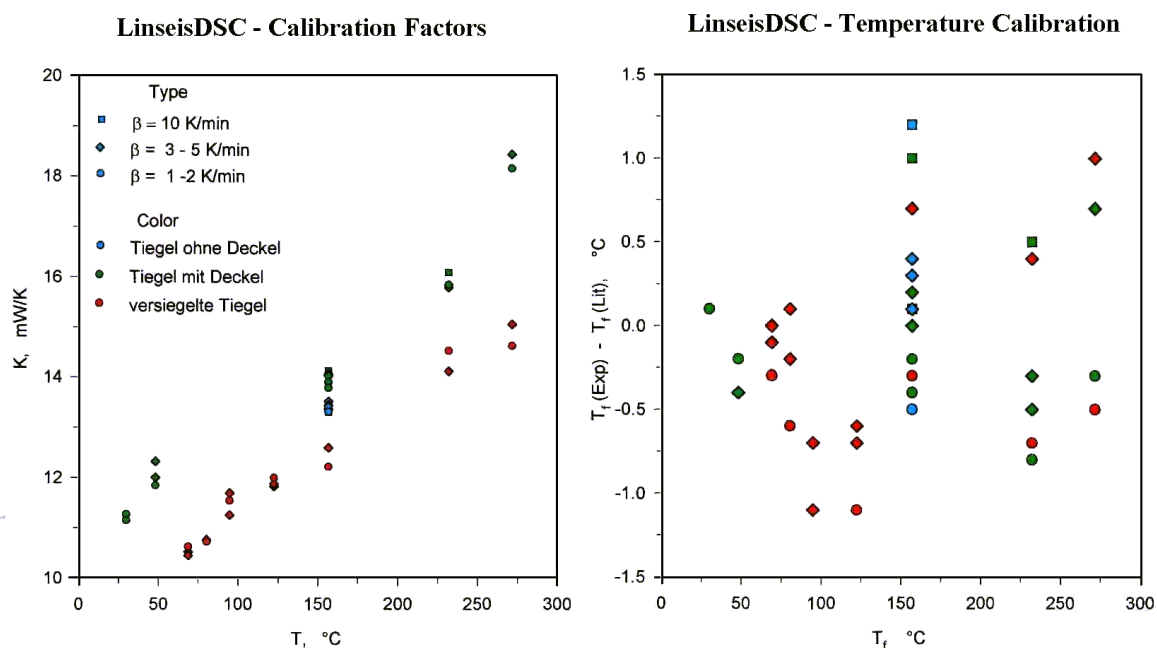**Figure A- 1**.   *Calibration factors for DSC analysis (temperature)*
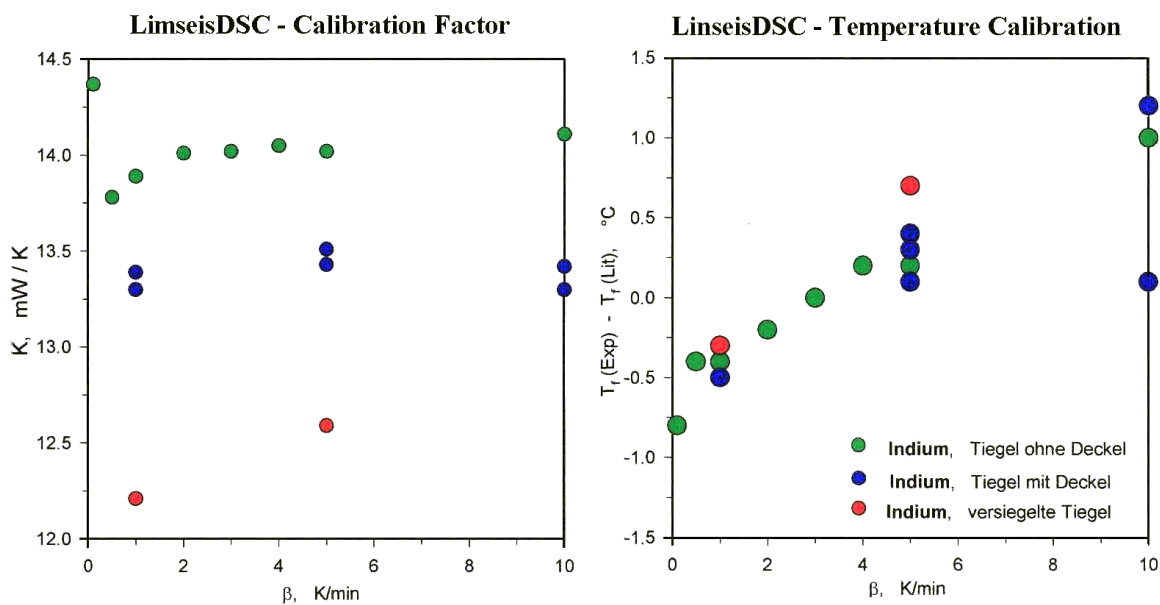

Figure A- 2. .   *Calibration factors for DSC analysis (temperature rising rate)*